

Université du Québec
Institut national de la recherche scientifique
Énergie, Matériaux et Télécommunications

Analysis and Compensation of Channel and RF Impairments in MIMO Wireless Communication Systems

By
Jian Qi

A dissertation submitted in partial fulfillment of the requirements for the degree of
Doctor of Philosophy (Ph.D.) in Telecommunications

Evaluation Jury

External examiner	Prof. Fadhel M. Ghannouchi University of Calgary
External examiner	Prof. Mohamed-Slim Alouini KAUST, Kingdom of Saudi Arabia
Internal examiner	Prof. Douglas O'Shaughnessy INRS-Énergie, Matériaux et Télécommunications
Internal examiner	Prof. Charles Despins INRS-Énergie, Matériaux et Télécommunications
Research director	Prof. Sonia Aïssa INRS-Énergie, Matériaux et Télécommunications

To my dear Mom and Dad.

Abstract

This dissertation presents analyses and compensation methods of channel and radio frequency (RF) impairments, including spatially-correlated and keyhole fading channels, impairments in mobile-to-mobile (M-to-M) communications, high-power amplifier (HPA) nonlinearity, in-phase and quadrature-phase (I/Q) imbalance and crosstalk, both separately and together for multiple-input multiple-output (MIMO) wireless communication systems.

Specifically, one cross-layer design scheme is proposed for MIMO systems employing orthogonal space-time block code (OSTBC) over spatially-correlated and keyhole Nakagami- m fading channels. In addition, the performance of M-to-M MIMO maximal ratio combining (MRC) systems is assessed, over double-correlated Rayleigh-and-Lognormal fading channels. In this regard, a three-dimensional (3D) channel model, which takes into account the effects of fast fading and shadowing, is used to obtain the transmit and receive spatial correlation functions.

On the other hand, we propose a constellation-based and a sequential Monte Carlo (SMC)-based compensation methods for HPA nonlinearity in the case with and without knowledge of the HPA parameters, respectively, for MIMO OSTBC systems. As for the HPA nonlinearity in MIMO transmit beamforming (TB) systems, the optimal TB scheme with the optimal beamforming weight vector and combining vector is proposed. Moreover, an alternative suboptimal but much simpler TB scheme, namely, quantized equal gain transmission (QEGT), is also evaluated in the presence of HPA nonlinearity. We also propose a compensation algorithm for I/Q imbalance in MIMO MRC systems, which first employs the least-squares (LS) rule to estimate the coefficients of the channel gain matrix, beamforming and combining weight vectors, and parameters of I/Q imbalance jointly, and then makes use of the received signal

together with its conjugation to detect the transmitted signal. Moreover, the performance of MIMO MRC in the presence of another RF impairment, namely, crosstalk, is evaluated.

Finally, a comprehensive compensation method for multiple RF impairments together in MIMO TB systems, is proposed.

Student

Research Director

Acknowledgments

First and foremost I would like to express my deepest gratitude to my supervisor Prof. Sonia Aïssa for her invaluable guidance, continuous encouragement and constant support throughout my research. I really appreciate her enthusiasm, insights and constructive suggestions on this research, which will still influence me in my further career.

I would like to thank my thesis committee members for their comments and suggestions on my dissertation.

I gratefully acknowledge the research funding from the Quebec Government Fonds Québécois de la Recherche sur la Nature et les Technologies (FQRNT) and from my supervisor.

Thanks to all professional and technical colleagues at Institut national de la recherche scientifique—Énergie, Matériaux et Télécommunications (INRS-EMT) and all my friends for their generous help.

Finally, my special thanks go to my family and most of all my parents for their love, encouragement, support and understanding.

Table of Contents

Abstract	i
Acknowledgments	iii
Table of Contents	v
List of Figures	ix
List of Tables	xvii
List of Acronyms	xix
1 Introduction	1
1.1 Background and Motivation	1
1.1.1 MIMO Wireless Communication Systems	1
1.1.2 Spatially-Correlated and Keyhole Fading Channels	2
1.1.3 Mobile-to-Mobile Communications	3
1.1.4 HPA Nonlinearity	4
1.1.5 I/Q Imbalance	5
1.1.6 Crosstalk	7
1.2 Research Objectives	8
1.3 Contribution of the Dissertation	9
1.3.1 Accomplishment	9
1.3.2 List of Original Publications	12
1.4 Organization of the Dissertation	14
2 MIMO Communications in Spatially-Correlated and Keyhole Fading Channels	17
2.1 Introduction	17
2.2 System and Channel Models	19
2.2.1 Spatially-Correlated MIMO Nakagami- m Fading Channels	20
2.2.2 Keyhole MIMO Nakagami- m Fading Channels	21

2.3	Cross-layer Design	22
2.3.1	Physical and Link layer Parameters	23
2.3.2	PER Approximation for AWGN channels	24
2.3.3	SNR Thresholds for MCS	25
2.4	Performance Analysis	26
2.4.1	Average Packet Loss Rate	26
2.4.2	Average Spectral Efficiency	29
2.4.3	Probability of Outage	30
2.5	Numerical Results and Discussions	31
2.6	Summary	36
3	Mobile-to-Mobile Communications	41
3.1	Introduction	41
3.2	System model	43
3.3	Space-Time Correlation Function	45
3.4	Performance Analysis	51
3.4.1	Average SEP	51
3.4.2	Ergodic Capacity	54
3.4.3	Outage Probability	57
3.5	Numerical Results	58
3.6	Summary	63
4	Analysis and Compensation of HPA Nonlinearity	65
4.1	Analysis and Compensation of HPA Nonlinearity in MIMO OSTBC Systems	66
4.1.1	System and HPA Models	67
4.1.2	Signal Detection with Knowledge of the HPA Parameters	70
4.1.3	SMC Receiver without Knowledge of the HPA Parameters	77
4.1.4	Numerical and Simulation Results	83
4.2	MIMO Transmit Beamforming Systems with Nonlinear HPAs	88
4.2.1	System and High-Power Amplifier Models	89
4.2.2	Channel Estimation under HPA Nonlinearity	90
4.2.3	Optimal Beamforming Scheme in the Presence of HPA Nonlinearity	92
4.2.4	QEGT/MRC: A Simple and Feasible Beamforming Scheme under HPA Nonlinearity	99
4.2.5	Numerical and Simulation Results	106
4.3	Summary	111
5	Analysis and Compensation of I/Q Imbalance	115
5.1	Introduction	115
5.2	System and I/Q Imbalance Models	116
5.3	Signal Detection without I/Q Imbalance Compensation	118

5.3.1	Proposed Channel Estimation Algorithm	119
5.3.2	Detection of the Transmitted Signal	121
5.4	Pilot-Based I/Q Imbalance Compensation Algorithm	123
5.4.1	Estimation of the Coefficients $K_1 \mathbf{z}^H \mathbf{H} \mathbf{w}$ and $K_2 (\mathbf{z}^H \mathbf{H} \mathbf{w})^*$	123
5.4.2	Signal Detection Using I/Q Imbalance Compensation	125
5.5	Performance Analysis	126
5.5.1	Performance without I/Q Imbalance Compensation	126
5.5.2	Performance with the Proposed I/Q Imbalance Compensation Algorithm	131
5.6	Numerical and Simulation Results	133
5.7	Summary	138
6	Analysis of the Effects of Crosstalk	141
6.1	Introduction	141
6.2	System Model	142
6.3	Performance Analysis	145
6.3.1	Average Symbol Error Probability	145
6.3.2	System capacity	146
6.4	Numerical Results	147
6.5	Summary	149
7	Compensation for Multiple RF Impairments	151
7.1	Introduction	151
7.2	System Model	153
7.3	Estimation of the Equivalent Channel Under HPA Nonlinearity, I/Q Imbalance and Crosstalk	156
7.4	Compensation for HPA Nonlinearity, I/Q Imbalance and Crosstalk	157
7.4.1	Optimal TB Scheme	157
7.4.2	Estimation of Coefficients $K_1 \mathbf{z}^H \mathbf{H}_e \mathbf{v}$ and $K_2 (\mathbf{z}^H \mathbf{H}_e \mathbf{v})^*$	158
7.4.3	Signal Detection Using Compensation for RF Impairments	159
7.5	Performance Analysis	160
7.5.1	Average Symbol Error Probability	161
7.5.2	System Capacity	162
7.6	Numerical Results	163
7.7	Summary	166
8	Conclusions and Further Research	167
8.1	Conclusions of the Dissertation	167
8.2	Topics for Future Research	170
A	Appendix	171
A.1	Proof of Proposition 1	171
A.2	Proof of Theorem 1	173

Bibliography	177
B Résumé	R-1
B.1 Introduction	R-1
B.1.1 Contexte et Motivation	R-1
B.1.2 Objectifs de la Recherche	R-5
B.1.3 Contribution de la Dissertation	R-6
B.2 Canaux à Évanouissements Spatialement Corrélés et à <i>Keyhole</i>	R-8
B.3 Communications Mobile-à-Mobile	R-10
B.4 Analyse et Rémunération de la Nonlinéarité HPA	R-12
B.4.1 Analyse et Rémunération de la Nonlinéarité HPA dans le Systèmes MIMO OSTBC	R-12
B.4.2 Nonlinéarité HPA dans le Systèmes MIMO TB	R-14
B.5 Analyse et Rémunération des Déséquilibre I/Q	R-15
B.6 Analyse des Effets de la Diaphonie	R-17
B.7 Indemnisation des Multiples Déficiences RF	R-19
B.8 Conclusions et Recherches Supplémentaires	R-20
B.8.1 Conclusions de la Dissertation	R-20
B.8.2 Thèmes pour de Futures Recherches	R-21

List of Figures

2.1	Block diagram for the cross layer design based MIMO-OSTBC systems.	23
2.2	Average spectral efficiency of cross layer design based MIMO-OSTBC in the spatially-correlated Nakagami- m fading channel case for different antenna configurations: $n_T = 2$ and (a) $n_R = 1$, (b) $n_R = 2$, and (c) $n_R = 4$.	32
2.3	Average packet loss rate of cross layer design based MIMO-OSTBC in the spatially-correlated Nakagami- m fading channel case for different values of N_r^{\max} .	33
2.4	Outage probability of cross layer design based MIMO-OSTBC in the spatially-correlated Nakagami- m fading channel case for different antenna configurations: $n_T = 2$ and (a) $n_R = 1$, (b) $n_R = 2$, and (c) $n_R = 4$.	34
2.5	Average spectral efficiency of cross layer design based MIMO-OSTBC in the spatially-correlated Nakagami- m fading channel case for different ρ_T , ρ_R , and m .	35
2.6	Average packet loss rate of cross layer design based MIMO-OSTBC in the spatially-correlated Nakagami- m fading channel case for different ρ_T , ρ_R , and m .	36
2.7	Outage probability of cross layer design based MIMO-OSTBC in the spatially-correlated Nakagami- m fading channel case for different ρ_T , ρ_R , and m .	37

2.8	PDFs for the output SNR of cross layer design based MIMO-OSTBC in the spatially-correlated Nakagami- m fading channel case for different ρ_T, ρ_R ($m = 2, \bar{\gamma} = 10$ dB).	37
2.9	Average spectral efficiency of cross layer design based MIMO-OSTBC in the keyhole Nakagami- m fading channel case for different antenna configurations: $n_T = 2$ and (a) $n_R = 1$, (b) $n_R = 2$, and (c) $n_R = 4$	38
2.10	Average packet loss rate of cross layer design based MIMO-OSTBC in the keyhole Nakagami- m fading channel case for different values of N_r^{\max}	38
2.11	Outage probability of cross layer design based MIMO-OSTBC in the keyhole Nakagami- m fading channel case for different antenna configurations: $n_T = 2$ and (a) $n_R = 1$, (b) $n_R = 2$, and (c) $n_R = 4$	39
2.12	Average spectral efficiency of cross layer design based MIMO-OSTBC in the keyhole Nakagami- m fading channel case for different m	39
2.13	Average packet loss rate of cross layer design based MIMO-OSTBC in the keyhole Nakagami- m fading channel case for different m	40
2.14	Outage probability of cross layer design based MIMO-OSTBC in the keyhole Nakagami- m fading channel case for different m	40
3.1	The two-cylinder model for M-to-M MIMO channel.	46
3.2	Space-time correlation function versus normalized time delay of M-to-M MIMO NLoS channels in the case with $n_T = n_R = 4$	58
3.3	Space-time correlation function $\rho_{11,22}(\delta_T, \delta_R, 0)$ for different values of $\delta_T, \delta_R, \beta_T^{\max}$, and β_R^{\max} of M-to-M MIMO NLoS channels in the case with $n_T = n_R = 4$	59
3.4	Average SEP versus orientation angle θ_T of M-to-M MIMO MRC for different values of ζ_T and μ_T in the case with $n_T = n_R = 2, a = 2, b = 0.5$ and $\bar{\gamma} = 20$ dB.	60
3.5	Average SEP versus shadowing standard derivation of M-to-M MIMO MRC for different values of D and δ_T in the case with $n_T = n_R = 2, r = 3, a = 2$ and $b = 0.5$	61

3.6	Outage probability versus SNR threshold of M-to-M MIMO MRC for different value of k_T in the case with $n_T = n_R = 2$ and $\bar{\gamma} = 20$ dB. . .	62
3.7	Outage probability versus SNR threshold of M-to-M MIMO MRC for different values of β_T^{\max} and r in the case with $n_T = n_R = 2$ and $\sigma = 8$ dB. 63	63
3.8	Ergodic capacity versus average SNR per receive antenna of M-to-M MIMO MRC for different values of β_T^{\max} in the case with $n_T = n_R = 2$. 64	64
4.1	Block diagram for the considered MIMO-OSTBC system in the presence of nonlinear HPA.	68
4.2	Rectangular 16-QAM constellation and decision regions: (a) ideal case, (b) with HPA distortion.	72
4.3	Average SEP versus $\bar{\gamma}$ of MIMO-OSTBC for different modulation formats in the case with knowledge of the HPA parameters ($n_T = n_R = 2$, $A_{os} = 1$, $\beta = 2$): linear (L) vs nonlinear (NL).	80
4.4	Average SEP versus $\bar{\gamma}$ of MIMO-OSTBC for different values of β in the case with knowledge of the HPA parameters ($n_T = n_R = 2$, $A_{os} = 1$, 16QAM)	81
4.5	TD versus OBO of MIMO-OSTBC for different values of n_T, n_R ($A_{os} = 1$, $\beta = 2$, 16QAM, $P_s = 10^{-4}$).	82
4.6	Upper and lower bounds on system capacity of MIMO-OSTBC versus $\bar{\gamma}$ for different values of β ($n_T = n_R = 2$, $A_{os} = 1$).	83
4.7	Average SEP versus $\bar{\gamma}$ of MIMO-OSTBC for different modulation formats in the cases with and without knowledge of the HPA parameters ($n_T = n_R = 2$, $A_{os} = 1$, $\bar{\beta} = 2$, $N = 30$).	84
4.8	Average SEP versus $\bar{\gamma}$ of MIMO-OSTBC for different values of N in the cases with and without knowledge of the HPA parameters ($n_T = n_R = 2$, 16QAM, $A_{os} = 1$, $\bar{\beta} = 2$)	85
4.9	Average SEP versus $\bar{\gamma}$ of MIMO-OSTBC for different cases of parameter knowledge ($n_T = n_R = 2$, 64QAM, $\bar{A}_{os} = 1$, $\bar{\beta} = 2$, $N = 30$) . . .	86

4.10	Total degradation versus OBO of MIMO-OSTBC for different cases of parameter knowledge ($n_T = 2$, $n_R = 4$, 16QAM, $\bar{A}_{os} = 1$, $\bar{\beta} = 2$, $N = 30$).	87
4.11	Block diagram of the considered MIMO TB system with nonlinear HPAs.	89
4.12	Lower and upper bounds on the average SEP versus $\bar{\gamma}$ of the optimal beamforming with HPA nonlinearity for different modulation formats ($n_T = n_R = 2$, $\beta = 1$, $V = 16$).	107
4.13	Lower and upper bounds on the average SEP versus $\bar{\gamma}$ of the optimal beamforming with HPA nonlinearity for different values of β ($n_T = n_R = 2$, 16QAM, $V = 16$).	108
4.14	Lower and upper bounds on the average SEP versus $\bar{\gamma}$ of the optimal beamforming with HPA nonlinearity for different values of V ($n_T = n_R = 2$, 16QAM, $\beta = 1$).	109
4.15	Lower and upper bounds on the mutual information under Gaussian input versus $\bar{\gamma}$ of the optimal beamforming with HPA nonlinearity for different values of β and n_T ($V = 16$).	110
4.16	Lower and upper bounds on the mutual information under Gaussian input versus $\bar{\gamma}$ of the optimal beamforming with HPA nonlinearity for different values of V and n_T ($\beta = 1$).	111
4.17	Average SEP versus $\bar{\gamma}$ of the optimal beamforming and QEGT/MRC schemes with HPA nonlinearity for different modulation formats ($n_T = n_R = 2$, $\beta = 1$, $V = 16$, $N = 16$).	112
4.18	Average SEP versus $\bar{\gamma}$ of the optimal beamforming and QEGT/MRC schemes with HPA nonlinearity for different values of N ($n_T = n_R = 2$, 16QAM, $\beta = 1$, $V = 16$).	113
4.19	Upper bounds on the mutual information under Gaussian input versus $\bar{\gamma}$ of the optimal beamforming and QEGT/MRC schemes with HPA nonlinearity for different values of β and n_T ($V = 16$, $N = 16$).	113

4.20	Upper bounds on the mutual information under Gaussian input versus $\bar{\gamma}$ of the optimal beamforming and QEGT/MRC schemes with HPA nonlinearity for different values of N ($\beta = 0.6$, $V = 16$).	114
5.1	Block diagram for the considered MIMO MRC system in the presence of I/Q imbalance.	117
5.2	Average SEP versus average SNR per receive antenna of MIMO MRC for different modulation formats in the cases with or without I/Q imbalance ($n_T = n_R = 2$).	133
5.3	Upper bound on average SEP versus average SNR per receive antenna of MIMO MRC for different values of ILR and V in the cases with or without I/Q imbalance ($n_T = n_R = 2$, 16QAM).	134
5.4	Outage probability versus SNR threshold γ_{th} of MIMO MRC for different values of n_T and n_R in the cases with or without I/Q imbalance ($\bar{\gamma} = 10$ dB, $V = 8$).	135
5.5	Lower bound on ergodic capacity versus average SNR per receive antenna of MIMO MRC for different values of ILR and V in the cases with or without I/Q imbalance ($n_T = n_R = 2$).	136
5.6	Average SEP versus average SNR per receive antenna of MIMO MRC for different modulation formats in the cases with or without compensation (perfect channel estimation, $n_T = n_R = 2$).	137
5.7	Average SEP versus average SNR per receive antenna of MIMO MRC for different values of U in the case with I/Q imbalance compensation (perfect channel estimation, $n_T = n_R = 2$, 16QAM).	138
5.8	Outage probability versus SNR threshold of MIMO MRC for different values of n_T , n_R and U in the case with I/Q imbalance compensation (perfect channel estimation, $\bar{\gamma} = 10$ dB).	139
5.9	Ergodic capacity versus average SNR per receive antenna of MIMO MRC for different values of n_T and n_R in the cases with and without I/Q imbalance compensation (perfect channel estimation).	140

6.1	Block diagram of the MIMO MRC system with crosstalk.	143
6.2	Average SEP versus $\bar{\gamma}$ of MIMO MRC with crosstalk for different modulation formats ($n_T = n_R = 2$).	147
6.3	Average SEP versus $\bar{\gamma}$ of MIMO MRC with crosstalk for different values of n_T and n_R (8PSK).	148
6.4	System capacity versus $\bar{\gamma}$ of MIMO MRC with crosstalk for different values of α_T and α_R ($n_T = n_R = 2$).	149
6.5	System capacity versus crosstalk of MIMO MRC for different values of n_T and n_R ($\alpha_T = \alpha_R = \alpha$, $\bar{\gamma} = 10$ dB).	150
7.1	Block diagram of the MIMO TB system in the presence of HPA non-linearity, I/Q imbalance and crosstalk.	153
7.2	Average SEP versus $\bar{\gamma}$ of MIMO TB with RF impairments for different modulations formats ($n_T = n_R = 2$, $\beta = 1$, $ILR = -20$ dB, $U=32$, $\alpha_T = \alpha_R = -10$ dB).	163
7.3	Average SEP versus $\bar{\gamma}$ of MIMO TB with RF impairments for different values of α_T , α_R and β ($n_T = 3$, $n_R = 2$, QPSK, $ILR = -20$ dB, $U=32$).	164
7.4	System capacity versus $\bar{\gamma}$ of MIMO TB with RF impairments for different values of α_T , α_R and ILR ($n_T = n_R = 2$, $\beta = 1$, $U=32$).	165
7.5	System capacity versus crosstalk of MIMO TB with RF impairments for different values of n_T , n_R and β ($\alpha_T = \alpha_R = \alpha$, $\bar{\gamma} = 10$ dB, $ILR = -20$ dB).	166
B.1	Schéma pour la conception inter-couches basée sur les MIMO-OSTBC systèmes.	R-9
B.2	Le modèle à deux cylindres pour canal M-to-M MIMO.	R-11
B.3	Schéma pour le système considéré MIMO-OSTBC dans le présence de non linéaires HPA.	R-13
B.4	Schéma du système MIMO TB considéré avec HPA nonlinéaire.	R-14
B.5	Schéma pour le système considéré MIMO MRC dans le présence d'I/Q déséquilibre.	R-16

B.6	Schéma du système MIMO MRC avec diaphonie.	R-18
B.7	Schéma du système MIMO TB en présence de nonlinarité HPA, I/Q déséquilibre et de la diaphonie.	R-19

List of Tables

2.1 Fitting parameters of MCS transmission modes for packet length $N_p =$
1080 bits. 24

List of Acronyms

3D	Three-Dimensional
3GPP	3rd Group Partnership Project
AAoA	Azimuth Angle of Arrival
AAoD	Azimuth Angle of Departure
AM/AM	Amplitude-to-Amplitude
AM/PM	Amplitude-to-Phase
AMC	Adaptive Modulation and Coding
ARQ	Automatic Repeat Request
ASE	Average Spectral Efficiency
AWGN	Additive White Gaussian Noise
BER	Bit Error Rate
CAD	Computer Aided Design
CDF	Cumulative Distribution Function
CRC	Cyclic Redundancy Check
CSI	Channel State Information
DSP	Digital Signal Processing
EAoA	Elevation Angle of Arrival
EAoD	Elevation Angle of Departure
EGT	Equal Gain Transmission
EVM	Error Vector Magnitude
FFT	Fast Fourier Transform

FPGA	Field-Programmable Gate Array
F-to-M	Fixed-to-Mobile
HPA	High-Power Amplifier
IEEE	Institute of Electrical and Electronics Engineers
i.i.d	Independent and Identically Distributed
I/Q	In-Phase/Quadrature-Phase
LNA	Low-Noise Amplifier
LS	Least-Squares
LTE	Long Term Evolution
M-to-M	Mobile-to-Mobile
MBWA	Mobile Broadband Wireless Access
MCS	Modulation and Coding Scheme
MIMO	Multiple-Input Multiple-Output
ML	Maximum Likelihood
MMSE	Minimum Mean Square Error
MRC	Maximal Ratio Combining
MRT	Maximal Ratio Transmission
MSE	Mean Square Error
NACK	Negative Acknowledgment
NLoS	Non-Line-of-Sight
OBO	Output Back-Off
OFDM	Orthogonal Frequency-Division Multiplexing
OSTBC	Orthogonal Space-Time Block Code
PAPR	Peak-to-Average Power Ratio
PCB	Printed Circuit Board
PDF	Probability Density Function
PER	Packet Error Rate
PLR	Packet Loss Rate
PSK	Phase-Shift Keying
QAM	Quadrature Amplitude Modulation
QEGT	Quantized Equal Gain Transmission

QPSK	Quadrature Phase-Shift Keying
RF	Radio Frequency
RVQ	Random Vector Quantization
SEL	Soft-Envelope Limiter
SEP	Symbol Error Probability
SISO	Signal-Input Single-Output
SMC	Sequential Monte Carlo
SNR	Signal-to-Noise Ratio
SSPA	Solid State Power Amplifier
STBC	Space-Time Block Code
STTC	Space-Time Trellis Code
T-ARQ	Truncated Automatic Repeat Request
TB	Transmit Beamforming
TD	Total Degradation
TWTA	Travelling Wave Tube Amplifier
VoIP	Voice over Internet Protocol
WiMAX	Worldwide Interoperability for Microwave Access
WLAN	Wireless Local Area Networks

Chapter 1

Introduction

1.1 Background and Motivation

1.1.1 MIMO Wireless Communication Systems

The unprecedented growth, over the past decades, in the demand for reliable high-speed wireless communications in order to support multifarious applications and services, e.g., voice, video, Voice over Internet Protocol (VoIP), email and web browsing, highlights the need for new promising transmission techniques. In the late 1990s, multiple-input multiple-output (MIMO) technology was invented, which represents efficient means to enhance channel capacity and transmission reliability, i.e., diversity gain and multiplexing gain, respectively. MIMO techniques can be categorized into several kinds, namely, space-time block code (STBC), space-time trellis code (STTC), layered space-time code, and MIMO maximal ratio combining (MRC) systems with transmit beamforming (TB) [1]. The STBC scheme can achieve transmit and receive diversity using a simple yet effective transmit/receive processing. The STTC may achieve coding gain over the STBC at the cost of increased decoding complexity, where trellis structure determines the coded symbols to be transmitted from different antenna elements. As for the layered space-time code, the technique focuses on the spatial multiplexing gain. On the other hand, if the channel state information (CSI) is perfectly known at the transmitter, TB and water-filling techniques associated with

MRC can be used to achieve full diversity gain and higher capacity. Owing to the great benefits, MIMO techniques have been included in several standards for future wireless communication systems, such as the 3rd Generation Partnership Project (3GPP) Long Term Evolution (LTE) and LTE-Advanced [2], Institute of Electrical and Electronics Engineers (IEEE) 802.11 Wireless Local Area Networks (WLAN) [3, 4] and IEEE 802.16e Worldwide Interoperability for Microwave Access (WiMAX) [5], and also considered for IEEE 802.20 Mobile Broadband Wireless Access (MBWA) [6] and IEEE 802.22 Wireless Regional Area Networks (WRAN) [7]. Furthermore, the implementation of MIMO schemes is also investigated in cooperative communications and cognitive radio networks.

However, the MIMO schemes are baseband techniques, which are related to the channel conditions and the radio frequency (RF) operations. In practice, the system performance is affected by channel and RF impairments, such as spatially-correlated and keyhole fading, impairments in mobile-to-mobile (M-to-M) channels, high-power amplifier (HPA) nonlinearity, in-phase and quadrature-phase (I/Q) imbalance, crosstalk, low-noise amplifier (LNA) nonlinearity, antenna coupling, phase noise, frequency offset, imperfect timing synchronization and echo. In this dissertation, we focus on the issues related to the spatially-correlated and keyhole fading channels, mobile-to-mobile channels, HPA nonlinearity, I/Q imbalance and crosstalk.

1.1.2 Spatially-Correlated and Keyhole Fading Channels

In practice, the fading channels over which the MIMO schemes operate may not be independent and identically distributed (i.i.d.), due to spatial fading correlation or keyhole phenomena [8]. Spatial correlation can arise when elements of the transmit/receive antenna arrays are not spaced sufficiently apart and/or due to poor scattering conditions [9–18]. The capacity of spatially-correlated MIMO Rayleigh fading channels without CSI at the transmitter has been widely discussed in the literature (cf. [19, 20] and references therein). In addition, the capacity of MIMO systems associated with orthogonal space-time block code (OSTBC) over correlated Rayleigh and Ricean flat-fading channels under different adaptive transmission techniques, such as

optimal power and rate allocation, total channel inversion with fixed rate policy and its truncated variant, was studied in [21]. On the other hand, in the presence of the keyhole phenomenon in the MIMO propagation environment, the radio wave sent from the transmitter to the receiver must propagate through the keyhole in space [22]. The properties of spatial fading correlations and keyholes have been investigated in [23], where canonical physical examples of keyholes are presented. In [24], the bit error rate (BER) performance of OSTBC in Nakagami- m keyhole channels was analyzed. Moreover, in the scenario with CSI at the transmitter and receiver, the impact of spatial fading correlations and keyholes in MIMO systems has been assessed from a capacity perspective in [25].

1.1.3 Mobile-to-Mobile Communications

In wireless communication systems, such as cooperative MIMO networks, cognitive radio networks and vehicle-to-vehicle communication systems, transmitters and receivers may both be in motion, and the channel is referred to as an M-to-M communication channel. In order to describe the propagation model of such a channel, a two-ring scattering model for MIMO systems has been proposed in [26]. This model is different from the one-ring model proposed in [27] for fixed-to-mobile (F-to-M) channels. In both of these models, the scattered waves are assumed to travel in the horizontal plane, which is only valid for poor-scattering environments, e.g., rural areas. In rich-scattering environments, e.g., urban areas with high density of buildings, the scattered waves may not diffuse in the horizontal plane only. In this case, three-dimensional (3D) geometrical modeling represents an adequate tool for describing the wireless propagation environment. In [28], a 3D model has been used for F-to-M multi-carrier propagation channels, where the cross-correlation function between two sub-channels of an outdoor MIMO channel with non-isotropic wave propagation was derived.

For M-to-M communication systems equipped with low elevation antennas and multi-antenna mobile transceivers, the 3D scattering channels can be characterized by the two-cylinder model, with one cylinder around the transmitter and another

around the receiver [29], which extends the one-cylinder model described in [30–32] for F-to-M channel. Recently, the space-time correlation function of 3D M-to-M MIMO fast fading channels has been derived in [33], and used to assess its influence on capacity in the scenario with no CSI at the transmitter and perfect CSI at the receiver, through simulations.

In the above-mentioned works on M-to-M channel modeling, only the effects of fast fading factors caused by multipath, such as random phase shift, propagation delay and Doppler shift, were considered in the modeling of the time-varying channel impulse response.

1.1.4 HPA Nonlinearity

HPA, e.g., travelling wave tube amplifier (TWTA), solid state power amplifier (SSPA) and soft-envelope limiter (SEL), is a primary block of wireless communication systems, wherein it operates at the RF level. In general, when analyzing the performance of wireless systems, the HPA is assumed to operate in its linear region in order to ensure that the characteristics of the symbols at the modulator's output are not affected by the power amplification process; an assumption that is not necessarily valid in practical situations, especially when the HPA operates at the medium and high-power signal levels. Indeed, in such cases, nonlinear distortions, including amplitude and phase distortions, are introduced into the transmitted symbols, which in turn can cause adjacent channel interference and power losses. Therefore, it is crucial to consider the HPA imperfections when evaluating the performance of wireless communication systems and designing such systems.

Nonlinear HPAs can be described by two kinds of models: memoryless models with frequency-flat responses and memory models with frequency-selective responses [34]. Memoryless HPA models, such as the one introduced in [35] for TWTA, the SSPA model [36], the SEL model for amplifiers with ideal predistortion [37], and the polynomial model [38], are characterized by their amplitude-to-amplitude (AM/AM) and amplitude-to-phase (AM/PM) conversions, which depend only on the current input signal at the HPA. On the other hand, HPAs may be characterized by more realistic

memory models, such as the Volterra, Wiener, Hammerstein, Wiener-Hammerstein, and memory polynomial models [34]. Recent research effort has dealt with the issue of HPA nonlinearity in MIMO systems. For instance, the effect of HPA nonlinearity on the symbol error probability (SEP) was studied in [39] for MIMO systems employing STTC, using the Saleh nonlinearity model [35] for TWTA. In addition, based on a memoryless polynomial model, the effect of HPA nonlinearity on the BER of quadrature amplitude modulation (QAM) was analyzed in [40] for MIMO systems with zero-forcing receivers in uncorrelated frequency non-selective Rayleigh fading channels. The latter study also highlighted the degrading effect of channel estimation error on the BER performance. On the other hand, the HPA nonlinearity in orthogonal frequency division multiplexing (OFDM) systems was investigated in [41], where the output at the HPA is expressed as the summation of the input signal multiplied by a complex scale factor, and an additive Gaussian noise, which is uncorrelated with the input signal.

The performance degradation due to the HPA nonlinearity highlights the need for compensation schemes in order to eliminate or mitigate the effects of nonlinearity. In this regard, several compensation schemes for the HPA nonlinearity have been proposed, which can be classified into two categories: compensation at the transmitter or at the receiver. Methods implemented at the transmitter include power back-off, peak-to-average power ratio (PAPR) reduction techniques, and linearization techniques [34, 42, 43]; for instance, feedforward method, feedback method and predistortion, represent linearization techniques. On the other hand, the uplink transmission scenario requires compensation of HPA nonlinearity at the receiver, e.g., postdistortion, nonlinear equalization and the iterative detection method [34].

1.1.5 I/Q Imbalance

One of the RF impairments associated with analog processing is I/Q imbalance at the transmitter and the receiver, which refers to the mismatch between the components in the I and Q branches, i.e., the mismatch between the real and imaginary parts of complex signals [44–48]. This happens due to the limited accuracy of the

analog hardware, such as finite tolerances of capacitors and resistors. In most articles discussing baseband communication techniques, the effect of I/Q imbalance is ignored in the design and performance analysis since it is normally considered in the RF front-end design. However, in practice, such an assumption is unrealistic, especially in multi-carrier communication systems. Indeed, in such cases, the I/Q imbalance, including amplitude imbalance and phase imbalance, is introduced into the received signal after analog processing, which in turn can cause interference and power loss. Since the performance of baseband digital design depends on that of the RF analog processing, it is crucial to consider the I/Q imbalance in the design and performance evaluation of wireless communication systems.

Recent research effort has dealt with the issue of I/Q imbalance in MIMO systems and OFDM systems. For instance, the effect of I/Q imbalance on the performance of MIMO systems employing STBC was studied in [49], where the SEP was evaluated through simulations. As for the capacity of OFDM systems in the presence of I/Q imbalance, its analytical expression was derived in [50], followed by an upper bound provided for a fixed channel realization in Rayleigh fading. In addition, the performance of M-ary QAM-OFDM in the presence of I/Q imbalance was investigated in terms of the error vector magnitude (EVM), which is a modulation quality metric used to evaluate the effects of imperfections in digital communication systems [51].

The performance degradation due to I/Q imbalance highlights the need for compensation schemes in order to eliminate or at least mitigate the effect of I/Q imbalance on the performance of wireless communication systems. Recently, several compensation schemes for I/Q imbalance have been proposed, which can be divided into two kinds: compensation methods with and without estimation of the parameters of I/Q imbalance, respectively. For instance, interference cancellation-based compensation and blind source separation-based compensation, which do not require any training signals, represent compensation methods without estimation of the parameters of I/Q imbalance [52, 53]. On the other hand, the transmitted signal can be detected after the channel gain and parameters of I/Q imbalance are estimated using training signals. For instance, a compensation method based on algebraic properties of

the derived signal models combined with proper pilot data was proposed for MIMO STBC systems in [49]. Besides, the effect of I/Q imbalance on OFDM systems was investigated in [54], followed by estimation-based system-level algorithms proposed to compensate for the distortions, including least-squares (LS) equalization, adaptive equalization, post-fast fourier transform (FFT) LS, as well as pre-FFT correction using adaptive channel/distortion estimation and special pilot tones to enable accurate and fast training. A framework for eliminating I/Q distortions through digital signal processing was also developed for MIMO OFDM systems in [55], where the complexity of the system at the receiver grows from dimensions $(n_R \times n_T)$ for ideal I/Q branches to $(2n_R \times 2n_T)$ in the presence of I/Q imbalance, with n_T and n_R denoting the numbers of transmit and receive antennas, respectively. In addition, a digital pre-distortion structure was provided in [56] to compensate for the I/Q imbalance at the transmitter, where the parameters of I/Q imbalance are estimated using an iterative approach.

1.1.6 Crosstalk

In the printed circuit board (PCB) design, one of several important aspects is crosstalk, which refers to the unintended electromagnetic coupling between traces, wires, PCB lands, and any other electrical component subject to electromagnetic field disturbance that are in close proximity to each other [57–63]. Crosstalk concerns the intrasystem interference performance; that is, the source of the electromagnetic emission and the receptor of this emission are within the same system. Moreover, the crosstalk can be classified into two kinds: linear crosstalk that occurs after the nonlinear HPAs and nonlinear crosstalk before the nonlinear HPAs.

In most articles discussing baseband MIMO communication techniques, the effect of crosstalk is ignored in the design and performance analysis, since it is assumed as an issue related to the PCB design. However, in practice, such assumption is unrealistic for MIMO systems. Indeed, since the performance of baseband digital design depends on that of the PCB design, it is crucial to consider the crosstalk in the design and performance analysis of multi-antenna wireless communication systems.

Recent research effort has dealt with the issue of crosstalk in MIMO systems. For instance, crossover digital predistorter was proposed in [64] for the compensation of HPA nonlinearly and crosstalk in MIMO systems, and simulation results showing the performance of the proposed method were provided.

To prevent crosstalk within the PCB, several design and layout techniques have been proposed, such as maximizing the separation distance between components, bringing the traces closer to a reference plane, minimizing parallel routed trace lengths, reducing trace impedance and signal drive level, locating components away from I/Q interconnects and other areas susceptible to data corruption and coupling, and providing proper terminations on impedance-controlled traces [65]. However, because crosstalk effects cannot be completely eliminated in the PCB design, baseband compensation methods are required to eliminate or mitigate the effects of residual crosstalk.

1.2 Research Objectives

As highlighted in the above, in the case with channel and RF impairments, the benefits of MIMO systems, such as diversity gain and multiplexing gain, become not visible or cannot be achieved anymore. For instance, the orthogonal structure of OSTBC and its decoupling operation at the receiver may be disturbed. In MIMO MRC systems with TB, the beamforming weight vector will not be optimal anymore. Therefore, it is crucial to investigate the impact of channel and RF impairments on MIMO wireless communication systems and then seek efficient compensation methods to eliminate or mitigate these impairments, so as to improve the performance of MIMO wireless communication systems in practical scenarios and environments, thus providing better service to the subscribers of wireless voice and data plans.

Recent research effort has dealt with the issue of channel and RF impairments in MIMO systems. However, most works use simulations to evaluate the effects of channel and RF impairments on the performance of MIMO systems. The research theme of this dissertation aims at investigating channel and RF impairments in MIMO

wireless communication systems. First of all, we will understand the concepts of the above-mentioned channel and RF impairments and evaluate their impacts on the performance of MIMO systems through theoretical analysis and computer-aided simulations. Specifically, the modified MIMO system models taking into account channel and RF impairments will be provided, followed by the corresponding expressions for important performance metrics in closed-form or approximate form. Based on this, we will provide techniques for MIMO system design, such as compensation methods for the impairments and parameter adjusting for transceiver design. The research will make the diversity gain and multiplexing gain easy to be achieved in practical system implementations. Moreover, it will provide a comprehensive method to analyze the impairments in other communication systems such as cognitive radio networks, cooperative communications and “green” networks.

1.3 Contribution of the Dissertation

1.3.1 Accomplishment

The research addressed the issues on the analysis and compensation of channel and RF impairments both separately and together for MIMO wireless communication systems. The contribution of this dissertation can be summarized in several respects as follows:

In Chapter 2, a cross-layer design scheme that combines physical layer adaptive modulation and coding (AMC) with link layer truncated ARQ (T-ARQ) is proposed for MIMO systems employing OSTBC. The performance of the proposed cross-layer design is evaluated in terms of achievable average spectral efficiency (ASE), average packet loss rate (PLR) and outage probability, for which analytical expressions are derived, considering transmission over two types of MIMO fading channels, namely, spatially-correlated Nakagami- m fading channels and keyhole Nakagami- m fading channels. Furthermore, the effects of the maximum number of ARQ retransmissions, numbers of transmit and receive antennas, Nakagami fading parameter and spatial correlation parameters, are studied and discussed based on numerical results

and comparisons. The core of this chapter corresponds to the publications [66–69].

In Chapter 3, we consider M-to-M MIMO MRC system and assess its performance in spatially correlated channels. The analysis assumes double-correlated Rayleigh-and-Lognormal fading channels and is performed in terms of average SEP, outage probability and ergodic capacity. To obtain the receive and transmit spatial correlation functions needed for the performance analysis, a 3D M-to-M MIMO channel model, which takes into account the effects of fast fading and shadowing, is used. The expressions for the considered metrics are derived as a function of the average signal-to-noise ratio (SNR) per receive antenna in closed-form, and further approximated using the recursive adaptive Simpson quadrature method. Numerical results are provided to show the effects of system parameters, such as distance between antenna elements, maximum elevation angle of scatterers, orientation angle of antenna array in the x-y plane, angle between the x-y plane and the antenna array orientation, and degree of scattering in the x-y plane, on the system performance. The core of this chapter corresponds to the publications [70, 71].

In Chapter 4, MIMO OSTBC in the presence of nonlinear HPAs is investigated. Specifically, we propose a constellation-based compensation method for HPA nonlinearity in the case with knowledge of the HPA parameters at the transmitter and receiver, where the constellation and decision regions of the distorted transmitted signal are derived in advance. Furthermore, in the scenario without knowledge of the HPA parameters, a sequential Monte Carlo (SMC)-based compensation method for HPA nonlinearity is proposed, which first estimates the channel gain matrix by means of the SMC method, and then uses the SMC-based algorithm to detect the desired signal. The performance of the MIMO-OSTBC system under study is evaluated in terms of average SEP, total degradation (TD) and system capacity, in uncorrelated Nakagami- m fading channels. Numerical and simulation results are provided, and show the effects of several system parameters, such as the parameters of HPA model, output back-off (OBO) of nonlinear HPA, numbers of transmit and receive antennas, modulation order of QAM, and number of SMC samples, on performance. In particular, it is shown that the constellation-based compensation method can efficiently

mitigate the effect of HPA nonlinearity with low complexity, and that the SMC-based detection scheme is efficient to compensate for HPA nonlinearity in the case without knowledge of the HPA parameters. On the other hand, MIMO TB systems in the presence of HPA nonlinearity are also investigated in Chapter 4. Specifically, due to the suboptimality of the conventional maximal ratio transmission (MRT)/MRC under HPA nonlinearity, we propose an optimal TB scheme with an optimal beamforming weight vector and combining vector, for MIMO systems with nonlinear HPAs. Moreover, an alternative suboptimal but much simpler TB scheme, namely, quantized equal gain transmission (QEGT), is proposed. The latter profits from the property that the elements of the beamforming weight vector have the same constant modulus. The performance of the proposed optimal TB scheme and QEGT/MRC technique in the presence of HPA nonlinearity is evaluated in terms of average SEP and mutual information with Gaussian input, considering transmission over uncorrelated quasi-static frequency-flat Rayleigh fading channels. Numerical results are provided and show the effects on performance of several system parameters, namely, the HPA parameters, numbers of antennas, QAM modulation order, number of pilot symbols, and cardinality of the beamforming weight vector codebook for QEGT. The core of this chapter corresponds to the publications [72–76].

In Chapter 5, we investigate the effect of I/Q imbalance on the performance of MIMO MRC systems that perform the combining at the RF level, thereby requiring only one RF chain. In order to perform the MIMO MRC, we propose a channel estimation algorithm that accounts for the I/Q imbalance. Moreover, a compensation algorithm for the I/Q imbalance in MIMO MRC systems is proposed, which first employs the least-square (LS) rule to estimate the coefficients of the channel gain matrix, beamforming and combining weight vectors, and parameters of I/Q imbalance jointly, and then makes use of the received signal together with its conjugation to detect the transmitted signal. The performance of the MIMO MRC system under study is evaluated in terms of average SEP, outage probability and ergodic capacity, which are derived considering transmission over Rayleigh fading channels. Numerical results are provided and show that the proposed compensation algorithm can effi-

ciently mitigate the effect of I/Q imbalance. The core of this chapter corresponds to the publications [77, 78].

Moreover, the performance of MIMO MRC systems in the presence of crosstalk is evaluated in Chapter 6. The effect of crosstalk on the performance of MIMO MRC is investigated in terms of average SEP and system capacity, considering transmission over uncorrelated Rayleigh fading channels. Numerical results are provided and show the effects of several system parameters, namely, crosstalk, numbers of transmit and receive antennas, and modulation order, on performance. For instance, the crosstalk is shown to yield a constructive effect on the average SEP in the low SNR range, and a destructive effect at high SNRs. The core of this chapter corresponds to the publication [79].

Finally, in Chapter 7, we investigate the joint effects of HPA nonlinearity, I/Q imbalance and crosstalk, on the performance of MIMO TB systems, and propose a compensation method for the three impairments together. The performance of the MIMO TB system equipped with the proposed compensation scheme is evaluated in terms of average SEP and capacity when transmissions are performed over uncorrelated Rayleigh fading channels. Numerical results are provided and show the effects on performance of several system parameters, namely, the HPA parameters, image-leakage ratio, crosstalk, numbers of antennas, length of pilot symbols and PSK modulation order. The core of this chapter corresponds to the publications [80–82].

1.3.2 List of Original Publications

- [1] Jian Qi and Sonia Aïssa, “Analysis and compensation of I/Q imbalance in MIMO transmit-receive diversity systems,” *IEEE Trans. Commun.*, vol. 58, no. 5, pp. 1546–1556, May 2010.
- [2] Jian Qi and Sonia Aïssa, “Analysis and compensation of power amplifier nonlinearity in MIMO transmit diversity systems,” *IEEE Trans. Veh. Technol.*, vol. 59, no. 6, pp. 2921–2931, July 2010.
- [3] Jian Qi, Sonia Aïssa and Amine Maaref, “Cross-layer design for MIMO

systems over spatially correlated and keyhole Nakagami- m fading channels,” *Wiley Journal Wireless Commun. and Mobile Computing*, vol. 10, no. 8, pp. 1055–1067, Aug. 2010; online publication, July 2009.

- [4] Jian Qi and Sonia Aïssa, “Cross-layer design for multiuser MIMO MRC systems with feedback constraints,” *IEEE Trans. Veh. Technol.*, vol. 58, no. 7, pp. 3347–3360, Sept. 2009.
- [5] Jian Qi and Sonia Aïssa, “On the power amplifier nonlinearity in MIMO transmit beamforming systems,” *IEEE Trans. Commun.*, revised.
- [6] Jian Qi and Sonia Aïssa, “Mobile-to-mobile MIMO transmit-receive diversity systems: analysis and performance in 3D double-correlated channels,” *Wiley Journal Wireless Commun. and Mobile Computing*, revised.
- [7] Jian Qi and Sonia Aïssa, “Adaptive switching for spatial transmission modes in MIMO systems with RF impairments,” *IEEE Trans. Wireless Commun.*, to be submitted.
- [8] Jian Qi and Sonia Aïssa, “Joint compensation of multiple RF impairments in MIMO STBC systems,” *IEEE Int. Symp. Personal Indoor and Mobile Radio Commun. (PIMRC’11)*, submitted.
- [9] Jian Qi and Sonia Aïssa, “Analysis and compensation for the joint effects of HPA nonlinearity, I/Q imbalance and crosstalk in MIMO beamforming systems,” in *Proc. IEEE Wireless Commun. and Networking Conf. (WCNC’11)*, Cancun, Quintana-Roo, Mexico, Mar. 2011, pp. 328–333.
- [10] Jian Qi and Sonia Aïssa, “Compensation for HPA nonlinearity and I/Q imbalance in MIMO beamforming system,” in *Proc. IEEE Int. Conf. on Wireless and Mobile Computing, Networking and Commun. (WiMob’10)*, Niagara Falls, Canada, Oct. 2010, pp. 78–82.
- [11] Jian Qi and Sonia Aïssa, “Optimal beamforming in MIMO systems with HPA nonlinearity,” in *Proc. IEEE Int. Symp. Personal Indoor and Mobile*

Radio Commun. (PIMRC'10), Istanbul, Turkey, Sept. 2010, pp. 910–914.

- [12] Jian Qi and Sonia Aïssa, “Beamforming for MIMO transmit-receive diversity systems with crosstalk,” in *Proc. IEEE Int. Conf. Commun. (ICC'10)*, Cape Town, South Africa, May 2010.
- [13] Jian Qi and Sonia Aïssa, “Impact of HPA nonlinearity on MIMO systems with quantized equal gain transmission,” in *Proc. IEEE Int. Symp. Personal Indoor and Mobile Radio Commun. (PIMRC'09)*, Tokyo, Japan, Sept. 2009.
- [14] Jian Qi and Sonia Aïssa, “On the effect of I/Q imbalance on MIMO transmit-receive diversity systems,” in *Proc. IEEE Wireless Commun. and Networking Conf. (WCNC'09)*, Budapest, Hungary, Apr. 2009.
- [15] Jian Qi and Sonia Aïssa, “On the effect of power amplifier nonlinearity on MIMO transmit diversity systems,” in *Proc. IEEE Int. Conf. Commun. (ICC'09)*, Dresden, Germany, June 2009.
- [16] Jian Qi and Sonia Aïssa, “Performance analysis of MIMO MRC systems in 3D mobile-to-mobile double-correlated channel,” in *Proc. IEEE Global Telecommun. Conf. (Globecom'08)*, New Orleans, LA, USA, Nov.–Dec. 2008.
- [17] Jian Qi and Sonia Aïssa, “Cross-layer design of enhanced AMC with truncated ARQ protocols,” in *Proc. IEEE Global Telecommun. Conf. (Globecom'07)*, Washington D.C., USA, Nov. 2007, pp. 3353–3357.
- [18] Jian Qi, Sonia Aïssa, and Xinsheng Zhao, “Optimal frame length for keeping normalized goodput with lowest requirement on BER,” in *Proc. IEEE Int. Conf. Innovations in Inf. Technol. (Innovations'07)*, Dubai, Nov. 2007, pp. 715–719.

1.4 Organization of the Dissertation

The remainder of the dissertation is organized as follows.

Chapter 2 investigates the cross-layer design for wireless MIMO OSTBC systems over spatially correlated and keyhole Nakagami- m fading channels. In Chapter 3, the performance analysis is carried out for M-to-M MIMO MRC systems in 3D double-correlated channels, taking into account the effects of fast fading and shadowing.

In Chapter 4, compensation methods are proposed for HPA nonlinearity in MIMO OSTBC systems considering the scenarios with and without knowledge of the HPA parameters. In addition, we propose the optimal TB scheme and investigate the QEGT mechanism in the presence of HPA nonlinearity. Compensation methods for I/Q imbalance in MIMO MRC systems are proposed in Chapter 5, followed by the corresponding performance analysis. In Chapter 6, we evaluate the effect of crosstalk on the performance of MIMO TB systems. In Chapter 7, comprehensive compensation methods for multiple RF Impairments are proposed for MIMO TB systems.

Finally, the dissertation conclusions and topics for further research are provided in Chapter 8.

Chapter 2

MIMO Communications in Spatially-Correlated and Keyhole Fading Channels

2.1 Introduction

It is well known that the performance of wireless communication systems suffers from severe channel impairments such as small-scale multi-path fading. In order to enhance the throughput and increase the transmission reliability, adaptive techniques were proposed to adjust the system parameters, such as power and rate, according to the CSI. For instance, AMC at the physical layer is used to enhance the spectral efficiency of wireless systems, by selecting the appropriate modulation and coding scheme (MCS) in accordance with the variations of the received SNR while satisfying the system's requirement on PLR [83–85]. Automatic repeat request (ARQ) in the link layer can also be used to increase the transmission reliability by resending a data packet whenever a failure of a previous transmission attempt is detected. Cross-layer design, combining AMC with ARQ for data transmission over fading channels, can improve the throughput performance and ensure the required quality of service is met [86, 87].

The background and current research on the spatially-correlated fading channels and keyhole fading channels have been presented in Section 1.1.2. In this chapter, we propose a cross-layer design combining physical layer AMC and link layer T-ARQ schemes for MIMO systems. MIMO techniques can be categorized into three kinds, namely, spatial diversity, multiplexing and opportunistic beamforming [1]. Herein, we consider one special MIMO technique, known as OSTBC, which achieves full diversity over fading channels and allows simple maximum-likelihood decoding at the receiver [88–90], and present a cross-layer scheme that manages packet-data transmissions in MIMO systems employing OSTBC over Nakagami- m fading channels where the use of AMC is combined with T-ARQ.

Accordingly, the contribution of this chapter can be seen in several respects: i) We propose a cross-layer scheme combining AMC and T-ARQ technologies for OSTBC systems over MIMO Nakagami- m fading channels. Specifically, the MIMO channels are converted into an equivalent signal-input single-output (SISO) scalar one so that the MCSs can be selected according to the effective SNR over the equivalent channel. ii) The effects of channel impairments, namely, spatial fading correlation and keyhole phenomena on the performance of our cross-layer mechanism are assessed. iii) The system performance is investigated in terms of ASE, average PLR and probability of outage, for which analytical expressions are derived. Furthermore, the effects on the system performance of various parameters such as the maximum number of ARQ retransmissions, numbers of transmit and receive antennas, Nakagami fading parameter and spatial correlation parameters, are investigated.

The remainder of this chapter is organized as follows. Section 2.2 presents the system models with spatial correlation and keyhole, respectively. In Section 2.3, a cross-layer design combining AMC and T-ARQ is proposed for MIMO OSTBC systems. The performance of the proposed cross-layer design in terms of ASE, average PLR and outage probability is then analyzed in Section 2.4. Numerical results are presented in Section 2.5, followed by the summary provided in Section 2.6.

2.2 System and Channel Models

Consider a MIMO OSTBC system equipped with n_T transmit and n_R receive antennas, and assume a discrete-time baseband quasi-static frequency-flat fading channel model. The channel characteristics are assumed to remain constant for T symbol durations, where T denotes the time duration of the OSTBC transmission matrix. The corresponding MIMO signal model within one frame is given by

$$\mathbf{Y} = \mathbf{H}\mathbf{X} + \mathbf{N}, \quad (2.1)$$

where \mathbf{Y} denotes the $n_R \times T$ received signal matrix, \mathbf{X} stands for the $n_T \times T$ transmitted symbol matrix, \mathbf{N} refers to the $n_R \times T$ noise matrix with elements belonging to i.i.d. complex Gaussian distribution $\mathcal{CN}(0, N_0)$ uncorrelated with the transmitted symbols, and $\mathbf{H} = [h_{k,l}]_{k,l=1}^{n_R, n_T}$ expresses the $n_R \times n_T$ channel gain matrix with $h_{k,l}$ representing the channel gain coefficient between the l th transmit and k th receive antennas. It is assumed that the knowledge on the channel gain matrix is perfectly known at the receiver.

OSTBC is designed to transmit R complex input symbols in T time slots, thus, the achieved information code rate is given by $R_c \triangleq R/T$. Owing to the decoupling property of the signals transmitted from different antennas, such MIMO channel can be converted into an equivalent SISO scalar one. The effective SNR at the receiver's output can be expressed as [91]

$$\gamma^{\text{OSTBC}} = \frac{\bar{\gamma}}{n_T R_c} \|\mathbf{H}\|_F^2, \quad (2.2)$$

where $\|\cdot\|_F$ refers to the Frobenius norm, and $\bar{\gamma} = P_0/N_0$ denotes the average SNR with P_0 representing the average transmit power per symbol over the n_T transmit antennas.

In the following, the channel models under consideration, namely, spatially-correlated MIMO Nakagami- m fading channel and keyhole MIMO Nakagami- m fading channel, are introduced.

2.2.1 Spatially-Correlated MIMO Nakagami- m Fading Channels

Herein, the random matrix $\mathbf{H}_{\text{SC}} = [h_{k,l}]_{k,l=1}^{n_{\text{R}},n_{\text{T}}}$ is used to denote the $n_{\text{R}} \times n_{\text{T}}$ channel gain matrix of spatially-correlated MIMO Nakagami- m fading channels, with $h_{k,l}$ representing the channel gain coefficient between the l th transmit and k th receive antennas. The channel gain coefficient $h_{k,l}$ is further defined as $h_{k,l} \triangleq \alpha_{k,l} e^{j\phi_{k,l}}$, where $j^2 = -1$ and $\alpha_{k,l}$ denotes the path gain. The probability density function (PDF) of the $\mathcal{K} = n_{\text{T}}n_{\text{R}}$ path gains $\alpha_{k,l}$ is given by

$$p_{\alpha_{k,l}}(\alpha) = 2 \left(\frac{m}{\Omega_{k,l}} \right)^m \frac{\alpha^{2m-1}}{\Gamma(m)} \exp\left(-m \frac{\alpha^2}{\Omega_{k,l}}\right), \quad \alpha \geq 0, \quad (2.3)$$

where $\Gamma(\cdot)$ denotes the Gamma function, m is the Nakagami fading parameter satisfying $m \geq 1/2$, and $\Omega_{k,l} = E[\alpha_{k,l}^2]$ refers to the average fading power with $E[\cdot]$ representing the expectation operator. The phase $\phi_{k,l}$, pertaining to $h_{k,l}$, is uniformly distributed over $[0, 2\pi)$.

Using the definition of the Frobenius norm, the effective output SNR of MIMO OSTBC systems can be rewritten as

$$\gamma^{\text{OSTBC}} = \frac{\bar{\gamma}}{n_{\text{T}}R_c} \sum_{k=1}^{n_{\text{R}}} \sum_{l=1}^{n_{\text{T}}} \gamma_{k,l}, \quad (2.4)$$

where $\gamma_{k,l} \triangleq \alpha_{k,l}^2$ denotes the elementary fading power corresponding to the path between the l th transmit and k th receive antennas. Then, the effective output SNR is the sum of \mathcal{K} correlated Gamma random variables. The spatial correlation in the case of OSTBC can be expressed as the following $\mathcal{K} \times \mathcal{K}$ covariance matrix [91]

$$\Phi_{\text{cc}} = E \left[(\text{vec}(\Gamma) - E[\text{vec}(\Gamma)]) (\text{vec}(\Gamma) - E[\text{vec}(\Gamma)])^T \right], \quad (2.5)$$

where $\text{vec}(\cdot)$ denotes the vectorizing operator, which maps the elements of the $n_{\text{R}} \times n_{\text{T}}$ matrix Γ into the $\mathcal{K} \times 1$ vector $\text{vec}(\Gamma) \triangleq [\gamma_{1,1}, \gamma_{2,1}, \dots, \gamma_{n_{\text{R}},1}, \gamma_{1,2}, \gamma_{2,2}, \dots, \gamma_{n_{\text{R}},n_{\text{T}}}]^T$, formed by stacking the columns of Γ , and where $\Gamma = [\gamma_{k,l}]_{k,l=1}^{n_{\text{R}},n_{\text{T}}}$. Furthermore, it is

assumed that the fading is induced by separate physical processes at the transmitter and receiver, in which case the covariance matrix is of the form $\Phi_{cc} = \Phi_T \otimes \Phi_R$, where \otimes denotes the matrix Kronecker product, Φ_R and Φ_T represent the receive and transmit correlation matrices, i.e., the covariance matrices of the rows and columns of \mathbf{H}_{SC} [27]. Moreover, it is assumed that the covariance matrix Φ_{cc} is positive-definite; hence, its eigenvalues are real and positive. Let $\lambda_1, \lambda_2, \dots, \lambda_K$ denote K ($K \leq \mathcal{K}$) distinct eigenvalues of Φ_{cc} and μ_k represent the multiplicity of the eigenvalue λ_k . Then, we have the identity $\sum_{k=1}^K \mu_k = \mathcal{K}$. When the Nakagami parameter m is integer, the PDF of the output SNR of MIMO OSTBC systems over spatially-correlated Nakagami- m fading channels can be expressed as [91, eq. (59)]

$$p_{\gamma_{SC}^{OSTBC}}(\gamma) = \sum_{k=1}^K \sum_{j_k=1}^{m\mu_k} \beta_{k,j_k} \frac{\gamma^{j_k-1}}{\Gamma(j_k)} \left(\frac{n_T R_c}{\lambda_k \bar{\gamma}} \right)^{j_k} \exp\left(-\frac{n_T R_c}{\lambda_k \bar{\gamma}} \gamma\right), \quad \gamma \geq 0, \quad (2.6)$$

where the coefficient β_{k,j_k} is given by

$$\beta_{k,j_k} = \frac{1}{(m\mu_k - j_k)! \left(-\frac{\bar{\gamma}}{n_T R_c} \lambda_k\right)^{m\mu_k - j_k}} \times \frac{d^{m\mu_k - j_k}}{ds^{m\mu_k - j_k}} \left[\prod_{n=1, n \neq k}^K \left(1 - s \frac{\bar{\gamma}}{n_T R_c} \lambda_n\right)^{-m\mu_k} \right] \Bigg|_{s = \frac{n_T R_c}{\lambda_k \bar{\gamma}}}, \quad (2.7)$$

with $\frac{d^{m\mu_k - j_k}}{ds^{m\mu_k - j_k}}$ referring to the derivative of order $m\mu_k - j_k$, with respect to s , for $j_k = 1, \dots, \mu_k$.

2.2.2 Keyhole MIMO Nakagami- m Fading Channels

In certain MIMO propagation environments, the radio wave sent from the transmitter to the receiver must propagate through the keyhole in space. The channel gain matrix of a keyhole MIMO Nakagami- m fading channel can be expressed as [92]

$$\mathbf{H}_{Kh} = \mathbf{h}_R \mathbf{h}_T^H, \quad (2.8)$$

where \mathbf{h}_T and \mathbf{h}_R denote the $n_T \times 1$ and $n_R \times 1$ random vectors modeling the fading coefficients for the transmitter and receiver sides, respectively. The elements of \mathbf{h}_T and \mathbf{h}_R are given by $\left\{ \alpha_l^T e^{j\phi_l^T} \right\}_{l=1}^{n_T}$ and $\left\{ \alpha_k^R e^{j\phi_k^R} \right\}_{k=1}^{n_R}$, respectively, with the PDF of α_l^T and α_k^R expressed as

$$p_{\alpha_l^T}(\alpha) = 2 \left(\frac{m_T}{\Omega_l^T} \right)^{m_T} \frac{\alpha^{2m_T-1}}{\Gamma(m_T)} \exp\left(-\frac{m_T \alpha^2}{\Omega_l^T}\right), \quad \alpha \geq 0, \quad (2.9)$$

$$p_{\alpha_k^R}(\alpha) = 2 \left(\frac{m_R}{\Omega_k^R} \right)^{m_R} \frac{\alpha^{2m_R-1}}{\Gamma(m_R)} \exp\left(-\frac{m_R \alpha^2}{\Omega_k^R}\right), \quad \alpha \geq 0, \quad (2.10)$$

where m_T and m_R are the Nakagami fading parameters satisfying $m_T, m_R \geq 1/2$, $\Omega_l^T = E\left[(\alpha_l^T)^2\right]$, and $\Omega_k^R = E\left[(\alpha_k^R)^2\right]$. The phases ϕ_l^T and ϕ_k^R are uniformly distributed over $[0, 2\pi)$. Note that all entries of the channel gain matrix \mathbf{H}_{Kh} are uncorrelated, but $\text{rank}(\mathbf{H}_{\text{Kh}}) = 1$. Then, making use of (2.2) and [92, eq. (31)], the PDF of the output SNR of MIMO OSTBC systems over keyhole Nakagami- m fading channels can be expressed as

$$p_{\gamma_{\text{Kh}}^{\text{OSTBC}}}(\gamma) = \frac{2\gamma^{\frac{m_T n_T + m_R n_R}{2} - 1}}{\Gamma(m_T n_T) \Gamma(m_R n_R)} \left(\frac{m_T m_R n_T R_c}{\bar{\gamma}} \right)^{\frac{m_T n_T + m_R n_R}{2}} \times K_{m_T n_T - m_R n_R} \left(2\sqrt{\frac{m_T m_R n_T R_c}{\bar{\gamma}}} \gamma \right), \quad \gamma \geq 0, \quad (2.11)$$

where $K_v(\cdot)$ denotes the v th-order modified Bessel function of the second kind [93, eq. (8.432.6)], given by

$$K_v(u) = \frac{1}{2} \left(\frac{u}{2} \right)^v \int_0^\infty \frac{1}{t^{v+1}} \exp\left(-t - \frac{u^2}{4t}\right) dt, \quad |\arg u| < \frac{\pi}{2}, \quad \text{Re}\{u^2\} > 0. \quad (2.12)$$

2.3 Cross-layer Design

In this section, we investigate the cross-layer framework combining AMC with T-ARQ for MIMO OSTBC systems over spatially-correlated and keyhole Nakagami- m fading channels. The corresponding block diagram is shown in Fig. 2.1.

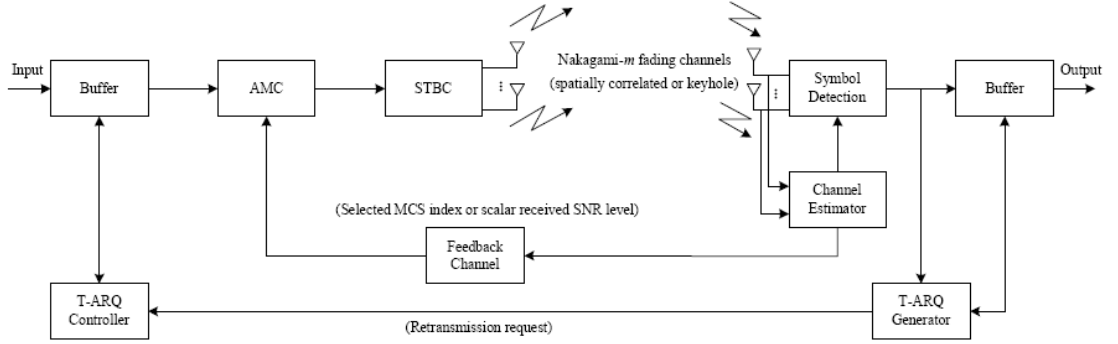


Figure 2.1: Block diagram for the cross layer design based MIMO-OSTBC systems.

2.3.1 Physical and Link layer Parameters

We adopt the packet and frame structure illustrated in [86, Fig. 3]. Frame transmission is considered at the physical layer. A frame contains a fixed number of symbols, N_f , and a variable number of packets N_b originating from the data link layer. N_b is modulation-dependent, as packets are mapped into a set of symbols belonging to a family of M-quadrature QAM signal constellations of size $M_n = 2^n$, $n = 1, 2, \dots, N$, where N is the total number of M-QAM constellations. This yields a finite set of available discrete data rates $\{n = \log_2(M_n) : n = 1, \dots, N\}$. Each N_p -bit packet, at the data link layer, comprises its own cyclic redundancy check (CRC) for ARQ error detection purposes as well as a payload content. After modulation at a given rate n , the N_p bits of each packet are mapped into N_p/n symbols to which N_c control symbols are added to form a frame at the physical layer. Accordingly, the frame length satisfies the relationship $N_f = N_c + N_b N_p/n$.

A link layer T-ARQ protocol controls packet retransmissions, initiating a retransmission request and sending it back to the transmitter whenever a packet is detected in error at the receiver. Due to limits on the service delay requirements and buffer sizes, in practice, the maximum number of ARQ retransmissions has to be bounded [94]. Denote this maximum number by N_r^{\max} . On the other hand, the service is considered to be characterized by a packet loss requirement, P_{loss} , which has to be satisfied for each data packet before it is delivered to the user. This can be translated into a physical layer target packet error rate (PER), $P_p = P_{\text{loss}}^{1/(N_r^{\max}+1)}$. Note that a packet

Table 2.1: Fitting parameters of MCS transmission modes for packet length $N_p = 1080$ bits.

	Mode 1	Mode 2	Mode 3	Mode 4	Mode 5	Mode 6	Mode 7
Modulation	BPSK	QPSK	8-QAM	16-QAM	32-QAM	64-QAM	128-QAM
Rate (bits/sym.)	1	2	3	4	5	6	7
a_n	107.95	109.06	93.44	85.01	74.41	67.46	61.07
g_n	1.0224	0.5117	0.1706	0.1025	0.0394	0.0244	0.0097
γ_{pn} (dB)	6.7	9.7	14.7	16.7	20.6	22.7	26.6

is declared to be lost whenever the maximum number of retransmissions is reached while the former has not been correctly decoded.

To proceed, the following adopted assumptions are listed: 1) the wireless channel is assumed to remain invariant during transmission of a frame and may vary from frame to frame. 2) The channel estimation at the receiver is error-free. The estimated scalar SNR level of OSTBC systems (in the case that the MCS is determined at the transmitter) or the discrete MCS index (in the case that the MCS is determined at the receiver) can be conveyed to the transmitter via an error-free and zero-delay feedback link. 3) The transmission errors can be perfectly detected through CRC, and that negative acknowledgments (NACK), sent from the receiver to the transmitter as retransmission requests, are error-free.

In the following, we seek to achieve the target PER, P_p , through constant-power discrete-rate adaptive M-QAM and OSTBC at the physical layer, subject to truncated ARQ retransmissions at the data link layer.

2.3.2 PER Approximation for AWGN channels

The aim of this section is to present a useful approximation for the instantaneous PER experienced by a set of M-QAM signal constellations for additive white Gaussian noise (AWGN) channels. Invoking the OSTBC SISO equivalency, the effective output SNR for each symbol to be transmitted is given by γ^{OSTBC} , which is previously defined in (2.2). For packets containing N_p bits, partitioned into N_p/n equally-likely symbols using coherent M_n -QAM ($M_n = 2^n$) with two-dimensional Gray coding, we use the

widely accepted approximate expression for the PER [86]:

$$P_n(\gamma) \approx \begin{cases} 1, & \text{if } 0 < \gamma < \gamma_{pn}, \\ a_n \exp(-g_n \gamma), & \text{if } \gamma \geq \gamma_{pn}, \end{cases} \quad (2.13)$$

where n denotes the MCS index, γ is the output SNR of MIMO OSTBC systems ¹, and $\{a_n, g_n, \gamma_{pn}\}$ are MCS and packet-size dependent constants which are evaluated by least-square fitting the PER expression in (2.13) to the exact PER given by [86, eq. (23)]

$$P_n(\gamma) = 1 - \prod_{i=1}^{\log_2 I} (1 - P_I^i(\gamma))^{\frac{N_p}{n}} \prod_{j=1}^{\log_2 J} (1 - P_J^j(\gamma))^{\frac{N_p}{n}}. \quad (2.14)$$

In (2.14), $I = \lfloor n/2 \rfloor$ and $J = \lceil n/2 \rceil$ with $\lfloor \cdot \rfloor$ and $\lceil \cdot \rceil$ respectively denoting floor function and ceiling function, while $P_I^i, i \in \{1, \dots, \log_2 I\}$, and $P_J^j, j \in \{1, \dots, \log_2 J\}$, are, respectively, the exact BER expressions corresponding to the i th and j th bits of two independent I -ary and J -ary one-dimensional amplitude modulations, whose expressions are provided by [95, eq. (9)]. Note that (2.14) rigorously captures the MIMO OSTBC performance under the ideal maximum likelihood detection since the transmitted symbols from different antennas can be decoupled and detected separately at the receiver. Since the expressions for exact PER varies for different modulation scheme and packet size, the fitting parameters $\{a_n, g_n, \gamma_{pn}\}$ depend on the packet size, N_p , and modulation order of QAM, n . An example of fitting parameters with $N_p = 1080$ bits is shown in Table 2.1.

2.3.3 SNR Thresholds for MCS

We partition the range of the output SNR, γ , into $N + 1$ non-overlapping consecutive intervals, with boundary points denoted as $\{\gamma_n\}_{n=0}^{N+1}$, and apply constant-power discrete-rate adaptive M-QAM on a frame-by-frame basis. Whenever the SNR sent back to the transmitter falls within the interval $[\gamma_n, \gamma_{n+1})$, the constellation size M_n is selected for all symbols sent from n_T transmit antennas, with $M_0 = 0$ referring to the

¹For notational brevity, we denote the output SNR by γ instead of γ^{OSTBC} .

case where no data are transmitted. Having set the target PER for the physical layer to P_p , the threshold levels $\{\gamma_n\}$ are set to the required SNR to achieve this target PER. Generally we have $P_p < 1$. Hence, using (2.13) leads to the following switching threshold values:

$$\gamma_n = \begin{cases} 0, & n = 0, \\ K_n/g_n, & n = 1, \dots, N, \\ +\infty, & n = N + 1, \end{cases} \quad (2.15)$$

where $K_n = -\ln(P_p/a_n)$ is a power penalty factor incurred by choosing modulation level n .

2.4 Performance Analysis

In this section, the performance of the proposed MIMO cross-layer design in spatially-correlated Nakagami- m fading channels and keyhole Nakagami- m fading channels is assessed in terms of three metrics: average PLR, ASE and probability of outage. Next, we derive analytical expressions for these metrics using the PDFs of the output SNR as provided in (2.6) and (2.11). It is assumed that received SNRs pertaining to several transmission attempts of a packet, constituting the CSI used by the transmitter, are i.i.d. random variables.

2.4.1 Average Packet Loss Rate

Adaptive modulation operates at an average PER smaller than the target PER to be achieved at the physical layer, i.e., P_p . This is due to the fact that our rate adaptive policy is conservative in the sense that we choose the constellation that guarantees an instantaneous PER no larger than P_p . In order to evaluate the average PER, we first calculate the probability that the constellation of size $M_n = 2^n$ is selected. For the spatially-correlated MIMO Nakagami- m fading channel case, this probability is

given by

$$\begin{aligned}
 Pr_n^{\text{SC}} &= \int_{\gamma_n}^{\gamma_{n+1}} p_{\gamma_{\text{SC}}^{\text{OSTBC}}}(\gamma) d\gamma \\
 &= \int_{\gamma_n}^{\gamma_{n+1}} \sum_{k=1}^K \sum_{j_k}^{m\mu_k} \beta_{k,j_k} \frac{\gamma^{j_k-1}}{\Gamma(j_k)} \left(\frac{n_{\text{T}} R_c}{\lambda_k \bar{\gamma}} \right)^{j_k} \exp\left(-\frac{n_{\text{T}} R_c}{\lambda_k \bar{\gamma}} \gamma\right) d\gamma \\
 &= \sum_{k=1}^K \sum_{j_k}^{m\mu_k} \frac{\beta_{k,j_k}}{\Gamma(j_k)} \left[\Gamma\left(j_k, \frac{n_{\text{T}} R_c \gamma_n}{\lambda_k \bar{\gamma}}\right) - \Gamma\left(j_k, \frac{n_{\text{T}} R_c \gamma_{n+1}}{\lambda_k \bar{\gamma}}\right) \right], \tag{2.16}
 \end{aligned}$$

where $\Gamma(m, x) := \int_x^\infty t^{m-1} e^{-t} dt$ denotes the upper incomplete Gamma function. As for the keyhole MIMO Nakagami- m fading case, the probability that the constellation of size $M_n = 2^n$ is chosen can be expressed as

$$\begin{aligned}
 Pr_n^{\text{Kh}} &= \int_{\gamma_n}^{\gamma_{n+1}} p_{\gamma_{\text{Kh}}^{\text{OSTBC}}}(\gamma) d\gamma \\
 &= \int_{\gamma_n}^{\gamma_{n+1}} \frac{2\gamma^{\frac{m_{\text{T}}n_{\text{T}}+m_{\text{R}}n_{\text{R}}}{2}-1}}{\Gamma(m_{\text{T}}n_{\text{T}})\Gamma(m_{\text{R}}n_{\text{R}})} \left(\frac{m_{\text{T}}m_{\text{R}}n_{\text{T}}R_c}{\bar{\gamma}} \right)^{\frac{m_{\text{T}}n_{\text{T}}+m_{\text{R}}n_{\text{R}}}{2}} \\
 &\quad \times K_{m_{\text{T}}n_{\text{T}}-m_{\text{R}}n_{\text{R}}} \left(2\sqrt{\frac{m_{\text{T}}m_{\text{R}}n_{\text{T}}R_c}{\bar{\gamma}}} \gamma \right) d\gamma. \tag{2.17}
 \end{aligned}$$

By changing the integral order of γ and t in the definition of $K_\nu(\cdot)$ specified in (2.12), (2.17) can be rewritten as

$$\begin{aligned}
 Pr_n^{\text{Kh}} &= \int_{\gamma_n}^{\gamma_{n+1}} \left(\frac{m_{\text{T}}m_{\text{R}}n_{\text{T}}R_c}{\bar{\gamma}} \right)^{\frac{m_{\text{T}}n_{\text{T}}+m_{\text{R}}n_{\text{R}}}{2}} \left(\sqrt{\frac{m_{\text{T}}m_{\text{R}}n_{\text{T}}R_c}{\bar{\gamma}}} \gamma \right)^{m_{\text{T}}n_{\text{T}}-m_{\text{R}}n_{\text{R}}} \\
 &\quad \times \frac{\gamma^{\frac{m_{\text{T}}n_{\text{T}}+m_{\text{R}}n_{\text{R}}}{2}-1}}{\Gamma(m_{\text{T}}n_{\text{T}})\Gamma(m_{\text{R}}n_{\text{R}})} \left[\int_0^\infty \frac{1}{t^{m_{\text{T}}n_{\text{T}}-m_{\text{R}}n_{\text{R}}+1}} \exp\left(-t - \frac{m_{\text{T}}m_{\text{R}}n_{\text{T}}R_c\gamma}{\bar{\gamma}t}\right) dt \right] d\gamma \\
 &= \int_0^\infty t^{m_{\text{R}}n_{\text{R}}-1} e^{-t} \left[\int_{\gamma_n}^{\gamma_{n+1}} \exp\left(-\frac{m_{\text{T}}m_{\text{R}}n_{\text{T}}R_c\gamma}{\bar{\gamma}t}\right) \right. \\
 &\quad \times \left. \frac{\gamma^{m_{\text{T}}n_{\text{T}}-1}}{\Gamma(m_{\text{T}}n_{\text{T}})\Gamma(m_{\text{R}}n_{\text{R}})} \left(\frac{m_{\text{T}}m_{\text{R}}n_{\text{T}}R_c}{\bar{\gamma}t} \right)^{m_{\text{T}}n_{\text{T}}} d\gamma \right] dt \\
 &= \int_0^\infty \frac{t^{m_{\text{R}}n_{\text{R}}-1} e^{-t}}{\Gamma(m_{\text{T}}n_{\text{T}})\Gamma(m_{\text{R}}n_{\text{R}})}
 \end{aligned}$$

$$\times \left[\Gamma \left(m_{\text{T}} n_{\text{T}}, \frac{m_{\text{T}} m_{\text{R}} n_{\text{T}} R_{\text{c}} \gamma_n}{\bar{\gamma} t} \right) - \Gamma \left(m_{\text{T}} n_{\text{T}}, \frac{m_{\text{T}} m_{\text{R}} n_{\text{T}} R_{\text{c}} \gamma_{n+1}}{\bar{\gamma} t} \right) \right] dt. \quad (2.18)$$

Now, let constellation size $M_n = 2^n$ be selected, then the average PER when transmitting with the corresponding QAM constellation, denoted by \bar{P}_n , is obtained by averaging the expression of $P_n(\gamma)$ (2.13), over the distribution of the Nakagami fading channel when the received SNR falls within the interval $[\gamma_n, \gamma_{n+1})$. Then, the average PER for mode n over spatially-correlated Nakagami- m fading channel can be expressed as

$$\begin{aligned} \bar{P}_n^{\text{SC}} &= \frac{1}{P r_n^{\text{SC}}} \int_{\gamma_n}^{\gamma_{n+1}} P_n(\gamma) p_{\gamma_{\text{SC}}^{\text{OSTBC}}}(\gamma) d\gamma \\ &= \frac{1}{P r_n^{\text{SC}}} \int_{\gamma_n}^{\gamma_{n+1}} a_n e^{-g_n \gamma} \sum_{k=1}^K \sum_{j_k}^{m \mu_k} \beta_{k,j_k} \frac{\gamma^{j_k-1}}{\Gamma(j_k)} \left(\frac{n_{\text{T}} R_{\text{c}}}{\lambda_k \bar{\gamma}} \right)^{j_k} \exp \left(-\frac{n_{\text{T}} R_{\text{c}}}{\lambda_k \bar{\gamma}} \gamma \right) d\gamma \\ &= \frac{a_n}{P r_n^{\text{SC}}} \sum_{k=1}^K \sum_{j_k}^{m \mu_k} \frac{\beta_{k,j_k}}{\Gamma(j_k)} \left(\frac{n_{\text{T}} R_{\text{c}}}{\lambda_k \bar{\gamma} b_{n,k}} \right)^{j_k} [\Gamma(j_k, b_{n,k} \gamma_n) - \Gamma(j_k, b_{n,k} \gamma_{n+1})], \end{aligned} \quad (2.19)$$

where $b_{n,k} \triangleq g_n + \frac{n_{\text{T}} R_{\text{c}}}{\lambda_k \bar{\gamma}}$. For transmission over keyhole MIMO Nakagami- m fading channel, it becomes

$$\begin{aligned} \bar{P}_n^{\text{Kh}} &= \frac{1}{P r_n^{\text{Kh}}} \int_{\gamma_n}^{\gamma_{n+1}} P_n(\gamma) p_{\gamma_{\text{Kh}}^{\text{OSTBC}}}(\gamma) d\gamma \\ &= \frac{1}{P r_n^{\text{SC}}} \int_{\gamma_n}^{\gamma_{n+1}} a_n e^{-g_n \gamma} \frac{2\gamma^{\frac{m_{\text{T}} n_{\text{T}} + m_{\text{R}} n_{\text{R}}}{2} - 1}}{\Gamma(m_{\text{T}} n_{\text{T}}) \Gamma(m_{\text{R}} n_{\text{R}})} \left(\frac{m_{\text{T}} m_{\text{R}} n_{\text{T}} R_{\text{c}}}{\bar{\gamma}} \right)^{\frac{m_{\text{T}} n_{\text{T}} + m_{\text{R}} n_{\text{R}}}{2}} \\ &\quad \times K_{m_{\text{T}} n_{\text{T}} - m_{\text{R}} n_{\text{R}}} \left(2 \sqrt{\frac{m_{\text{T}} m_{\text{R}} n_{\text{T}} R_{\text{c}}}{\bar{\gamma}}} \gamma \right) d\gamma. \end{aligned} \quad (2.20)$$

Similar to (2.17), (2.20) can be re-expressed as

$$\begin{aligned} \bar{P}_n^{\text{Kh}} &= \frac{1}{P r_n^{\text{Kh}}} \int_{\gamma_n}^{\gamma_{n+1}} a_n e^{-g_n \gamma} \frac{2\gamma^{\frac{m_{\text{T}} n_{\text{T}} + m_{\text{R}} n_{\text{R}}}{2} - 1}}{\Gamma(m_{\text{T}} n_{\text{T}}) \Gamma(m_{\text{R}} n_{\text{R}})} \left(\sqrt{\frac{m_{\text{T}} m_{\text{R}} n_{\text{T}} R_{\text{c}}}{\bar{\gamma}}} \gamma \right)^{m_{\text{T}} n_{\text{T}} - m_{\text{R}} n_{\text{R}}} \\ &\quad \times \left(\frac{m_{\text{T}} m_{\text{R}} n_{\text{T}} R_{\text{c}}}{\bar{\gamma}} \right)^{\frac{m_{\text{T}} n_{\text{T}} + m_{\text{R}} n_{\text{R}}}{2}} \left[\int_0^{\infty} \frac{1}{t^{m_{\text{T}} n_{\text{T}} - m_{\text{R}} n_{\text{R}} + 1}} \exp \left(-t - \frac{m_{\text{T}} m_{\text{R}} n_{\text{T}} R_{\text{c}} \gamma}{\bar{\gamma} t} \right) dt \right] d\gamma \end{aligned}$$

$$\begin{aligned}
 &= \frac{1}{Pr_n^{\text{Kh}}} \int_0^\infty t^{m_R n_R - 1} e^{-t} \left[\int_{\gamma_n}^{\gamma_{n+1}} \exp\left(-\frac{m_T m_R n_T R_c \gamma}{\bar{\gamma} t}\right) \right. \\
 &\quad \times \left. \frac{a_n e^{-g_n \gamma} \gamma^{m_T n_T - 1}}{\Gamma(m_T n_T) \Gamma(m_R n_R)} \left(\frac{m_T m_R n_T R_c}{\bar{\gamma} t}\right)^{m_T n_T} d\gamma \right] dt \\
 &= \frac{a_n}{Pr_n^{\text{Kh}}} \int_0^\infty \frac{t^{m_R n_R - 1} e^{-t}}{\Gamma(m_T n_T) \Gamma(m_R n_R)} \left(\frac{m_T m_R n_T R_c}{\bar{\gamma} t b_n}\right)^{m_T n_T} \\
 &\quad \times [\Gamma(m_T n_T, b_n \gamma_n) - \Gamma(m_T n_T, b_n \gamma_{n+1})] dt, \tag{2.21}
 \end{aligned}$$

where $b_n \triangleq g_n + \frac{m_T m_R n_T R_c}{\bar{\gamma} t}$.

The overall average PER at the physical layer corresponds to the ratio of the average number of erroneously received packets over the total average number of transmitted packets, and can be expressed as (cf. [96, eq. 35])

$$\bar{P} = \frac{\sum_{n=1}^N R_n Pr_n \bar{P}_n}{\sum_{n=1}^N R_n Pr_n}, \tag{2.22}$$

where R_n , in bits per channel use, is the information rate of the combined AMC and OSTBC diversity scheme. Hence, $R_n = R_c \frac{\log_2(M_n)}{W T_s}$, T_s representing the fixed symbol duration and W denoting the signalling bandwidth. Assuming ideal Nyquist data pulses for each constellation yields $W = 1/T_s$, which in turn implies that $R_n = n R_c$ for the set of uncoded M-QAM constellations. Then, accounting for the N_r^{max} -truncated ARQ, the corresponding average PLR at the data link layer can be expressed in terms of \bar{P} as follows:

$$\bar{P}_{\text{loss}} = \bar{P}^{N_r^{\text{max}} + 1}. \tag{2.23}$$

2.4.2 Average Spectral Efficiency

To evaluate the average spectral efficiency, $\overline{\text{SE}}$, we should account for the packet retransmissions at the data link layer induced by the ARQ protocol. Since a packet can be transmitted up to $N_r^{\text{max}} + 1$ times, we can compute the average number of transmissions, \bar{N} , needed for a packet to be either correctly received or discarded due to the ARQ truncation, as a function of the maximum number of retransmissions,

N_r^{\max} , and the average PER, \bar{P} . In a similar way to [86, eq. (10)] (SISO channel), the average number of packet transmissions for the OSTBC diversity scheme over both types of Nakagami- m fading channels considered in this work, is given by

$$\begin{aligned}\bar{N}(N_r^{\max}, \bar{P}) &= \sum_{i=1}^{N_r^{\max}+1} \bar{P}^{i-1} \\ &= \frac{1 - \bar{P}^{N_r^{\max}+1}}{1 - \bar{P}}.\end{aligned}\quad (2.24)$$

As can be seen, when $N_r^{\max} = 0$ (no retransmission), $\bar{N}(0, \bar{P}) = 1$, which corresponds to the case of AMC only with no ARQ implemented at the packet level.

The overall ASE is the sum of the information rates of each modulation level weighted by the probability Pr_n that the output SNR falls within the corresponding SNR threshold interval, divided by the average number of transmissions per packet $\bar{N}(N_r^{\max}, \bar{P})$. It is then given by (cf. [86, eq. 13])

$$\overline{\text{SE}} = \frac{\sum_{n=1}^N R_n Pr_n}{\bar{N}(N_r^{\max}, \bar{P})}.\quad (2.25)$$

2.4.3 Probability of Outage

Since no packets are transmitted successfully when the output SNR falls below the threshold γ_1 , the probability of outage, $P_{\text{out}}^{\text{SC}}$, induced by the adaptive M-QAM for the first packet transmission over the spatially-correlated Nakagami- m fading is given by

$$\begin{aligned}P_{\text{out}}^{\text{SC}}(\gamma_1) &= \int_0^{\gamma_1} p_{\gamma_{\text{SC}}^{\text{OSTBC}}}(\gamma) d\gamma \\ &= 1 - \sum_{k=1}^K \sum_{j_k}^{m\mu_k} \frac{\beta_{k,j_k}}{\Gamma(j_k)} \Gamma\left(j_k, \frac{n_{\text{T}} R_c \gamma_1}{\lambda_k \bar{\gamma}}\right).\end{aligned}\quad (2.26)$$

On the other hand, for the OSTBC scheme over keyhole MIMO Nakagami- m fading channels, it can be expressed as

$$\begin{aligned}
 P_{\text{out}}^{\text{Kh}}(\gamma_1) &= \int_0^{\gamma_1} p_{\gamma_{\text{Kh}}}^{\text{OSTBC}}(\gamma) d\gamma \\
 &= 1 - \int_0^{\infty} \frac{t^{m_{\text{R}}n_{\text{R}}-1} e^{-t}}{\Gamma(m_{\text{T}}n_{\text{T}})\Gamma(m_{\text{R}}n_{\text{R}})} \Gamma\left(m_{\text{T}}n_{\text{T}}, \frac{m_{\text{T}}m_{\text{R}}n_{\text{T}}R_c\gamma_1}{\bar{\gamma}t}\right) dt. \quad (2.27)
 \end{aligned}$$

The probability of outage, $P_{\text{out},N_r^{\text{max}}}$, given up to N_r^{max} allowable retransmissions, can then be expressed as

$$\begin{aligned}
 P_{\text{out},N_r^{\text{max}}}(\gamma_1) &= P_{\text{out}}(\gamma_1) \sum_{i=1}^{N_r^{\text{max}}+1} \bar{P}^{i-1} \\
 &= P_{\text{out}}(\gamma_1) \bar{N}(N_r^{\text{max}}, \bar{P}). \quad (2.28)
 \end{aligned}$$

Note that for the no-retransmission case, i.e., when $N_r^{\text{max}} = 0$, we have $\bar{N}(0, \bar{P}) = 1$, which implies that the probability of outage $P_{\text{out},N_r^{\text{max}}}(\gamma_1)$, given by (2.28), reduces to (2.26) and (2.27) for MIMO OSTBC over spatially-correlated and keyhole Nakagami- m fading channels, respectively.

2.5 Numerical Results and Discussions

In this section, we present numerical results illustrating the ASE, average PLR and outage probability for the cross-layer scheme combining AMC and T-ARQ in MIMO OSTBC systems over spatially-correlated and keyhole Nakagami- m fading channels, respectively. All the curves shown in the figures are obtained on the basis of the analytical results, i.e., (2.23), (2.25) and (2.28). Herein, we consider the full-rate Alamouti OSTBC ($R_c = 1$, $n_{\text{T}} = 2$). We set the packet length to $N_p = 1080$ bits and the number of M-QAM constellations to $N = 7$. With these parameters, least-square fitting the approximate PER expression (2.13) to the exact expression (2.14), yields the set of modulation-level and packet-size dependent constants $\{a_n, g_n, \gamma_{pn}\}$ that are listed in Table 2.1. In addition, the system PLR requirement is set to $P_{\text{loss}} = 10^{-4}$.

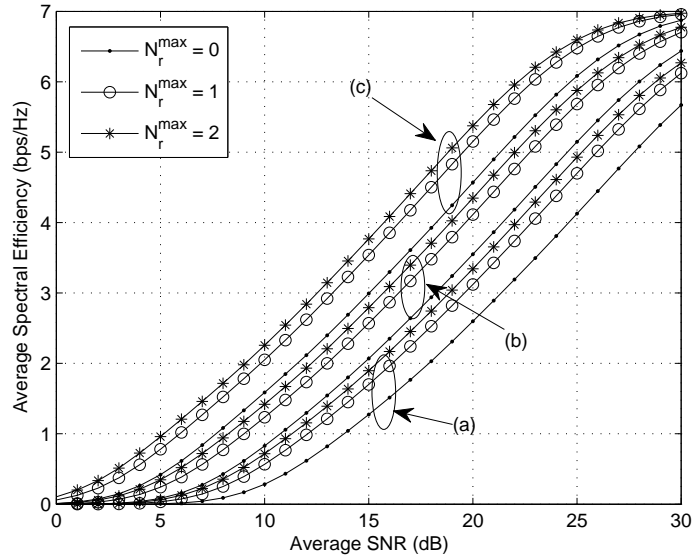


Figure 2.2: Average spectral efficiency of cross layer design based MIMO-OSTBC in the spatially-correlated Nakagami- m fading channel case for different antenna configurations: $n_T = 2$ and (a) $n_R = 1$, (b) $n_R = 2$, and (c) $n_R = 4$.

First, we consider transmission over spatially-correlated Nakagami- m fading channels. The exponential correlation model [97] is used to model the elements of the receive and transmit correlation matrices, Φ_R and Φ_T , according to [97, equation (13)]

$$\begin{aligned}\Phi_R(i, j) &= \rho_R^{|i-j|}, 0 < |\rho_R| < 1, \\ \Phi_T(i, j) &= \rho_T^{|i-j|}, 0 < |\rho_T| < 1.\end{aligned}\quad (2.29)$$

Fig. 2.2 shows the variation of the ASE as a function of the average SNR for various values of N_r^{\max} , n_T and n_R , in the scenario with $m = 1$, $\rho_T = 0.5$, and $\rho_R = 0.9$. It is observed that using the T-ARQ protocol helps increasing the ASE as compared to the achievable spectral efficiency when ARQ is not used ($N_r^{\max} = 0$). The ASE increases as N_r^{\max} becomes larger. However, the increment of spectral efficiency degrades as N_r^{\max} increases, which implies that there is no benefit from employing large N_r^{\max} . In addition, increasing the number of receive antennas improves the achieved ASE. The corresponding results in terms of average PLR are provided in Fig. 2.3. As

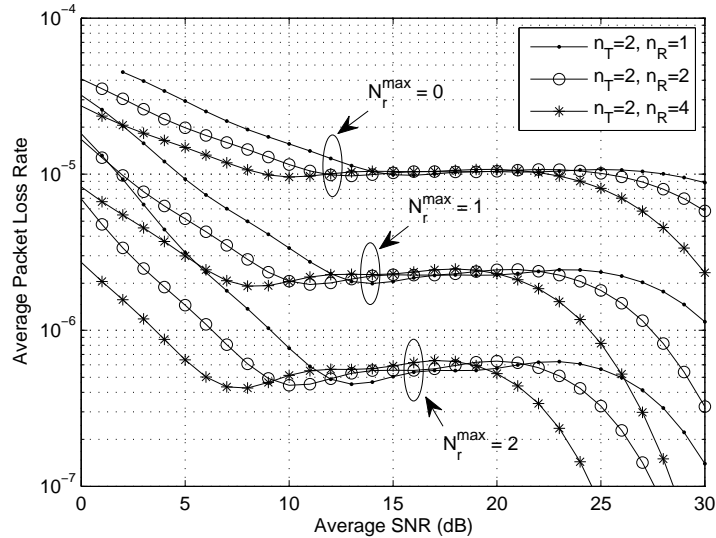


Figure 2.3: Average packet loss rate of cross layer design based MIMO-OSTBC in the spatially-correlated Nakagami- m fading channel case for different values of N_r^{\max} .

can be expected, the combined AMC and T-ARQ cross-layer design achieves the target $P_{\text{loss}} = 10^{-4}$ for any value of the average SNR, which is not the case for the nonadaptive scheme. This figure also shows how increasing N_r^{\max} improves the system performance in terms of average PLR, which explains the improvement in ASE observed in Fig. 2.2. Moreover, it is shown in Fig. 2.4 that increasing the values of N_r^{\max} , n_T and n_R , reduces the probability of outage.

To further illustrate the cross-layer scheme over spatially-correlated Nakagami- m fading channels, the influence of the spatial correlation parameters, ρ_T and ρ_R , and Nakagami fading parameter m , on the ASE, average PLR and probability of outage, are illustrated in Fig. 2.5, Fig. 2.6 and Fig. 2.7, respectively, where $N_r^{\max} = 1$ and $n_T = n_R = 2$. The effect of spatial correlation on performance is discussed first, followed by the impact of the Nakagami fading parameter. As observed, the probability of outage is larger with higher spatial correlation. The ASE becomes more and more discrete, and the oscillatory behavior of the average PLR curves increases as the spatial correlation becomes smaller. Fig. 2.8 illustrates PDFs of the output SNR for different ρ_T , ρ_R in the case with $m = 2$, $\bar{\gamma} = 10$ dB. It can be observed that as the spatial correlation decreases, the variance of the instantaneous

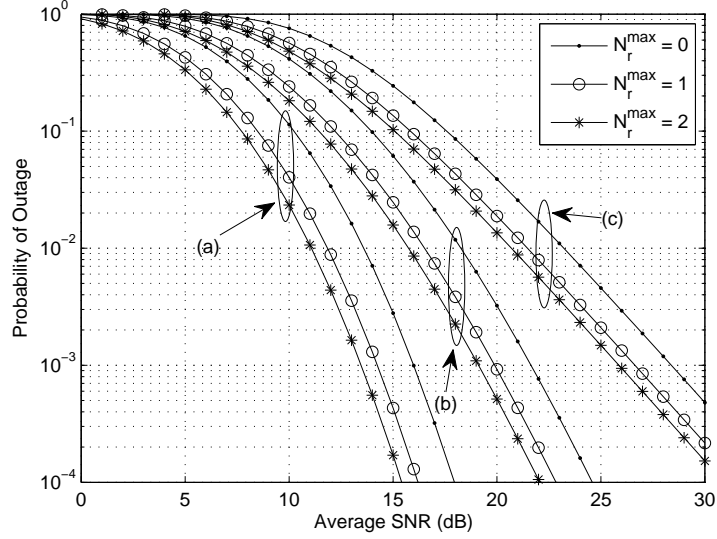


Figure 2.4: Outage probability of cross layer design based MIMO-OSTBC in the spatially-correlated Nakagami- m fading channel case for different antenna configurations: $n_T = 2$ and (a) $n_R = 1$, (b) $n_R = 2$, and (c) $n_R = 4$.

output SNR decreases. In this scenario, when the average SNR $\bar{\gamma} \in [\gamma_n, \gamma_{n+1})$, MCS n will be selected with high probability and, thus, the ASE will be approximately constant. As for the average PLR, for low spatial correlation, the AMC scheme will select MCS with higher index when $\bar{\gamma}$ exceeds the SNR threshold. Consequently, the oscillatory behavior of the average PLR curves becomes more visible as the spatial correlation becomes smaller. On the other hand, when spatial correlation becomes high, the variance of the instantaneous output SNR is very high. The high variability of the instantaneous output SNR allows the cross-layer scheme to select different MCS and, thus, the discrete characterization of the ASE and the oscillatory behavior of the average PLR decrease. In addition, it can be observed that the larger the Nakagami parameter m is, the larger the ASE will be, and the lower the outage probability will become. Moreover, the ASE becomes more and more discrete and the oscillatory behavior of the average PLR curves increases as m gets larger.

We now analyze the effect of system parameters on the ASE, average PLR and outage probability of the cross-layer MIMO OSTBC system for the keyhole Nakagami- m fading case. Fig. 2.9, Fig. 2.10 and Fig. 2.11 show the effect of N_r^{\max} and the

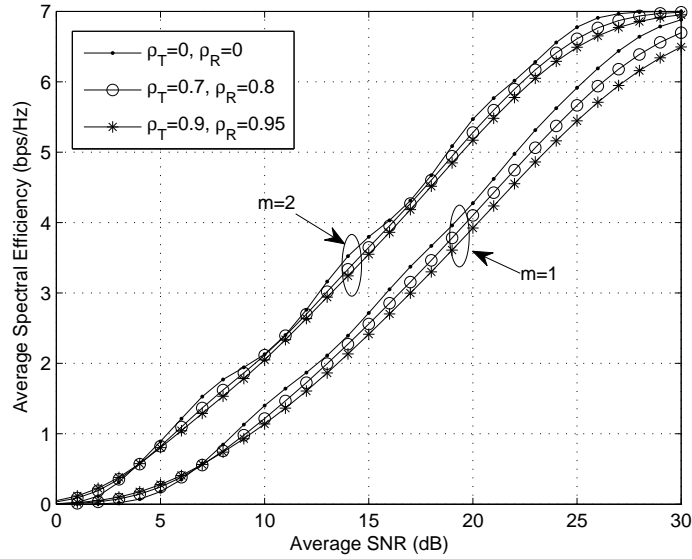


Figure 2.5: Average spectral efficiency of cross layer design based MIMO-OSTBC in the spatially-correlated Nakagami- m fading channel case for different ρ_T , ρ_R , and m .

numbers of transmit and receive antennas on the the ASE, average PLR and outage probability, respectively, in the scenario with $m_T = m_R = 1$. As observed, higher values for the parameter N_r^{\max} in the cross-layer design result in higher ASE, lower average PLR and lower outage probability. Furthermore, the ASE and diversity order increase as the number of receive antennas n_R becomes larger.

Finally, the ASE, average PLR and outage probability versus average SNR, taking m_T and m_R as the varying parameters in the scenario with $N_r^{\max} = 1$ and $n_T = n_R = 2$, are plotted and compared in Fig. 2.12, Fig. 2.13 and Fig. 2.14, respectively. Transmission over keyhole Nakagami- m fading channels yields reduced ASE and lower diversity order compared to the i.i.d. Nakagami- m case. This performance degradation is due to the fact that there is only one degree of freedom for keyhole channels. Due to the similar reason explained for Fig. 2.5 and Fig. 2.6, the discrete property of the ASE and the oscillatory behavior of the average PLR curves become less visible. Additionally, the system performance, in terms of ASE and outage probability, improves as m becomes larger.

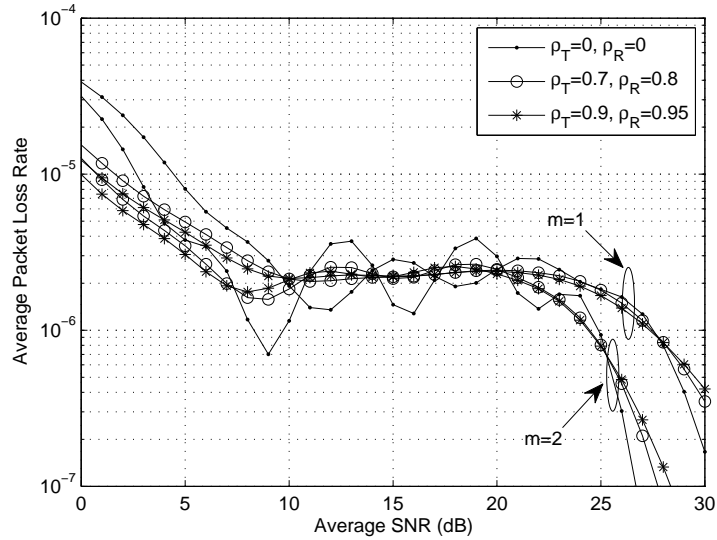


Figure 2.6: Average packet loss rate of cross layer design based MIMO-OSTBC in the spatially-correlated Nakagami- m fading channel case for different ρ_T , ρ_R , and m .

2.6 Summary

In this chapter, we proposed a cross-layer design for MIMO OSTBC over spatially-correlated and keyhole Nakagami- m fading channels. The performance was evaluated in terms of ASE, average PLR and probability of outage. Numerical results were presented to illustrate the effects of various parameters on the system performance. In particular, the ASE becomes more and more discrete and the oscillatory behavior of the average PLR curves increases as the spatial correlation becomes smaller. In addition, the discrete property of the ASE and the oscillatory behavior of the average PLR curves become less visible in keyhole Nakagami- m fading channels, compared to the i.i.d. Nakagami- m case. In the next chapter, investigation of the performance of another channel impairment, namely impairments in M-to-M communications, on MIMO wireless communication systems will be addressed.

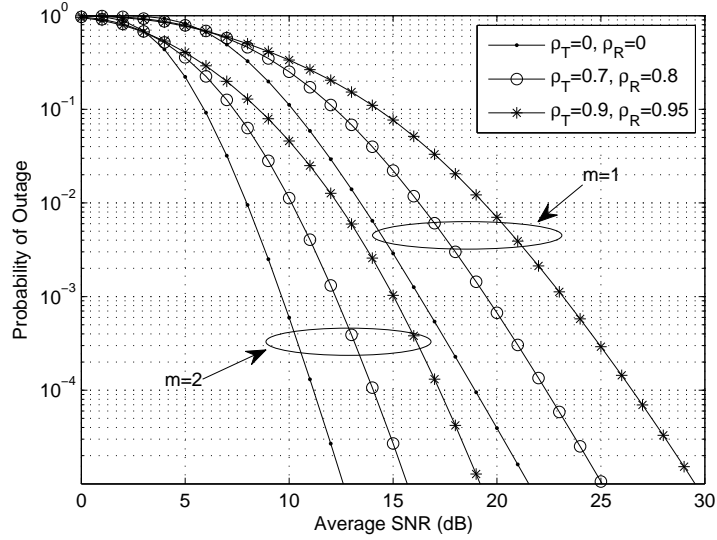


Figure 2.7: Outage probability of cross layer design based MIMO-OSTBC in the spatially-correlated Nakagami- m fading channel case for different ρ_T , ρ_R , and m .

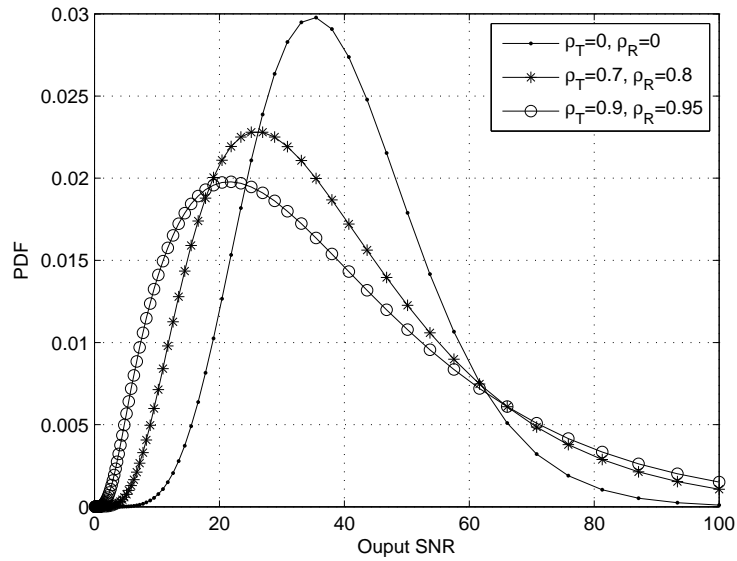


Figure 2.8: PDFs for the output SNR of cross layer design based MIMO-OSTBC in the spatially-correlated Nakagami- m fading channel case for different ρ_T , ρ_R ($m = 2$, $\bar{\gamma} = 10$ dB).

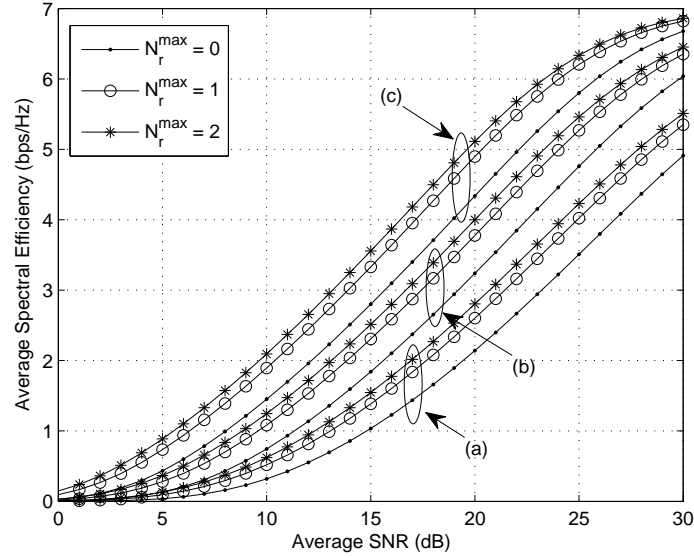


Figure 2.9: Average spectral efficiency of cross layer design based MIMO-OSTBC in the keyhole Nakagami- m fading channel case for different antenna configurations: $n_T = 2$ and (a) $n_R = 1$, (b) $n_R = 2$, and (c) $n_R = 4$.

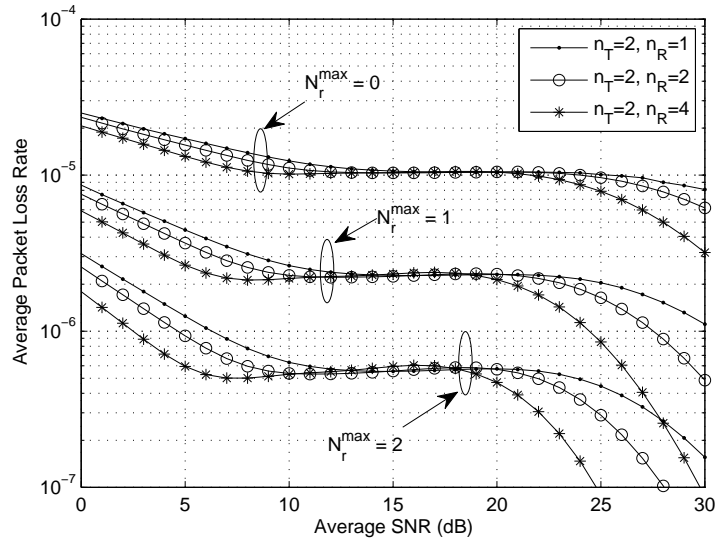


Figure 2.10: Average packet loss rate of cross layer design based MIMO-OSTBC in the keyhole Nakagami- m fading channel case for different values of N_r^{\max} .

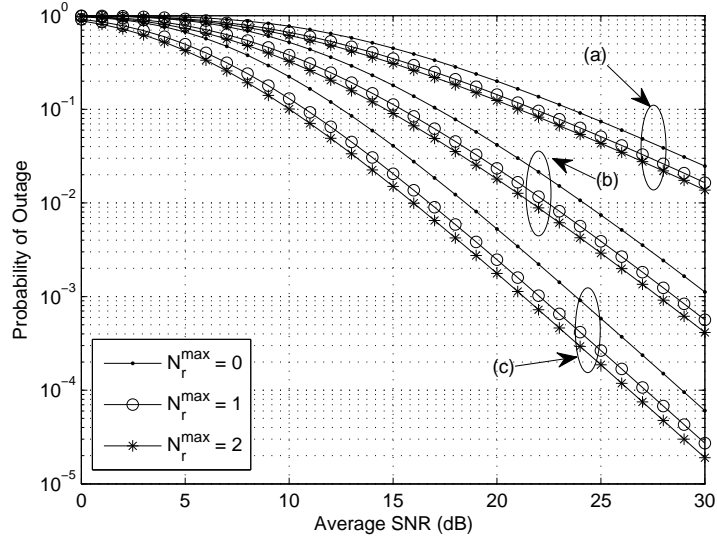


Figure 2.11: Outage probability of cross layer design based MIMO-OSTBC in the keyhole Nakagami- m fading channel case for different antenna configurations: $n_T = 2$ and (a) $n_R = 1$, (b) $n_R = 2$, and (c) $n_R = 4$.

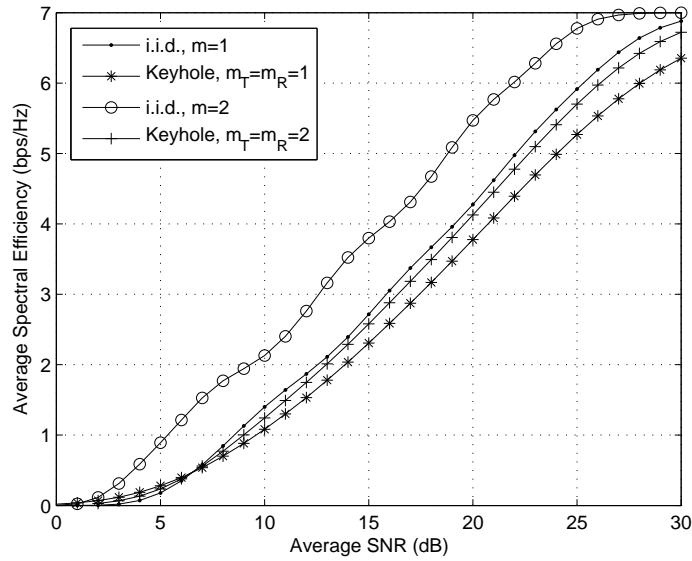


Figure 2.12: Average spectral efficiency of cross layer design based MIMO-OSTBC in the keyhole Nakagami- m fading channel case for different m .

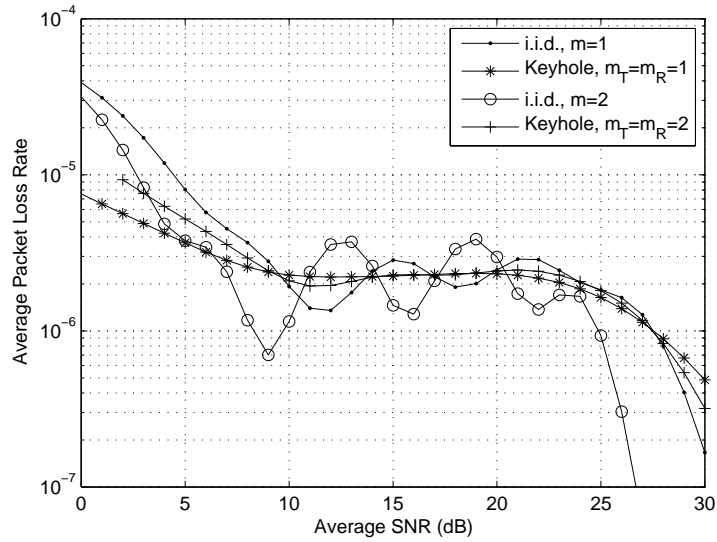


Figure 2.13: Average packet loss rate of cross layer design based MIMO-OSTBC in the keyhole Nakagami- m fading channel case for different m .

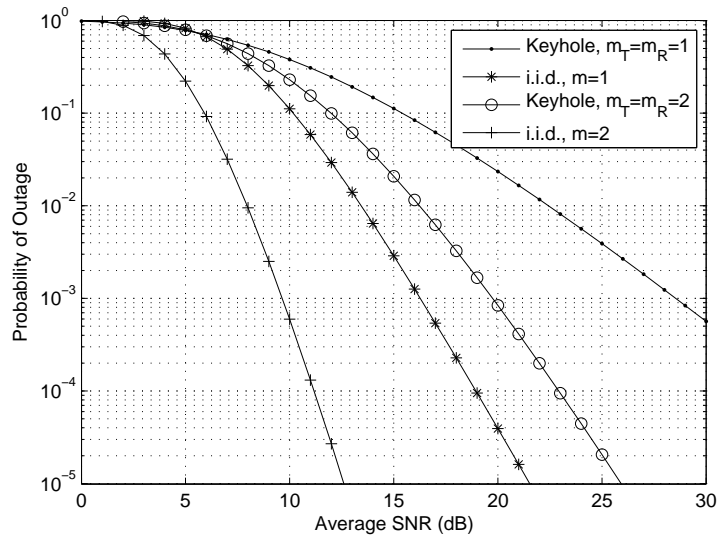


Figure 2.14: Outage probability of cross layer design based MIMO-OSTBC in the keyhole Nakagami- m fading channel case for different m .

Chapter 3

Mobile-to-Mobile Communications

3.1 Introduction

3D M-to-M channels can be considered as a general kind of double-correlated fading channels, where the transmit and receive correlations are due to scattering and shadowing. Herein, we consider MIMO MRC over 3D M-to-M double-correlated fading channels. MIMO MRC systems implement TB through full CSI availability at the transmitter, and can achieve high system capacity and full diversity gain ¹. The performance of MIMO MRC in uncorrelated and semi-correlated Rayleigh fading channels has been respectively analyzed in [98] and [99] in terms of SEP. MIMO MRC over double-correlated Rayleigh fading channels was also investigated in recent works. In particular, the cumulative distribution function (CDF) and PDF of the output SNR under double-correlated Rayleigh fading, which are related to the transmit and receive correlation matrices, were provided in [100] and used for deriving the average SEP in the special case with two antennas at either the transmitter or the receiver, i.e., for $2 \times n_R$ or $n_T \times 2$ MIMO configurations (n_T and n_R denote the numbers of transmit and receive antennas). Because the CDF expression for the output SNR in [100] is too complex to achieve tractable performance analysis, an approximation

¹Since it is difficult to obtain perfect CSI in the scenario with mobile transceivers, more pilot/training symbols are required to perform the channel estimation in M-to-M MIMO MRC systems.

in the low SNR range was used in [101] for arbitrary $n_T \times n_R$ MIMO configurations.

As represented in Section 1.1.3, current works on M-to-M channel modeling only consider the effects of fast fading factors caused by multipath, such as random phase shift, propagation delay and Doppler shift, in the modeling of the time-varying channel impulse response. In this chapter, the effect of spatial correlation on the performance of the M-to-M MIMO MRC system under study is assessed for transmissions over double-correlated Rayleigh-and-Lognormal fading channels considering fast fading and shadowing. We derive the expression for the average SEP as a function of the average SNR per receive antenna, $\bar{\gamma}$, in the $2 \times n_R$ or $n_T \times 2$ MIMO MRC system configurations in closed-form using an approach that is much simpler than the one taken in [100] to derive the expression for the average SEP under double-correlated Rayleigh fading channels. Besides, the expressions for the ergodic capacity and outage probability as a function of average SNR per receive antenna are derived in closed-form, which has not been done in previous works, for instance [100] or [101]. Results corresponding to the averaging over the variations of the average SNR per receive antenna are approximated using the recursive adaptive Simpson quadrature method. Furthermore, numerical results are provided and the effect of system parameters, such as distance between antenna elements, maximum elevation angle of scatterers, orientation angle of antenna array in the x-y plane, angle between the x-y plane and the antenna array orientation, and degree of scattering in the x-y plane, on the system performance, are studied and discussed.

In the remainder of this chapter, Section 3.2 introduces the MIMO MRC system considering data transmission over double-correlated Rayleigh-and-Lognormal fading channels. In Section 3.3, the space-time correlation function of 3D M-to-M MIMO channels is presented taking into account fast fading and shadowing. The performance of the M-to-M MIMO MRC system is analyzed in Section 3.4 in terms of average SEP, ergodic capacity and outage probability. Numerical results and comparisons are presented in Section 3.5, followed by the summary provided in Section 3.6.

3.2 System model

Consider a MIMO system, equipped with n_T transmit and n_R receive antennas, to operate under TB and MRC. The received signal model can be expressed as

$$\mathbf{y} = \mathbf{H}\mathbf{w}x + \mathbf{n}, \quad (3.1)$$

where x denotes the transmitted symbol with average power P_0 , \mathbf{w} refers to the $n_T \times 1$ unit TB weight vector, and \mathbf{n} is the $n_R \times 1$ noise vector with elements belonging to independent and identically distributed (i.i.d.) complex Gaussian distribution $\mathcal{CN}(0, N_0)$ that is uncorrelated with the transmitted symbols. In (3.1), \mathbf{H} is the $n_R \times n_T$ channel gain matrix, which follows the common Kronecker structure [27], according to

$$\mathbf{H} = \mathbf{\Phi}_R^{1/2} \mathbf{H}_w \mathbf{\Phi}_T^{1/2} \sim \mathcal{CN}_{n_R, n_T}(\mathbf{0}_{n_R \times n_T}, \mathbf{\Phi}_R \otimes \mathbf{\Phi}_T), \quad (3.2)$$

where $\mathbf{H}_w \sim \mathcal{CN}_{n_R, n_T}(\mathbf{0}_{n_R \times n_T}, \mathbf{I}_{n_R} \otimes \mathbf{I}_{n_T})$ with \mathbf{I}_n denoting the identity matrix of size $n \times n$, and $\mathbf{\Phi}_R$ and $\mathbf{\Phi}_T$ represent the receive and transmit correlation matrices, respectively. Accordingly, the channel is called a double-correlated fading channel. Let $n = \min(n_T, n_R)$, $m = \max(n_T, n_R)$, and denote $\mathbf{\Omega} \in \mathcal{C}^{n \times n}$ and $\mathbf{\Sigma} \in \mathcal{C}^{m \times m}$ as the Hermitian positive-definite matrices defined as

$$\mathbf{\Omega} \triangleq \begin{cases} \mathbf{\Phi}_R, & n_R \leq n_T \\ \mathbf{\Phi}_T, & n_R > n_T \end{cases}, \quad \mathbf{\Sigma} \triangleq \begin{cases} \mathbf{\Phi}_T, & n_R \leq n_T \\ \mathbf{\Phi}_R, & n_R > n_T \end{cases}, \quad (3.3)$$

with eigenvalues $\omega_1 < \dots < \omega_n$ and $\sigma_1 < \dots < \sigma_m$, respectively. At the receiver, the signals collected from all receive antenna branches are combined with the $n_R \times 1$ weight vector \mathbf{z} . A receiver where \mathbf{z} maximizes $|\mathbf{z}^H \mathbf{H}\mathbf{w}|$ given \mathbf{w} is called a MRC receiver [98]. Furthermore, MRT is employed to maximize the output SNR with respect to \mathbf{w} . The MIMO system under consideration implementing MRC and MRT is generally referred to as a MIMO MRC system. Above all, set $\|\mathbf{w}\|_F = 1$ to keep a constant average transmit power, irrespective of n_T , where $\|\cdot\|_F$ refers to the Frobenius norm. Then, denoting λ_{\max} as the largest eigenvalue of the double-correlated complex

Wishart matrix $\mathbf{H}^H \mathbf{H}$, the output SNR is given by [98]

$$\gamma = \bar{\gamma} \lambda_{\max}, \quad (3.4)$$

where $\bar{\gamma}$ denotes the average SNR per receive antenna. In the scenario with shadowing, $\bar{\gamma}$ is assumed to be Lognormally distributed according to the PDF

$$p_{\bar{\gamma}}(\bar{\gamma}) = \frac{\xi}{\sqrt{2\pi\sigma\bar{\gamma}}} \exp\left[-\frac{(10 \log_{10} \bar{\gamma} - \eta_p)^2}{2\sigma^2}\right], \quad (3.5)$$

where $\xi = 10/\ln 10$, $\eta_p = 10 \log_{10} [P_0 (D/d_0)^{-r}/N_0] - L_0$, with r representing the pathloss exponent, d_0 denoting the close-in reference distance which is determined from measurements close to the transmitter, and L_0 expressing the pathloss in [dB] at distance d_0 , and where σ denotes the shadowing standard deviation.

As for λ_{\max} , its exact CDF and PDF are derived in [100]. However, the provided expressions are too complex to achieve tractable performance analysis, such as average SEP, ergodic capacity and outage probability, for arbitrary $n_T \times n_R$ MIMO configurations. Herein, we concentrate on the special case with $2 \times m$ or $m \times 2$ MIMO MRC configurations in double-correlated channels, for which the CDF of λ_{\max} is given by [100]:

$$F_{\lambda_{\max}}(\lambda) = \frac{\det(\mathbf{\Omega})}{\Delta_2(\mathbf{\Omega}) \Delta_m(\mathbf{\Sigma})} \sum_{s=1}^m \sum_{t=1, t \neq s}^m (-1)^{s+\vartheta(t)} (\sigma_s \sigma_t)^{m-1} \Delta_{m-2}(\sigma^{[s,t]}) Q_{s,t}(\lambda), \quad (3.6)$$

where

$$\vartheta(t) = \begin{cases} t, & t < s, \\ t-1, & t > s, \end{cases} \quad (3.7)$$

$$\sigma^{[s,t]} = \{\sigma_k; k = 1, \dots, m \setminus \{s, t\}\}, \quad (3.8)$$

$$Q_{s,t}(\lambda) = \frac{1}{\lambda} e^{-\frac{\lambda}{\omega_2 \sigma_s}} \mathbf{P}\left(m, -\frac{\lambda}{\omega_2 \sigma_s}\right) e^{-\frac{\lambda}{\omega_1 \sigma_t}} \mathbf{P}\left(m, -\frac{\lambda}{\omega_1 \sigma_t}\right), \quad (3.9)$$

with $\mathbf{P}(\ell, y) = 1 - e^{-y} \sum_{k=0}^{\ell-1} \frac{y^k}{k!}$ and $\Delta_m(\cdot)$ denoting a Vandermonde determinant in the

eigenvalues of the m -dimensional matrix argument, expressed as

$$\Delta_m(\Sigma) = \prod_{k < l}^m (\sigma_l - \sigma_k). \quad (3.10)$$

By differentiating (3.6), the PDF of λ_{\max} can be obtained as follows:

$$\begin{aligned} p_{\lambda_{\max}}(\lambda) &= \frac{\det(\Omega)}{\Delta_2(\Omega) \Delta_m(\Sigma)} \sum_{s=1}^m \sum_{t=1, t \neq s}^m (-1)^{s+\vartheta(t)} (\sigma_s \sigma_t)^{m-1} \Delta_{m-2}(\sigma^{[s,t]}) \\ &\times \left\{ -\frac{1}{\lambda^2} e^{-\frac{\lambda}{\omega_2 \sigma_s}} \mathbb{P}\left(m, -\frac{\lambda}{\omega_2 \sigma_s}\right) e^{-\frac{\lambda}{\omega_2 \sigma_s}} \mathbb{P}\left(m, -\frac{\lambda}{\omega_1 \sigma_t}\right) \right. \\ &\quad - \frac{1}{\omega_2 \sigma_s \lambda} \left[e^{-\frac{\lambda}{\omega_2 \sigma_s}} + \sum_{k=0}^{m-2} \frac{(-1)^{k+1}}{k!} \left(\frac{\lambda}{\omega_2 \sigma_s}\right)^k \right] e^{-\frac{\lambda}{\omega_1 \sigma_t}} \mathbb{P}\left(m, -\frac{\lambda}{\omega_1 \sigma_t}\right) \\ &\quad \left. - \frac{1}{\omega_1 \sigma_t \lambda} \left[e^{-\frac{\lambda}{\omega_1 \sigma_t}} + \sum_{k=0}^{m-2} \frac{(-1)^{k+1}}{k!} \left(\frac{\lambda}{\omega_1 \sigma_t}\right)^k \right] e^{-\frac{\lambda}{\omega_2 \sigma_s}} \mathbb{P}\left(m, -\frac{\lambda}{\omega_2 \sigma_s}\right) \right\}. \end{aligned} \quad (3.11)$$

Finally, the CDF of the output SNR (3.4) can be obtained by averaging the CDF of λ_{\max} over the variations of $\bar{\gamma}$, i.e.,

$$F_{\gamma}(\gamma) = \int_0^{\infty} F_{\lambda_{\max}}\left(\frac{\gamma}{\bar{\gamma}}\right) p_{\bar{\gamma}}(\bar{\gamma}) d\bar{\gamma}, \quad (3.12)$$

3.3 Space-Time Correlation Function

In this section, we derive the receive and transmit correlation matrices, Φ_{R} and Φ_{T} , of a narrow-band M-to-M MIMO system. The transmitter and receiver are mobile and denoted by T_x and R_x , respectively. We consider a 3D scattering environment with NLoS propagation, which can be characterized by the two-cylinder model illustrated in [29, Fig. 1].²

It is assumed that P fixed omnidirectional scatterers are located on the surface of the cylinder with radius R_{T} around T_x , denoted by $S_{\text{T}}^{(p)}$ ($p = 1, 2, \dots, P$) following

²For convenience, this illustration is shown in Fig. 3.1.

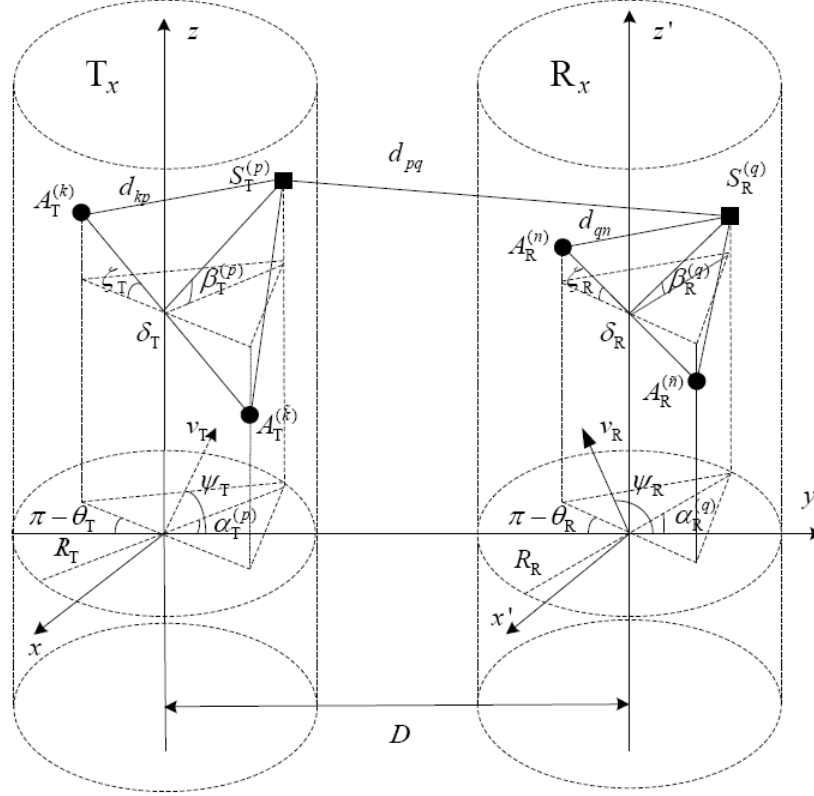


Figure 3.1: The two-cylinder model for M-to-M MIMO channel.

notations used in [29]. Also, Q fixed omnidirectional scatterers $S_R^{(q)}$ ($q = 1, 2, \dots, Q$) are located on the surface of the cylinder with radius R_R around R_x . Let D denote the distance between the centers of T_x and R_x cylinders. We consider the scenario where T_x and R_x antennas are located in linear and equal-distance arrays, with δ_T and δ_R denoting the distance between the adjacent antenna elements at T_x and R_x , respectively. It is assumed that $\max\{R_T, R_R\} \ll D$ and $\max\{\delta_T, \delta_R\} \ll \min\{R_T, R_R\}$. In Fig. 3.1, tilt angles θ_T and θ_R represent the orientation of T_x and R_x antenna arrays in the x - y plane, respectively, with respect to the x -axis. Analogously, angles between the x - y plane and the orientation of T_x and R_x antenna arrays are denoted by ζ_T and ζ_R , respectively. As for the scatterer orientation, the azimuth angle of departure (AAoD) and the azimuth angle of arrival (AAoA) are expressed as $\alpha_T^{(p)}$ and $\alpha_R^{(q)}$, respectively. The symbols $\beta_T^{(p)}$ and $\beta_R^{(q)}$ denote the elevation angle of departure (EAoD) and the elevation angle of arrival (EAoA), respectively. Furthermore, it is

assumed that T_x and R_x move with speeds v_T and v_R , according to the direction angles ψ_T and ψ_R with respect to x-axis in the x-y plane, respectively. Finally, the propagation distances pertaining to links $\overrightarrow{A_T^{(k)} S_T^{(p)}}$, $\overrightarrow{S_T^{(p)} S_R^{(q)}}$ and $\overrightarrow{S_R^{(q)} A_R^{(n)}}$, are respectively denoted by d_{kp} , d_{pq} and d_{qn} , where $A_T^{(k)}$ and $A_R^{(n)}$ refer to the k th transmit and n th receive antennas. In the above-described model, it can be observed that the waves emitted from the antenna elements at T_x are transmitted by the scatterers at T_x and R_x cylinders, before arriving at the R_x antennas. Furthermore, it is assumed that all wave branches from each transmit antenna are equal in power.

Herein, we take into account fast fading and shadowing in the M-to-M MIMO channel modeling. Since the fast fading and shadowing are uncorrelated random processes, the space-time correlation function between two complex faded envelopes corresponding to transmission links $\overrightarrow{A_T^{(k)} A_R^{(n)}}$ and $\overrightarrow{A_T^{(\tilde{k})} A_R^{(\tilde{n})}}$ can be written as

$$\rho_{nk, \tilde{n}\tilde{k}}(\delta_T, \delta_R, \tau) = \rho_{nk, \tilde{n}\tilde{k}}^{\text{Sh}}(\delta_T, \delta_R, \tau) \rho_{nk, \tilde{n}\tilde{k}}^{\text{NS}}(\delta_T, \delta_R, \tau), \quad (3.13)$$

where $\rho_{nk, \tilde{n}\tilde{k}}^{\text{NS}}(\delta_T, \delta_R, \tau)$ represents the space-time correlation without consideration of shadowing, and $\rho_{nk, \tilde{n}\tilde{k}}^{\text{Sh}}(\delta_T, \delta_R, \tau)$ is the correlation component with shadowing only. The correlation components $\rho_{nk, \tilde{n}\tilde{k}}^{\text{NS}}(\delta_T, \delta_R, \tau)$ and $\rho_{nk, \tilde{n}\tilde{k}}^{\text{Sh}}(\delta_T, \delta_R, \tau)$ are independent of scatterer indices, p and q , due to the fact that the numbers of scatterers around T_x and R_x are assumed infinite. Specifically, all the discrete random variables that have influence on $\rho_{nk, \tilde{n}\tilde{k}}^{\text{NS}}(\delta_T, \delta_R, \tau)$ and $\rho_{nk, \tilde{n}\tilde{k}}^{\text{Sh}}(\delta_T, \delta_R, \tau)$, such as AAoD $\{\alpha_T^{(p)}\}$, AAoA $\{\alpha_R^{(q)}\}$, EAoD $\{\beta_T^{(p)}\}$, and EAoA $\{\beta_R^{(q)}\}$, approach continuous random variables that are independent of scatterer indices [29]. The correlation component for shadowing in the M-to-M scenario, $\rho_{nk, \tilde{n}\tilde{k}}^{\text{Sh}}(\delta_T, \delta_R, \tau)$, is given as extension of [102, eq. (8)] for the F-to-M case by

$$\rho_{nk, \tilde{n}\tilde{k}}^{\text{Sh}}(\delta_T, \delta_R, \tau) = e^{-\eta \lambda_c (f_T^{\text{max}} + f_R^{\text{max}}) \tau} [A \cos(\Delta_{nk, \tilde{n}\tilde{k}}) + B], \quad (3.14)$$

where λ_c denotes the carrier wavelength, f_T^{max} and f_R^{max} represent the maximum Doppler shifts of T_x and R_x , respectively, and η is a propagation-related coefficient (a value of $\eta = 1/20$ is suggested for suburban and urban environments [103]). A and

B are two non-negative coefficients satisfying $A + B \leq 1$. In order to calculate the geometrical angle between the two links $\overrightarrow{A_T^{(k)} A_R^{(n)}}$ and $\overrightarrow{A_T^{(\tilde{k})} A_R^{(\tilde{n})}}$, i.e., $\Delta_{nk, \tilde{n}\tilde{k}}$, we start by presenting the coordinates of the transmit and receive antennas:

$$A_T^{(k)} = \left(-\frac{\delta_T (n_T + 1 - 2k)}{2} \cos \zeta_T \cos \theta_T, \right. \\ \left. \frac{\delta_T (n_T + 1 - 2k)}{2} \cos \zeta_T \sin \theta_T, \frac{\delta_T (n_T + 1 - 2k)}{2} \sin \zeta_T \right), \quad (3.15)$$

$$A_R^{(n)} = \left(D - \frac{\delta_R (n_R + 1 - 2n)}{2} \cos \zeta_R \cos \theta_R, \right. \\ \left. \frac{\delta_R (n_R + 1 - 2n)}{2} \cos \zeta_R \sin \theta_R, \frac{\delta_R (n_R + 1 - 2n)}{2} \sin \zeta_R \right). \quad (3.16)$$

Then, based on the coordinates of $A_T^{(k)}$ and $A_R^{(n)}$, we get the square of the distance between $A_T^{(k)}$ and $A_R^{(n)}$ as follows

$$\left| \overrightarrow{A_T^{(k)} A_R^{(n)}} \right|^2 = D\delta_T (n_T + 1 - 2k) \cos \zeta_T \cos \theta_T - D\delta_R (n_R + 1 - 2n) \cos \zeta_R \cos \theta_R \\ + D^2 + \left[\frac{\delta_T (n_T + 1 - 2k)}{2} \right]^2 + \left[\frac{\delta_R (n_R + 1 - 2n)}{2} \right]^2 \\ - \frac{\delta_T (n_T + 1 - 2k) \delta_R (n_R + 1 - 2n)}{2} [(\cos \zeta_T \cos \zeta_R \cos (\theta_T - \theta_R) + \sin \zeta_T \sin \zeta_R)]. \quad (3.17)$$

Note that $\left| \overrightarrow{A_T^{(\tilde{k})} A_R^{(\tilde{n})}} \right|^2$ has the same form as $\left| \overrightarrow{A_T^{(k)} A_R^{(n)}} \right|^2$ except for replacing k by \tilde{k} and n by \tilde{n} in (3.17). In addition, the inner product of $\overrightarrow{A_T^{(k)} A_R^{(n)}}$ and $\overrightarrow{A_T^{(\tilde{k})} A_R^{(\tilde{n})}}$ can be expressed as

$$\left\langle \overrightarrow{A_T^{(k)} A_R^{(n)}}, \overrightarrow{A_T^{(\tilde{k})} A_R^{(\tilde{n})}} \right\rangle = \frac{1}{4} \delta_T^2 (n_T + 1 - 2k) (n_T + 1 - 2\tilde{k}) \\ + \frac{1}{4} \delta_R^2 (n_R + 1 - 2n) (n_R + 1 - 2\tilde{n}) + D^2$$

$$\begin{aligned}
& - \frac{\delta_T \delta_R}{4} [(\cos \zeta_T \cos \zeta_R \cos (\theta_T - \theta_R) + \sin \zeta_T \sin \zeta_R)] \\
& \times \left[(n_T + 1 - 2k)(n_R + 1 - 2\tilde{n}) + (n_T + 1 - 2\tilde{k})(n_R + 1 - 2n) \right] \\
& + D\delta_T (n_T + 1 - k - \tilde{k}) \cos \zeta_T \cos \theta_T + D\delta_R (n_R + 1 - n - \tilde{n}) \cos \zeta_R \cos \theta_R. \quad (3.18)
\end{aligned}$$

Hence, $\cos(\Delta_{nk, \tilde{n}\tilde{k}})$ in (3.14) can be obtained by substituting (3.17) and (3.18) into

$$\cos(\Delta_{nk, \tilde{n}\tilde{k}}) = \frac{\left\langle \overrightarrow{A_T^{(k)} A_R^{(n)}}, \overrightarrow{A_T^{(\tilde{k})} A_R^{(\tilde{n})}} \right\rangle}{\left| \overrightarrow{A_T^{(k)} A_R^{(n)}} \right| \left| \overrightarrow{A_T^{(\tilde{k})} A_R^{(\tilde{n})}} \right|}. \quad (3.19)$$

For the space-time correlation function without consideration of shadowing, i.e., $\rho_{nk, \tilde{n}\tilde{k}}^{\text{NS}}(\delta_T, \delta_R, \tau)$, we adopt the von Mises distribution for α_T and α_R [104]

$$p(\alpha_T) = \frac{1}{2\pi I_0(k_T)} \exp[k_T(\alpha_T - \mu_T)], \quad (3.20)$$

$$p(\alpha_R) = \frac{1}{2\pi I_0(k_R)} \exp[k_R(\alpha_R - \mu_R)], \quad (3.21)$$

where $I_0(\cdot)$ refers to the zeroth-order modified Bessel function of the first kind, μ_T and μ_R denote the mean value of α_T and α_R , respectively, and k_T and k_R are the parameters controlling the spread of scatterers around these mean values, which represent the degrees of scattering. As for β_T and β_R , their PDFs are given by [31]

$$p(\beta_T) = \frac{\pi}{4|\beta_T^{\max}|} \cos\left(\frac{\pi\beta_T}{2\beta_T^{\max}}\right), \quad |\beta_T| \leq |\beta_T^{\max}| \leq \frac{\pi}{2}, \quad (3.22)$$

$$p(\beta_R) = \frac{\pi}{4|\beta_R^{\max}|} \cos\left(\frac{\pi\beta_R}{2\beta_R^{\max}}\right), \quad |\beta_R| \leq |\beta_R^{\max}| \leq \frac{\pi}{2}, \quad (3.23)$$

where β_T^{\max} and β_R^{\max} are the maximum elevation angles of the scatterers around T_x and R_x , respectively.

Consequently, the overall space-time correlation function taking into account fast fading and shadowing can be obtained by substituting (3.14) and the expression of

$\rho_{nk, \tilde{n}\tilde{k}}^{\text{NS}}(\delta_{\text{T}}, \delta_{\text{R}}, \tau)$ provided in [29, eq. (14)] into (3.13), thus yielding

$$\begin{aligned} \rho_{nk, \tilde{n}\tilde{k}}(\delta_{\text{T}}, \delta_{\text{R}}, \tau) &\approx e^{-\eta\lambda_c(f_{\text{T}}^{\text{max}}+f_{\text{R}}^{\text{max}})\tau} [A \cos(\Delta_{nk, \tilde{n}\tilde{k}}) + B] \\ &\times \frac{I_0\left(\sqrt{y_{\text{T}}^2+z_{\text{T}}^2}\right) \cos\left[\frac{2\pi}{\lambda_c}\beta_{\text{T}}^{\text{max}}\delta_{\text{T}}(\tilde{k}-k)\sin\zeta_{\text{T}}\right]}{I_0(k_{\text{T}}) \left[1 - \left(\frac{4\beta_{\text{T}}^{\text{max}}\delta_{\text{T}}(\tilde{k}-k)\sin\zeta_{\text{T}}}{\lambda_c}\right)^2\right]} \\ &\times \frac{I_0\left(\sqrt{y_{\text{R}}^2+z_{\text{R}}^2}\right) \cos\left[\frac{2\pi}{\lambda_c}\beta_{\text{R}}^{\text{max}}\delta_{\text{R}}(\tilde{n}-n)\sin\zeta_{\text{R}}\right]}{I_0(k_{\text{R}}) \left[1 - \left(\frac{4\beta_{\text{R}}^{\text{max}}\delta_{\text{R}}(\tilde{n}-n)\sin\zeta_{\text{R}}}{\lambda_c}\right)^2\right]}, \end{aligned} \quad (3.24)$$

where parameters y_{T} , z_{T} , y_{R} and z_{R} are given in [29] and provided in (3.25) for completeness,

$$\begin{aligned} y_{\text{T}} &= j2\pi\delta_{\text{T}}(\tilde{k}-k)\cos\theta_{\text{T}}\cos\zeta_{\text{T}}/\lambda - j2\pi\tau f_{\text{T}}^{\text{max}}\cos\psi_{\text{T}} + k_{\text{T}}\cos\mu_{\text{T}}, \\ z_{\text{T}} &= j2\pi\delta_{\text{T}}(\tilde{k}-k)\sin\theta_{\text{T}}\cos\zeta_{\text{T}}/\lambda - j2\pi\tau f_{\text{T}}^{\text{max}}\sin\psi_{\text{T}} + k_{\text{T}}\sin\mu_{\text{T}}, \\ y_{\text{R}} &= j2\pi\delta_{\text{R}}(\tilde{n}-n)\cos\theta_{\text{R}}\cos\zeta_{\text{R}}/\lambda - j2\pi\tau f_{\text{R}}^{\text{max}}\cos\psi_{\text{R}} + k_{\text{R}}\cos\mu_{\text{R}}, \\ z_{\text{R}} &= j2\pi\delta_{\text{R}}(\tilde{n}-n)\sin\theta_{\text{R}}\cos\zeta_{\text{R}}/\lambda - j2\pi\tau f_{\text{R}}^{\text{max}}\sin\psi_{\text{R}} + k_{\text{R}}\sin\mu_{\text{R}}. \end{aligned} \quad (3.25)$$

Finally, the elements of the receive and transmit correlation matrices defined in (3.2) can respectively be expressed as

$$\{\Phi_{\text{R}}\}_{n\tilde{n}} = \frac{1}{n_{\text{T}}} \sum_{k=\tilde{k}=1}^{n_{\text{T}}} \rho_{nk, \tilde{n}\tilde{k}}(\delta_{\text{T}}, \delta_{\text{R}}, 0), \quad (3.26)$$

$$\{\Phi_{\text{T}}\}_{k\tilde{k}} = \frac{1}{n_{\text{R}}} \sum_{n=\tilde{n}=1}^{n_{\text{R}}} \rho_{nk, \tilde{n}\tilde{k}}(\delta_{\text{T}}, \delta_{\text{R}}, 0). \quad (3.27)$$

Remark 1 *The cross-correlation of shadowing, $A \cos(\Delta_{nk, \tilde{n}\tilde{k}}) + B$, can be divided into two kinds: angle-independent ($A = 0$) and angle-dependent ($A \neq 0$). It is noticed that the geometrical angle $\Delta_{nk, \tilde{n}\tilde{k}}$ is infinitesimally small if $\max\{\delta_{\text{T}}, \delta_{\text{R}}\} \ll D$. When parameters A, B are such that $A + B = 1$, the impact of the shadowing on the receive and transmit correlations specified in (3.26) and (3.27) becomes negligible.*

3.4 Performance Analysis

In this section, we derive the average SEP, ergodic capacity and outage probability of MIMO MRC systems under the above-described 3D M-to-M Rayleigh-and-Lognormal fading channels.

3.4.1 Average SEP

The general expression of average SEP for many modulation mechanisms can be expressed as [105]

$$P_s = E_\gamma \left\{ aQ \left(\sqrt{2b\gamma} \right) \right\}, \quad (3.28)$$

where $E \{ \cdot \}$ denotes the expectation operator, $Q(\cdot)$ represents the Gaussian Q-function, and a and b are modulation-specific constants. A useful alternative expression for (3.28) using integration by parts is given by

$$P_s = \frac{a\sqrt{b}}{2\sqrt{\pi}} \int_0^\infty \frac{e^{-bu}}{\sqrt{u}} F_\gamma(u) du, \quad (3.29)$$

which can be adapted to our channel variations according to

$$\begin{aligned} P_s &= \frac{a\sqrt{b}}{2\sqrt{\pi}} \int_0^\infty \int_0^\infty \frac{e^{-bu}}{\sqrt{u}} F_{\lambda_{\max}} \left(\frac{u}{\bar{\gamma}} \right) p_{\bar{\gamma}}(\bar{\gamma}) d\bar{\gamma} du \\ &= \int_0^\infty \left[\frac{a\sqrt{b}}{2\sqrt{\pi}} \int_0^\infty \frac{e^{-bu}}{\sqrt{u}} F_{\lambda_{\max}} \left(\frac{u}{\bar{\gamma}} \right) du \right] p_{\bar{\gamma}}(\bar{\gamma}) d\bar{\gamma}. \end{aligned} \quad (3.30)$$

Let $P_s(\bar{\gamma}) = \frac{a\sqrt{b}}{2\sqrt{\pi}} \int_0^\infty \frac{e^{-bu}}{\sqrt{u}} F_{\lambda_{\max}} \left(\frac{u}{\bar{\gamma}} \right) du$, then, the average SEP as a function of $\bar{\gamma}$ can be expressed as

$$\begin{aligned} P_s(\bar{\gamma}) &= \frac{a\sqrt{b}}{2\sqrt{\pi}} \int_0^\infty \frac{e^{-bu}}{\sqrt{u}} \frac{\det(\mathbf{\Omega})}{\Delta_2(\mathbf{\Omega}) \Delta_m(\mathbf{\Sigma})} \\ &\quad \times \sum_{s=1}^m \sum_{t=1, t \neq s}^m (-1)^{s+\vartheta(t)} (\sigma_s \sigma_t)^{m-1} \Delta_{m-2}(\sigma^{[s,t]}) Q_{s,t} \left(\frac{u}{\bar{\gamma}} \right) du \end{aligned}$$

$$\begin{aligned}
&= \frac{a\sqrt{b} \det(\mathbf{\Omega})}{2\sqrt{\pi} \Delta_2(\mathbf{\Omega}) \Delta_m(\mathbf{\Sigma})} \sum_{s=1}^m \sum_{t=1, t \neq s}^m (-1)^{s+\vartheta(t)} (\sigma_s \sigma_t)^{m-1} \Delta_{m-2}(\sigma^{[s,t]}) \\
&\quad \times \int_0^\infty \frac{e^{-bu} \bar{\gamma}}{\sqrt{u} u} \left[e^{-\frac{u}{\omega_2 \sigma_s \bar{\gamma}}} - \sum_{k=0}^{m-1} \frac{(-1)^k}{k!} \left(\frac{u}{\omega_2 \sigma_s \bar{\gamma}} \right)^k \right] \\
&\quad \times \left[e^{-\frac{u}{\omega_1 \sigma_t \bar{\gamma}}} - \sum_{k=0}^{m-1} \frac{(-1)^k}{k!} \left(\frac{u}{\omega_1 \sigma_t \bar{\gamma}} \right)^k \right] du. \tag{3.31}
\end{aligned}$$

To proceed with our derivation, we introduce the following identity [93]

$$\int_0^\infty t^{n-1} e^{-\mu t} dt = \frac{\Gamma(n)}{\mu^n} \quad n > 0, \mu > 0, \tag{3.32}$$

where $\Gamma(\cdot)$ denotes the Gamma function. Then noting that

$$\Gamma(n + 1/2) = \frac{(2n - 1)!! \sqrt{\pi}}{2^n}, \tag{3.33}$$

for nonnegative integer n , where $(2n - 1)!! \triangleq 1 \times 3 \times \dots \times (2n - 1)$ and $(-1)!! \triangleq 1$, and applying (3.32) to (3.31), $P_s(\bar{\gamma})$ can be expressed as

$$\begin{aligned}
P_s(\bar{\gamma}) &= \frac{a\sqrt{b} \det(\mathbf{\Omega})}{2\sqrt{\pi} \Delta_2(\mathbf{\Omega}) \Delta_m(\mathbf{\Sigma})} \sum_{s=1}^m \sum_{t=1, t \neq s}^m (-1)^{s+\vartheta(t)} (\sigma_s \sigma_t)^{m-1} \Delta_{m-2}(\sigma^{[s,t]}) \\
&\quad \times \left\{ \mathfrak{S} + \int_0^\infty \frac{e^{-bu} \bar{\gamma}}{\sqrt{u} u} \left[\sum_{k,l \in \{0, \dots, m-1\} \setminus \{k=l=0\}} \frac{(-1)^{k+l}}{k!l! (\omega_2 \sigma_s)^k (\omega_1 \sigma_t)^l \bar{\gamma}^{k+l}} u^{k+l} \right] du \right. \\
&\quad \left. - \int_0^\infty \frac{e^{-bu} \bar{\gamma}}{\sqrt{u} u} \left[e^{-\frac{u}{\omega_2 \sigma_s \bar{\gamma}}} \sum_{k=1}^{m-1} \frac{(-1)^k}{k!} \left(\frac{u}{\omega_1 \sigma_t \bar{\gamma}} \right)^k + e^{-\frac{u}{\omega_1 \sigma_t \bar{\gamma}}} \sum_{k=1}^{m-1} \frac{(-1)^k}{k!} \left(\frac{u}{\omega_2 \sigma_s \bar{\gamma}} \right)^k \right] du \right\}, \tag{3.34}
\end{aligned}$$

where

$$\mathfrak{S} = \int_0^\infty \frac{e^{-bu} \bar{\gamma}}{\sqrt{u} u} \left[e^{-\frac{u}{\omega_2 \sigma_s \bar{\gamma}} - \frac{u}{\omega_1 \sigma_t \bar{\gamma}}} - e^{-\frac{u}{\omega_2 \sigma_s \bar{\gamma}}} - e^{-\frac{u}{\omega_1 \sigma_t \bar{\gamma}}} + 1 \right] du. \tag{3.35}$$

Now by making use of the following identity

$$\int_0^{\infty} u^{-3/2} [e^{-\alpha u} - e^{-\beta u}] du = 2\sqrt{\pi\beta} - 2\sqrt{\pi\alpha}, \quad (3.36)$$

the integral \mathfrak{S} (3.35) can be rewritten as

$$\begin{aligned} \mathfrak{S} = & 2\bar{\gamma} \left[\sqrt{\pi \left(b + \frac{1}{\omega_2 \sigma_s \bar{\gamma}} \right)} + \sqrt{\pi \left(b + \frac{1}{\omega_1 \sigma_t \bar{\gamma}} \right)} \right. \\ & \left. - \sqrt{\pi \left(b + \frac{1}{\omega_2 \sigma_s \bar{\gamma}} + \frac{1}{\omega_1 \sigma_t \bar{\gamma}} \right)} - \sqrt{\pi b} \right]. \end{aligned} \quad (3.37)$$

Then substituting (3.32), (3.33) and (3.37) into (3.34), we obtain the following expression for the average SEP given $\bar{\gamma}$:

$$\begin{aligned} P_s(\bar{\gamma}) = & \frac{a\sqrt{b} \det(\mathbf{\Omega})}{2\sqrt{\pi} \Delta_2(\mathbf{\Omega}) \Delta_m(\mathbf{\Sigma})} \sum_{s=1}^m \sum_{t=1, t \neq s}^m (-1)^{s+\vartheta(t)} (\sigma_s \sigma_t)^{m-1} \Delta_{m-2}(\sigma^{[s,t]}) \\ & \times \left\{ 2\bar{\gamma} \left[\sqrt{\pi \left(b + \frac{1}{\omega_2 \sigma_s \bar{\gamma}} + \frac{1}{\omega_1 \sigma_t \bar{\gamma}} \right)} - \sqrt{\pi \left(b + \frac{1}{\omega_2 \sigma_s \bar{\gamma}} \right)} - \sqrt{\pi \left(b + \frac{1}{\omega_1 \sigma_t \bar{\gamma}} \right)} + \sqrt{\pi b} \right] \right. \\ & + \sum_{k,l \in \{0, \dots, m-1\} \setminus \{k=l=0\}} \frac{(-1)^{k+l} (2k+2l-3)!! \sqrt{\pi}}{k! l! (\omega_2 \sigma_s)^k (\omega_1 \sigma_t)^l (2\bar{\gamma})^{k+l-1} b^{k+l-\frac{1}{2}}} \\ & \left. - \sum_{k=1}^{m-1} \frac{(-1)^k (2k-3)!! \sqrt{\pi}}{k! (2\bar{\gamma})^{k-1}} \left[\frac{1}{(\omega_1 \sigma_t)^k} \left(\frac{1}{\omega_2 \sigma_s \bar{\gamma}} + b \right)^{\frac{1}{2}-k} + \frac{1}{(\omega_2 \sigma_s)^k} \left(\frac{1}{\omega_1 \sigma_t \bar{\gamma}} + b \right)^{\frac{1}{2}-k} \right] \right\}. \end{aligned} \quad (3.38)$$

Observing the operator $\sum_{s=1}^m \sum_{t=1, t \neq s}^m (-1)^{s+\vartheta(t)}$ in (3.38), some similar parties can be counteracted. Accordingly, the average SEP as a function of $\bar{\gamma}$ is derived as

$$\begin{aligned} P_s(\bar{\gamma}) = & \frac{a\sqrt{b} \det(\mathbf{\Omega})}{2\sqrt{\pi} \Delta_2(\mathbf{\Omega}) \Delta_m(\mathbf{\Sigma})} \sum_{s=1}^m \sum_{t=1, t \neq s}^m (-1)^{s+\vartheta(t)} (\sigma_s \sigma_t)^{m-1} \Delta_{m-2}(\sigma^{[s,t]}) \\ & \times \left\{ 2\bar{\gamma} \left[\sqrt{\pi \left(b + \frac{1}{\omega_2 \sigma_s \bar{\gamma}} \right)} + \sqrt{\pi \left(b + \frac{1}{\omega_1 \sigma_t \bar{\gamma}} \right)} - \sqrt{\pi \left(b + \frac{1}{\omega_2 \sigma_s \bar{\gamma}} + \frac{1}{\omega_1 \sigma_t \bar{\gamma}} \right)} \right] \right\} \end{aligned}$$

$$\begin{aligned}
& + \sum_{k=1}^{m-1} \frac{(-1)^k (2k-3)!! \sqrt{\pi}}{k! (2\bar{\gamma})^{k-1}} \\
& \times \left[\frac{b^{\frac{1}{2}-k}}{(\omega_1 \sigma_t)^k} + \frac{b^{\frac{1}{2}-k}}{(\omega_2 \sigma_s)^k} - \frac{1}{(\omega_1 \sigma_t)^k} \left(\frac{1}{\omega_2 \sigma_s \bar{\gamma}} + b \right)^{\frac{1}{2}-k} - \frac{1}{(\omega_2 \sigma_s)^k} \left(\frac{1}{\omega_1 \sigma_t \bar{\gamma}} + b \right)^{\frac{1}{2}-k} \right] \Bigg\}. \tag{3.39}
\end{aligned}$$

Remark 2 *The method used to obtain the above expression for the average SEP as a function of $\bar{\gamma}$ is much simpler than that in [100].*

Finally, the average SEP in the double-correlated Rayleigh-and-Lognormal fading channel can be expressed as $P_s = \int_0^\infty P_s(\bar{\gamma}) p_{\bar{\gamma}}(\bar{\gamma}) d\bar{\gamma}$, where $P_s(\bar{\gamma})$ and $p_{\bar{\gamma}}(\bar{\gamma})$ are provided in (3.39) and (3.5), respectively. It is noticed that deriving P_s in closed-form is intractable. As such, illustration of the SEP performance in the numerical results section is performed using the recursive adaptive Simpson quadrature method.

3.4.2 Ergodic Capacity

The ergodic capacity of M-to-M MIMO MRC systems in double-correlated Rayleigh-and-Lognormal fading channels can be expressed in [bits/s/Hz] as

$$\begin{aligned}
C &= E_\gamma \{ \log_2(1 + \gamma) \} \\
&= \int_0^\infty \log_2(1 + \gamma) p_\gamma(\gamma) d\gamma. \tag{3.40}
\end{aligned}$$

Substituting (3.12) into (3.40), the ergodic capacity can be rewritten as

$$\begin{aligned}
C &= \int_0^\infty \log_2(1 + \gamma) \left[\int_0^\infty \frac{1}{\bar{\gamma}} p_{\lambda_{\max}} \left(\frac{\gamma}{\bar{\gamma}} \right) p_{\bar{\gamma}}(\bar{\gamma}) d\bar{\gamma} \right] d\gamma \\
&= \int_0^\infty p_{\bar{\gamma}}(\bar{\gamma}) \left[\int_0^\infty \frac{\ln(1 + \gamma)}{\bar{\gamma} \ln 2} p_{\lambda_{\max}} \left(\frac{\gamma}{\bar{\gamma}} \right) d\gamma \right] d\bar{\gamma}. \tag{3.41}
\end{aligned}$$

It is observed that the ergodic capacity can be obtained by averaging the capacity expression given $\bar{\gamma}$ over the distribution of the latter, i.e., $C = \int_0^\infty C(\bar{\gamma}) p_{\bar{\gamma}}(\bar{\gamma}) d\bar{\gamma}$, where $C(\bar{\gamma}) = \int_0^\infty \frac{\ln(1+\gamma)}{\bar{\gamma} \ln 2} p_{\lambda_{\max}} \left(\frac{\gamma}{\bar{\gamma}} \right) d\gamma$ denotes the ergodic capacity as a function of

$\bar{\gamma}$. Then, inserting the PDF expression of λ_{\max} (3.11), $C(\bar{\gamma})$ can be expressed as

$$\begin{aligned}
C(\bar{\gamma}) &= \frac{\det(\mathbf{\Omega})}{\bar{\gamma} \ln 2 \Delta_2(\mathbf{\Omega}) \Delta_m(\mathbf{\Sigma})} \sum_{s=1}^m \sum_{t=1, t \neq s}^m (-1)^{s+\vartheta(t)} (\sigma_s \sigma_t)^{m-1} \Delta_{m-2}(\sigma^{[s,t]}) \\
&\times \left\{ -\bar{\gamma}^2 \left[\mathfrak{N}_{-1} \left(\frac{1}{\omega_2 \sigma_s \bar{\gamma}} + \frac{1}{\omega_1 \sigma_t \bar{\gamma}} \right) - \mathfrak{N}_{-1} \left(\frac{1}{\omega_2 \sigma_s \bar{\gamma}} \right) - \mathfrak{N}_{-1} \left(\frac{1}{\omega_1 \sigma_t \bar{\gamma}} \right) + \mathfrak{N}_{-1}(0) \right] \right. \\
&+ \sum_{k,l \in \{0, \dots, m-1\} \setminus \{k=l=0\}} \frac{(-1)^{k+l}}{k!l! (\omega_2 \sigma_s)^k (\omega_1 \sigma_t)^l \bar{\gamma}^{k+l}} \mathfrak{N}_{k+l-1}(0) \\
&- \sum_{k=1}^{m-1} \frac{(-1)^k}{k!} \left(\frac{1}{\omega_1 \sigma_t \bar{\gamma}} \right)^k \mathfrak{N}_{k-1} \left(\frac{1}{\omega_2 \sigma_s \bar{\gamma}} \right) - \sum_{k=1}^{m-1} \frac{(-1)^k}{k!} \left(\frac{1}{\omega_2 \sigma_s \bar{\gamma}} \right)^k \mathfrak{N}_{k-1} \left(\frac{1}{\omega_1 \sigma_t \bar{\gamma}} \right) \left. \right] \\
&- \frac{\bar{\gamma}}{\omega_2 \sigma_s} \left[\mathfrak{N}_0 \left(\frac{1}{\omega_2 \sigma_s \bar{\gamma}} + \frac{1}{\omega_1 \sigma_t \bar{\gamma}} \right) - \sum_{k=0}^{m-2} \sum_{l=0}^{m-1} \frac{(-1)^{k+l+1}}{k!l! (\omega_2 \sigma_s)^k (\omega_1 \sigma_t)^l \bar{\gamma}^{k+l}} \mathfrak{N}_{k+l}(0) \right. \\
&+ \sum_{k=0}^{m-2} \frac{(-1)^{k+1}}{k!} \left(\frac{1}{\omega_2 \sigma_s \bar{\gamma}} \right)^k \mathfrak{N}_k \left(\frac{1}{\omega_1 \sigma_t \bar{\gamma}} \right) - \sum_{k=0}^{m-1} \frac{(-1)^k}{k!} \left(\frac{1}{\omega_1 \sigma_t \bar{\gamma}} \right)^k \mathfrak{N}_k \left(\frac{1}{\omega_2 \sigma_s \bar{\gamma}} \right) \left. \right] \\
&- \frac{\bar{\gamma}}{\omega_1 \sigma_t} \left[\mathfrak{N}_0 \left(\frac{1}{\omega_2 \sigma_s \bar{\gamma}} + \frac{1}{\omega_1 \sigma_t \bar{\gamma}} \right) - \sum_{k=0}^{m-2} \sum_{l=0}^{m-1} \frac{(-1)^{k+l+1}}{k!l! (\omega_1 \sigma_t)^k (\omega_2 \sigma_s)^l \bar{\gamma}^{k+l}} \mathfrak{N}_{k+l}(0) \right. \\
&+ \sum_{k=0}^{m-2} \frac{(-1)^{k+1}}{k!} \left(\frac{1}{\omega_1 \sigma_t \bar{\gamma}} \right)^k \mathfrak{N}_k \left(\frac{1}{\omega_2 \sigma_s \bar{\gamma}} \right) - \sum_{k=0}^{m-1} \frac{(-1)^k}{k!} \left(\frac{1}{\omega_2 \sigma_s \bar{\gamma}} \right)^k \mathfrak{N}_k \left(\frac{1}{\omega_1 \sigma_t \bar{\gamma}} \right) \left. \right] \left. \right\}, \tag{3.42}
\end{aligned}$$

which can further be simplified as follows

$$\begin{aligned}
C(\bar{\gamma}) &= \frac{\det(\mathbf{\Omega})}{\bar{\gamma} \ln 2 \Delta_2(\mathbf{\Omega}) \Delta_m(\mathbf{\Sigma})} \sum_{s=1}^m \sum_{t=1, t \neq s}^m (-1)^{s+\vartheta(t)} (\sigma_s \sigma_t)^{m-1} \Delta_{m-2}(\sigma^{[s,t]}) \\
&\left\{ -\bar{\gamma}^2 \left[\mathfrak{N}_{-1} \left(\frac{1}{\omega_2 \sigma_s \bar{\gamma}} + \frac{1}{\omega_1 \sigma_t \bar{\gamma}} \right) - \mathfrak{N}_{-1} \left(\frac{1}{\omega_2 \sigma_s \bar{\gamma}} \right) - \mathfrak{N}_{-1} \left(\frac{1}{\omega_1 \sigma_t \bar{\gamma}} \right) + \mathfrak{N}_{-1}(0) \right] \right. \\
&- \left(\frac{\bar{\gamma}}{\omega_2 \sigma_s} + \frac{\bar{\gamma}}{\omega_1 \sigma_t} \right) \mathfrak{N}_0 \left(\frac{1}{\omega_2 \sigma_s \bar{\gamma}} + \frac{1}{\omega_1 \sigma_t \bar{\gamma}} \right) + \frac{\bar{\gamma}}{\omega_2 \sigma_s} \mathfrak{N}_0 \left(\frac{1}{\omega_2 \sigma_s \bar{\gamma}} \right) + \frac{\bar{\gamma}}{\omega_1 \sigma_t} \mathfrak{N}_0 \left(\frac{1}{\omega_1 \sigma_t \bar{\gamma}} \right) \\
&+ \sum_{k=1}^{m-1} \sum_{l=1}^{m-1} \frac{(-1)^{k+l}}{k!l! (\omega_2 \sigma_s)^k (\omega_1 \sigma_t)^l \bar{\gamma}^{k+l-2}} \mathfrak{N}_{k+l-1}(0) \left. \right\}
\end{aligned}$$

$$+ \left. \sum_{k=1}^{m-1} \frac{(-1)^k}{k!} \left[\frac{\bar{\gamma}}{\omega_2 \sigma_s} \left(\frac{1}{\omega_1 \sigma_t \bar{\gamma}} \right)^k \aleph_k \left(\frac{1}{\omega_2 \sigma_s \bar{\gamma}} \right) + \frac{\bar{\gamma}}{\omega_1 \sigma_t} \left(\frac{1}{\omega_2 \sigma_s \bar{\gamma}} \right)^k \aleph_k \left(\frac{1}{\omega_1 \sigma_t \bar{\gamma}} \right) \right] \right\}, \quad (3.43)$$

where $\aleph_n(\mu) = \int_0^\infty t^{n-1} \ln(1+t) e^{-\mu t} dt$. In particular, for the case with positive integer n , $\aleph_n(\mu)$ is given by [106]

$$\aleph_n(\mu) = (n-1)! e^\mu \sum_{k=1}^n \frac{\Gamma(-n+k, \mu)}{\mu^k}, \quad \mu > 0; n = 1, 2, \dots \quad (3.44)$$

where $\Gamma(\cdot, \cdot)$ is the complementary incomplete Gamma function defined by $\Gamma(\alpha, x) = \int_x^\infty t^{\alpha-1} e^{-t} dt$. On the other hand, $\aleph_{-1}(\mu)$ for $\mu > 0$ can be derived as follows

$$\begin{aligned} \aleph_{-1}(\mu) &= \int_0^\infty t^{-2} \ln(1+t) e^{-\mu t} dt \\ &= [-t^{-1} \ln(1+t) e^{-\mu t}]|_0^\infty + \int_0^\infty \frac{t^{-1}}{1+t} e^{-\mu t} dt - \mu \int_0^\infty t^{-1} \ln(1+t) e^{-\mu t} dt \\ &= [-t^{-1} \ln(1+t) e^{-\mu t}]|_0^\infty + \int_0^\infty \frac{t^{-1}}{1+t} e^{-\mu t} dt - \mu \aleph_0(\mu). \end{aligned} \quad (3.45)$$

Now defining $\Xi(\mu) = [-t^{-1} \ln(1+t) e^{-\mu t}]|_0^\infty$ and $\Theta(\mu) = \int_0^\infty \frac{t^{-1}}{1+t} e^{-\mu t} dt$, we can show that for $\mu_1, \mu_2 > 0$, we have

$$\Xi(\mu_1) - \Xi(\mu_2) = 0, \quad (3.46)$$

and

$$\begin{aligned} \Theta(\mu_1) - \Theta(\mu_2) &= \int_0^\infty \left(\frac{1}{t} - \frac{1}{1+t} \right) (e^{-\mu_1 t} - e^{-\mu_2 t}) dt \\ &= \ln \mu_2 - \ln \mu_1 - \int_1^\infty \frac{1}{t} (e^{-\mu_1(t-1)} - e^{-\mu_2(t-1)}) dt \\ &= \ln \mu_2 - \ln \mu_1 - e^{\mu_1} E_1(\mu_1) + e^{\mu_2} E_1(\mu_2), \end{aligned} \quad (3.47)$$

where $E_1(\cdot)$ is the exponential integral function of the first order, defined as $E_1(\mu) = \int_1^\infty \frac{e^{-\mu t}}{t} dt$. Finally, substituting (3.44) and (3.45) into (3.43) and performing further

simplifications, the ergodic capacity can be expressed as

$$\begin{aligned}
C(\bar{\gamma}) &= \frac{\det(\mathbf{\Omega})}{\bar{\gamma} \ln 2 \Delta_2(\mathbf{\Omega}) \Delta_m(\mathbf{\Sigma})} \sum_{s=1}^m \sum_{t=1, t \neq s}^m (-1)^{s+\vartheta(t)} (\sigma_s \sigma_t)^{m-1} \Delta_{m-2}(\sigma^{[s,t]}) \\
&\quad \left\{ -\bar{\gamma}^2 \left[\Theta\left(\frac{1}{\omega_2 \sigma_s \bar{\gamma}} + \frac{1}{\omega_1 \sigma_t \bar{\gamma}}\right) - \Theta\left(\frac{1}{\omega_2 \sigma_s \bar{\gamma}}\right) - \Theta\left(\frac{1}{\omega_1 \sigma_t \bar{\gamma}}\right) \right] \right. \\
&\quad \left. + \sum_{k=1}^{m-1} \frac{(-1)^k}{k!} \left[\frac{\bar{\gamma}}{\omega_2 \sigma_s} \left(\frac{1}{\omega_1 \sigma_t \bar{\gamma}}\right)^k \mathfrak{N}_k\left(\frac{1}{\omega_2 \sigma_s \bar{\gamma}}\right) + \frac{\bar{\gamma}}{\omega_1 \sigma_t} \left(\frac{1}{\omega_2 \sigma_s \bar{\gamma}}\right)^k \mathfrak{N}_k\left(\frac{1}{\omega_1 \sigma_t \bar{\gamma}}\right) \right] \right\} \\
&= \frac{\det(\mathbf{\Omega})}{\bar{\gamma} \ln 2 \Delta_2(\mathbf{\Omega}) \Delta_m(\mathbf{\Sigma})} \sum_{s=1}^m \sum_{t=1, t \neq s}^m (-1)^{s+\vartheta(t)} (\sigma_s \sigma_t)^{m-1} \Delta_{m-2}(\sigma^{[s,t]}) \\
&\quad \left\{ \bar{\gamma}^2 \left[\ln\left(\frac{1}{\omega_2 \sigma_s \bar{\gamma}} + \frac{1}{\omega_1 \sigma_t \bar{\gamma}}\right) - \ln\left(\frac{1}{\omega_2 \sigma_s \bar{\gamma}}\right) - \ln\left(\frac{1}{\omega_1 \sigma_t \bar{\gamma}}\right) \right] \right. \\
&\quad \left. + e^{\frac{1}{\omega_2 \sigma_s \bar{\gamma}} + \frac{1}{\omega_1 \sigma_t \bar{\gamma}}} E_1\left(\frac{1}{\omega_2 \sigma_s \bar{\gamma}} + \frac{1}{\omega_1 \sigma_t \bar{\gamma}}\right) - e^{\frac{1}{\omega_2 \sigma_s \bar{\gamma}}} E_1\left(\frac{1}{\omega_2 \sigma_s \bar{\gamma}}\right) - e^{\frac{1}{\omega_1 \sigma_t \bar{\gamma}}} E_1\left(\frac{1}{\omega_1 \sigma_t \bar{\gamma}}\right) \right] \\
&\quad + \sum_{k=1}^{m-1} \frac{(-1)^k}{k} \left[\left(\frac{1}{\omega_1 \sigma_t}\right)^k e^{\frac{1}{\omega_2 \sigma_s \bar{\gamma}}} \sum_{l=1}^k \bar{\gamma}^{l-k+1} \left(\frac{1}{\omega_2 \sigma_s}\right)^{1-l} \Gamma\left(-k+l, \frac{1}{\omega_2 \sigma_s \bar{\gamma}}\right) \right. \\
&\quad \left. + \left(\frac{1}{\omega_2 \sigma_s}\right)^k e^{\frac{1}{\omega_1 \sigma_t \bar{\gamma}}} \sum_{l=1}^k \bar{\gamma}^{l-k+1} \left(\frac{1}{\omega_1 \sigma_t}\right)^{1-l} \Gamma\left(-k+l, \frac{1}{\omega_1 \sigma_t \bar{\gamma}}\right) \right] \left. \right\}. \quad (3.48)
\end{aligned}$$

The overall ergodic capacity averaging over $\bar{\gamma}$ is also approximated by using the recursive adaptive Simpson quadrature method.

3.4.3 Outage Probability

The outage probability denotes the probability that the output SNR, γ , drops below a predefined SNR threshold γ_{th} . Using the CDF expression of λ_{max} in (3.6), the outage probability as a function of $\bar{\gamma}$, of M-to-M MIMO MRC systems in double-correlated Rayleigh-and-Lognormal fading channels, can be expressed as

$$\begin{aligned}
P_{\text{out}}(\gamma_{\text{th}}, \bar{\gamma}) &= \Pr(\gamma \leq \gamma_{\text{th}}) \\
&= F_{\lambda_{\text{max}}}\left(\frac{\gamma_{\text{th}}}{\bar{\gamma}}\right)
\end{aligned}$$

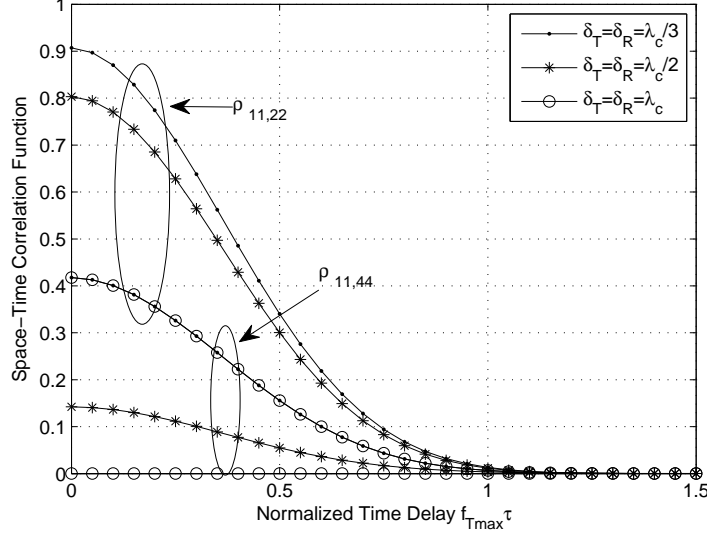


Figure 3.2: Space-time correlation function versus normalized time delay of M-to-M MIMO NLoS channels in the case with $n_T = n_R = 4$.

$$= \frac{\det(\mathbf{\Omega})}{\Delta_2(\mathbf{\Omega}) \Delta_m(\mathbf{\Sigma})} \sum_{s=1}^m \sum_{t=1, t \neq s}^m (-1)^{s+\vartheta(t)} (\sigma_s \sigma_t)^{m-1} \Delta_{m-2}(\sigma^{[s,t]}) Q_{s,t} \left(\frac{\gamma_{\text{th}}}{\bar{\gamma}} \right). \quad (3.49)$$

Taking into account the variation of average SNR per receive antenna $\bar{\gamma}$ due to shadow fading, the outage probability is given by $P_{\text{out}}(\gamma_{\text{th}}) = \int_0^\infty P_{\text{out}}(\gamma_{\text{th}}, \bar{\gamma}) p_{\bar{\gamma}}(\bar{\gamma}) d\bar{\gamma}$. Herein, similar to section 3.4.1, the outage probability can be approximated by using the recursive adaptive Simpson quadrature method.

3.5 Numerical Results

In this section, we present numerical results illustrating the space-time correlation function of the M-to-M MIMO NLoS channel model, as well as the average SEP, outage probability and ergodic capacity of M-to-M MIMO MRC systems. It is assumed that the carrier frequency is 800 MHz, thus the wavelength is $\lambda_c = 0.375$ m. In addition, we set the distance between the centers of T_x and R_x to $D = 200$ m, and the parameters of normalized shadowing spatial correlation function to $A = B = 0.5$. Unless otherwise specified, the other system parameters are as follows: $\delta_T = \lambda_c$,

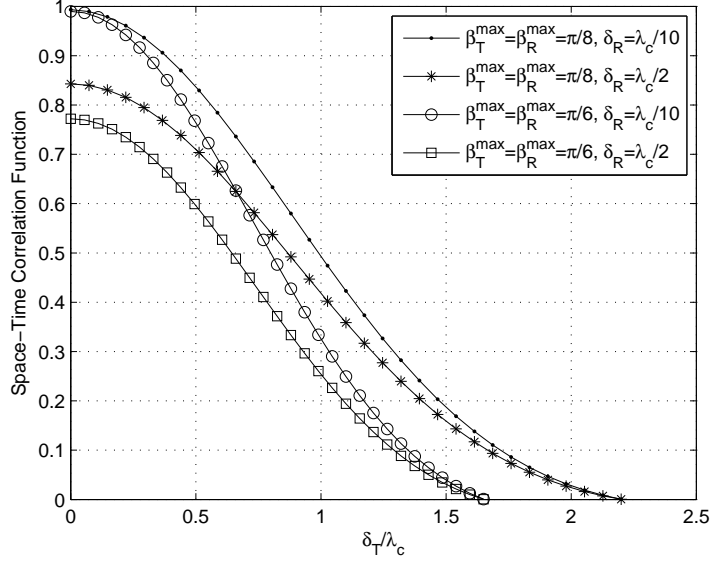


Figure 3.3: Space-time correlation function $\rho_{11,22}(\delta_T, \delta_R, 0)$ for different values of δ_T , δ_R , β_T^{\max} , and β_R^{\max} of M-to-M MIMO NLoS channels in the case with $n_T = n_R = 4$.

$\delta_R = \lambda_c/10$, $\beta_T^{\max} = \beta_R^{\max} = \pi/12$, $\theta_T = \theta_R = \pi/4$, $\zeta_T = \zeta_R = \pi/3$, $\psi_T = 0$, $\psi_R = \pi$, $k_T = k_R = 10$, $f_T^{\max} = f_R^{\max} = 5$, $\mu_T = \pi/2$, and $\mu_R = 3\pi/2$.

First, we examine the space-time correlation function in the case with $n_T = n_R = 4$. Fig. 3.2 shows the variation of $\rho_{11,22}(\delta_T, \delta_R, \tau)$ and $\rho_{11,44}(\delta_T, \delta_R, \tau)$ as a function of the normalized time delay $f_T^{\max}\tau$ for various values of δ_T and δ_R . It can be observed that the correlation decreases as the difference between antenna indices or the distance separating adjacent antenna elements at T_x and R_x , i.e., δ_T and δ_R , become larger. Furthermore, as the normalized time-delay increases, the correlation function converges to zero. It can also be observed that the range of values of normalized time-delay over which the space-time correlation is essentially nonzero, i.e., coherence time, is independent of the values of δ_T and δ_R .

In Fig. 3.3, we illustrate the effects of δ_T , δ_R and maximum elevation angles of the scatterers around T_x and R_x , i.e., β_T^{\max} and β_R^{\max} , on the spatial correlation function $\rho_{11,22}(\delta_T, \delta_R, 0)$. Notice that for a given value of β_T^{\max} and β_R^{\max} , when the spatial correlation function approaches zero, the values of δ_T/λ_c are the same, irrespective of the value of δ_R . However, increasing the maximum elevation angles of the scatterers,

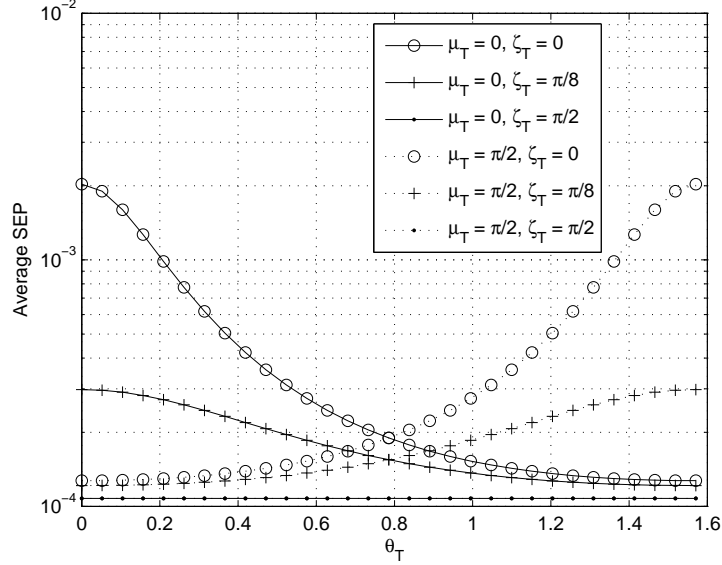


Figure 3.4: Average SEP versus orientation angle θ_T of M-to-M MIMO MRC for different values of ζ_T and μ_T in the case with $n_T = n_R = 2$, $a = 2$, $b = 0.5$ and $\bar{\gamma} = 20$ dB.

β_T^{\max} and β_R^{\max} , from $\pi/8$ to $\pi/6$ makes the non-correlation distance drop from $2.2\lambda_c$ to $1.7\lambda_c$.

We now analyze the effect of the spatial correlation on the average SEP, outage probability and ergodic capacity of M-to-M MIMO MRC system. First, we assess the metrics as a function of the average SNR per receive antenna, $\bar{\gamma}$. Then, results corresponding to the averaging over the variations of $\bar{\gamma}$ are approximated using the recursive adaptive Simpson quadrature method implemented in Matlab.

Fig. 3.4 illustrates the average SEP versus the orientation angle θ_T of T_x antenna arrays in the x-y plane, taking ζ_T as a parameter, for $n_T = n_R = 2$ and $\bar{\gamma} = 20$ dB in the case with $a = 2$ and $b = 0.5$, i.e., QPSK, which is considered hereafter. It can be observed that the average SEP depends on the relative angles between the antenna array and the local scatterers around T_x and R_x , i.e., $|\theta_T - \mu_T|$ and $|\theta_R - \mu_R|$, similar to the phenomenon observed in the outage capacity results presented in [29]. Furthermore, the angles between the x-y plane and the orientation of the T_x and R_x antenna arrays, i.e., ζ_T and ζ_R , play an important role on the SEP performance. For the case with $\zeta_R = \pi/3$, when $\zeta_T = \pi/2$ the average SEP is the lowest and $\theta_T - \mu_T$

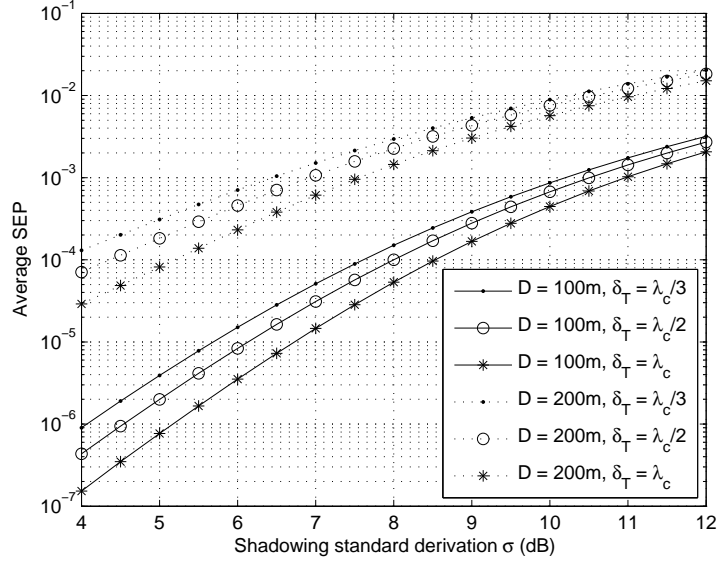


Figure 3.5: Average SEP versus shadowing standard derivation of M-to-M MIMO MRC for different values of D and δ_T in the case with $n_T = n_R = 2$, $r = 3$, $a = 2$ and $b = 0.5$.

has no influence on it. A value of $\zeta_T = 0$ results in the highest SEP. On the other hand, as ζ_T decreases, the average SEP drops dramatically with increasing values of $|\theta_T - \mu_T|$. Similar observations can be made by fixing the value of ζ_T and varying that of ζ_R .

In Fig. 3.5, the average SEP as a function of shadowing standard derivation taking into account the Rayleigh-and-Lognormal fading is shown for different δ_T and D in the case with $n_T = n_R = 2$ and $r = 3$. The total transmit power is $P_0 = -43$ dBm in 5MHz bandwidth. We can see that the average SEP increases as the shadowing standard derivation σ increases. In addition, the average SNR per receive antenna drops as D increases, due to the severe path loss, resulting in worse SEP. Besides, the average SEP drops when the distance between transmit antennas, δ_T , increases.

Fig. 3.6 demonstrates the impact of the degrees of scattering around T_x and R_x in the x-y plane, i.e., k_T , which controls the spread of scatterers around the mean values of α_T , on the outage probability with $n_T = n_R = 2$ and $\bar{\gamma} = 20$ dB, compared to that under uncorrelated Rayleigh fading. As observed, the larger k_T is, the higher the outage probability will be due to the higher non-isotropic scattering. In Fig. 3.7,

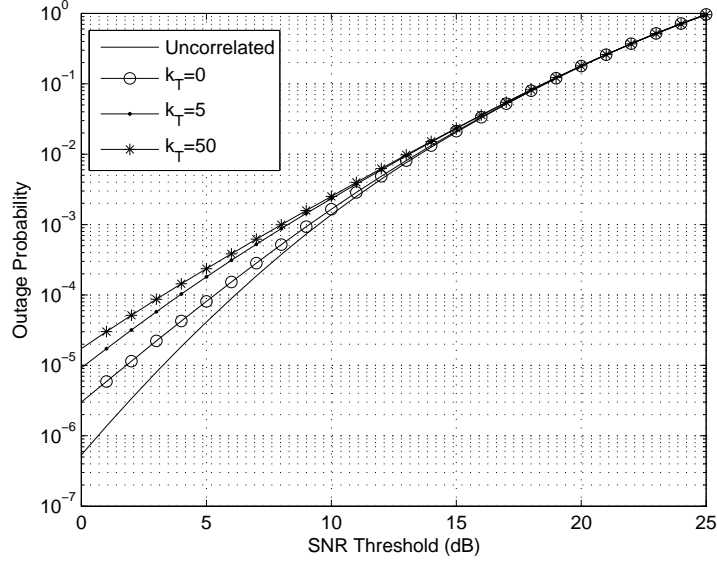


Figure 3.6: Outage probability versus SNR threshold of M-to-M MIMO MRC for different value of k_T in the case with $n_T = n_R = 2$ and $\bar{\gamma} = 20$ dB.

we examine the effect of pathloss exponent r and maximum elevation angle β_T^{\max} on the outage probability in the scenario with $n_T = n_R = 2$ and $\sigma = 8$ dB. As observed, increasing r results in a degradation of the outage probability. Also, the higher β_T^{\max} is, the lower the outage probability will be. Note that the impact of r is more severe than that of β_T^{\max} , meaning that the effect of pathloss on performance is more visible than that of spatial correlation.

Finally Fig. 3.8 plots the ergodic capacity as a function of the average SNR per receive antenna for the case with $n_T = n_R = 2$. It is observed that increasing the maximum elevation angle β_T^{\max} yields a favorable influence on the ergodic capacity. Additionally, shadowing results in a reduction in the ergodic capacity; a decrease that is not of major significance as it can be seen from the plots. In this figure, results corresponding to the case with no CSI at the transmitter and perfect CSI at the receiver, pertaining to the MIMO system with no MRC, are plotted to serve as reference and quantify the advantages of MRC.

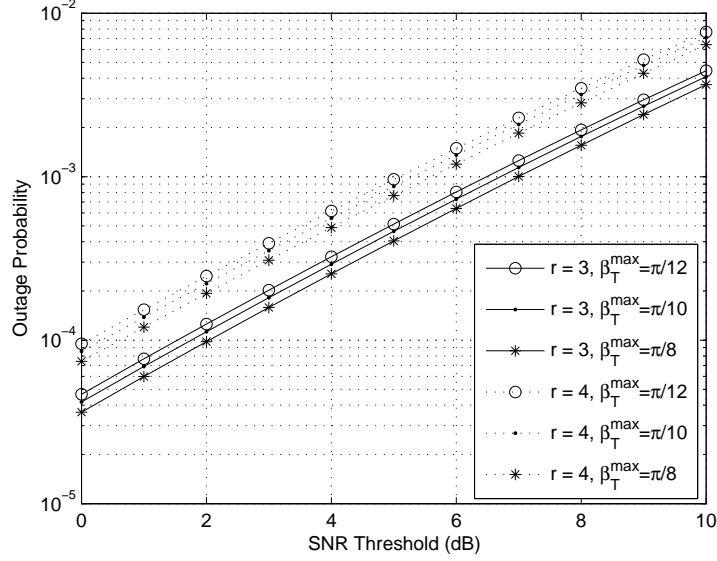


Figure 3.7: Outage probability versus SNR threshold of M-to-M MIMO MRC for different values of β_T^{\max} and r in the case with $n_T = n_R = 2$ and $\sigma = 8$ dB.

3.6 Summary

In this chapter, the performance of M-to-M MIMO MRC systems in double-correlated channels was evaluated in terms of average SEP, ergodic capacity and outage probability. The receive and transmit correlation functions were investigated taking into account fast fading and shadowing in a 3D M-to-M MIMO channel model. Furthermore, numerical results and comparisons were presented to illustrate the effects of various parameters on the system performance. In particular, the average SEP performance as a function of the relative angles between the antenna array and the local scatterers around the transmitter and receiver, i.e., $|\theta_T - \mu_T|$ and $|\theta_R - \mu_R|$, was shown to decrease dramatically with increasing values of $|\theta_T - \mu_T|$ when the angle between the x-y plane and the transmit antenna array orientation decreases. In addition, the average SEP increases as the shadowing standard deviation increases. It was also shown that the larger the degree of scattering around the transmitter in the x-y plane is, the higher the outage probability will be due to the higher non-isotropic scattering, and that the effect of path loss on performance is more visible than that of spatial correlation.

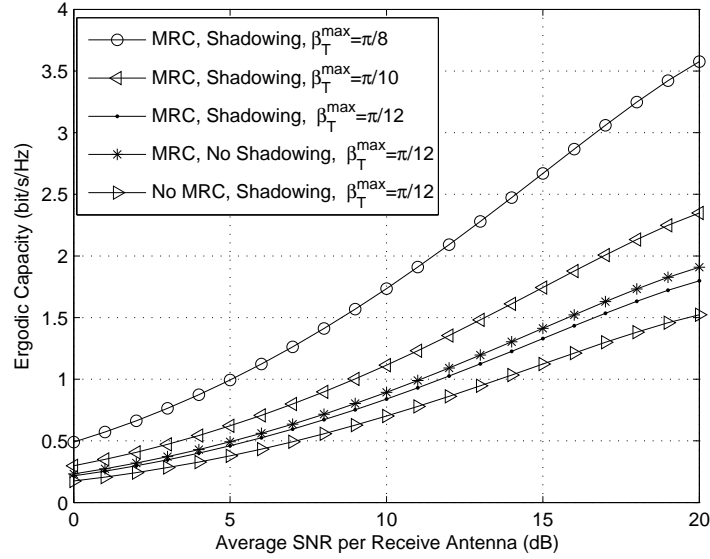


Figure 3.8: Ergodic capacity versus average SNR per receive antenna of M-to-M MIMO MRC for different values of β_T^{\max} in the case with $n_T = n_R = 2$.

In addition to the channel impairments investigated in Chapters 2 and 3, RF impairments, such as HPA nonlinearity, I/Q imbalance and crosstalk, also affect the performance of MIMO wireless communication systems. Analysis and compensation of these kinds of RF impairments will be investigated in the following chapters.

Chapter 4

Analysis and Compensation of HPA Nonlinearity

HPA represents a crucial block of wireless communication systems, which operates at the RF level. In general, the HPA is assumed to operate in its linear region in order to ensure that the characteristics of the symbols at the modulator's output are not affected by the power amplification process, when carrying out design and performance analysis of wireless communication systems.

However, in practice, the HPA may operate in its nonlinear region, especially when it operates at the medium and high-power signal levels. Indeed, in such cases, nonlinear distortions, including amplitude and phase distortions, are introduced into the transmitted symbols, which in turn can cause adjacent channel interference and power losses. Therefore, the nonlinearity of HPA has a crucial effect on the performance of MIMO wireless communication systems.

Review of current research on the performance analysis and compensation methods for HPA nonlinearity has been presented in Section 1.1.4.

4.1 Analysis and Compensation of HPA Nonlinearity in MIMO OSTBC Systems

In this section, we focus on HPA nonlinearity in OSTBC systems. For the case when the HPA parameters are perfectly known at the transmitter and receiver, we propose a compensation scheme that derives the constellation and decision regions of the distorted transmitted signal in advance. In this way, the complexity of the transmitter can be efficiently reduced by using the proposed compensation scheme, compared to other compensation methods implemented at the transmitter only, which is crucial for system implementation, especially in uplink transmission scenarios. For the outlined transmission chain, we derive the expressions for the average SEP and the TD, and obtain upper and lower bounds on the system capacity, which are valued for memoryless nonlinear HPA models, considering operation under quasi-static frequency-flat uncorrelated Nakagami- m fading. In some cases, the parameters of the nonlinear HPAs may be unknown or time-varying due to manufacturing or environmental variations such as aging and temperature [107]. In this scenario, the SMC method was employed to compensate for the nonlinearity of SSPA in single-antenna systems over AWGN channels without fading [107]. The SMC (or particle filtering) technique is a common recursive computation of relevant probability distributions using the concept of importance sampling and approximation of probability distributions with discrete random measures (see [108–112] and references therein). In this section, we also propose a compensation algorithm for HPA nonlinearity in MIMO-OSTBC systems without knowledge of the HPA parameters. Specifically, the channel gain matrix is first estimated by means of the SMC method. Then, we make use of the SMC-based algorithm to detect the desired signal. Numerical and simulation results along with comparisons for the cases with and without knowledge of the HPA parameters are provided, and show the effects of system parameters, such as the parameters of the HPA model, OBO of nonlinear HPA, numbers of transmit and receive antennas, QAM modulation order, and number of SMC samples, on the MIMO-OSTBC system performance.

Accordingly, the contribution of this section can be seen in several respects: (i) we propose a compensation method for HPA nonlinearity in MIMO OSTBC systems when the HPA parameters are known at the transmitter and receiver. Specifically, we take the signals distorted due to HPA nonlinearity as the signals to be detected using the maximum likelihood (ML) method, where the decision regions for the ML decoding are determined as per the constellation of the distorted signals. The proposed constellation-based compensation method can efficiently mitigate the effect of HPA nonlinearity compared to the usual case, where the original signals before the nonlinear HPAs are taken as the desired signals and detected using the ML rule. Furthermore, the system performance is investigated in terms of average SEP, TD and system capacity, for which analytical expressions are derived; (ii) in the case without knowledge of the HPA parameters, a SMC-based compensation method for the HPA nonlinearity in the considered MIMO OSTBC system is proposed, which first estimates the channel gain matrix by means of the SMC method, and then uses the SMC-based algorithm to detect the desired signal. The proposed SMC-based detection scheme is shown to be efficient in compensating the HPA nonlinearity in the case without knowledge of the HPA parameters.

The remainder of Section 4.1 is organized as follows: Section 4.1.1 introduces the MIMO-OSTBC system model and the models for memoryless nonlinear HPAs. In Section 4.1.2, we propose a constellation-based compensation method for HPA nonlinearity in the case when the knowledge of the HPA parameters is available, and evaluate the system performance in terms of average SEP, TD and capacity. The SMC-based compensation algorithm in the case without knowledge of the HPA parameters is presented in 4.1.3. Numerical and simulation results are then presented in Section 4.1.4.

4.1.1 System and HPA Models

We consider a MIMO-OSTBC system equipped with n_T transmit and n_R receive antennas, and assume a discrete-time baseband channel model subject to quasi-static frequency-flat Nakagami- m fading. The channel state remains constant in each frame

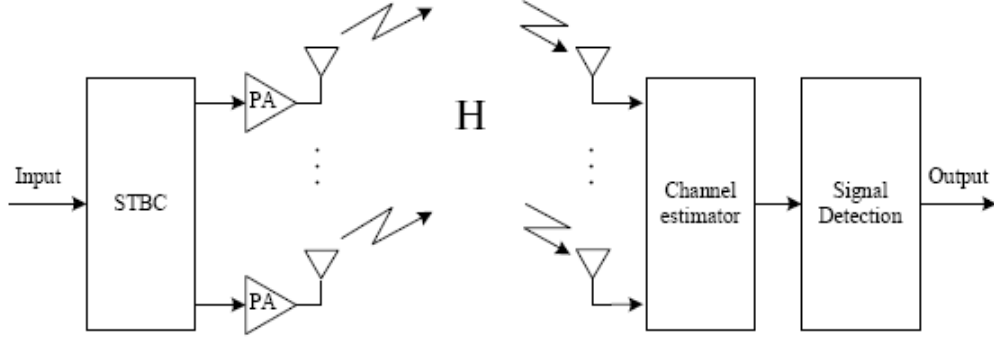


Figure 4.1: Block diagram for the considered MIMO-OSTBC system in the presence of nonlinear HPA.

with T symbol durations and may vary from frame to frame, where T denotes the time duration of the OSTBC transmission matrix. The received signal within one frame can be expressed as

$$\mathbf{Y} = \mathbf{H}\mathbf{X} + \mathbf{N}, \quad (4.1)$$

where \mathbf{Y} denotes the $n_R \times T$ received signal matrix, \mathbf{X} stands for the $n_T \times T$ transmitted symbol matrix, \mathbf{N} represents the $n_R \times T$ noise matrix with elements belonging to independent and identically distributed (i.i.d.) complex Gaussian distribution $\mathcal{CN}(0, N_0)$ uncorrelated with the transmitted symbols, and $\mathbf{H} = [h_{k,l}]_{k,l=1}^{n_R, n_T}$ indicates the $n_R \times n_T$ channel gain matrix with $h_{k,l}$ representing the channel coefficient between the l th transmit and k th receive antennas. OSTBC is designed to transmit R complex input symbols in T time slots, hence the information code rate is given by $R_c = R/T$. The block diagram for the considered MIMO-OSTBC system is shown in Fig. 4.1.

In the transmission scheme, the modulated signal is amplified by the HPA at the RF module. In practice, the HPA may operate in its nonlinear region, thus causing amplitude distortion and phase distortion on the transmitted data. Specifically, denote the polar coordinates of the input signal, x , as

$$x = re^{j\theta}, \quad (4.2)$$

where r and θ are the amplitude and phase of x , respectively, and $j^2 = -1$. Then,

the symbol at the output of the nonlinear HPA can be expressed as

$$\hat{x} = f_A(r) e^{j f_P(r)} e^{j\theta}, \quad (4.3)$$

where functions $f_A(\cdot)$ and $f_P(\cdot)$ denote the AM/AM and AM/PM conversions, respectively. Next, we introduce these functions for three different HPA models.

The TWTA can be characterized by the Saleh model, whose AM/AM and AM/PM functions are given by [35]:

$$f_A(r) = A_{is}^2 \frac{r}{r^2 + A_{is}^2}, \quad f_P(r) = \frac{\pi}{3} \frac{r^2}{r^2 + A_{is}^2}, \quad (4.4)$$

where A_{is} represents the input saturation voltage.

The AM/AM and AM/PM conversions of the SSPA model [36] can be expressed as:

$$f_A(r) = \frac{r}{\left[1 + \left(\frac{r}{A_{os}}\right)^{2\beta}\right]^{1/2\beta}}, \quad f_P(r) = 0, \quad (4.5)$$

where A_{os} represents the output saturation voltage, and β indicates the smoothness of the transition from linear operation to saturation.

The SEL, used to model the HPA with ideal predistortion, can be described by the following AM/AM and AM/PM functions [37]:

$$f_A(r) = \begin{cases} r, & r \leq A_{is} \\ A_{is}, & r > A_{is} \end{cases} \quad f_P(r) = 0. \quad (4.6)$$

Note that $A_{is} = A_{os}$ for the SEL model.

4.1.2 Signal Detection with Knowledge of the HPA Parameters

Recall that our objective is to detect the desired signal in the presence of nonlinear HPA. The behavior of the HPA plays an important role in the data detection process. In this section, the HPA parameters are assumed to be perfectly known at the transmitter and receiver. The scenario without knowledge of the HPA parameters at the transmitter and receiver will be considered in Section 4.1.3.

In this section, for simplicity of the analysis, the HPAs at all the transmitting branches are assumed to exhibit the same nonlinear behavior. As such, the MIMO-OSTBC signal model (4.1) in the presence of HPA nonlinearity can be rewritten as

$$\mathbf{Y} = \mathbf{H}\hat{\mathbf{X}} + \mathbf{N}, \quad (4.7)$$

where $\hat{\mathbf{X}}$ denotes the distorted version of the transmitted symbol matrix. Let P_0 denote the average transmit power per symbol duration over the n_T transmit antennas, then we may define the pre-processing average signal-to-noise ratio (SNR) as $\bar{\gamma} = P_0/N_0$. Thus, the average power per symbol is given by $P_s = E[r^2] = \frac{P_0}{cn_T R_c}$, where $E[\cdot]$ denotes the expectation operator, and c is a code-dependent constant based on the OSTBC mapping. Consequently, the average power per symbol at the output of the nonlinear HPA can be expressed as $P_s^{\text{HPA}} = E[f_A^2(r)]$. The relationship between P_s^{HPA} and $\bar{\gamma}$ depends on the HPA characteristics and the distribution of the input symbol power. Based on the system model described in (4.7), the channel gain matrix can be estimated using the minimum mean square error (MMSE) or LS rules as in the case with linear HPA. It is assumed in this section that the channel gain matrix is perfectly estimated at the receiver.

In this following, we investigate the performance of MIMO-OSTBC systems over uncorrelated Nakagami- m fading channels in the presence of HPA nonlinearity, in terms of average SEP and system capacity.

PDF of the Output SNR

Owing to the decoupling property of the signals transmitted through the different antennas, the MIMO-OSTBC model can be converted into an equivalent SISO scalar one, yielding

$$y = c \|\mathbf{H}\|_F^2 \hat{x} + \tilde{n}, \quad (4.8)$$

where $\|\cdot\|_F$ denotes the Frobenius norm, \hat{x} represents the distorted version of the transmitted symbol with average power P_s^{HPA} , and \tilde{n} is the noise term after OSTBC decoding with distribution $\mathcal{CN}(0, c \|\mathbf{H}\|_F^2 N_0)$. Then, the effective SNR at the output of the decoder can be expressed as

$$\begin{aligned} \gamma^{\text{STBC}} &= \frac{c^2 \|\mathbf{H}\|_F^4 E[f_A^2(r)]}{c \|\mathbf{H}\|_F^2 N_0} \\ &= \frac{c E[f_A^2(r)]}{N_0} \|\mathbf{H}\|_F^2. \end{aligned} \quad (4.9)$$

The channel coefficient between the l th transmit and k th receive antennas is defined as $h_{k,l} \triangleq \alpha_{k,l} e^{j\varphi_{k,l}}$, where $\alpha_{k,l}$ and $\varphi_{k,l}$ denote the path gain and phase, respectively. Under Nakagami- m fading, the probability density function (PDF) of the $\mathcal{K} = n_T n_R$ path gains $\alpha_{k,l}$ is given by [91]

$$p_{\alpha_{k,l}}(\alpha) = 2 \left(\frac{m}{\Omega_{k,l}} \right)^m \frac{\alpha^{2m-1}}{\Gamma(m)} \exp\left(-m \frac{\alpha^2}{\Omega_{k,l}}\right), \quad \alpha \geq 0, \quad (4.10)$$

where $\Gamma(\cdot)$ denotes the Gamma function, $m \geq 1/2$, and $\Omega_{k,l} = E[\alpha_{k,l}^2] = m$ represents the average fading power. The phase $\varphi_{k,l}$ pertaining to $h_{k,l}$ is uniformly distributed over $[0, 2\pi)$. Using the Frobenius norm definition, the effective output SNR of the MIMO-OSTBC system can be rewritten as

$$\gamma^{\text{STBC}} = \frac{c E[f_A^2(r)]}{N_0} \sum_{k=1}^{n_R} \sum_{l=1}^{n_T} \gamma_{k,l}, \quad (4.11)$$

where $\gamma_{k,l} \triangleq \alpha_{k,l}^2$ denotes the elementary fading power corresponding to the path between the l th transmit and k th receive antennas. Then, the PDF of the output

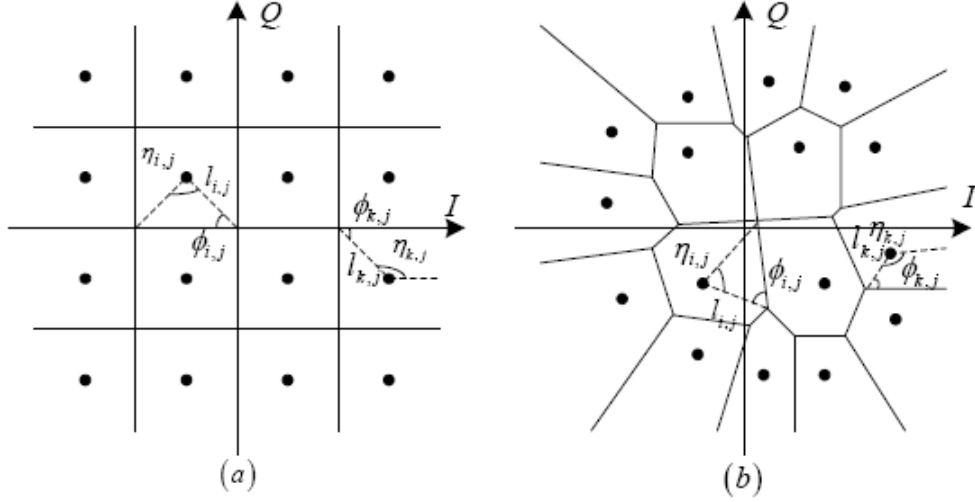


Figure 4.2: Rectangular 16-QAM constellation and decision regions: (a) ideal case, (b) with HPA distortion.

SNR for the MIMO-OSTBC system with nonlinear HPA can be expressed as

$$p_{\gamma_{\text{STBC}}}(\gamma) = \frac{\gamma^{m\mathcal{K}-1}}{\Gamma(m\mathcal{K})} \left\{ \frac{N_0}{cE[f_A^2(r)]} \right\}^{m\mathcal{K}} \exp \left\{ -\frac{N_0\gamma}{cE[f_A^2(r)]} \right\}. \quad (4.12)$$

Average SEP

We recall that the HPA nonlinearity results in amplitude and phase distortions in the input signal. Hence, the constellation and decision regions of arbitrary two-dimensional modulation get changed as compared to the ideal case where the power amplification process is assumed linear. Note that the ML detection method used for the ideal case can be also applied for the OSTBC system with nonlinear HPA. However, the decision regions for the ML decoding are changed as per the constellation of the distorted signals. An example illustrating such distortion is shown in Fig. 4.2, where we present the constellation and decision regions of rectangular 16-QAM without and with HPA distortion.

Based on the constellation and decision regions of the distorted version of the transmitted signal, the SEP, as a function of the instantaneous output SNR for arbitrary two-dimensional modulations, can be expressed using the Craig's method [113],

according to

$$P_s(\gamma) = \sum_{i=1}^M \sum_{j=1}^{D_i} \frac{P(s_i)}{2\pi} \int_0^{\eta_{i,j}} \exp \left[-\frac{c_{i,j} \gamma \sin^2 \phi_{i,j}}{\sin^2(\vartheta + \phi_{i,j})} \right] d\vartheta, \quad (4.13)$$

where M denotes the number of symbols in the constellation, $P(s_i)$ represents the *a priori* probability that symbol s_i is transmitted, D_i is the number of sub-regions for symbol s_i , γ refers to the output SNR of the MIMO-OSTBC system, and $c_{i,j} = l_{i,j}/E[f_A^2(r)]$ is the scaling factor. Parameters $l_{i,j}$, $\eta_{i,j}$ and $\phi_{i,j}$ are related to symbol s_i and sub-region j , and determined by the decision region geometry [113].

The average SEP using such decision region boundaries can be found using

$$P_s = \int_0^\infty P_s(\gamma) p_{\gamma^{\text{STBC}}}(\gamma) d\gamma. \quad (4.14)$$

Substituting (4.13) into (4.14) and making use of the moment generating function (MGF)-based approach [114], the average SEP can be rewritten as

$$P_s = \sum_{i=1}^M \sum_{j=1}^{D_i} \frac{P(s_i)}{2\pi} \int_0^{\eta_{i,j}} \Psi_{\gamma^{\text{STBC}}} \left[-\frac{c_{i,j} \sin^2 \phi_{i,j}}{\sin^2(\vartheta + \phi_{i,j})} \right] d\vartheta, \quad (4.15)$$

where $\Psi_{\gamma^{\text{STBC}}}(j\omega)$ denotes the characteristic function of γ^{STBC} and is given by

$$\Psi_{\gamma^{\text{STBC}}}(j\omega) = \left\{ 1 - j\omega \frac{cE[f_A^2(r)]}{N_0} \right\}^{-m\kappa}. \quad (4.16)$$

Then, substituting (4.16) into (4.15), the average SEP of MIMO-OSTBC over uncorrelated Nakagami- m fading channels with HPA nonlinearity can be expressed as

$$P_s = \sum_{i=1}^M \sum_{j=1}^{D_i} \frac{P(s_i)}{2\pi} \int_0^{\eta_{i,j}} \left\{ \frac{\sin^2(\vartheta + \phi_{i,j})}{\sin^2(\vartheta + \phi_{i,j}) + c_{i,j} \gamma \sin^2 \phi_{i,j} \frac{cE[f_A^2(r)]}{N_0}} \right\}^{m\kappa} d\vartheta. \quad (4.17)$$

Finally, making use of [114, App. C], the expression for the average SEP of the

considered system can be obtained as

$$\begin{aligned}
P_s = & \sum_{i=1}^M \sum_{j=1}^{D_i} \frac{P(s_i)}{2\pi} \left\{ \eta_{i,j} + \phi_{i,j} - \beta_{i,j} \left[\left(\frac{\pi}{2} + \arctan \alpha_{i,j} \right) \right. \right. \\
& \times \sum_{k=0}^{m\mathcal{K}-1} \binom{2k}{k} \frac{1}{4^k (1 + \zeta_{i,j})^k} + \sin(\arctan \alpha_{i,j}) \\
& \left. \left. \times \sum_{k=1}^{m\mathcal{K}-1} \sum_{l=1}^k \frac{T_{l,k}}{(1 + \zeta_{i,j})^k} (\cos(\arctan \alpha_{i,j}))^{2(k-l)+1} \right] \right\}, \quad (4.18)
\end{aligned}$$

where $\zeta_{i,j} = c_{i,j} \frac{cE[f_A^2(r)]}{N_0} \sin^2 \phi_{i,j}$, $\beta_{i,j} = \sqrt{\frac{\zeta_{i,j}}{1+\zeta_{i,j}}} \operatorname{sgn}(\eta_{i,j} + \phi_{i,j})$, $\alpha_{i,j} = -\beta_{i,j} \cot(\eta_{i,j} + \phi_{i,j})$, and

$$T_{l,k} = \binom{2k}{k} \Big/ \left[\binom{2(k-l)}{k-l} 4^l (2(k-l) + 1) \right].$$

Total Degradation

The TD is a performance metric that quantifies the degradation due to the non-linear distortion, and is defined by [115]

$$\text{TD(dB)} = \bar{\gamma}_T^{\text{NL}}(\text{dB}) - \bar{\gamma}_T^{\text{L}}(\text{dB}) + \text{OBO(dB)}, \quad (4.19)$$

where $\text{OBO(dB)} = f_A^2(A_{is})(\text{dB}) - E[f_A^2(r)](\text{dB})$ denotes the difference in decibels between the maximum output power and the effective mean output power pertaining to the HPA module, and where $\bar{\gamma}_T^{\text{NL}}(\text{dB})$ and $\bar{\gamma}_T^{\text{L}}(\text{dB})$ are the pre-processing average SNR required to meet the target SEP with and without HPA nonlinearity, respectively.

System Capacity

Under the assumption that the transmitter does not have knowledge of the channel gain matrix, the capacity of the MIMO-OSTBC system in the presence of HPA

nonlinearity can be expressed in [bps/Hz] as [116]

$$\begin{aligned} C &= R_c E_{\mathbf{H}} \left[\max_{P(x|\mathbf{H})} I(y; x | \mathbf{H}) \right] \\ &= R_c E_{\mathbf{H}} \left[\max_{P(x|\mathbf{H})} h(y | \mathbf{H}) - h(y | x, \mathbf{H}) \right], \end{aligned} \quad (4.20)$$

where $P(x | \mathbf{H})$ denotes the probability distribution of the input signal x given \mathbf{H} , $I(y; x | \mathbf{H})$ refers to the mutual information between the received signal y and the transmitted signal x given \mathbf{H} , and $h(\cdot)$ represents the entropy function.

1) Upper Bound

In the scenario where the nonlinearity coefficients are deterministic and known at the transmitter, the distorted version of the transmitted signal, \hat{x} , is fixed (given x). Therefore, the remaining uncertainty at the output is only the noise term with complex Gaussian distribution (\tilde{n} expressed in (4.8)). Then, the entropy $h(y | x, \mathbf{H})$ is given by

$$h(y | x, \mathbf{H}) = \log_2 2\pi e c N_0 \|\mathbf{H}\|_F^2. \quad (4.21)$$

On the other hand, due to the fact that the Gaussian distribution maximizes the corresponding entropy over all the distributions with the same variance, the entropy $h(y | \mathbf{H})$ can be upper bounded as follows:

$$\begin{aligned} h(y | \mathbf{H}) &\leq \log_2 2\pi e \left[c^2 \|\mathbf{H}\|_F^4 E[f_A^2(r)] + c \|\mathbf{H}\|_F^2 N_0 \right] \\ &= \log_2 2\pi e \left[c^2 \|\mathbf{H}\|_F^4 E\left[f_A^2\left(\sqrt{r^2}\right)\right] + c \|\mathbf{H}\|_F^2 N_0 \right] \\ &\leq \log_2 2\pi e \left[c^2 \|\mathbf{H}\|_F^4 f_A^2\left(\sqrt{E(r^2)}\right) + c \|\mathbf{H}\|_F^2 N_0 \right] \\ &= \log_2 2\pi e \left[c^2 \|\mathbf{H}\|_F^4 f_A^2\left(\sqrt{\frac{N_0 \bar{\gamma}}{c n_T R_c}}\right) + c \|\mathbf{H}\|_F^2 N_0 \right], \end{aligned} \quad (4.22)$$

where the second inequality is obtained by applying the Jensen's inequality, using the fact that $g(x) = \sqrt{x}$ and each type of the AM/AM conversion functions ($f_A(\cdot)$ presented in Section 4.1.1) are convex [34]. Note that in this case, the signal at the

output of the nonlinear HPA is Gaussian distributed. Substituting (4.21) and (4.22) into (4.20), we obtain the following upper bound on the system capacity

$$C_{\text{up}} = R_c E_{\mathbf{H}} \left\{ \log_2 \left[1 + \|\mathbf{H}\|_F^2 \frac{c f_A^2 \left(\sqrt{\frac{N_0 \bar{\gamma}}{c n_T R_c}} \right)}{N_0} \right] \right\}. \quad (4.23)$$

Consequently, making use of [106, App. B], an upper bound on the system capacity of the MIMO-OSTBC system over uncorrelated Nakagami- m channels taking into account the HPA nonlinearity is given by

$$C_{\text{up}} = R_c \log_2(e) \exp \left[\frac{N_0}{c f_A^2 \left(\sqrt{\frac{N_0 \bar{\gamma}}{c n_T R_c}} \right)} \sum_{j=1}^{m\mathcal{K}} E_{m\mathcal{K}+1-j} \left[\frac{N_0}{c f_A^2 \left(\sqrt{\frac{N_0 \bar{\gamma}}{c n_T R_c}} \right)} \right] \right], \quad (4.24)$$

where $E_l(u) = \int_1^\infty \frac{e^{-ux}}{x^l} dx$ denotes the exponential integral function.

2) Lower Bound

Using Bussgang's theorem [117], when the transmitted symbol x is Gaussian distributed, the output of the nonlinear HPA can be expressed as [41]

$$\hat{x} = K_0 x + d, \quad (4.25)$$

where K_0 denotes a deterministic complex factor, and d is an additive zero-mean Gaussian noise uncorrelated with the input signal x .

The value of K_0 is given by [41, eq. (19)]

$$K_0 = \frac{1}{2} E \left[\hat{x}'(r) + \frac{\hat{x}(r)}{r} \right], \quad (4.26)$$

where $\hat{x}'(r)$ denotes the differential of $\hat{x}(r)$. Furthermore, the variance of d is given by [41, eq. (37)]

$$\sigma_d^2 = E[f_A^2(r)] - |K_0|^2 E(r^2). \quad (4.27)$$

Specifically, for the SEL model, the values of K_0 and σ_d^2 can be obtained using [41, eq.

(42)] as follows:

$$K_0 = 1 - e^{-\lambda^2} + \frac{1}{2}\sqrt{\pi}\lambda\text{erfc}(\lambda), \quad (4.28)$$

$$\sigma_d^2 = P_s \left[1 - e^{-\lambda^2} - K_0^2 \right], \quad (4.29)$$

where $\lambda = A_{is}/\sqrt{P_s}$ denotes the clipping level. In addition, the evaluation of parameters K_0 and σ_d^2 for the TWTA and SSPA models are listed in [41, Table I].

Then, a lower bound on the system capacity can be expressed as

$$\begin{aligned} C_{\text{low}} &= R_c E_{\mathbf{H}} \left[\log_2 \left(\frac{c^2 \|\mathbf{H}\|_F^4 (|K_0|^2 P_s + \sigma_d^2) + c \|\mathbf{H}\|_F^2 N_0}{c^2 \|\mathbf{H}\|_F^4 \sigma_d^2 + c \|\mathbf{H}\|_F^2 N_0} \right) \right] \\ &= R_c E_{\mathbf{H}} \left[\log_2 \left(1 + c \|\mathbf{H}\|_F^2 \frac{|K_0|^2 P_s + \sigma_d^2}{N_0} \right) \right] - R_c E_{\mathbf{H}} \left[\log_2 \left(1 + c \|\mathbf{H}\|_F^2 \frac{\sigma_d^2}{N_0} \right) \right]. \end{aligned} \quad (4.30)$$

Finally, making use of [106, App. B], the lower bound on the system capacity is given by

$$C_{\text{low}} = R_c \log_2(e) e^\mu \sum_{j=1}^{m\mathcal{K}} E_{m\mathcal{K}+1-j}(\mu) - R_c \log_2(e) e^{\frac{N_0}{c\sigma_d^2}} \sum_{j=1}^{m\mathcal{K}} E_{m\mathcal{K}+1-j} \left(\frac{N_0}{c\sigma_d^2} \right), \quad (4.31)$$

where $\mu = \frac{N_0}{c(|K_0|^2 P_s + \sigma_d^2)}$.

4.1.3 SMC Receiver without Knowledge of the HPA Parameters

In Section 4.1.2, we studied the signal detection and system performance of MIMO-OSTBC systems for the case when the HPA parameters are perfectly known at the transmitter and receiver. However, the parameters of the nonlinear HPAs may be sometimes unknown or time-varying. These variations are due to handover processes as in cellular networks, manufacturing limitations, or environmental effects such as temperature and aging [107]. In this section, we propose a compensation algorithm for HPA nonlinearity in MIMO-OSTBC systems without knowledge of the HPA pa-

rameters. First of all, the channel gain matrix is estimated by means of the SMC method. Then, we make use of the SMC technique to detect the desired signal.

SMC-Based Channel Estimation

It is assumed that the channel is quasi-static, which implies that the channel gain matrix remains invariant in each frame transmission and may vary from frame to frame. Based on this, $n_T \times N_p$ pilot symbol matrix, \mathbf{X}_p , with power ξ_p for each pilot symbol, is inserted at the beginning of each transmit frame in order to perform the channel estimation. In the presence of HPA nonlinearity, the received signal model for the pilot symbols can be expressed as

$$\mathbf{Y}_p = \mathbf{H}\hat{\mathbf{X}}_p + \mathbf{N}_p, \quad (4.32)$$

where \mathbf{Y}_p denotes the $n_R \times N_p$ received signal matrix, \mathbf{N}_p represents the $n_R \times N_p$ noise matrix with elements belonging to i.i.d. complex circular Gaussian distribution $\mathcal{CN}(0, N_0)$ uncorrelated with the transmitted pilot symbols, \mathbf{H} expresses the same $n_R \times n_T$ channel gain matrix as for the data symbol transmission, and $\hat{\mathbf{X}}_p$ is the $n_T \times N_p$ transmitted pilot symbols amplified by the nonlinear HPAs.

Herein, we use the LS method to estimate the unknown channel coefficients, \mathbf{H} . The LS estimate of \mathbf{H} is given by [118]

$$\hat{\mathbf{H}}_{LS} = \arg \min_{\hat{\mathbf{H}}} \left\| \hat{\mathbf{H}}\hat{\mathbf{X}}_p - \mathbf{Y}_p \right\|_F^2. \quad (4.33)$$

Since the parameters of the nonlinear HPAs are unknown or time-varying, it is not straightforward to obtain a closed-form solution for the above estimation problem. Instead, we apply the well-known Rao-Blackwellization technique (see [107, 110]) to tackle the channel estimation problem, according to

$$\hat{\mathbf{H}}_{LS} = \arg \min_{\hat{\mathbf{H}}} \int \left\| \hat{\mathbf{H}}\hat{\mathbf{X}}_p(\Psi) - \mathbf{Y}_p \right\|_F^2 p(\Psi) d\Psi, \quad (4.34)$$

where $p(\Psi)$ represents the PDF of Ψ , $\Psi = \{\psi_1, \psi_2, \dots, \psi_{n_T}\}$, with ψ_l denoting the

set of the HPA parameters at the l th transmit antenna, and $\hat{\mathbf{X}}_p(\Psi)$ is the amplified signal matrix as a function of Ψ . For instance, $\psi_l = \{A_{is}\}$ for the TWTA model, $\psi_l = \{A_{os}, \beta\}$ for the SSPA model, and $\psi_l = \{A_{is}\}$ for the SEL model. Since the solution derivation for (4.34) is not straightforward due to the integral over Ψ , we use the SMC method to obtain the estimate of the channel gain matrix. Specifically, the PDF of Ψ is approximated by

$$p(\Psi) \approx \frac{1}{W} \sum_{i_1=1}^N \sum_{i_2=1}^N \cdots \sum_{i_{n_T}=1}^N w_{i_1, i_2, \dots, i_{n_T}} \delta(\Psi - \Psi_{i_1, i_2, \dots, i_{n_T}}), \quad (4.35)$$

where $\delta(\cdot)$ denotes the Dirac delta function, $\Psi_{i_1, i_2, \dots, i_{n_T}} = \{\psi_{i_1}, \psi_{i_2}, \dots, \psi_{i_{n_T}}\}$ is a random sample of the parameter set Ψ , and $W = \sum_{i_1=1}^N \sum_{i_2=1}^N \cdots \sum_{i_{n_T}=1}^N w_{i_1, i_2, \dots, i_{n_T}}$ with $w_{i_1, i_2, \dots, i_{n_T}}$ indicating the weight of the sample $\Psi_{i_1, i_2, \dots, i_{n_T}}$. Herein, a *properly weighted sample* is defined as the pair $(\Psi_{i_1, i_2, \dots, i_{n_T}}, w_{i_1, i_2, \dots, i_{n_T}})$ [111]. Then, substituting (4.35) into (4.34), the channel estimation can be rewritten as

$$\hat{\mathbf{H}}_{LS} \approx \arg \min_{\hat{\mathbf{H}}} \frac{1}{W} \times \sum_{i_1=1}^N \sum_{i_2=1}^N \cdots \sum_{i_{n_T}=1}^N w_{i_1, i_2, \dots, i_{n_T}} \left\| \hat{\mathbf{H}} \hat{\mathbf{X}}_p(\Psi_{i_1, i_2, \dots, i_{n_T}}) - \mathbf{Y}_p \right\|_F^2. \quad (4.36)$$

Proposition 1 *The LS estimate of the MIMO channel gain matrix in the presence of HPA nonlinearity, based on the SMC method, is given by*

$$\begin{aligned} \hat{\mathbf{H}}_{LS} &\approx \sum_{i_1=1}^N \sum_{i_2=1}^N \cdots \sum_{i_{n_T}=1}^N w_{i_1, i_2, \dots, i_{n_T}} \mathbf{Y}_p \hat{\mathbf{X}}_p^H(\Psi_{i_1, i_2, \dots, i_{n_T}}) \\ &\times \left[\sum_{i_1=1}^N \sum_{i_2=1}^N \cdots \sum_{i_{n_T}=1}^N w_{i_1, i_2, \dots, i_{n_T}} \hat{\mathbf{X}}_p(\Psi_{i_1, i_2, \dots, i_{n_T}}) \hat{\mathbf{X}}_p^H(\Psi_{i_1, i_2, \dots, i_{n_T}}) \right]^{-1}. \end{aligned} \quad (4.37)$$

Proof: The proof of the above proposition is provided in Appendix A.1.

Remark 3 *The properly weighted sample can be obtained using recursive importance sampling method [111]¹. We use the idea of importance sampling to generate the*

¹For completeness, the strategy is illustrated in this chapter.

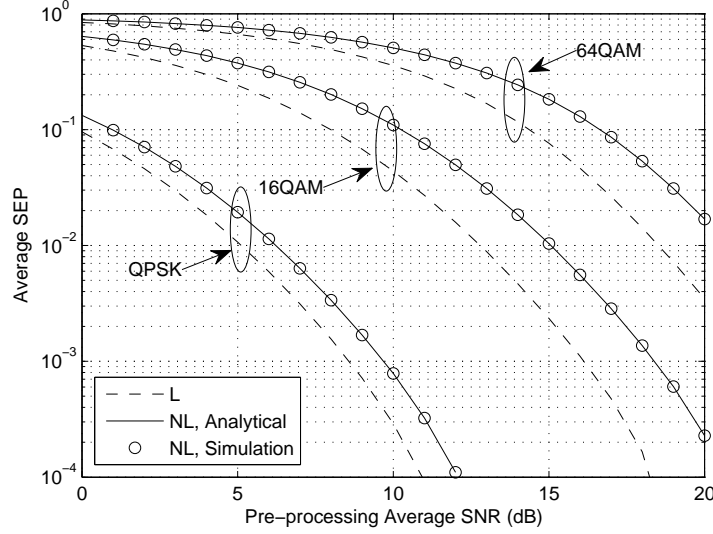


Figure 4.3: Average SEP versus $\bar{\gamma}$ of MIMO-OSTBC for different modulation formats in the case with knowledge of the HPA parameters ($n_T = n_R = 2$, $A_{os} = 1$, $\beta = 2$): linear (L) vs nonlinear (NL).

samples from the trial distribution $\pi(\Psi^{0:t})$, known as the importance function, and assign weights according to

$$w_{i_1, i_2, \dots, i_{n_T}}^t = \frac{p(\Psi_{i_1, i_2, \dots, i_{n_T}}^{0:t})}{\pi(\Psi_{i_1, i_2, \dots, i_{n_T}}^{0:t})}, \quad (4.38)$$

where $\Psi^{0:t} = (\Psi^0, \Psi^1, \dots, \Psi^t)$ with Ψ^i representing the set of the HPA parameters in the i th frame, $\Psi_{i_1, i_2, \dots, i_{n_T}}^{0:t}$ denotes a sample of $\Psi^{0:t}$, and $w_{i_1, i_2, \dots, i_{n_T}}^t$ indicates the weight in the t th frame. Generally, a Gaussian-distributed function is used for the importance function [109]. Then, in the $(t+1)$ th frame, draw samples $\Psi_{i_1, i_2, \dots, i_{n_T}}^{t+1}$ with respect to a trial function $\pi(\Psi^{t+1} | \Psi_{i_1, i_2, \dots, i_{n_T}}^{0:t})$, and let $\Psi_{i_1, i_2, \dots, i_{n_T}}^{0:t+1} = (\Psi_{i_1, i_2, \dots, i_{n_T}}^{0:t}, \Psi_{i_1, i_2, \dots, i_{n_T}}^{t+1})$. Consequently, the weights in the $(t+1)$ th frame are given by

$$w_{i_1, i_2, \dots, i_{n_T}}^{t+1} = w_{i_1, i_2, \dots, i_{n_T}}^t \frac{p(\Psi_{i_1, i_2, \dots, i_{n_T}}^{0:t+1})}{p(\Psi_{i_1, i_2, \dots, i_{n_T}}^{0:t}) \pi(\Psi^{t+1} | \Psi_{i_1, i_2, \dots, i_{n_T}}^{0:t})}. \quad (4.39)$$

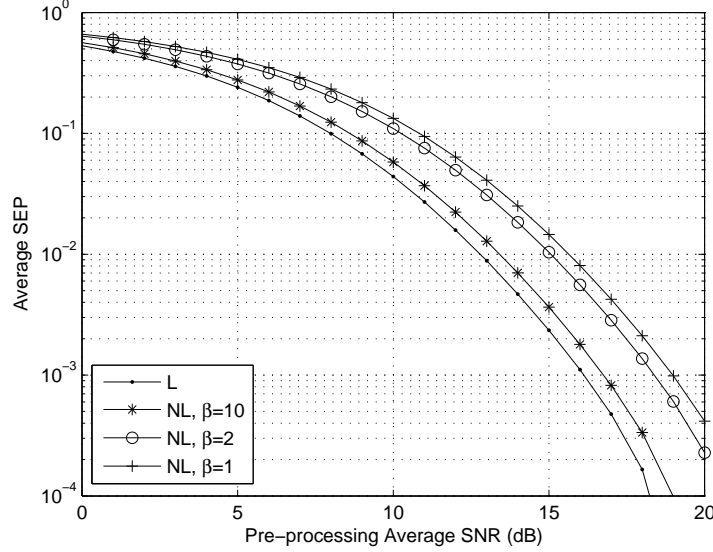


Figure 4.4: Average SEP versus $\bar{\gamma}$ of MIMO-OSTBC for different values of β in the case with knowledge of the HPA parameters ($n_T = n_R = 2$, $A_{os} = 1$, 16QAM)

SMC-Based Signal Detection

Due to the time-variation of the HPA parameters, the orthogonality of OSTBC cannot be maintained. Thereby, the system can not be converted to a SISO one. We apply the ML rule to detect the transmitted signal. Conditioned on the channel gain estimate, $\hat{\mathbf{H}}_{LS}$, described in Section 4.1.3, the detection of the transmitted signal, \mathbf{X} , is given by

$$\mathbf{X}_{ML} = \arg \min_{\mathbf{X}_C} \Pr \left(\mathbf{Y} | \mathbf{X}_C, \hat{\mathbf{H}}_{LS} \right), \quad (4.40)$$

where the candidates of the desired signal, \mathbf{X}_C , are chosen with respect to the modulation scheme. Using the Rao-Blackwellization method, (4.40) can be rewritten as

$$\begin{aligned} \mathbf{X}_{ML} &= \arg \min_{\mathbf{X}_C} \int \Pr \left(\mathbf{Y} | \mathbf{X}_C, \Psi, \hat{\mathbf{H}}_{LS} \right) p(\Psi) d\Psi \\ &= \arg \min_{\mathbf{X}_C} \int \exp \left(- \frac{\left\| \hat{\mathbf{H}}_{LS} \hat{\mathbf{X}}_C(\Psi) - \mathbf{Y} \right\|_F^2}{N_0} \right) p(\Psi) d\Psi, \end{aligned} \quad (4.41)$$

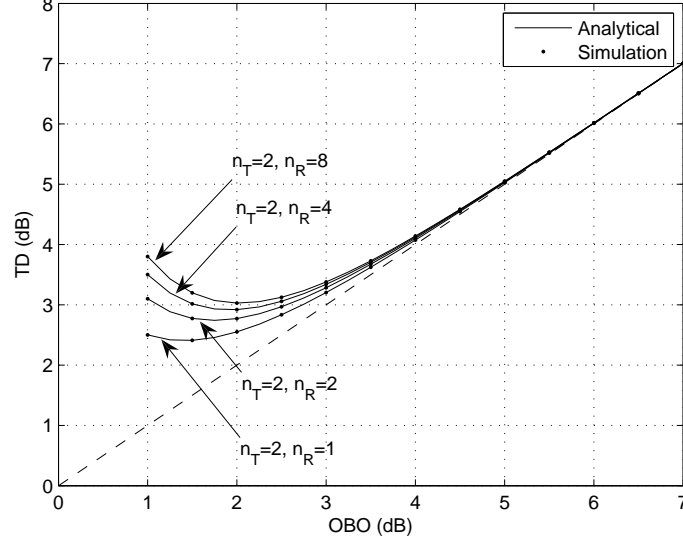


Figure 4.5: TD versus OBO of MIMO-OSTBC for different values of n_T , n_R ($A_{os} = 1$, $\beta = 2$, 16QAM, $P_s = 10^{-4}$).

where Ψ is the set of the HPA parameters, previously defined in Section 4.1.3, and $\hat{\mathbf{X}}_C(\Psi)$ denotes the amplified version of \mathbf{X}_C as a function of Ψ .

Furthermore, we use the SMC method to simplify the detection problem (4.41), according to

$$\mathbf{X}_{ML} \approx \arg \min_{\mathbf{X}_C} \frac{1}{W} \sum_{i_1=1}^N \sum_{i_2=1}^N \cdots \sum_{i_{n_T}=1}^N w_{i_1, i_2, \dots, i_{n_T}} \exp \left(\frac{\|\hat{\mathbf{H}}_{LS} \hat{\mathbf{X}}_C(\Psi_{i_1, i_2, \dots, i_{n_T}}) - \mathbf{Y}\|_F^2}{N_0} \right), \quad (4.42)$$

where the parameters W , N , $\Psi_{i_1, i_2, \dots, i_{n_T}}$, and $w_{i_1, i_2, \dots, i_{n_T}}$ have been previously defined in Section 4.1.3. Note that the properly weighted sample, $(\Psi_{i_1, i_2, \dots, i_{n_T}}, w_{i_1, i_2, \dots, i_{n_T}})$, is obtained using recursive importance sampling as specified in *Remark 3*. The complexity of the SMC-based channel estimation and signal detection is N^{n_T} times that of the ideal case without HPA nonlinearity.

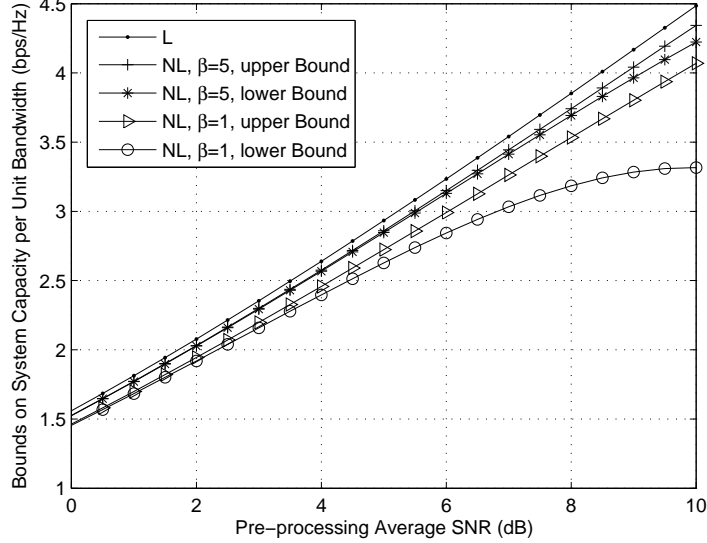


Figure 4.6: Upper and lower bounds on system capacity of MIMO-OSTBC versus $\bar{\gamma}$ for different values of β ($n_T = n_R = 2$, $A_{os} = 1$).

4.1.4 Numerical and Simulation Results

In this section, we present sample numerical and simulation results representing the performance of the MIMO-OSTBC system with the proposed compensation methods for HPA nonlinearity in the cases with and without knowledge of the HPA parameters, specifically on the average SEP, TD and bounds on the system capacity. The full-rate Alamouti code ($R_c = 1$, $c = 1$, $n_T = 2$) in the presence of HPA nonlinearity is investigated. Hereafter, we set the Nakagami parameter to $m = 1$ and consider the SSPA model for nonlinear HPAs. Unless otherwise specified, the output saturation voltage of the SSPA is set to $A_{os} = 1$.

First, we evaluate the average SEP versus the pre-processing average SNR $\bar{\gamma}$ for the 2×2 MIMO configuration, taking the modulation order as parameter, in the case with knowledge of the HPA parameters. We consider SSPA with $\beta = 2$. The curves are obtained on the basis of the analytical results, i.e., using eq. (4.18), and simulation results. Fig. 4.3 shows that the analytical and simulation results are in perfect match. It can be observed that the residual degradation of average SEP, caused by the HPA nonlinearity after the corresponding compensation, varies with $\bar{\gamma}$.

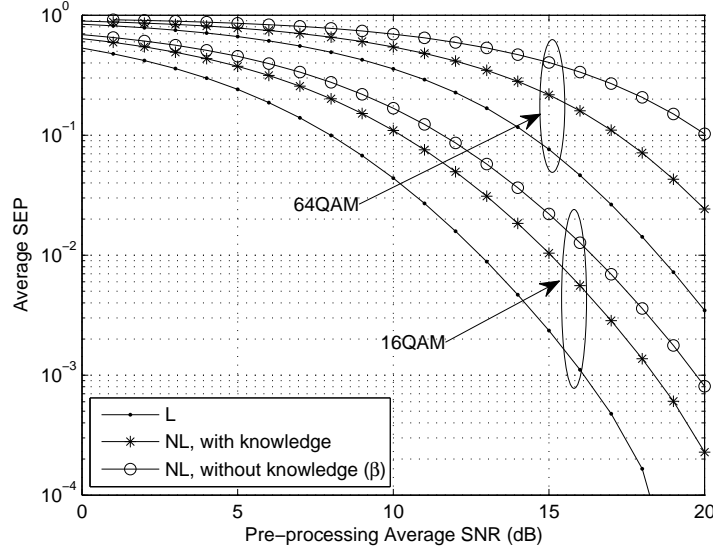


Figure 4.7: Average SEP versus $\bar{\gamma}$ of MIMO-OSTBC for different modulation formats in the cases with and without knowledge of the HPA parameters ($n_T = n_R = 2$, $A_{os} = 1$, $\bar{\beta} = 2$, $N = 30$).

The degradation increases as $\bar{\gamma}$ gets larger, since the impact of nonlinearity becomes more notable in the high SNR region. In addition, given the same requirement on the average SEP, the $\bar{\gamma}$ penalty is the largest for 64-QAM and the least for QPSK. Indeed, as 64-QAM works in the high SNR region more degradation is caused by the HPA nonlinearity.

To further illustrate the effect of nonlinearity in the case with knowledge of the HPA parameters, the average SEP for different values of β , taking 16QAM as the modulation scheme in the $n_T = n_R = 2$ MIMO configuration is shown in Fig. 4.4. The result curves are obtained as per (4.18). As noticed, the smaller the HPA parameter β is, the larger the average SEP will be. This phenomenon is due to the fact that the nonlinear distortion caused by HPA increases as the parameter β becomes smaller.

Fig. 4.5 plots analytical and simulation results for the TD versus OBO with $\beta = 2$ in the case with knowledge of the HPA parameters. Using 16-QAM modulation and setting the target average SEP P_s at 10^{-4} , the results illustrate the effects of n_T and n_R on the TD. It is observed that there is an optimal value of OBO corresponding to the lowest TD for each antenna configuration, which indicates the best tradeoff

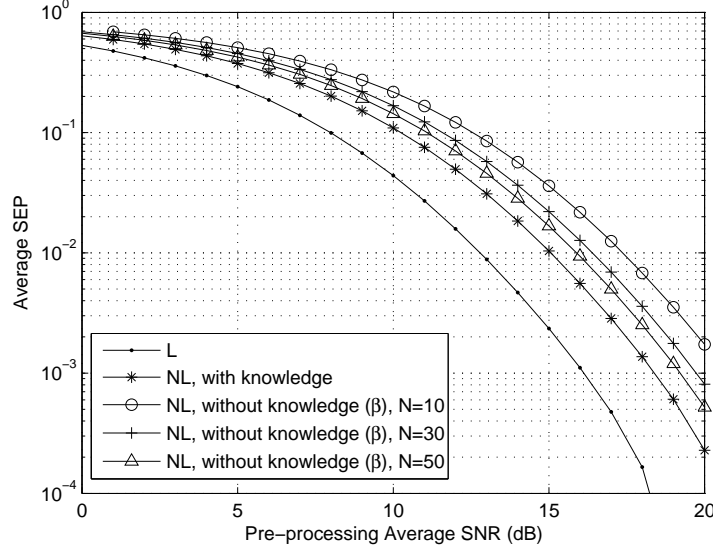


Figure 4.8: Average SEP versus $\bar{\gamma}$ of MIMO-OSTBC for different values of N in the cases with and without knowledge of the HPA parameters ($n_T = n_R = 2$, 16QAM, $A_{os} = 1$, $\bar{\beta} = 2$)

between the power efficiency of the amplifier and the system performance. Moreover, the optimal value of the OBO varies for different antenna configurations. The TD is worse for higher numbers of n_R .

In Fig. 4.6, we show the upper and lower bounds on the system capacity as a function of the pre-processing average SNR, taking into account the HPA nonlinearity, for the case with $n_T = n_R = 2$. Herein, we consider the SSPA model with different values of β . The result curves are obtained according to (4.24) and (4.31). As observed, the distortion due to HPA nonlinearity results in a degradation of the bounds, which is larger for smaller values of β . Furthermore, the difference between the upper bound and lower bound on the capacity decreases as β gets larger. The lower bound also saturates at high pre-processing average SNRs, due to the fact that the saturation point of HPA limits the system performance in such SNR range.

Next, we investigate the proposed SMC compensation scheme in the case without knowledge of the HPA parameters, and compare its performance with that of the case with knowledge of the HPA parameters. Comparisons are shown for the average SEP. In the following, the curves for the case without knowledge of the HPA parameters

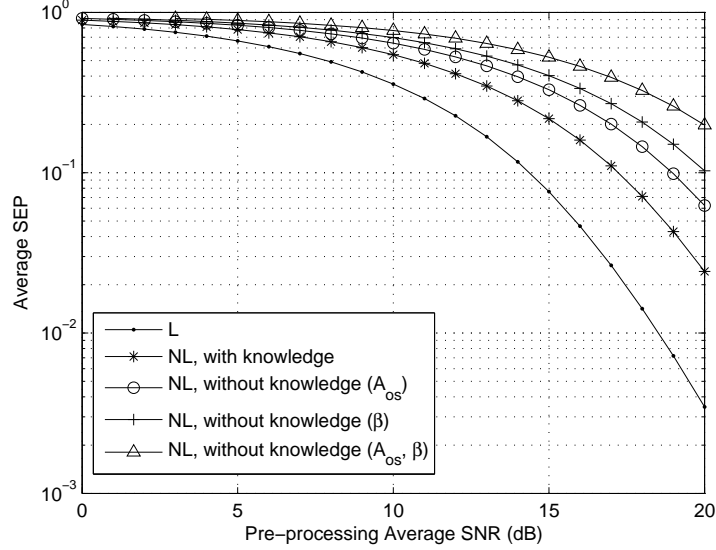


Figure 4.9: Average SEP versus $\bar{\gamma}$ of MIMO-OSTBC for different cases of parameter knowledge ($n_T = n_R = 2$, 64QAM, $\bar{A}_{os} = 1$, $\bar{\beta} = 2$, $N = 30$)

are obtained on the basis of simulation, while the curves for the case with knowledge of the HPA parameters are plotted on the basis of analytical results.

Fig. 4.7 shows the average SEP as a function of the pre-processing average SNR in the $n_T = n_R = 2$ MIMO configuration for different modulation formats in the cases with and without knowledge of the HPA parameters. For the case without knowledge of the HPA parameters, we consider that the parameter β is unknown at the transmitter and receiver. For simulation purposes, we choose the average value of β as $\bar{\beta} = 2$, and set the number of SMC samples to $N = 30$. It can be observed that the proposed compensation algorithm in the case without knowledge of the HPA parameters can efficiently mitigate the effect of nonlinearity, even though the corresponding average SEP is larger than in the case with knowledge of the HPA parameters.

In Fig. 4.8, the effect of the number of SMC samples on the average SEP in the case without knowledge of the HPA parameters is analyzed for the 2×2 MIMO configuration with 16QAM. The average value of β is set to $\bar{\beta} = 2$. As noticed, by increasing the number of SMC samples, the average SEP can be reduced to approach

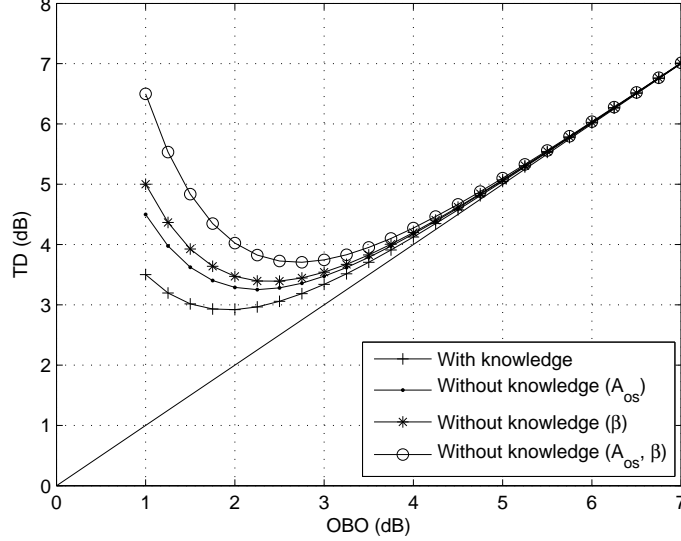


Figure 4.10: Total degradation versus OBO of MIMO-OSTBC for different cases of parameter knowledge ($n_T = 2$, $n_R = 4$, 16QAM, $\bar{A}_{os} = 1$, $\bar{\beta} = 2$, $N = 30$).

the performance with knowledge of the HPA parameters. This is due to the fact that the probability distributions of the HPA parameters can be better simulated by using more SMC samples. Moreover, there is a performance gap between the results of the ideal case, i.e., without HPA nonlinearity, and the compensated case with knowledge of the HPA parameters. Specifically, the compensation for the HPA nonlinearity makes use of the ML detection method. However, the ideal constellation of the input signals is disturbed due to HPA nonlinearity. Consequently, the decision regions for the ML decoding are changed as per the constellation of the distorted signals, which results in the above-mentioned performance gap.

Fig. 4.9 plots the average SEP for different cases of parameter knowledge, taking 64QAM as the modulation scheme, in the case with $N = 30$. We can observe that the average SEP in the case without knowledge of (A_{os}, β) is larger than in the case without knowledge of β , and the latter is larger than in the case without knowledge of A_{os} , since the parameter β has a more important effect on the nonlinear behavior of the SSPA than the parameter A_{os} .

Finally, Fig. 4.10 shows the TD versus OBO for different cases of parameter

knowledge in the 2×4 MIMO configuration. We consider 16-QAM modulation, set the target average SEP P_s at 10^{-4} , and fix the number of SMC samples to $N = 30$. It is observed that there is an optimal value for the OBO which yields the lowest TD for each case. The corresponding TD is worse in the case without knowledge of A_{os} and β .

4.2 MIMO Transmit Beamforming Systems with Nonlinear HPAs

In this section, we focus on the closed-loop MIMO TB technique in the presence of HPA nonlinearity [98]. The conventional MRT/MRC scheme becomes suboptimal in the presence of HPA nonlinearity. Herein, our objectives are to seek the optimal beamforming weight vector and combining vector to adapt MIMO TB systems for operation under HPA nonlinearity, by maximizing the output SNR. In addition, profiting from the property that the elements of the beamforming weight vector have the same constant modulus, we also investigate an alternative suboptimal but much simpler TB scheme, namely, QEGT, which is an effective mechanism in the case with nonlinear HPA.

For the proposed optimal TB scheme, we derive lower and upper bounds on the average SEP and on the mutual information with Gaussian input, considering that the system operates under uncorrelated quasi-static frequency-flat Rayleigh fading. Moreover, a lower bound on the average SEP and an upper bound on the mutual information with Gaussian input are provided for the QEGT/MRC scheme. Numerical results are provided and show the effects of system parameters, such as the HPA parameters, numbers of antennas, QAM order, number of pilot symbols, and cardinality of the beamforming weight vector codebook for QEGT, on performance.

The remainder of Section 4.2 is organized as follows: Section 4.2.1 introduces the MIMO TB system model with HPA nonlinearity. In Section 4.2.2, we present the channel estimation algorithm under HPA nonlinearity in order to get the full knowledge of the channel gain of each transmit-receive antenna link. In Section 4.2.3,

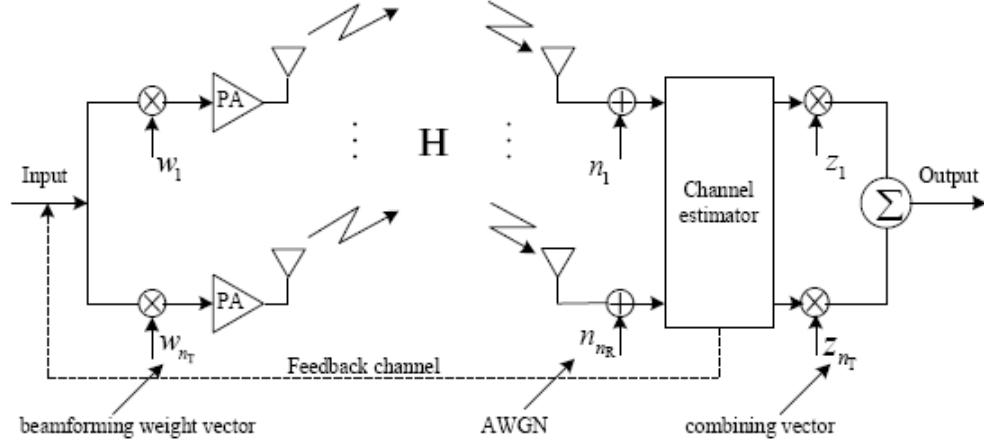


Figure 4.11: Block diagram of the considered MIMO TB system with nonlinear HPAs.

we propose the optimal TB scheme with the optimal beamforming weight vector and combining vector, and evaluate the system performance in terms of average SEP and mutual information. The QEGT/MRC technique is investigated and evaluated in Section 4.2.4. Numerical and simulation results are then presented in Section 4.2.5.

4.2.1 System and High-Power Amplifier Models

We consider a MIMO TB system with n_T transmit and n_R receive antennas, and assume a discrete-time baseband channel model subject to uncorrelated quasi-static frequency-flat Rayleigh fading. The received signal can be expressed as

$$\mathbf{y} = \mathbf{H}\mathbf{w}x + \mathbf{n}, \quad (4.43)$$

where x represents the transmitted symbol with average power P_0 , \mathbf{w} is the $n_T \times 1$ unit-norm beamforming weight vector, \mathbf{n} denotes the $n_R \times 1$ noise vector with elements belonging to i.i.d. complex circular Gaussian distribution $\mathcal{CN}(0, N_0)$ uncorrelated with the transmitted symbols, and $\mathbf{H} = [h_{k,l}]_{k,l=1}^{n_R, n_T}$ defines the channel gain matrix with $h_{k,l}$ denoting the channel coefficient between the l th transmit and k th receive antennas. The entries of the channel gain matrix are i.i.d. complex Gaussian random variables, each with a $\mathcal{CN}(0, 1)$ distribution.

In practice, the transmitted signal has to be amplified at RF through the HPA, which may operate in its nonlinear region, thus causing amplitude distortion and phase distortion on the input signal. The block diagram of the MIMO TB system under study is shown in Fig. 4.11. The behavior of the HPA plays an important role in the data detection process. Assuming the HPA parameters to be known at the transmitter and receiver and, for simplicity of the analysis, that the HPAs at all the transmitting branches exhibit the same nonlinear behavior, the MIMO TB signal model in the presence of HPA nonlinearity can be expressed as

$$\mathbf{y}_{\text{NL}} = \mathbf{H}\mathbf{u} + \mathbf{n}, \quad (4.44)$$

where $\mathbf{u} = [u_1, u_2, \dots, u_{n_T}]^T$ denotes the distorted version of the weighted transmit symbol vector. Based on the transfer function of the memoryless HPAs in (4.3), the weighted and distorted signal u_i ($i = 1, 2, \dots, n_T$) is of the form

$$u_i = f_A(|w_i x|) \exp[j(\theta_x + \varphi_i + f_P(|w_i x|))], \quad (4.45)$$

where θ_x and φ_i denote the phases of the input signal x and the beamforming weight w_i , respectively.

4.2.2 Channel Estimation under HPA Nonlinearity

In this section, we present the channel estimation algorithm taking into account the HPA nonlinearity. Full knowledge of the channel gain of each transmit-receive antenna link, i.e., the channel gain matrix, is required in MIMO TB systems. As the channels are assumed to be quasi-static, the channel gain matrix remains invariant in each frame and may vary from frame to frame. Under this setting, $n_T \times V$ pilot symbol matrix \mathbf{S}_p , with an average power of ξ_p per pilot, is used for the channel estimation in each transmit frame. The received signal in the presence of HPA nonlinearity can be expressed as

$$\mathbf{Y}_p = \mathbf{H}\tilde{\mathbf{S}}_p + \mathbf{N}_p, \quad (4.46)$$

where $\tilde{\mathbf{S}}_p$ represents the pilot symbol matrix after nonlinear amplification, and \mathbf{N}_p denotes the $n_R \times V$ noise matrix with elements belonging to i.i.d. complex circular Gaussian distribution $\mathcal{CN}(0, N_0)$ uncorrelated with the transmitted pilot symbols.

Using LS rule, the channel estimate $\hat{\mathbf{H}}$ can be obtained as

$$\hat{\mathbf{H}} = \mathbf{Y}_p \tilde{\mathbf{S}}_p^H \left(\tilde{\mathbf{S}}_p \tilde{\mathbf{S}}_p^H \right)^{-1}. \quad (4.47)$$

In this case, the pilot symbol matrix \mathbf{S}_p should be chosen to satisfy the constraint that the matrix $\tilde{\mathbf{S}}_p \tilde{\mathbf{S}}_p^H$ has full rank. The necessary condition is that $V \geq n_T$. The resulting mean square error (MSE) can be expressed as

$$\begin{aligned} \sigma_e^2 &= E \left[\left\| \mathbf{H} - \hat{\mathbf{H}} \right\|_F^2 \right] \\ &= E \left[\left\| \mathbf{N}_p \tilde{\mathbf{S}}_p^H \left(\tilde{\mathbf{S}}_p \tilde{\mathbf{S}}_p^H \right)^{-1} \right\|_F^2 \right] \\ &= n_R N_0 \text{tr} \left[\left(\tilde{\mathbf{S}}_p \tilde{\mathbf{S}}_p^H \right)^{-1} \right]. \end{aligned} \quad (4.48)$$

The minimal MSE is achieved when the matrix $\tilde{\mathbf{S}}_p$ has orthogonal rows, i.e.,

$$\tilde{\mathbf{S}}_p \tilde{\mathbf{S}}_p^H = V \xi_p \mathbf{I}_{n_T}. \quad (4.49)$$

Then, the lower bound on the MSE between \mathbf{H} and $\hat{\mathbf{H}}$ is given by

$$\sigma_{e,\text{low}}^2 = \frac{n_R n_T N_0}{V f_A^2 (\sqrt{\xi_p})}. \quad (4.50)$$

Accordingly, the estimation error for each element of \mathbf{H} can be expressed as $\sigma_h^2 = \frac{\sigma_e^2}{n_T n_R}$, and the relationship between \mathbf{H} and $\hat{\mathbf{H}}$ can be expressed as [119]

$$\mathbf{H} = \rho_h \hat{\mathbf{H}} + \mathbf{\Theta}, \quad (4.51)$$

where $\rho_h = \frac{1}{1+\sigma_h^2}$, and each component of $\mathbf{\Theta}$ is complex Gaussian distributed variable, with zero mean and variance $\sigma_{\mathbf{\Theta}}^2 = \frac{\sigma_h^2}{1+\sigma_h^2}$, uncorrelated with the elements of \mathbf{H} .

4.2.3 Optimal Beamforming Scheme in the Presence of HPA Nonlinearity

In this section, our objectives are to investigate the effect of HPA nonlinearity on the performance of MIMO TB and seek the optimal beamforming weight vector and combining vector to adapt the MIMO TB system for operation under HPA nonlinearity, through maximization of the output SNR.

Conventional MRT/MRC under HPA Nonlinearity

In the absence of HPA nonlinearity, the detected signal after MRC at the receiver, \hat{y} , conditioned on the channel gain matrix \mathbf{H} and the beamforming weight vector \mathbf{w} , is given by

$$\hat{y} = \mathbf{z}^H \mathbf{H} \mathbf{w} x + \mathbf{z}^H \mathbf{n}. \quad (4.52)$$

A receiver where \mathbf{z} maximizes $|\mathbf{z}^H \mathbf{H} \mathbf{w}|$ given \mathbf{w} is called an MRC receiver, according to $\mathbf{z} = \mathbf{H} \mathbf{w} / \|\mathbf{H} \mathbf{w}\|_F$ [98]. Due to the imperfect channel estimation, the combining vector is given by $\mathbf{z} = \hat{\mathbf{H}} \mathbf{w} / \|\hat{\mathbf{H}} \mathbf{w}\|_F$. Furthermore, MRT is employed to maximize the output SNR. However, in the case with HPA nonlinearity, the combined signal at the receiver, \hat{y}_{NL} , conditioned on the channel gain matrix \mathbf{H} and HPA nonlinearity, becomes

$$\hat{y}_{\text{NL}} = \mathbf{z}^H \mathbf{H} \mathbf{u} + \mathbf{z}^H \mathbf{n}, \quad (4.53)$$

where the elements of \mathbf{u} are as defined in (4.45). Since the term $\mathbf{z}^H \mathbf{H} \mathbf{u}$ is not a linear combination of the desired signal anymore, spatial diversity cannot be efficiently achieved by the MRC. Therefore, the conventional MRT/MRC is suboptimal in the case with HPA nonlinearity.

Optimal Beamforming Scheme under HPA Nonlinearity

We now determine the optimal beamforming scheme with optimal beamforming weight vector and combining vector under HPA nonlinearity. The weighted and distorted signal at the output of the nonlinear HPAs, u_i in (4.45), can be rewritten

as

$$u_i = v_i x, \quad (4.54)$$

where

$$v_i = \frac{f_A(|w_i x|)}{|x|} \exp [j (\varphi_i + f_P(|w_i x|))]. \quad (4.55)$$

Then, the MIMO TB signal model in the presence of HPA nonlinearity can be expressed as

$$\mathbf{y}_{\text{NL}} = \mathbf{H} \mathbf{v} x + \mathbf{n}, \quad (4.56)$$

where $\mathbf{v} = [v_1, v_2, \dots, v_{n_T}]^T$. At the receiver, the signals from all the receive antenna branches are weighted by the $n_R \times 1$ combining vector \mathbf{z} . Then, the detected signal at the receiver, \hat{y}_{NL} , is given by

$$\hat{y}_{\text{NL}} = \mathbf{z}^H \mathbf{H} \mathbf{v} x + \mathbf{z}^H \mathbf{n}. \quad (4.57)$$

In a beamforming and combining system, the key problem is to choose \mathbf{w} and \mathbf{z} that maximize the output SNR in order to minimize the SEP. A receiver where \mathbf{z} maximizes $|\mathbf{z}^H \mathbf{H} \mathbf{v}|$ given \mathbf{v} is called MRC receiver, according to $\mathbf{z}_{\text{op}} = \hat{\mathbf{H}} \mathbf{v} / \|\hat{\mathbf{H}} \mathbf{v}\|_F$, due to the imperfect channel estimation. Consequently, substituting the expression for \mathbf{z} along with (4.51) into (4.57), the detected signal can further be expressed as

$$\hat{y}_{\text{op}} = \rho_h \frac{\mathbf{v}^H \hat{\mathbf{H}}^H \hat{\mathbf{H}} \mathbf{v}}{\|\hat{\mathbf{H}} \mathbf{v}\|_F} x + \frac{\mathbf{v}^H \hat{\mathbf{H}}^H \mathbf{\Theta} \mathbf{v}}{\|\hat{\mathbf{H}} \mathbf{v}\|_F} x + \frac{\mathbf{v}^H \hat{\mathbf{H}}^H}{\|\hat{\mathbf{H}} \mathbf{v}\|_F} \mathbf{n}. \quad (4.58)$$

Furthermore, MRT is employed to maximize the output SNR with respect to \mathbf{v} . In this scenario, \mathbf{v} is the eigenvector of the Wishart matrix $\hat{\mathbf{H}}^H \hat{\mathbf{H}} / (1 + \sigma_h^2)$ associated with its largest eigenvalue λ_{max} . Consequently, \mathbf{v} can be rewritten as

$$\mathbf{v} = d \tilde{\mathbf{w}}, \quad (4.59)$$

where $\tilde{\mathbf{w}}$ denotes the unit-norm eigenvector of $\hat{\mathbf{H}}^H \hat{\mathbf{H}} / (1 + \sigma_h^2)$ associated with its largest eigenvalue, i.e., the conventional beamforming weight vector. Accordingly, the optimal combining vector, \mathbf{z}_{op} , can be further expressed as $\mathbf{z}_{\text{op}} = \hat{\mathbf{H}} \tilde{\mathbf{w}} / \|\hat{\mathbf{H}} \tilde{\mathbf{w}}\|_F$.

Then, making use of a similar methodology as that in [120], the output SNR is given by

$$\begin{aligned} \gamma_{\text{op}} &= \frac{d^2 \rho_h^2 P_0 \tilde{\mathbf{w}}^H \hat{\mathbf{H}}^H \hat{\mathbf{H}} \tilde{\mathbf{w}}}{d^2 P_0 \sigma_{\Theta}^2 + N_0} \\ &= \frac{d^2 \bar{\gamma}}{1 + \sigma_h^2 (1 + d^2 \bar{\gamma})} \lambda_{\max}, \end{aligned} \quad (4.60)$$

where $\bar{\gamma} = P_0/N_0$ denotes the average SNR per receive antenna.

In the following, we seek the values of the optimal beamforming weight vector \mathbf{w}_{op} , and the coefficient d . Regarding (4.54), (4.55) and (4.59), the values of \mathbf{w}_{op} and d can be obtained by solving the following set of equations:

$$\begin{cases} \varphi_i^{\text{op}} = \tilde{\varphi}_i - f_P(|w_i^{\text{op}} x|), i = 1, 2, \dots, n_T, \\ f_A(|w_i^{\text{op}} x|) = d |\tilde{w}_i x|, i = 1, 2, \dots, n_T, \\ \sum_{i=1}^{n_T} |w_i^{\text{op}}|^2 = 1, \end{cases} \quad (4.61)$$

where φ_i^{op} and $\tilde{\varphi}_i$ represent the phases of w_i^{op} and \tilde{w}_i , respectively.

Remark 4 *The numbers of the equations and the unknown variables, d , $|w_i^{\text{op}}|$ and φ_i^{op} , for $i = 1, 2, \dots, n_T$, are both $2n_T + 1$ so that there are solutions for the values of the beamforming weight vector, \mathbf{w}_{op} , and the coefficient d . Specifically, the value of \mathbf{w}_{op} depends on the estimated channel gain matrix $\hat{\mathbf{H}}$, amplitude of the input symbol x and the HPA characteristics. On the other hand, the combining vector \mathbf{z}_{op} is only related to the estimated channel gain matrix $\hat{\mathbf{H}}$.*

The solution of the equation group (4.61) can be expressed as follows,

$$\begin{cases} |w_i^{\text{op}}| = \frac{f_A^{-1}(d|\tilde{w}_i x|)}{|x|}, i = 1, 2, \dots, n_T, \\ \varphi_i^{\text{op}} = \tilde{\varphi}_i - f_P[f_A^{-1}(d|\tilde{w}_i x|)], i = 1, 2, \dots, n_T, \end{cases} \quad (4.62)$$

where the coefficient d is the solution of the following equation:

$$\sum_{i=1}^{n_T} [f_A^{-1}(d|\tilde{w}_i x|)]^2 = |x|^2. \quad (4.63)$$

Since the derived expression for the output SNR of the optimal MIMO beamforming system under study is too complicated, deriving the probability distribution function (PDF) of the output SNR in closed-form is not straightforward. Herein, we provide upper and lower bounds on the coefficient d . An upper bound on d can be expressed as

$$d_{\text{up}} = \sqrt{\frac{n_T}{P_0}} f_A \left(\sqrt{\frac{P_0}{n_T}} \right), \quad (4.64)$$

which is achieved when $|\tilde{w}_i| = |\tilde{w}_j|$ ($i, j = 1, 2, \dots, n_T$). On the other hand, a lower bound on d is obtained if $|\tilde{w}_i| = 1, |\tilde{w}_j| = 0$ ($j = 1, 2, \dots, n_T, j \neq i$). The lower bound is given by

$$d_{\text{low}} = \sqrt{\frac{1}{P_0}} f_A \left(\sqrt{P_0} \right). \quad (4.65)$$

The above-mentioned upper and lower bounds are obtained based on the fact that each type of the AM/AM conversion functions, $f_A(\cdot)$ presented in Section 4.2.1, are convex functions [34].

Since the entries of $\hat{\mathbf{H}}/\sqrt{1+\sigma_h^2}$ are i.i.d. complex Gaussian random variables, each with a $\mathcal{CN}(0, 1)$ distribution, the PDF of the largest eigenvalue of the Hermitian matrix $\hat{\mathbf{H}}^H \hat{\mathbf{H}}/(1+\sigma_h^2)$, is given by [98]

$$p_{\lambda_{\max}}(\lambda) = \sum_{k=1}^p \sum_{l=q-p}^{(p+q-2k)k} \frac{d_{k,l}}{l!} k^{l+1} \lambda^l e^{-k\lambda}, \quad (4.66)$$

where $p = \min\{n_T, n_R\}$, $q = \max\{n_T, n_R\}$, and coefficients $d_{k,l}$ are obtained using the algorithm proposed in [121]. It can be observed that $p_{\lambda_{\max}}(\lambda)$ is a finite linear combination of elementary Gamma PDFs with parameter $l + 1$ and mean $l + 1/k$.

In the remainder of this section, we analyze the performance of the optimal MIMO beamforming system in uncorrelated quasi-static frequency-flat Rayleigh fading channels in the presence of HPA nonlinearity, in terms of average SEP and mutual information.

Average Symbol Error Probability

Since the channel estimation error matrix Θ is complex Gaussian, the interference introduced by the imperfect channel estimation $\frac{\mathbf{v}^H \hat{\mathbf{H}}^H \Theta \mathbf{v}}{\|\hat{\mathbf{H}} \mathbf{v}\|_F} x$ and the noise term $\frac{\mathbf{v}^H \hat{\mathbf{H}}^H \mathbf{n}}{\|\hat{\mathbf{H}} \mathbf{v}\|_F}$, specified in (4.58), are complex Gaussian distributed (given $\hat{\mathbf{H}}$ and x). Then, the average SEP of MQAM in the optimal MIMO beamforming system in the case with HPA nonlinearity can be expressed as [98, eq. 35]:

$$P_{s,\text{op}} = \frac{4}{\pi} \left(1 - \frac{1}{\sqrt{M}}\right) \int_0^{\pi/2} \Psi_{\gamma_{\text{op}}} \left(-\frac{g_{\text{MQAM}}}{\sin^2 \theta}\right) d\theta - \frac{4}{\pi} \left(1 - \frac{1}{\sqrt{M}}\right)^2 \int_0^{\pi/4} \Psi_{\gamma_{\text{op}}} \left(-\frac{g_{\text{MQAM}}}{\sin^2 \theta}\right) d\theta, \quad (4.67)$$

where $g_{\text{MQAM}} = 3/[2(M-1)]$, and $\Psi_{\gamma_{\text{op}}}(\cdot)$ denotes the characteristic function of γ_{op} , i.e.,

$$\Psi_{\gamma_{\text{op}}}(j\omega) = \sum_{k=1}^p \sum_{l=q-p}^{(p+q-2k)k} \frac{d_{k,l}}{\left(1 - \frac{j\omega}{k} \frac{d^2 \bar{\gamma}}{1 + \sigma_h^2 (1 + d^2 \bar{\gamma})}\right)^{l+1}}. \quad (4.68)$$

Furthermore, taking into account the value of the coefficient d , we obtain lower and upper bounds on the average SEP. Specifically, substituting (4.68) into (4.67), the lower bound on the average SEP can be expressed as

$$P_{s,\text{op}}^{\text{low}} = 2 \left(1 - \frac{1}{\sqrt{M}}\right) \sum_{k=1}^p \sum_{l=q-p}^{(p+q-2k)k} d_{k,l} \left\{ 1 - \frac{1}{\sqrt{1 + \frac{1}{\zeta_k}}} \sum_{m=0}^l \binom{2m}{m} \frac{1}{4^m (1 + \zeta_k)^m} \right\}$$

$$\begin{aligned}
& + \frac{4}{\pi} \left(1 - \frac{1}{\sqrt{M}}\right)^2 \sum_{k=1}^p \sum_{l=q-p}^{(p+q-2k)k} d_{k,l} \left\{ \frac{\pi}{4} - \beta_k \left[\left(\frac{\pi}{2} - \arctan \beta_k \right) \sum_{m=0}^l \binom{2m}{m} \right. \right. \\
& \left. \left. \times \frac{1}{[4(1+\zeta_k)]^m} - \sin(\arctan \beta_k) \sum_{m=1}^l \sum_{n=1}^m \frac{T_{nm}}{(1+\zeta_k)^m} (\cos(\arctan \beta_k))^{2(m-n)+1} \right] \right\}, \tag{4.69}
\end{aligned}$$

where the first and second terms make use of [98, eq. 29] and [114, eq. 74], respectively, and where $\beta_k = \sqrt{\zeta_k/(1+\zeta_k)}$, $\zeta_k = (d_{\text{up}}^2 \bar{\gamma} g_{\text{M-QAM}})/\{k [1 + \sigma_h^2 (1 + d_{\text{up}}^2 \bar{\gamma})]\}$ and

$$T_{nm} = \binom{2m}{m} / \left[\binom{2(m-n)}{m-n} 4^n (2(m-n)+1) \right].$$

On the other hand, the expression for the upper bound on the average SEP is similar to that for the lower bound, after replacing d_{up}^2 with d_{low}^2 .

Mutual Information

In the presence of imperfect channel estimation and HPA nonlinearity, deriving the expression for the capacity of the MIMO system under study in closed-form is not straightforward. Herein, it is assumed that the input signal x is Gaussian distributed, which is not necessarily the capacity achieving distribution when the channel estimation is not perfect [122, 123]. However, we provide lower and upper bounds on the mutual information, by making use of a similar methodology as that in [124].

By taking into account the lower bound on the coefficient d , the lower bound on the mutual information of the optimal MIMO beamforming system under the consideration of HPA nonlinearity and channel estimation error can be expressed in [bps/Hz] as

$$\begin{aligned}
I_{\text{op}}^{\text{low}}(x; \hat{y}_{\text{op}}) &= E_{\lambda_{\text{max}}} \left\{ \log_2 \left(1 + \frac{d_{\text{low}}^2 \bar{\gamma}}{1 + \sigma_h^2 (1 + d_{\text{low}}^2 \bar{\gamma})} \lambda_{\text{max}} \right) \right\} \\
&= \log_2 e \sum_{k=1}^p \exp \left\{ \frac{k [1 + \sigma_h^2 (1 + d_{\text{low}}^2 \bar{\gamma})]}{d_{\text{low}}^2 \bar{\gamma}} \right\}
\end{aligned}$$

$$\times \left\{ \sum_{l=q-p}^{(p+q-2k)k} d_{k,l} \sum_{j=1}^{l+1} E_{l+2-j} \left\{ \frac{k [1 + \sigma_h^2 (1 + d_{\text{low}}^2 \bar{\gamma})]}{d_{\text{low}}^2 \bar{\gamma}} \right\} \right\}, \quad (4.70)$$

where the second equality makes use of [121, eq. (20)], and $E_l(a) = \int_1^\infty \frac{e^{-ax}}{x^l} dx$ denotes the exponential integral function of the l th order. On the other hand, the expression for the upper bound on the mutual information is given by

$$\begin{aligned} I_{\text{op}}^{\text{up}}(x; \hat{y}_{\text{op}}) &= E_{\lambda_{\text{max}}} \left\{ \log_2 \left(1 + \frac{d_{\text{up}}^2 \bar{\gamma}}{1 + \sigma_h^2 (1 + d_{\text{up}}^2 \bar{\gamma})} \lambda_{\text{max}} \right) \right\} + \Delta \\ &= \Delta + \log_2 e \sum_{k=1}^p \exp \left\{ \frac{k [1 + \sigma_h^2 (1 + d_{\text{up}}^2 \bar{\gamma})]}{d_{\text{up}}^2 \bar{\gamma}} \right\} \\ &\quad \times \left\{ \sum_{l=q-p}^{(p+q-2k)k} d_{k,l} \sum_{j=1}^{l+1} E_{l+2-j} \left\{ \frac{k [1 + \sigma_h^2 (1 + d_{\text{up}}^2 \bar{\gamma})]}{d_{\text{up}}^2 \bar{\gamma}} \right\} \right\}, \end{aligned} \quad (4.71)$$

where the second term in the second equality is given by

$$\Delta = E_x \left[\log_2 \frac{N_0 (1 + \sigma_h^2) + d_{\text{up}}^2 \sigma_h^2 P_0}{N_0 (1 + \sigma_h^2) + d_{\text{up}}^2 \sigma_h^2 |x|^2} \right]. \quad (4.72)$$

Note that in the case with high signal power, Δ can be expressed as

$$\begin{aligned} \lim_{P_0 \rightarrow \infty} \Delta &= \lim_{P_0 \rightarrow \infty} [\log_2 P_0 - E_x (\log_2 |x|^2)] \\ &= \lim_{P_0 \rightarrow \infty} \left[\log_2 P_0 - \left(\log_2 P_0 - \frac{\gamma_{\text{Eu}}}{\ln 2} \right) \right] \\ &= \frac{\gamma_{\text{Eu}}}{\ln 2} \\ &\approx 0.83, \end{aligned} \quad (4.73)$$

where the second equality makes use of [124, eq. (51)] and where

$\gamma_{\text{Eu}} = \lim_{n \rightarrow \infty} (\sum_{k=1}^n 1/k - \ln n) \approx 0.577$ denotes Euler's constant.

4.2.4 QEGT/MRC: A Simple and Feasible Beamforming Scheme under HPA Nonlinearity

The optimal beamforming scheme with the optimal weight vector and combining vector in the presence of HPA nonlinearity was proposed in Section 4.2.3. In this section, we investigate an alternative suboptimal but much simpler TB scheme, namely, equal gain transmission (EGT).

In this case, the element of the beamforming weight vector is given by $w_i^{\text{EGT}} = \frac{1}{\sqrt{n_T}} \exp(j\varphi_i^{\text{EGT}})$ ($i = 1, 2, \dots, n_T$), where φ_i^{EGT} denotes the phase of w_i^{EGT} . Then, the signal u_i in (4.45) can be further expressed as

$$\begin{aligned} u_i^{\text{EGT}} &= f_A \left(\frac{|x|}{\sqrt{n_T}} \right) \exp \left[j \left(\theta_x + \varphi_i^{\text{EGT}} + f_P \left(\frac{|x|}{\sqrt{n_T}} \right) \right) \right] \\ &= \underbrace{w_i^{\text{EGT}} \sqrt{n_T} f_A \left(\frac{|x|}{\sqrt{n_T}} \right) \exp \left[j \left(\theta_x + f_P \left(\frac{|x|}{\sqrt{n_T}} \right) \right) \right]}_{\hat{x}}, \end{aligned} \quad (4.74)$$

where \hat{x} is the post-distortion symbol, which is independent of the beamforming weight vector. The average power of \hat{x} is given by $P_0^{\text{HPA}} = n_T E \left[f_A^2 \left(\frac{|x|}{\sqrt{n_T}} \right) \right]$. The relationship between P_0^{HPA} and the pre-distortion average signal-to-noise ratio (SNR), $\bar{\gamma} = P_0/N_0$, depends on the distribution of the input symbol power. Consequently, the average SNR after HPA is given by $\bar{\gamma}_{\text{NL}} = \frac{n_T E[f_A^2(|x|/\sqrt{n_T})]}{N_0}$.

By substituting (4.74) and (4.51) into (4.53), the detected signal can be rewritten as

$$\hat{y}_{\text{EGT}} = \rho_h \mathbf{z}^H \hat{\mathbf{H}} \mathbf{w}_{\text{EGT}} \hat{x} + \mathbf{z}^H \mathbf{\Theta} \mathbf{w}_{\text{EGT}} \hat{x} + \mathbf{z}^H \mathbf{n}. \quad (4.75)$$

Note that the term $\rho_h \mathbf{z}^H \hat{\mathbf{H}} \mathbf{w}_{\text{EGT}} \hat{x}$ in (4.75) is a linear combination of \hat{x} . Then, the input signal can be efficiently detected, profiting from the property that the elements of the beamforming weight vector have the same constant modulus. Moreover, the MRC receiver that maximizes $\mathbf{z}^H \hat{\mathbf{H}} \mathbf{w}^{\text{EGT}}$ given \mathbf{w}^{EGT} is implemented, according to

$\mathbf{z}_{\text{MRC}} = \hat{\mathbf{H}}\mathbf{w}_{\text{EGT}} / \left\| \hat{\mathbf{H}}\mathbf{w}_{\text{EGT}} \right\|_F$. Thus, the detected signal (4.75) is given by

$$\hat{y}_{\text{EGT/MRC}} = \rho_h \frac{\mathbf{w}_{\text{EGT}}^H \hat{\mathbf{H}}^H \hat{\mathbf{H}} \mathbf{w}_{\text{EGT}}}{\left\| \hat{\mathbf{H}} \mathbf{w}_{\text{EGT}} \right\|_F} \hat{x} + \frac{\mathbf{w}_{\text{EGT}}^H \hat{\mathbf{H}}^H \Theta \mathbf{w}_{\text{EGT}}}{\left\| \hat{\mathbf{H}} \mathbf{w}_{\text{EGT}} \right\|_F} \hat{x} + \frac{\mathbf{w}_{\text{EGT}}^H \hat{\mathbf{H}}^H}{\left\| \hat{\mathbf{H}} \mathbf{w}_{\text{EGT}} \right\|_F} \mathbf{n}. \quad (4.76)$$

For EGT/MRC systems, the optimal weight vector \mathbf{w}_{EGT} is chosen according to

$$\mathbf{w}^{\text{EGT}} = \arg \max_{|w_i|=1/\sqrt{n_T}} \left\| \hat{\mathbf{H}} \mathbf{w} \right\|_F^2. \quad (4.77)$$

However, solving the optimization problem (4.77) in closed-form is not straightforward [125]. In addition, due to the low rate of the feedback channel, it is impossible to send back high-precision beamforming weight vector data. Then, the beamforming weight vector should be quantized, according to the QEGT scheme [125]. The receiver and transmitter are supposed to both know a codebook Ψ from which the beamforming weight vector is selected. Let the cardinality of Ψ be N , $\Psi = \{\psi_1, \psi_2, \dots, \psi_N\}$ where ψ_i ($i = 1, 2, \dots, N$) is the beamforming weight vector selected for EGT. Then, information about the chosen beamforming vector can be conveyed to the transmitter using $\lceil \log_2 N \rceil$ bits of feedback, where $\lceil \cdot \rceil$ stands for the ceiling function. Such codebook design, defined as Grassmannian line packing, has been widely investigated in previous works [125–127]. By denoting the chosen codebook for QEGT as Ψ^* , the SNR-maximizing beamforming weight vector can be expressed according to

$$\mathbf{w}^{\text{QEGT}} = \arg \max_{\psi \in \Psi^*} \left\| \hat{\mathbf{H}} \psi \right\|_F^2. \quad (4.78)$$

Next, we analyze the performance of MIMO QEGT/MRC in uncorrelated quasi-static frequency-flat Rayleigh fading channels in the presence of HPA nonlinearity, in terms of average SEP and mutual information.

Average Symbol Error Probability

It has been assumed that the transfer function of nonlinear HPA is perfectly known at the MRC receiver. Thus, we can derive the constellation and decision regions of

arbitrary two-dimensional modulation in the case with HPA nonlinearity based on this knowledge. An example illustrating such distortion is shown in Fig. 4.2, where we present the constellation and decision regions of rectangular 16-QAM without and with HPA distortion.

Since the channel estimation error Θ is complex Gaussian distributed, both the interference term introduced by the imperfect channel estimation, $\frac{\mathbf{w}_{\text{EGT}}^H \hat{\mathbf{H}}^H \Theta \mathbf{w}_{\text{EGT}}}{\|\hat{\mathbf{H}} \mathbf{w}_{\text{EGT}}\|_F} \hat{x}$, and the noise, $\frac{\mathbf{w}_{\text{EGT}}^H \hat{\mathbf{H}}^H}{\|\hat{\mathbf{H}} \mathbf{w}_{\text{EGT}}\|_F} \mathbf{n}$, are complex Gaussian distributed (given $\hat{\mathbf{H}}$ and \hat{x}). Then, making use of the Craig's method [113], the instantaneous SEP for arbitrary two-dimensional modulations is given by

$$P_{s,\text{QE/M}}(\gamma_{\text{QE/M}}) = \sum_{i=1}^M \sum_{j=1}^{D_i} \frac{P(s_i)}{2\pi} \int_0^{\eta_{i,j}} \exp\left[-\frac{c_{i,j} \gamma_{\text{QE/M}} \sin^2 \phi_{i,j}}{\sin^2(\vartheta + \phi_{i,j})}\right] d\vartheta, \quad (4.79)$$

where M represents the number of symbols in the constellation, D_i indicates the number of sub-regions for symbol s_i , $P(s_i)$ denotes the *a priori* probability that symbol s_i is transmitted, and $c_{i,j} = l_{i,j} / [n_T E (f_A^2 (|x| / \sqrt{n_T}))]$ is the scaling factor. Parameters $l_{i,j}$, $\eta_{i,j}$ and $\phi_{i,j}$ are related to symbol s_i and sub-region j , and are determined by the decision region geometry [113]. In addition, $\gamma_{\text{QE/M}}$ in (4.79) refers to the output SNR of the MIMO QEGT/MRC system and can be expressed as

$$\begin{aligned} \gamma_{\text{QE/M}} &= \frac{\rho_h^2 \bar{\gamma}_{\text{NL}} \max_{\psi \in \Psi^*} \|\hat{\mathbf{H}} \psi\|_F^2}{\bar{\gamma}_{\text{NL}} \sigma_{\Theta}^2 + 1} \\ &= \frac{\bar{\gamma}_{\text{NL}}}{1 + \sigma_h^2 (1 + \bar{\gamma}_{\text{NL}})} \max_{\psi \in \Psi^*} \|\hat{\mathbf{H}} \psi\|_F^2 \\ &= \frac{\bar{\gamma}_{\text{NL}}}{1 + \sigma_h^2 (1 + \bar{\gamma}_{\text{NL}})} \|\hat{\mathbf{H}}\|_F^2 \max_{\psi \in \Psi^*} \|\tilde{\mathbf{H}} \psi\|_F^2 \\ &= \frac{\bar{\gamma}_{\text{NL}}}{1 + \sigma_h^2 (1 + \bar{\gamma}_{\text{NL}})} \|\hat{\mathbf{H}}\|_F^2 \left[1 - \min_{\psi \in \Psi^*} d^2(\tilde{\mathbf{H}}, \psi)\right], \end{aligned} \quad (4.80)$$

where $\tilde{\mathbf{H}} = \hat{\mathbf{H}} / \|\hat{\mathbf{H}}\|_F$ and $d^2(\tilde{\mathbf{H}}, \psi) = 1 - \|\tilde{\mathbf{H}} \psi\|_F^2$. To simplify the notation, we

define two independent random variables

$$\gamma_h := \|\mathbf{H}\|_F^2 \quad (4.81)$$

and

$$V := \min_{\psi \in \Psi^*} d^2(\tilde{\mathbf{H}}, \psi), \quad (4.82)$$

which we use to re-express the SNR in (4.80) according to

$$\gamma_{\text{QE/M}} = \frac{\bar{\gamma}_{\text{NL}}}{1 + \sigma_h^2(1 + \bar{\gamma}_{\text{NL}})} (1 - V) \gamma_h. \quad (4.83)$$

Denoting $\mathcal{K} := n_T \times n_R$, the PDF of γ_h is given by [106]

$$p(\gamma_h) = \frac{\gamma_h^{\mathcal{K}-1}}{\Gamma(\mathcal{K})} e^{-\gamma_h}, \quad (4.84)$$

where $\Gamma(\cdot)$ denotes the Gamma function. On the other hand, V is a random variable within the interval $[0, 1]$. By denoting $p(v)$ and $F_V(v)$ as the PDF and cumulative distribution function (CDF) of V , the characteristic function of $\gamma_{\text{QE/M}}$ can be expressed as

$$\Psi_{\gamma_{\text{QE/M}}}(j\omega) = \int_0^1 \left[1 - j\omega \frac{\bar{\gamma}_{\text{NL}}}{1 + \sigma_h^2(1 + \bar{\gamma}_{\text{NL}})} (1 - v) \right]^{-\mathcal{K}} dF_V(v). \quad (4.85)$$

Then, the average SEP is given by

$$P_{s,\text{QE/M}} = \int_0^\infty \int_0^1 P_{s,\text{QE/M}} \left(\frac{\bar{\gamma}_{\text{NL}}}{1 + \sigma_h^2(1 + \bar{\gamma}_{\text{NL}})} (1 - v) \gamma_h \right) p(\gamma_h) p(v) dv d\gamma_h. \quad (4.86)$$

Subsequently, substituting (4.79) into (4.86) and making use of the moment generating function (MGF)-based method, the average SEP can be expressed as

$$P_{s,\text{QE/M}} = \sum_{i=1}^M \sum_{j=1}^{D_i} \frac{P(s_i)}{2\pi}$$

$$\times \int_0^{\eta_{i,j}} \int_0^1 \left[1 + \frac{\bar{\gamma}_{\text{NL}}}{1 + \sigma_h^2 (1 + \bar{\gamma}_{\text{NL}})} \frac{c_{i,j} \sin^2 \phi_{i,j} (1 - v)}{\sin^2 (\vartheta + \phi_{i,j})} \right]^{-\mathcal{K}} dF_V(v) d\vartheta. \quad (4.87)$$

Deriving the average SEP in closed-form is not straightforward, since $F_V(v)$ depends on the particular codebook design. Herein, using a methodology similar to that in [128], we provide a lower bound on the average SEP:

$$\begin{aligned} P_{s,\text{QE}/\text{M}}^{\text{low}} &:= \sum_{i=1}^M \sum_{j=1}^{D_i} \frac{P(s_i)}{2\pi} \\ &\times \int_0^{\eta_{i,j}} \int_0^1 \left[1 + \frac{\bar{\gamma}_{\text{NL}}}{1 + \sigma_h^2 (1 + \bar{\gamma}_{\text{NL}})} \frac{c_{i,j} \sin^2 \phi_{i,j} (1 - v)}{\sin^2 (\vartheta + \phi_{i,j})} \right]^{-\mathcal{K}} d\tilde{F}_V(v) d\vartheta, \end{aligned} \quad (4.88)$$

conditioned on

$$F_V(v) \leq \tilde{F}_V(v), \quad 0 \leq v \leq 1. \quad (4.89)$$

The upper bound $\tilde{F}_V(v)$ is given by [128, eq. 31]

$$\tilde{F}_V(v) = \begin{cases} Nv^{\mathcal{K}-1}, & 0 \leq v < \left(\frac{1}{N}\right)^{\frac{1}{\mathcal{K}-1}} \\ 1, & v \geq \left(\frac{1}{N}\right)^{\frac{1}{\mathcal{K}-1}}. \end{cases} \quad (4.90)$$

Substituting (4.90) into (4.88), the lower bound on the average SEP of MIMO QEGT/MRC over uncorrelated Rayleigh fading channels in the presence of HPA nonlinearity can be further expressed as

$$\begin{aligned} P_{s,\text{QE}/\text{M}}^{\text{low}} &= \sum_{i=1}^M \sum_{j=1}^{D_i} \frac{P(s_i)}{2\pi} \int_0^{\eta_{i,j}} \left[1 + \frac{\bar{\gamma}_{\text{NL}}}{1 + \sigma_h^2 (1 + \bar{\gamma}_{\text{NL}})} \frac{c_{i,j} \sin^2 \phi_{i,j}}{\sin^2 (\vartheta + \phi_{i,j})} \right]^{-1} \\ &\times \left[1 + \left(1 - N^{-\frac{1}{\mathcal{K}-1}}\right) \frac{\bar{\gamma}_{\text{NL}}}{1 + \sigma_h^2 (1 + \bar{\gamma}_{\text{NL}})} \frac{c_{i,j} \sin^2 \phi_{i,j}}{\sin^2 (\vartheta + \phi_{i,j})} \right]^{1-\mathcal{K}} d\vartheta. \end{aligned} \quad (4.91)$$

Finally, making using of [114, App. C], the lower bound on the average SEP of the

considered system can be obtained as

$$P_{s,\text{QE/M}}^{\text{low}} = \sum_{i=1}^M \sum_{j=1}^{D_i} \frac{P(s_i)}{2\pi} I_{K-1} \left(\eta_{i,j}, \frac{\bar{\gamma}_{\text{NL}}}{1 + \sigma_h^2 (1 + \bar{\gamma}_{\text{NL}})} c_{i,j} \sin^2 \phi_{i,j}, \right. \\ \left. \left(1 - N^{-\frac{1}{K-1}} \right) \frac{\bar{\gamma}_{\text{NL}}}{1 + \sigma_h^2 (1 + \bar{\gamma}_{\text{NL}})} c_{i,j} \sin^2 \phi_{i,j} \right), \quad (4.92)$$

where $I_n(\cdot, \cdot, \cdot)$ is given in [114, eq. 79].

Mutual Information

Herein, we provide an upper bound on the mutual information of the MIMO QEGT/MRC in the presence of imperfect channel estimation and HPA nonlinearity. The mutual information of the MIMO QEGT/MRC system can be expressed in [bps/Hz] as

$$I_{\text{QE/M}}(x; \hat{y}_{\text{EGT/MRC}}) = E_{\hat{\mathbf{H}}} \left[h_{\text{QE/M}}(\hat{y}_{\text{EGT/MRC}} | \hat{\mathbf{H}}) - h_{\text{QE/M}}(\hat{y}_{\text{EGT/MRC}} | x, \hat{\mathbf{H}}) \right], \quad (4.93)$$

where $h(\cdot)$ represents the entropy function.

In the case that the HPA parameters are deterministic and known at the transmitter and since the channel estimation error matrix Θ is a complex Gaussian variable, the interference term introduced by the imperfect channel estimation, $\frac{\mathbf{w}_{\text{EGT}}^H \hat{\mathbf{H}}^H \Theta \mathbf{w}_{\text{EGT}}}{\|\hat{\mathbf{H}} \mathbf{w}_{\text{EGT}}\|_F} \hat{x}$, and the noise, $\frac{\mathbf{w}_{\text{EGT}}^H \hat{\mathbf{H}}^H \mathbf{n}}{\|\hat{\mathbf{H}} \mathbf{w}_{\text{EGT}}\|_F}$, are both complex Gaussian distributed (given $\hat{\mathbf{H}}$ and \hat{x}). Then, the entropy $h_{\text{QE/M}}(\hat{y} | x, \mathbf{H})$ is given by

$$h_{\text{QE/M}}(\hat{y}_{\text{EGT/MRC}} | x, \hat{\mathbf{H}}) = E_{\hat{x}} \left[\log_2 2\pi e \left(N_0 + \frac{\sigma_h^2}{1 + \sigma_h^2} |\hat{x}|^2 \right) \right]. \quad (4.94)$$

On the other hand, the maximal entropy over all the distributions with the same variance is the one with Gaussian distribution. Therefore, the entropy $h_{\text{QE/M}}(\hat{y}_{\text{EGT/MRC}} | \hat{\mathbf{H}})$

can be upper bounded as

$$\begin{aligned}
h_{\text{QE/M}} \left(\hat{y}_{\text{EGT/MRC}} \mid \hat{\mathbf{H}} \right) &\leq \log_2 2\pi e \left[\frac{\bar{\gamma}_{\text{NL}}}{1 + \sigma_h^2} \max_{\psi \in \Psi^*} \left\| \hat{\mathbf{H}}\psi \right\|_F^2 + N_0 \left(1 + \frac{\sigma_h^2}{1 + \sigma_h^2} \bar{\gamma}_{\text{NL}} \right) \right] \\
&= \log_2 \frac{2\pi e}{1 + \sigma_h^2} \left\{ n_{\text{T}} E \left(f_A^2 \left(\sqrt{|x|^2/n_{\text{T}}} \right) \right) \max_{\psi \in \Psi^*} \left\| \hat{\mathbf{H}}\psi \right\|_F^2 \right. \\
&\quad \left. + N_0 \left[1 + \sigma_h^2 \left(1 + n_{\text{T}} E \left(f_A^2 \left(\sqrt{|x|^2/n_{\text{T}}} \right) \right) \right) \right] \right\} \\
&\leq \log_2 \frac{2\pi e}{1 + \sigma_h^2} \left\{ n_{\text{T}} f_A^2 \left(\sqrt{E(|x|^2)/n_{\text{T}}} \right) \max_{\psi \in \Psi^*} \left\| \hat{\mathbf{H}}\psi \right\|_F^2 \right. \\
&\quad \left. + N_0 \left[1 + \sigma_h^2 \left(1 + n_{\text{T}} f_A^2 \left(\sqrt{E(|x|^2)/n_{\text{T}}} \right) \right) \right] \right\} \\
&= \log_2 \frac{2\pi e}{1 + \sigma_h^2} \left\{ n_{\text{T}} f_A^2 \left(\sqrt{N_0 \bar{\gamma}/n_{\text{T}}} \right) \max_{\psi \in \Psi^*} \left\| \hat{\mathbf{H}}\psi \right\|_F^2 \right. \\
&\quad \left. + \left[1 + \sigma_h^2 \left(1 + n_{\text{T}} f_A^2 \left(\sqrt{N_0 \bar{\gamma}/n_{\text{T}}} \right) \right) \right] \right\}, \tag{4.95}
\end{aligned}$$

where the second inequality is based on the Jensen's inequality, using the fact that $g(x) = \sqrt{x}$ and the AM/AM conversion function $f_A(\cdot)$ are convex. By substituting (4.94) and (4.95) into (4.93), the mutual information is upper-bounded as

$$I_{\text{QE/M}}(x; \hat{y}_{\text{EGT/MRC}}) \leq E_{\hat{\mathbf{H}}} \left\{ \log_2 \left[1 + \frac{\mu}{1 + \sigma_h^2(1 + \mu)} \max_{\psi \in \Psi^*} \left\| \hat{\mathbf{H}}\psi \right\|_F^2 \right] \right\} + \Delta_{\text{QE/M}}, \tag{4.96}$$

where $\mu = n_{\text{T}} f_A^2 \left(\sqrt{N_0 \bar{\gamma}/n_{\text{T}}} \right) / N_0$, and the second term in (4.96) can be expressed as

$$\Delta_{\text{QE/M}} = E_{\hat{x}} \left[\log_2 \frac{N_0(1 + \sigma_h^2) + \sigma_h^2 P_0^{\text{HPA}}}{N_0(1 + \sigma_h^2) + \sigma_h^2 |\hat{x}|^2} \right]. \tag{4.97}$$

In the case with high signal power, making use of a similar methodology as that taken to derive (4.73), $\Delta_{\text{QE/M}}$ is given by

$$\begin{aligned}
\lim_{P_0 \rightarrow \infty} \Delta_{\text{QE/M}} &= \frac{\gamma_{\text{Eu}}}{\ln 2} \\
&\approx 0.83. \tag{4.98}
\end{aligned}$$

Then, applying (4.81) and (4.82) in (4.96), the mutual information can be further

expressed as

$$I_{\text{QE/M}}(x; \hat{y}_{\text{EGT/MRC}}) \leq \Delta_{\text{QE/M}} + \int_0^\infty \int_0^1 \log_2 \left[1 + \frac{\mu}{1 + \sigma_h^2(1 + \mu)} (1 - v) \gamma_h \right] p(\gamma_h) p(v) dv d\gamma_h. \quad (4.99)$$

Consequently, making use of [106, App. B] and using the approach we employed in Section 4.2.4, an upper bound on the mutual information of the MIMO QEGT/MRC systems over uncorrelated Rayleigh channels taking into account the HPA nonlinearity can be obtained as

$$I_{\text{QE/M}}^{\text{up}}(x; \hat{y}_{\text{EGT/MRC}}) = \log_2 e \int_0^1 e^{\frac{1 + \sigma_h^2(1 + \mu)}{\mu(1 - v)}} \sum_{j=1}^{\mathcal{K}} E_{\mathcal{K}+1-j} \left(\frac{1 + \sigma_h^2(1 + \mu)}{\mu(1 - v)} \right) d\tilde{F}_V(v), \quad (4.100)$$

where $\tilde{F}_V(v)$ is as defined in (4.90).

4.2.5 Numerical and Simulation Results

In this section, we present numerical and simulation results illustrating the performance of the optimal beamforming and QEGT/MRC schemes in the presence of HPA nonlinearity in uncorrelated quasi-static frequency-flat Rayleigh fading channels, specifically on the average SEP and mutual information with Gaussian input. Herein, we consider the SSPA model for the nonlinear HPA. The output saturation voltage is set to $A_{os} = 1$. In addition, we set the ratio of the pilot power to the noise power spectral density to $\xi_p/N_0 = 10$ dB.

Above all, we show the lower and upper bounds on the average SEP versus the average SNR per receive antenna of the optimal beamforming, for the 2×2 MIMO configuration, taking the modulation order as parameter, in comparison with simulation results. We consider $\beta = 1$ in the SSPA model. Furthermore, we also set $V = 16$. The average SEP of the MIMO MRT/MRC system in the case without linear HPAs and perfect channel estimation is taken as the performance baseline. Fig.

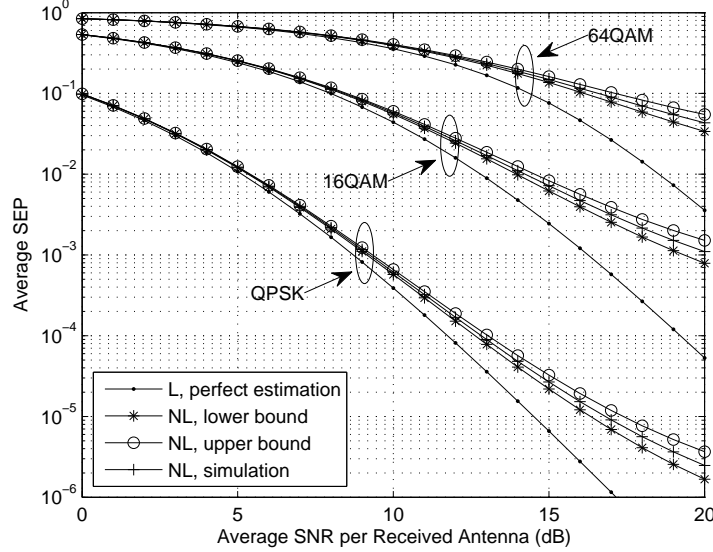


Figure 4.12: Lower and upper bounds on the average SEP versus $\bar{\gamma}$ of the optimal beamforming with HPA nonlinearity for different modulation formats ($n_T = n_R = 2$, $\beta = 1$, $V = 16$).

4.12 indicates that the degradation caused by the HPA nonlinearity on the average SEP increases as $\bar{\gamma}$ gets larger. Furthermore, the gap between the lower and upper bounds on the average SEP becomes larger as $\bar{\gamma}$ increases. The gap is also the largest for 64QAM and the least for quadrature phase-shift keying (QPSK).

To further demonstrate the effect of HPA nonlinearity on the average SEP, results for different values of β , taking 16QAM as the modulation scheme in the 2×2 MIMO configuration, are provided in Fig. 4.13. In this case, we set $V = 16$. As observed, the average SEP of the optimal MIMO beamforming system decreases as the parameter β becomes larger. Moreover, the HPA nonlinearity with $\beta \geq 1.6$ has little impact on the average SEP.

Fig. 4.14 illustrates the lower and upper bounds on the average SEP versus the average SNR per receive antenna, $\bar{\gamma}$, and shows the effects of V in the case with 2×2 MIMO configuration, 16QAM and $\beta = 1$. We see that the average SEP of the optimal beamforming using the proposed channel estimation is reduced at the cost of a high number of pilot symbols, due to the fact that the MSE of the channel estimation is lower in the case with more pilot symbols.

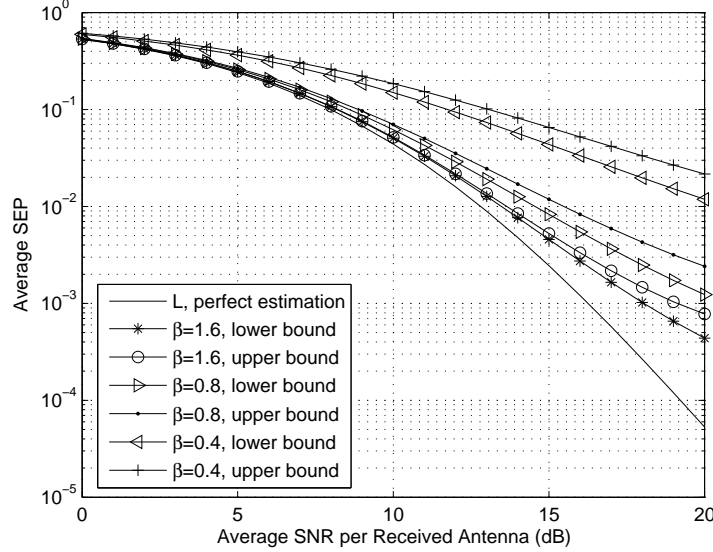


Figure 4.13: Lower and upper bounds on the average SEP versus $\bar{\gamma}$ of the optimal beamforming with HPA nonlinearity for different values of β ($n_T = n_R = 2$, 16QAM, $V = 16$).

In addition, in Fig. 4.15, we represent the upper and lower bounds on the mutual information with Gaussian input of the optimal beamforming, as a function of the average SNR per receive antenna, taking into account the HPA nonlinearity, for the case with $V = 16$. The effects of n_T and β on the performance are shown in this figure. As noticed, for arbitrary $n_T \times n_R$ MIMO configurations, the distortion due to HPA nonlinearity results in a degradation of the mutual information, which is larger for smaller values of β . Moreover, the HPA nonlinearity with $\beta \geq 0.8$ has little impact on the mutual information performance.

We further demonstrate the lower and upper bounds on the mutual information with Gaussian input of the optimal beamforming in Fig. 4.16, for different values of V and n_T , in the case with $\beta = 1$. It is observed that for arbitrary MIMO configurations, higher mutual information is attained by employing more pilot symbols to perform the channel estimation.

Next, we analyze the QEGT/MRC scheme, and compare its performance with that of the optimal beamforming scheme in the case with HPA nonlinearity. Comparisons are shown for the average SEP and mutual information with Gaussian input.

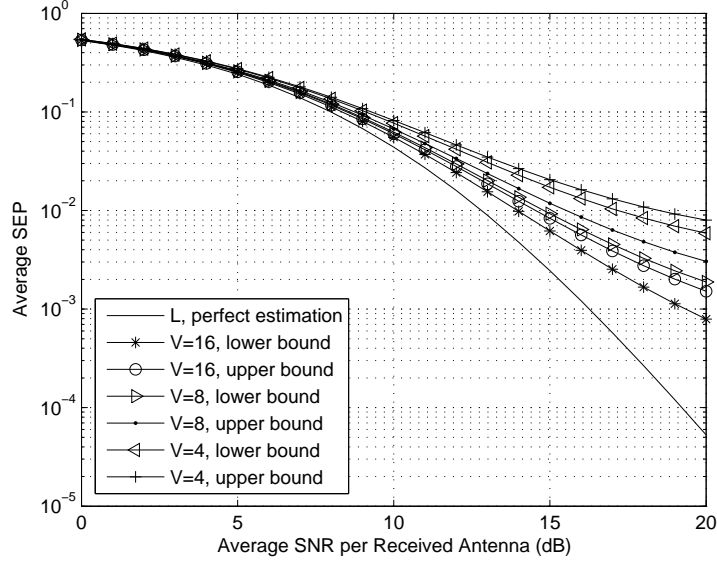


Figure 4.14: Lower and upper bounds on the average SEP versus $\bar{\gamma}$ of the optimal beamforming with HPA nonlinearity for different values of V ($n_T = n_R = 2$, 16QAM, $\beta = 1$).

Fig. 4.17 shows the average SEP versus the average SNR $\bar{\gamma}$ for the 2×2 MIMO configuration, taking the modulation order as parameter, in the cases with the optimal beamforming and QEGT/MRC. We consider $\beta = 1$ and $V = 16$. Additionally, the cardinality of the codebook pertaining to QEGT is set to $N = 16$. We observe that the lower bound on the average SEP of the QEGT/MRC is tight for different modulation formats. Given the same requirement on average SEP, the $\bar{\gamma}$ penalty of the QEGT/MRC is the largest for 64QAM and the least for QPSK. Indeed, as 64QAM works in the high SNR region, more degradation follows because of the HPA nonlinearity.

In Fig. 4.18, the effect of the cardinality of the beamforming weight vector codebook pertaining to QEGT, i.e., N , on the average SEP, is presented for the scenario with $n_T = n_R = 2$, $\beta = 1$ and $V = 16$. As noticed, the average SEP of the MIMO QEGT/MRC system can be reduced at the cost of large cardinality of the beamforming weight vector codebook. However, the average SEP of the MIMO QEGT/MRC cannot be reduced by employing a large-size codebook to approach the performance

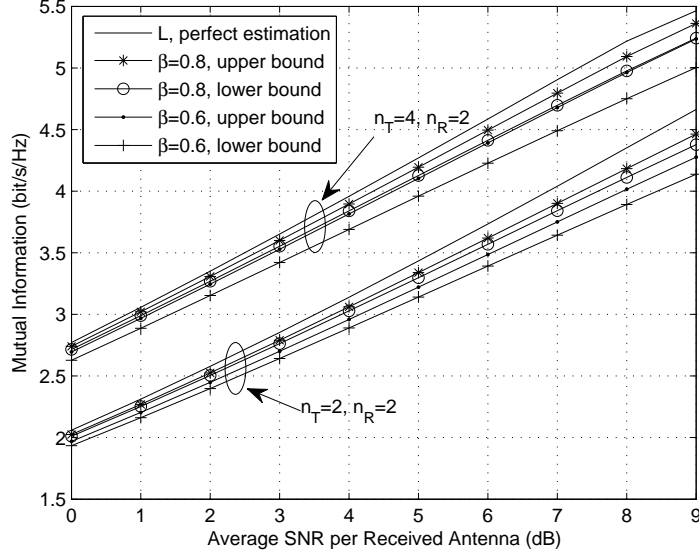


Figure 4.15: Lower and upper bounds on the mutual information under Gaussian input versus $\bar{\gamma}$ of the optimal beamforming with HPA nonlinearity for different values of β and n_T ($V = 16$).

of the MIMO MRT/MRC system without HPA nonlinearity.

Fig. 4.19 plots the upper bounds on the mutual information with Gaussian input of the optimal beamforming and QEGT/MRC as a function of the average SNR per receive antenna, $\bar{\gamma}$, taking β and n_T as the parameters, for the case with $V = 16$ and $N = 16$. We can notice that the distortion due to HPA nonlinearity results in a degradation of the mutual information, which is larger for smaller values of β . Furthermore, the HPA nonlinearity with $\beta \geq 1$ has little impact on the mutual information for both beamforming schemes.

Finally, we illustrate the upper bounds on the mutual information with Gaussian input of the QEGT/MRC scheme with different values of N , in the case with $\beta = 0.6$ and $V = 16$. As observed, the mutual information of the QEGT/MRC can be improved by increasing the cardinality of the beamforming weight vector codebook.

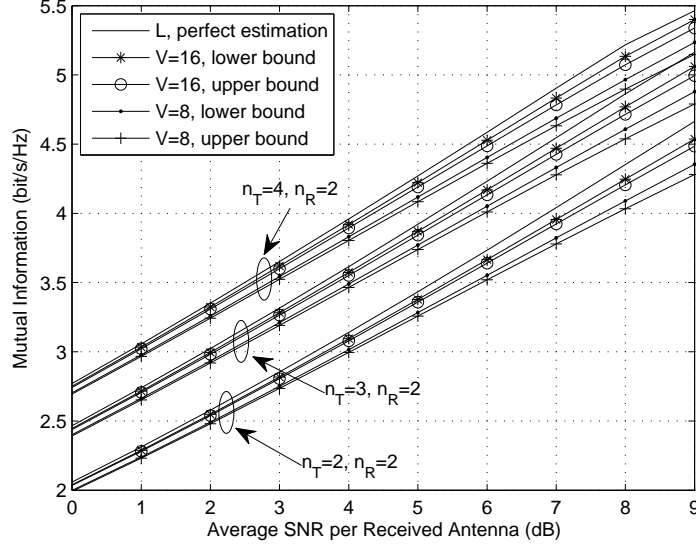


Figure 4.16: Lower and upper bounds on the mutual information under Gaussian input versus $\bar{\gamma}$ of the optimal beamforming with HPA nonlinearity for different values of V and n_T ($\beta = 1$).

4.3 Summary

In this chapter, a MIMO-OSTBC system that accounts for HPA nonlinearity was considered. We proposed a constellation-based compensation method and a SMC-based compensation algorithm for HPA nonlinearity in the case with and without knowledge of the HPA parameters, respectively. Using the proposed compensation schemes, the system performance was analyzed in terms of average SEP, TD and system capacity, when the system operates under uncorrelated Nakagami- m fading. Numerical results showing the effects of several system parameters, such as the parameters of the HPA model, OBO of nonlinear HPA, MIMO antenna configuration, modulation order of QAM, and number of SMC samples, were presented and discussed. It was shown that the constellation-based compensation method can efficiently mitigate the effect of HPA nonlinearity with low implementation complexity, and that the SMC-based compensation scheme is effective in the case without knowledge of the HPA parameters.

In addition, MIMO TB schemes with nonlinear HPAs were also studied. It was

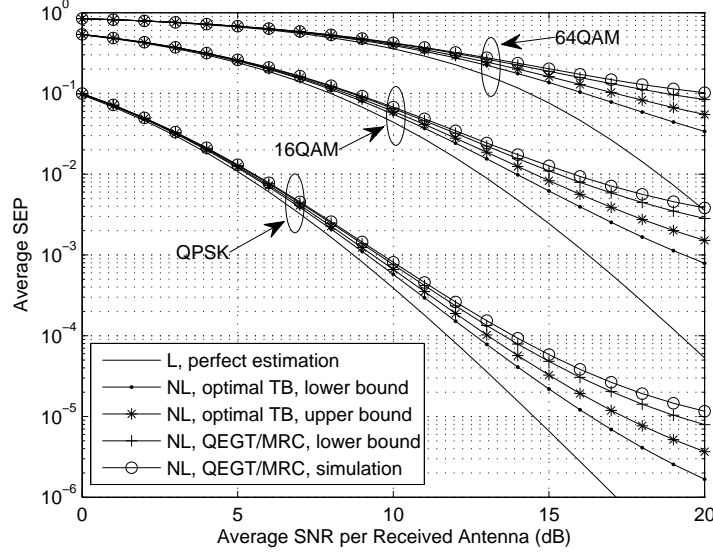


Figure 4.17: Average SEP versus $\bar{\gamma}$ of the optimal beamforming and QEGT/MRC schemes with HPA nonlinearity for different modulation formats ($n_T = n_R = 2$, $\beta = 1$, $V = 16$, $N = 16$).

illustrated that the conventional MRT/MRC scheme becomes suboptimal in the presence of HPA nonlinearity, where the spatial diversity cannot be efficiently obtained by the MRC. Then, we sought the optimal TB scheme with the optimal beamforming weight vector and combining vector for operation under HPA nonlinearity, by maximizing the output SNR. In addition, an alternative suboptimal but much simpler TB scheme, namely, QEGT/MRC, was investigated, which is feasible in the case with nonlinear HPA, profiting from the property that the elements of the beamforming weight vector have the same constant modulus. We derived lower and upper bounds on the average SEP and mutual information with Gaussian input for the proposed optimal TB scheme in the presence of HPA nonlinearity, when operating under uncorrelated quasi-static frequency-flat Rayleigh fading. Moreover, a lower bound on the average SEP and an upper bound on the mutual information were provided for the QEGT/MRC scheme. Numerical results showing the effects of several system parameters on performance were also presented and discussed.

In the next chapter, another RF impairment, namely, I/Q imbalance, in MIMO wireless communication systems, will be investigated.

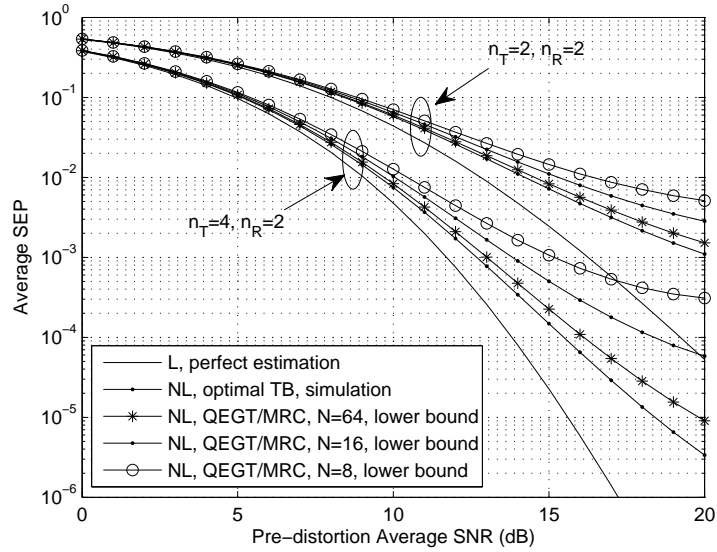


Figure 4.18: Average SEP versus $\bar{\gamma}$ of the optimal beamforming and QEGT/MRC schemes with HPA nonlinearity for different values of N ($n_T = n_R = 2$, 16QAM, $\beta = 1$, $V = 16$).

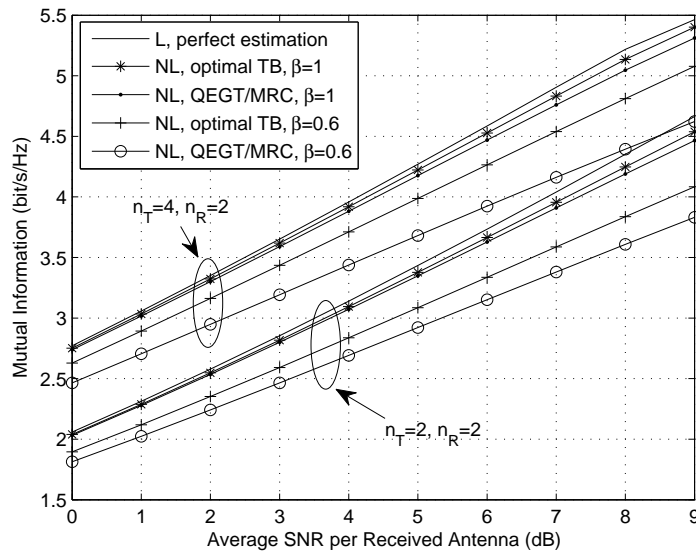


Figure 4.19: Upper bounds on the mutual information under Gaussian input versus $\bar{\gamma}$ of the optimal beamforming and QEGT/MRC schemes with HPA nonlinearity for different values of β and n_T ($V = 16$, $N = 16$).

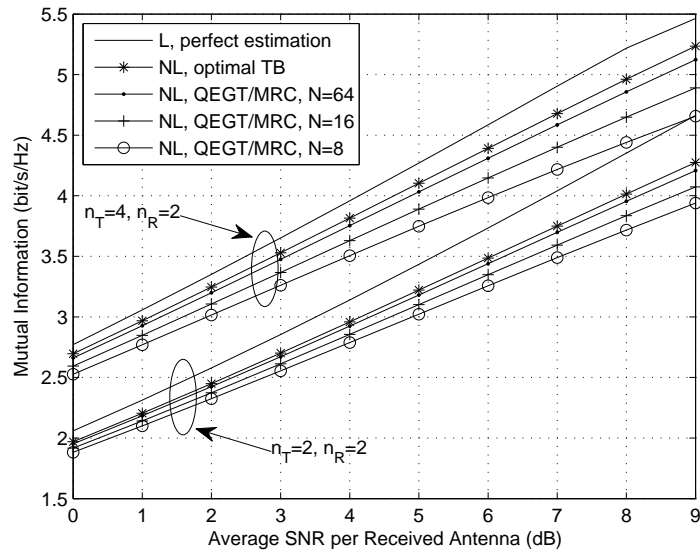


Figure 4.20: Upper bounds on the mutual information under Gaussian input versus $\bar{\gamma}$ of the optimal beamforming and QEGT/MRC schemes with HPA nonlinearity for different values of N ($\beta = 0.6$, $V = 16$).

Chapter 5

Analysis and Compensation of I/Q Imbalance

5.1 Introduction

One of the RF impairments associated with analog processing is the I/Q imbalance, which represents the mismatch between the components in the I and Q branches, i.e., the mismatch between the real and imaginary parts of complex signals. This happens due to the limited accuracy of the analog hardware, such as finite tolerances of capacitors and resistors. Section 1.1.5 introduced recent research effort on the issue of I/Q imbalance. The I/Q imbalance may occur at the transmitter and the receiver. Recently, several compensation schemes for I/Q imbalance have been proposed, which can be divided into two kinds: compensation methods with and without estimation of the parameters of I/Q imbalance, respectively.

In this chapter, we concentrate on the so-called MIMO MRC technique implementing MRT in the presence of the I/Q imbalance at the direct-conversion receiver. Herein, we consider such a system where the MRC is performed at the RF level, and present the corresponding system model considering the I/Q imbalance. We propose a channel estimation algorithm taking into account the I/Q imbalance, where the length of pilot symbols used to achieve the same performance of channel estimation

as in the case with ideal I/Q branches is twice as that in the latter. In the presence of imperfect channel estimation, the expressions for the PDF and CDF of the output SNR are obtained in closed-form, considering transmission over uncorrelated Rayleigh fading channels. Thereafter, we obtain an upper bound on the average SEP, derive the expression for the outage probability in closed-form, and provide a lower bound on the ergodic capacity. Furthermore, a compensation scheme for the I/Q imbalance is proposed, which first employs the LS rule to estimate the coefficients of the channel gain matrix, beamforming and combining weight vectors, and parameters of I/Q imbalance jointly, and then uses the received signal together with its conjugation to detect the transmitted signal. Subsequently, approximate expressions for the average SEP, outage probability and ergodic capacity of the MIMO MRC system under study over uncorrelated Rayleigh fading channels using the proposed compensation scheme are derived. Furthermore, numerical results and comparisons are provided and show the effects of system parameters, such as the image-leakage ratio, numbers of transmit and receive antennas, modulation order of QAM, and length of pilot symbols, on the MIMO MRC system performance in the presence of I/Q imbalance.

The remainder of this chapter is organized as follows: Section 5.2 introduces the MIMO MRC system model considering I/Q imbalance, including amplitude imbalance and phase imbalance. In Sections 5.3 and 5.4, we provide the signal detection without and with compensation for I/Q imbalance, respectively. In Section 5.5, the performance of the MIMO MRC system under study is analyzed in terms of average SEP, outage probability and ergodic capacity. Numerical results and comparisons are then presented in Section 5.6, followed by the summary in Section 5.7.

5.2 System and I/Q Imbalance Models

We consider a MIMO MRC system with n_T transmit and n_R receive antennas, and assume a discrete-time baseband channel model subject to quasi-static flat Rayleigh

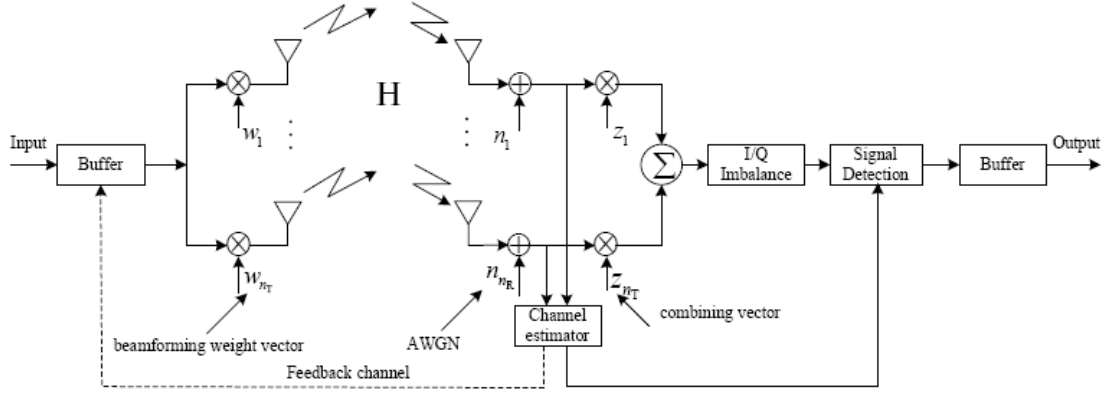


Figure 5.1: Block diagram for the considered MIMO MRC system in the presence of I/Q imbalance.

fading. The MIMO signal model can be expressed as

$$\mathbf{y} = \mathbf{H}\mathbf{w}x + \mathbf{n}, \quad (5.1)$$

where x denotes the transmitted symbol with average power P_0 , \mathbf{w} is the $n_T \times 1$ unit beamforming weight vector, \mathbf{n} refers to the $n_R \times 1$ noise vector with elements belonging to independent and identically distributed (i.i.d.) complex circular Gaussian distribution $\mathcal{CN}(0, N_0)$ uncorrelated with the transmitted symbols, and $\mathbf{H} = [h_{i,j}]_{i,j=1}^{n_R, n_T}$ expresses the $n_R \times n_T$ channel gain matrix with $h_{i,j}$ representing the channel coefficient between the j th transmit and i th receive antennas. The entries of the channel gain matrix are i.i.d. complex Gaussian random variables, each with a $\mathcal{CN}(0, 1)$ distribution.

In conventional MIMO MRC systems, the signals received from the antenna elements are combined at baseband, which results in high power cost due to the requirement of n_R RF receive chains according to n_R receive antennas. As the number of antenna elements increases, this receiver architecture becomes costly, especially for mobile devices. However, if the signal combining takes place at the RF level, only one receive chain is required, which produces essentially the same output as with the conventional MRC receiver [129]. Hereafter, we consider the approach that combines signals from antenna elements at the RF level. The block diagram for the considered

MIMO MRC system is shown in Fig. 5.1.

At the receiver side, the signals from all antenna branches are weighted by the $n_R \times 1$ combining vector \mathbf{z} . Then, the combined signal, \tilde{y} , conditioned on the channel gain matrix \mathbf{H} and the beamforming weight vector \mathbf{w} , is given by

$$\tilde{y} = \mathbf{z}^H \mathbf{H} \mathbf{w} x + \mathbf{z}^H \mathbf{n}. \quad (5.2)$$

However, in practice, I/Q imbalance occurs in the RF processing at the direct-conversion receiver. This happens due to the limited accuracy of the analog hardware, such as finite tolerances of capacitors and resistors. Herein, we describe such imbalance behavior using typical models from the literature (see, e.g., [49, 130]). Since the MRC is assumed to be performed at the RF level, the combined signal taking into account I/Q imbalance can be expressed as

$$\begin{aligned} \hat{y} &= K_1 \tilde{y} + K_2 \tilde{y}^* \\ &= K_1 (\mathbf{z}^H \mathbf{H} \mathbf{w} x + \mathbf{z}^H \mathbf{n}) + K_2 (\mathbf{z}^H \mathbf{H} \mathbf{w} x + \mathbf{z}^H \mathbf{n})^*, \end{aligned} \quad (5.3)$$

where $K_2 \tilde{y}^*$ denotes the image of signal $K_1 \tilde{y}$. The coefficients K_1 and K_2 are of the form $K_1 = (1 + g e^{-j\theta})/2$ and $K_2 = (1 - g e^{j\theta})/2$, where g and θ represent the gain imbalance and phase imbalance, respectively. It can be observed that the coefficients K_1 and K_2 are related through $K_2 = 1 - K_1^*$. Moreover, the image-rejection ratio can be expressed as $IRR = \left| \frac{K_1}{K_2} \right|^2$, and the image-leakage ratio is given by $ILR = \left| \frac{K_2}{K_1} \right|^2$.

5.3 Signal Detection without I/Q Imbalance Compensation

In this section, we propose a channel estimation algorithm taking into account the I/Q imbalance and then describe the detection of the transmitted signal when no compensation is used for such imbalance.

5.3.1 Proposed Channel Estimation Algorithm

As described in Section 5.2, full knowledge of the channel gain of each transmit-receive antenna link, i.e., channel gain matrix, is required in MIMO MRC systems implementing MRT. In conventional MIMO MRC systems, n_R RF receive chains according to n_R receive antennas are implemented at the receiver so as to estimate the channel gain matrix. In the case that received signals from all antenna elements are combined at the RF level, only one RF chain is implemented, as in the MIMO MRC system under study.

It is assumed that the channels are quasi-static, which implies that the channel gain matrix remains invariant in each frame and may vary from frame to frame. Under the above-mentioned assumption, the receive antenna elements can be multiplexed to the RF chain during the training period [129]. Based on this, $n_T \times V n_R$ pilot symbols $[\mathbf{S}_p \ \mathbf{S}_p \ \dots \ \mathbf{S}_p]$, with power ξ_p for each pilot symbol, are inserted at the beginning of each transmit frame in order to perform the channel estimation, where \mathbf{S}_p denotes the $n_T \times V$ transmitted pilot symbol matrix. The RF chain is connected to the first receive antenna during the first part of the pilot sequence, then to the second receive antenna during the second part, and so on. Thus, the required number of pilot symbols is n_R times that of conventional MIMO MRC systems. Then, the equivalent MIMO signal model for pilot symbol transmission in the presence of I/Q imbalance can be expressed as

$$\mathbf{Y}_p = K_1 (\mathbf{H}\mathbf{S}_p + \mathbf{N}_p) + K_2 (\mathbf{H}\mathbf{S}_p + \mathbf{N}_p)^*, \quad (5.4)$$

where \mathbf{Y}_p represents the $n_R \times V$ received signal matrix, \mathbf{N}_p refers to the $n_R \times V$ noise matrix with elements belonging to i.i.d. complex circular Gaussian distribution $\mathcal{CN}(0, N_0)$ uncorrelated with the transmitted pilot symbols, and \mathbf{H} expresses the same $n_R \times n_T$ channel gain matrix as that for data symbol transmission. Making use of the property $K_2 = 1 - K_1^*$, the MIMO signal model for pilot symbols can be rewritten as

$$\mathbf{Y}_p = K_1 \mathbf{H}\mathbf{S}_p - K_1^* \mathbf{H}^* \mathbf{S}_p^* + \mathbf{H}^* \mathbf{S}_p^* + K_1 \mathbf{N}_p - K_1^* \mathbf{N}_p^* + \mathbf{N}_p^*. \quad (5.5)$$

Accordingly, the conjugation of \mathbf{Y}_p is given by

$$\mathbf{Y}_p^* = K_1^* \mathbf{H}^* \mathbf{S}_p^* - K_1 \mathbf{H} \mathbf{S}_p + \mathbf{H} \mathbf{S}_p + K_1^* \mathbf{N}_p^* - K_1 \mathbf{N}_p + \mathbf{N}_p. \quad (5.6)$$

As such, we have

$$\mathbf{Y}_p + \mathbf{Y}_p^* = \mathbf{\Omega} \mathbf{Z}_p + \mathbf{N}_p + \mathbf{N}_p^*, \quad (5.7)$$

where $\mathbf{\Omega} = [\mathbf{H} \ \mathbf{H}^*]$ and $\mathbf{Z}_p = [\mathbf{S}_p \ \mathbf{S}_p^*]^T$. The channel estimation problem can be solved using the LS rule [118]. The LS estimate $\hat{\mathbf{\Omega}} = [\hat{\mathbf{H}} \ \hat{\mathbf{H}}^*]$ is given by

$$\hat{\mathbf{\Omega}} = (\mathbf{Y}_p + \mathbf{Y}_p^*) \mathbf{Z}_p^H (\mathbf{Z}_p \mathbf{Z}_p^H)^{-1}. \quad (5.8)$$

The pilot symbol matrix \mathbf{S}_p should be chosen to satisfy the constraint that the matrix $\mathbf{Z}_p \mathbf{Z}_p^H$ has full rank. It is obviously observed that the necessary condition is that $V \geq 2n_T$. The resulting mean square error (MSE) can be expressed as

$$\begin{aligned} \sigma_{\mathbf{\Omega}, \text{WI}}^2 &= E \left[\left\| \mathbf{\Omega} - \hat{\mathbf{\Omega}} \right\|_F^2 \right] \\ &= E \left[\left\| (\mathbf{N}_p + \mathbf{N}_p^*) \mathbf{Z}_p^H (\mathbf{Z}_p \mathbf{Z}_p^H)^{-1} \right\|_F^2 \right] \\ &= 2n_R N_0 \text{Tr} \left[(\mathbf{Z}_p \mathbf{Z}_p^H)^{-1} \right]. \end{aligned} \quad (5.9)$$

In order to minimize the MSE specified in (5.9), the matrix \mathbf{Z}_p should have orthogonal rows, i.e.,

$$\mathbf{Z}_p \mathbf{Z}_p^H = V \xi_p \mathbf{I}_{2n_T}, \quad (5.10)$$

that is,

$$\mathbf{S}_p \mathbf{S}_p^H = V \xi_p \mathbf{I}_{n_T}, \text{ and } \mathbf{S}_p \mathbf{S}_p^T = \mathbf{0}_{n_T}. \quad (5.11)$$

Then, the MSE using the LS estimation of the channel gain matrix \mathbf{H} is lower-bounded as

$$\sigma_{\mathbf{H}, \text{WI}}^2 = \frac{\sigma_{\mathbf{\Omega}, \text{WI}}^2}{2}$$

$$\geq \frac{2n_{\text{R}}n_{\text{T}}N_0}{V\xi_p}, \quad (5.12)$$

which is twice as that in the case with ideal I/Q branches (i.e., without I/Q imbalance). Note that “WI” in (5.12) refers to the case with I/Q imbalance. The average estimation error for each element of \mathbf{H} can be expressed as $\sigma_{h,\text{WI}}^2 = \frac{\sigma_{\hat{\mathbf{H}},\text{WI}}^2}{n_{\text{T}}n_{\text{R}}}$. The entries of $\hat{\mathbf{H}}$ are i.i.d. complex Gaussian random variables, each with a $\mathcal{CN}(0, 1 + \sigma_{h,\text{WI}}^2)$ distribution. The relationship between \mathbf{H} and $\hat{\mathbf{H}}$ can be expressed as [119]

$$\mathbf{H} = \rho_h \hat{\mathbf{H}} + \Theta, \quad (5.13)$$

where $\rho_h = \frac{1}{1 + \sigma_{h,\text{WI}}^2}$, and each component of Θ is complex Gaussian distributed variable, with zero mean and variance $\sigma_{\Theta}^2 = \frac{\sigma_{h,\text{WI}}^2}{1 + \sigma_{h,\text{WI}}^2}$, uncorrelated with the elements of \mathbf{H} . The proposed channel estimation algorithm can also be applied in the case with I/Q imbalance compensation. The effect of channel estimation error on the I/Q imbalance compensation scheme is analyzed in Section 5.4.2.

5.3.2 Detection of the Transmitted Signal

In a beamforming and combining system, the key problem is to choose \mathbf{w} and \mathbf{z} that maximize the output SNR in order to minimize the SEP. Without loss of generality, we fix $\|\mathbf{z}\|_F = 1$. A receiver where \mathbf{z} maximizes $|\mathbf{z}^H \mathbf{H} \mathbf{w}|$ given \mathbf{w} is called an MRC receiver, according to $\mathbf{z} = \mathbf{H} \mathbf{w} / \|\mathbf{H} \mathbf{w}\|_F$ [98]. Due to the imperfect channel estimation, the combining vector is given by $\mathbf{z} = \hat{\mathbf{H}} \mathbf{w} / \|\hat{\mathbf{H}} \mathbf{w}\|_F$. Accordingly, substituting the latter expression for \mathbf{z} along with (5.13) into (5.3), the received signal can further be expanded as

$$\begin{aligned} \hat{y} = & K_1 \rho_h \frac{\mathbf{w}^H \hat{\mathbf{H}}^H \hat{\mathbf{H}} \mathbf{w}}{\|\hat{\mathbf{H}} \mathbf{w}\|_F} x + K_2 \rho_h \frac{(\mathbf{w}^H \hat{\mathbf{H}}^H \hat{\mathbf{H}} \mathbf{w})^*}{\|\hat{\mathbf{H}} \mathbf{w}\|_F} x^* \\ & + K_1 \frac{\mathbf{w}^H \hat{\mathbf{H}}^H \Theta \mathbf{w}}{\|\hat{\mathbf{H}} \mathbf{w}\|_F} x + K_2 \frac{(\mathbf{w}^H \hat{\mathbf{H}}^H \Theta \mathbf{w})^*}{\|\hat{\mathbf{H}} \mathbf{w}\|_F} x^* \end{aligned}$$

$$+ K_1 \frac{\mathbf{w}^H \hat{\mathbf{H}}^H}{\|\hat{\mathbf{H}}\mathbf{w}\|_F} \mathbf{n} + K_2 \frac{(\mathbf{w}^H \hat{\mathbf{H}}^H)^*}{\|\hat{\mathbf{H}}\mathbf{w}\|_F} \mathbf{n}^*. \quad (5.14)$$

Under the assumption that the transmitted symbol x is circular, i.e., $E[x^2] = 0$, the output SNR in the case without compensation for the I/Q imbalance is given by

$$\begin{aligned} \gamma_{\text{WI\&WOC}}^{\text{MRC}} &= \frac{|K_1|^2 \rho_h^2 P_0 \mathbf{w}^H \hat{\mathbf{H}}^H \hat{\mathbf{H}} \mathbf{w}}{|K_2|^2 \rho_h^2 P_0 \mathbf{w}^H \hat{\mathbf{H}}^H \hat{\mathbf{H}} \mathbf{w} + (|K_1|^2 + |K_2|^2) P_0 \sigma_{\Theta}^2 + (|K_1|^2 + |K_2|^2) N_0} \\ &= \frac{\bar{\gamma} \mathbf{w}^H \hat{\mathbf{H}}^H \hat{\mathbf{H}} \mathbf{w} / (1 + \sigma_{h,\text{WI}}^2)}{ILLR \bar{\gamma} \mathbf{w}^H \hat{\mathbf{H}}^H \hat{\mathbf{H}} \mathbf{w} / (1 + \sigma_{h,\text{WI}}^2) + (1 + ILLR) [1 + \sigma_{h,\text{WI}}^2 (1 + \bar{\gamma})]}, \end{aligned} \quad (5.15)$$

where “WI&WOC” refers to the case with I/Q imbalance but without compensation for it, and $\bar{\gamma} = P_0/N_0$ denotes the average SNR per receive antenna. Furthermore, MRT is employed to maximize the output SNR with respect to \mathbf{w} . Above all, set $\|\mathbf{w}\|_F = 1$ to keep a constant average transmit power, irrespective of n_T , then denoting λ_{\max} as the largest eigenvalue of the Wishart matrix $\hat{\mathbf{H}}^H \hat{\mathbf{H}} / (1 + \sigma_{h,\text{WI}}^2)$, the output SNR can be rewritten as

$$\gamma_{\text{WI\&WOC}}^{\text{MRT/MRC}} = \frac{\alpha \bar{\gamma} \lambda_{\max}}{\beta \lambda_{\max} + 1}, \quad (5.16)$$

where the parameters α and β are given by

$$\begin{aligned} \alpha &= \frac{1}{(1 + ILLR) [1 + \sigma_{h,\text{WI}}^2 (1 + \bar{\gamma})]}, \\ \beta &= \frac{ILLR \bar{\gamma}}{(1 + ILLR) [1 + \sigma_{h,\text{WI}}^2 (1 + \bar{\gamma})]}. \end{aligned} \quad (5.17)$$

Herein, \mathbf{w} is the unit-norm eigenvector of the Wishart matrix $\hat{\mathbf{H}}^H \hat{\mathbf{H}} / (1 + \sigma_{h,\text{WI}}^2)$ associated with λ_{\max} , i.e., the unit-norm eigenvector of $\hat{\mathbf{H}}^H \hat{\mathbf{H}}$ associated with its

largest eigenvalue. Note that the output SNR becomes

$$\gamma_{\text{WOI}}^{\text{MRT/MRC}} = \frac{\bar{\gamma}\lambda_{\max}}{1 + \sigma_{h,\text{WOI}}^2(1 + \bar{\gamma})}, \quad (5.18)$$

for the case with ideal I/Q branches ($ILR = 0$), where “WOI” indicates the case without I/Q imbalance, and $\sigma_{h,\text{WOI}}^2 = \frac{N_0}{V\xi_p}$ is the estimation error for each element of the matrix \mathbf{H} in the case without I/Q imbalance.

5.4 Pilot-Based I/Q Imbalance Compensation Algorithm

The performance degradation caused by the I/Q imbalance specified in Section 5.3 highlights the need for compensation schemes in order to mitigate the effect of I/Q imbalance on the system performance. In this section, we propose a compensation algorithm for the I/Q imbalance in MIMO MRC systems. According to the data signal model described in (5.3), the proposed compensation scheme first estimates the coefficients $K_1\mathbf{z}^H\mathbf{H}\mathbf{w}$ and $K_2(\mathbf{z}^H\mathbf{H}\mathbf{w})^*$ using the LS method, and then makes use of the received signal and its conjugation to detect the transmitted signal.

5.4.1 Estimation of the Coefficients $K_1\mathbf{z}^H\mathbf{H}\mathbf{w}$ and $K_2(\mathbf{z}^H\mathbf{H}\mathbf{w})^*$

At the transmitter side, U pilot symbols different from those used for the channel estimation are inserted before the data symbols in each frame. Each pilot symbol is transmitted over the n_T transmit antennas similar to the data symbols. Taking the I/Q imbalance into account, the MIMO signal model for the pilot symbols can be expressed as

$$\hat{\mathbf{y}}_{p,C} = K_1\mathbf{z}^H\mathbf{H}\mathbf{w}\mathbf{s}_{p,C} + K_2(\mathbf{z}^H\mathbf{H}\mathbf{w})^*\mathbf{s}_{p,C}^* + K_1\mathbf{z}^H\mathbf{N}_{p,C} + K_2(\mathbf{z}^H\mathbf{N}_{p,C})^*, \quad (5.19)$$

where $\hat{\mathbf{y}}_{p,C}$ represents the $1 \times U$ combined received signal vector, $\mathbf{s}_{p,C}$ denotes the $1 \times U$ transmitted pilot symbol vector with power ξ_p for each element, $\mathbf{N}_{p,C}$ represents

the $n_R \times U$ noise matrix with elements belonging to i.i.d. complex circular Gaussian distribution $\mathcal{CN}(0, N_0)$ uncorrelated with the transmitted pilot symbols, and \mathbf{H} refers to the $n_R \times n_T$ channel gain matrix. The signal model in (5.19) can be rewritten as

$$\hat{\mathbf{y}}_{p,C} = \mathbf{\Phi}_C \mathbf{Q}_{p,C} + K_1 \mathbf{z}^H \mathbf{N}_{p,C} + K_2 (\mathbf{z}^H \mathbf{N}_{p,C})^*, \quad (5.20)$$

where $\mathbf{\Phi}_C = [\phi_{C,1} \ \phi_{C,2}] = [K_1 \mathbf{z}^H \mathbf{H} \mathbf{w} \ K_2 (\mathbf{z}^H \mathbf{H} \mathbf{w})^*]$ and $\mathbf{Q}_{p,C} = [\mathbf{s}_{p,C} \ \mathbf{s}_{p,C}^*]^T$. The estimation problem can be solved using the LS rule, according to

$$\hat{\mathbf{\Phi}}_C = \hat{\mathbf{y}}_{p,C} \mathbf{Q}_{p,C}^H (\mathbf{Q}_{p,C} \mathbf{Q}_{p,C}^H)^{-1}. \quad (5.21)$$

The pilot symbol vector $\mathbf{s}_{p,C}$ should be chosen such that $\mathbf{Q}_{p,C} \mathbf{Q}_{p,C}^H$ has full rank. For such, the necessary condition is that $U \geq 2$, and the resulting MSE for the estimation is given by

$$\begin{aligned} \sigma_C^2 &= E \left[\left\| \mathbf{\Phi}_C - \hat{\mathbf{\Phi}}_C \right\|_F^2 \right] \\ &= E \left[\left\| \mathbf{\Phi}_C - (\mathbf{\Phi}_C \mathbf{Q}_{p,C} + K_1 \mathbf{z}^H \mathbf{N}_{p,C} + K_2 (\mathbf{z}^H \mathbf{N}_{p,C})^*) \mathbf{Q}_{p,C}^H (\mathbf{Q}_{p,C} \mathbf{Q}_{p,C}^H)^{-1} \right\|_F^2 \right] \\ &= E \left[\left\| (K_1 \mathbf{z}^H \mathbf{N}_{p,C} + K_2 (\mathbf{z}^H \mathbf{N}_{p,C})^*) \mathbf{Q}_{p,C}^H (\mathbf{Q}_{p,C} \mathbf{Q}_{p,C}^H)^{-1} \right\|_F^2 \right] \\ &= (|K_1|^2 + |K_2|^2) N_0 \text{Tr} \left[(\mathbf{Q}_{p,C} \mathbf{Q}_{p,C}^H)^{-1} \right]. \end{aligned} \quad (5.22)$$

In order to minimize the MSE specified in (5.22), matrix $\mathbf{Q}_{p,C}$ should have orthogonal rows, i.e.,

$$\mathbf{Q}_{p,C} \mathbf{Q}_{p,C}^H = U \xi_p \mathbf{I}_2, \quad (5.23)$$

that is,

$$\mathbf{s}_{p,C} \mathbf{s}_{p,C}^H = U \xi_p, \text{ and } \mathbf{s}_{p,C} \mathbf{s}_{p,C}^T = 0. \quad (5.24)$$

Then, the MSE of the coefficient matrix $\mathbf{\Phi}_C$ using LS estimation is lower-bounded as

$$\sigma_C^2 \geq \frac{2 (|K_1|^2 + |K_2|^2) N_0}{U \xi_p}. \quad (5.25)$$

Then denoting Ψ as the estimation error, the relationship between $\hat{\Phi}_C$ and Φ_C can be expressed as

$$\hat{\Phi}_C = \Phi_C + \Psi, \quad (5.26)$$

where each element of vector $\Psi = [\psi_1 \ \psi_2]$ is a complex Gaussian distributed random variable, with zero mean and variance $\frac{\sigma_C^2}{2}$, uncorrelated with the elements of Φ_C .

5.4.2 Signal Detection Using I/Q Imbalance Compensation

Based on the coefficients $K_1 \mathbf{z}^H \mathbf{H} \mathbf{w}$ and $K_2 (\mathbf{z}^H \mathbf{H} \mathbf{w})^*$ estimated using the method specified in Section 5.4.1, the transmitted data signal can be detected consequently. The MIMO signal model in (5.3) can be rewritten as

$$\hat{y} = \phi_{C,1} x + \phi_{C,2} x^* + K_1 \mathbf{z}^H \mathbf{n} + K_2 (\mathbf{z}^H \mathbf{n})^*. \quad (5.27)$$

Then, combining (5.27) with the expression for \hat{y}^* , the received signal model is given by

$$\mathbf{Y} = \Phi_d \mathbf{X} + \mathbf{N}_d, \quad (5.28)$$

where $\mathbf{Y} = [\hat{y} \ \hat{y}^*]^T$, $\Phi_d = \begin{bmatrix} \phi_{C,1} & \phi_{C,2} \\ \phi_{C,2}^* & \phi_{C,1}^* \end{bmatrix}$, $\mathbf{N}_d = \begin{bmatrix} K_1 \mathbf{z}^H \mathbf{n} + K_2 (\mathbf{z}^H \mathbf{n})^* \\ K_2^* \mathbf{z}^H \mathbf{n} + K_1^* (\mathbf{z}^H \mathbf{n})^* \end{bmatrix}$, and $\mathbf{X} = [x \ x^*]^T$. Conditioned on the estimation of the Φ_C coefficients described in Section 5.4.1, the estimate of Φ_d can be expressed as

$$\hat{\Phi}_d = \Phi_d + \Psi_d, \quad (5.29)$$

where $\hat{\Phi}_d = \begin{bmatrix} \hat{\phi}_{C,1} & \hat{\phi}_{C,2} \\ \hat{\phi}_{C,2}^* & \hat{\phi}_{C,1}^* \end{bmatrix}$ and $\Psi_d = \begin{bmatrix} \psi_1 & \psi_2 \\ \psi_2^* & \psi_1^* \end{bmatrix}$. Then, the estimate of \mathbf{X} is given by

$$\hat{\mathbf{X}}_{\text{WI\&WC}} = \hat{\Phi}_d^{-1} \mathbf{Y}, \quad (5.30)$$

which is valid owing to the full rank property of $\hat{\Phi}_d$.

Theorem 1 *Under the assumption that $\sigma_C^2 \ll 1$ and $\sigma_{h,WI}^2 \ll 1$, the effective output*

SNR of the MIMO MRC system under study, using the channel estimation algorithm proposed in Section 5.3.1 and the coefficients estimation scheme specified in Section 5.4.1, can be approximated as (5.31)

$$\begin{aligned} \gamma_{WI\&WC}^{MRT/MRC} &\approx \frac{1}{\frac{(|K_1|^2+|K_2|^2)(1+\sigma_{h,WI}^2)}{(|K_1|^2-|K_2|^2)^2\lambda_{\max}} \left[1 + \left(\frac{|K_1|^2+|K_2|^2}{|K_1|^2-|K_2|^2} \right)^2 \frac{2\sigma_{h,WI}^2}{\lambda_{\max}} \right]} \\ &\times \frac{\bar{\gamma}}{\left\{ |K_1|^2 + |K_2|^2 + \bar{\gamma}\sigma_C^2 + \left(\frac{|K_1|^2+|K_2|^2}{|K_1|^2-|K_2|^2} \right)^2 \frac{\sigma_C^2(1+\sigma_{h,WI}^2)}{\lambda_{\max}} \left[1 + \left(\frac{|K_1|^2+|K_2|^2}{|K_1|^2-|K_2|^2} \right)^2 \frac{2\sigma_{h,WI}^2}{\lambda_{\max}} \right] \right\}}, \end{aligned} \quad (5.31)$$

where “WI&WC” refers to the case with I/Q imbalance and its compensation.

Proof: The proof of the above theorem is provided in Appendix A.2.

5.5 Performance Analysis

In this section, we analyze the performance of MIMO MRC systems without and with compensation for I/Q imbalance, respectively. Performance metrics, namely, average SEP, outage probability and ergodic capacity, are derived considering uncorrelated Rayleigh fading.

5.5.1 Performance without I/Q Imbalance Compensation

Since the entries of $\hat{\mathbf{H}}/\sqrt{1+\sigma_{h,WI}^2}$ are i.i.d. complex Gaussian random variables, each with a $\mathcal{CN}(0,1)$ distribution, the PDF for the largest eigenvalue of the Wishart matrix $\hat{\mathbf{H}}^H\hat{\mathbf{H}}/(1+\sigma_{h,WI}^2)$, is given by [98]

$$p_{\lambda_{\max}}(\lambda) = \sum_{k=1}^p \sum_{l=q-p}^{(p+q-2k)k} \frac{d_{k,l}}{l!} k^{l+1} \lambda^l e^{-k\lambda}, \quad (5.32)$$

where $p = \min\{n_T, n_R\}$, $q = \max\{n_T, n_R\}$, and the coefficient $d_{k,l}$ can be obtained using the algorithm proposed in [121]. It can be observed that $p_{\lambda_{\max}}(\lambda)$ is a finite

linear combination of elementary Gamma PDFs with parameter $l + 1$ and mean $(l + 1)/k$. Consequently, the PDF of the output SNR for the MIMO MRC system under consideration of I/Q imbalance can be derived as

$$p_{\gamma_{\text{WI\&WOC}}}(\gamma) = \alpha\bar{\gamma} \sum_{k=1}^p \sum_{l=q-p}^{(p+q-2k)k} \frac{d_{k,l}}{l!} k^{l+1} \gamma^l \phi(\gamma)^{-(l+2)} e^{-\frac{k\gamma}{\phi(\gamma)}}, \quad (5.33)$$

where α and β are as previously defined in (5.17), and $\phi(\gamma)$ is given by

$$\phi(\gamma) = \alpha\bar{\gamma} - \beta\gamma. \quad (5.34)$$

Moreover, it can be observed that the range of the output SNR is $(0, \alpha\bar{\gamma}/\beta)$. In addition, the CDF of the output SNR can be expressed according to

$$F_{\gamma_{\text{WI\&WOC}}}(\gamma) = \sum_{k=1}^p \sum_{l=q-p}^{(p+q-2k)k} d_{k,l} \left\{ 1 - \bar{\Gamma} \left[l + 1, \frac{k\gamma}{\phi(\gamma)} \right] \right\}, \quad (5.35)$$

where $\bar{\Gamma}(m, x) := \int_x^\infty t^{m-1} e^{-t} dt / \Gamma(m)$ denotes the normalized complementary incomplete Gamma function, with $\Gamma(\cdot)$ representing the Gamma function.

Average SEP

The average SEP for general modulation formats in AWGN channels can be expressed as [105]

$$P_s = E_\gamma \left\{ aQ \left(\sqrt{2b\gamma} \right) \right\}, \quad (5.36)$$

where $Q(\cdot)$ represents the Gaussian Q-function, and a and b are modulation-specific constants. For instance, $a \approx 4$ and $b \approx \frac{3}{2(M-1)}$ for M -QAM [105]. However, in the case with I/Q imbalance, the transmitted signal is interfered by not only AWGN, but also the distortion caused by the I/Q mismatch. Note that the self-interference due to I/Q imbalance is correlated with the transmitted symbol; hence, the summation of the interference and noise is not necessarily Gaussian distributed. Herein, we provide an upper bound on the average SEP, i.e., (5.36), under the assumption that the

interference and noise are Gaussian random variables; using the alternative expression for (5.36) based on integration by parts [131, eq. 32], this upper bound is given by

$$P_{\text{up}}^{\text{WI\&WOC}} = \frac{a\sqrt{b}}{2\sqrt{\pi}} \int_0^{\alpha\bar{\gamma}/\beta} \frac{e^{-bu}}{\sqrt{u}} F_{\gamma_{\text{WI\&WOC}}}(u) du. \quad (5.37)$$

Moreover, by using the following change of variable

$$u = \frac{\alpha\bar{\gamma}v}{1 + \beta v}, \quad (5.38)$$

it can be observed that the integration interval in (5.37) becomes $[0, \infty)$, which is convenient for further derivation. Accordingly, the average SEP is upper bounded as

$$P_{\text{up}}^{\text{WI\&WOC}} = \frac{a\sqrt{b\alpha\bar{\gamma}}}{2\sqrt{\pi}} \sum_{k=1}^p \sum_{l=q-p}^{(p+q-2k)k} d_{k,l} \underbrace{\int_0^{\infty} v^{-\frac{1}{2}} (1 + \beta v)^{-\frac{3}{2}} e^{-\frac{b\alpha\bar{\gamma}v}{1+\beta v}} [1 - \bar{\Gamma}(l+1, kv)] dv}_{:=\aleph(k,l)}. \quad (5.39)$$

Then, making use of the following identity [106]

$$\bar{\Gamma}(l+1, kv) = e^{-kv} \sum_{m=0}^l \frac{1}{m!} (kv)^m, \quad (5.40)$$

and applying the Taylor series expansion, the integral in (5.39) can be expressed as

$$\begin{aligned} \aleph(k, l) &= \int_0^{\infty} v^{-\frac{1}{2}} (1 + \beta v)^{-\frac{3}{2}} e^{-\frac{b\alpha\bar{\gamma}v}{1+\beta v}} dv \\ &\quad - \sum_{m=0}^l \frac{k^m}{m!} \int_0^{\infty} v^{m-\frac{1}{2}} (1 + \beta v)^{-\frac{3}{2}} e^{-kv} e^{-\frac{b\alpha\bar{\gamma}v}{1+\beta v}} dv \\ &= \int_0^{\infty} v^{-\frac{1}{2}} (1 + \beta v)^{-\frac{3}{2}} \left[\sum_{n=0}^{\infty} \frac{1}{n!} \left(\frac{-b\alpha\bar{\gamma}v}{1 + \beta v} \right)^n \right] dv \\ &\quad - \sum_{m=0}^l \frac{k^m}{m!} \int_0^{\infty} v^{m-\frac{1}{2}} (1 + \beta v)^{-\frac{3}{2}} e^{-kv} \left[\sum_{n=0}^{\infty} \frac{1}{n!} \left(\frac{b\alpha\bar{\gamma}v}{1 + \beta v} \right)^n \right] dv \end{aligned}$$

$$\begin{aligned}
&= \sum_{n=0}^{\infty} \frac{(-b\alpha\bar{\gamma})^n}{n!} \left(n + \frac{1}{2}\right)^{-1} \beta^{-(n+\frac{1}{2})} \\
&\quad - \sum_{m=0}^l \frac{k^m}{m!} \sum_{n=0}^{\infty} \frac{(-b\alpha\bar{\gamma})^n}{n!} \int_0^{\infty} v^{m+n-\frac{1}{2}} (1+\beta v)^{-n-\frac{3}{2}} e^{-kv} dv. \quad (5.41)
\end{aligned}$$

To proceed, we introduce the following integral representation

$$\begin{aligned}
\int_0^{\infty} v^n (1+\beta v)^y e^{-\frac{v}{a}} dv &= \frac{\Gamma(n+1) \Gamma(-1-n-y) {}_1F_1(1+n, n+y+2, 1/a\beta)}{\beta^{n+1} \Gamma(-y)} \\
&\quad + a^{n+1+y} \beta^y \Gamma(n+1+y) {}_1F_1(-y, -n-y, 1/a\beta), \quad (5.42)
\end{aligned}$$

which is valid for $n \geq 0$, $\text{Re}(a) > 0$, $\arg\{\beta\} \neq \pi$, where $\text{Re}(\cdot)$ represents the real part of a complex number and ${}_1F_1(\cdot, \cdot, \cdot)$ denotes the confluent Hypergeometric function [93]. Then, by applying (5.42) to (5.41) and substituting the latter into (5.39), the upper bound on the average SEP is given by

$$\begin{aligned}
P_{\text{up}}^{\text{WI\&WOC}} &= \frac{a\sqrt{b\alpha\bar{\gamma}}}{2\sqrt{\pi}} \sum_{k=1}^p \sum_{l=q-p}^{(p+q-2k)k} d_{k,l} \left\{ \sum_{n=0}^{\infty} \frac{(-b\alpha\bar{\gamma})^n}{n!} \left(n + \frac{1}{2}\right)^{-1} \beta^{-(n+\frac{1}{2})} \right. \\
&\quad - \sum_{m=0}^l \frac{k^m}{m!} \sum_{n=0}^{\infty} \frac{(-b\alpha\bar{\gamma})^n}{n!} \left[\frac{\Gamma(m+n+\frac{1}{2}) \Gamma(1-m)}{\beta^{m+n+\frac{1}{2}} \Gamma(n+\frac{3}{2})} {}_1F_1\left(m+n+\frac{1}{2}, m, \frac{k}{\beta}\right) \right. \\
&\quad \left. \left. + k^{1-m} \beta^{-n-\frac{3}{2}} \Gamma(m-1) {}_1F_1\left(n+\frac{3}{2}, 2-m, \frac{k}{\beta}\right) \right] \right\}. \quad (5.43)
\end{aligned}$$

Outage Probability

This metric denotes the probability that the output SNR drops below a predefined SNR threshold, say γ_{th} . The outage probability of the MIMO MRC system in the presence of I/Q imbalance, i.e., $\Pr(\gamma \leq \gamma_{\text{th}})$, is given by

$$P_{\text{out}}^{\text{WI\&WOC}}(\gamma_{\text{th}}) = \sum_{k=1}^p \sum_{l=q-p}^{(p+q-2k)k} d_{k,l} \left\{ 1 - \bar{\Gamma}\left[l+1, \frac{k\gamma_{\text{th}}}{\phi(\gamma_{\text{th}})}\right] \right\}, \quad (5.44)$$

where $\phi(\gamma_{\text{th}}) = \alpha\bar{\gamma} - \beta\gamma_{\text{th}}$.

Ergodic Capacity

The ergodic capacity of the MIMO MRC system can be expressed in [bps/Hz] as [105]

$$\begin{aligned} C &= E_{\hat{\mathbf{H}}} \left[\max_{P(x|\hat{\mathbf{H}})} I(\hat{y}; x | \hat{\mathbf{H}}) \right] \\ &= E_{\hat{\mathbf{H}}} \left[\max_{P(x|\hat{\mathbf{H}})} h(\hat{y} | \hat{\mathbf{H}}) - h(\hat{y} | x, \hat{\mathbf{H}}) \right], \end{aligned} \quad (5.45)$$

where $P(x | \hat{\mathbf{H}})$ denotes the probability distribution of the input signal x given $\hat{\mathbf{H}}$, $I(\hat{y}; x | \hat{\mathbf{H}})$ indicates the mutual information between the received signal \hat{y} and the transmitted signal x given $\hat{\mathbf{H}}$, and $h(\cdot)$ is the entropy function.

Since the interference due to I/Q imbalance and imperfect channel estimation is not necessarily Gaussian, deriving the ergodic capacity in closed-form is not straightforward. However, a lower bound on the training-based capacity can be obtained by replacing the summation of interference and noise by AWGN with the same power constraint [132]. In this case, the input signal x is Gaussian distributed. Under the above conditions and based on (5.14), the entropy $h(\hat{y} | x, \hat{\mathbf{H}})$ is given by

$$\begin{aligned} h(\hat{y} | x, \hat{\mathbf{H}}) &= \log_2 2\pi e \left[|K_2|^2 \rho_h^2 P_0 \lambda_{\max} \right. \\ &\quad \left. + (|K_1|^2 + |K_2|^2) P_0 \frac{\sigma_{h, \text{WI}}^2}{1 + \sigma_{h, \text{WI}}^2} + (|K_1|^2 + |K_2|^2) N_0 \right], \end{aligned} \quad (5.46)$$

and the term $h(\hat{y} | \hat{\mathbf{H}})$ can be expressed as

$$\begin{aligned} h(\hat{y} | \hat{\mathbf{H}}) &= \log_2 2\pi e \left[(|K_1|^2 + |K_2|^2) \rho_h^2 P_0 \lambda_{\max} \right. \\ &\quad \left. + (|K_1|^2 + |K_2|^2) P_0 \frac{\sigma_{h, \text{WI}}^2}{1 + \sigma_{h, \text{WI}}^2} + (|K_1|^2 + |K_2|^2) N_0 \right]. \end{aligned} \quad (5.47)$$

Then, substituting (5.46) and (5.47) into (5.45), a lower bound on the ergodic capacity

can be represented as

$$\begin{aligned} C_{\text{low}}^{\text{WI\&WOC}} &= E \left[\log_2 \left(\frac{\beta \lambda_{\max} + \alpha \bar{\gamma} \lambda_{\max} + 1}{\beta \lambda_{\max} + 1} \right) \right] \\ &= E [\log_2 (1 + (\alpha \bar{\gamma} + \beta) \lambda_{\max}) - \log_2 (1 + \beta \lambda_{\max})]. \end{aligned} \quad (5.48)$$

Finally, making use of [121, eq. (20)], the lower bound on the ergodic capacity of MIMO MRC systems over uncorrelated Rayleigh channels in the presence of I/Q imbalance is given by

$$C_{\text{low}}^{\text{WI\&WOC}} = \log_2 e \sum_{k=1}^p \sum_{l=q-p}^{(p+q-2k)k} \sum_{j=1}^{l+1} d_{k,l} \left[e^{\frac{k}{\alpha \bar{\gamma} + \beta}} E_{l+2-j} \left(\frac{k}{\alpha \bar{\gamma} + \beta} \right) - e^{\frac{k}{\beta}} E_{l+2-j} \left(\frac{k}{\beta} \right) \right]. \quad (5.49)$$

5.5.2 Performance with the Proposed I/Q Imbalance Compensation Algorithm

Since the derived expression for the output SNR in the case with I/Q imbalance compensation is too complex, deriving the PDF of the output SNR in closed-form is not straightforward.

Herein, we concentrate on the case with perfect channel estimation, i.e., $\sigma_{h,\text{WI}}^2 = 0$. Thus, the output SNR in (5.31) can be simplified as

$$\begin{aligned} \gamma_{\text{WI\&WC}} &\approx \frac{(|K_1|^2 - |K_2|^2)^2 \bar{\gamma} \lambda_{\max}^2}{(|K_1|^2 + |K_2|^2)} \\ &\quad \times \frac{1}{\left\{ (|K_1|^2 + |K_2|^2 + \bar{\gamma} \sigma_C^2) \lambda_{\max} + \left(\frac{|K_1|^2 + |K_2|^2}{|K_1|^2 - |K_2|^2} \right)^2 \sigma_C^2 \right\}}. \end{aligned} \quad (5.50)$$

Furthermore, the term $\left(\frac{|K_1|^2 + |K_2|^2}{|K_1|^2 - |K_2|^2} \right)^2 \sigma_C^2$ in (5.50) can be neglected under the above-mentioned assumption $\sigma_C^2 \ll 1$ and small values of $ILR = \left| \frac{K_2}{K_1} \right|^2$. Therefore, the

approximate output SNR can be expressed as

$$\hat{\gamma}_{\text{WI\&WC}} = \omega \lambda_{\max}, \quad (5.51)$$

$$\text{where } \omega = \frac{(|K_1|^2 - |K_2|^2)^2 \bar{\gamma}}{(|K_1|^2 + |K_2|^2)(|K_1|^2 + |K_2|^2 + \bar{\gamma} \sigma_c^2)}.$$

Average SEP

The entries of the effective post-processing noise $\tilde{\mathbf{N}}_d$ in the case with I/Q imbalance compensation, i.e., (A.7), are not necessarily Gaussian distributed. However, similar to Section 5.5.2, an upper bound on the average SEP in the case with perfect channel estimation is given by

$$\begin{aligned} P_{\text{up}}^{\text{WI\&WC}} &= E_{\hat{\gamma}_{\text{WI\&WC}}} \left\{ aQ \left(\sqrt{2b\hat{\gamma}_{\text{WI\&WC}}} \right) \right\} \\ &= \frac{a\sqrt{b}}{2\sqrt{\pi}} \sum_{k=1}^p \sum_{l=q-p}^{(p+q-2k)k} d_{k,l} \left[\sqrt{\frac{\pi}{b}} - \sum_{m=0}^l \frac{1}{m!} \left(\frac{k}{\omega} \right)^m \frac{\Gamma(m+1/2)}{(b+k/\omega)^{m+1/2}} \right], \end{aligned} \quad (5.52)$$

where the second equality makes use of [98, eq. 31].

Outage Probability

Using the same methodology as that in Section 5.5.1, the outage probability of the MIMO MRC system in the presence of the proposed I/Q imbalance compensation scheme can be expressed as

$$P_{\text{out}}^{\text{WI\&WC}}(\gamma_{\text{th}}) \approx \sum_{k=1}^p \sum_{l=q-p}^{(p+q-2k)k} d_{k,l} \left\{ 1 - \bar{\Gamma} \left[l+1, \frac{k\gamma_{\text{th}}}{\omega} \right] \right\}, \quad (5.53)$$

which is valid for the case with perfect channel estimation.

Ergodic Capacity

Using the same approach as that in Section 5.5.1, in the case with perfect channel estimation, a lower bound on the ergodic capacity of the MIMO MRC system

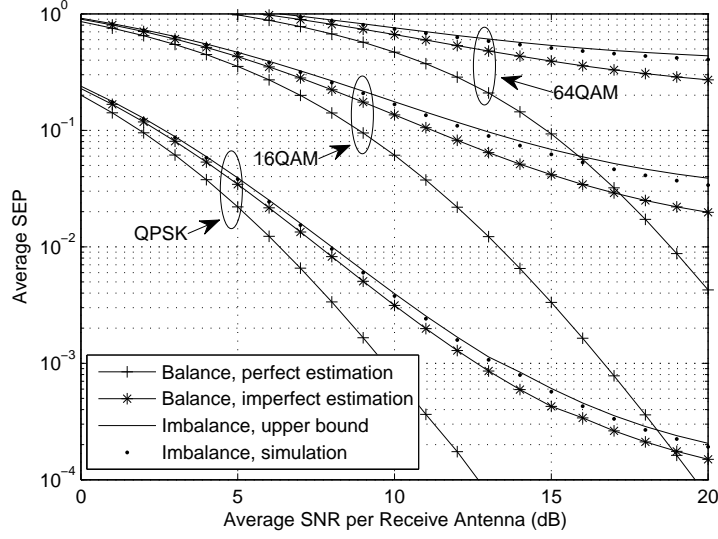


Figure 5.2: Average SEP versus average SNR per receive antenna of MIMO MRC for different modulation formats in the cases with or without I/Q imbalance ($n_T = n_R = 2$).

implementing I/Q imbalance compensation can be obtained in [bps/Hz] as

$$C_{\text{low}}^{\text{WI\&WC}} = \log_2 e \sum_{k=1}^p e^{\frac{k}{\omega}} \sum_{l=q-p}^{(p+q-2k)k} d_{k,l} \sum_{j=1}^{l+1} E_{l+2-j} \left(\frac{k}{\omega} \right). \quad (5.54)$$

5.6 Numerical and Simulation Results

In this section, we present numerical results to show the effect of I/Q imbalance on the performance of MIMO MRC systems, specifically on the average SEP, outage probability and ergodic capacity. For the comparisons between the cases with and without I/Q imbalance, the channel estimation errors are assumed to be at the same level, which requires the number of pilot symbols in the case with I/Q imbalance to be twice as that of the case with ideal I/Q branches. Moreover, numerical results representing the performance of the MIMO MRC system with the proposed I/Q imbalance compensation method, are provided to illustrate the performance gain over the case without compensation. We set the ratio of the pilot power to the noise power spectral density to $\xi_p/N_0 = 10$ dB.

First, we evaluate the upper bound on the average SEP versus average SNR per

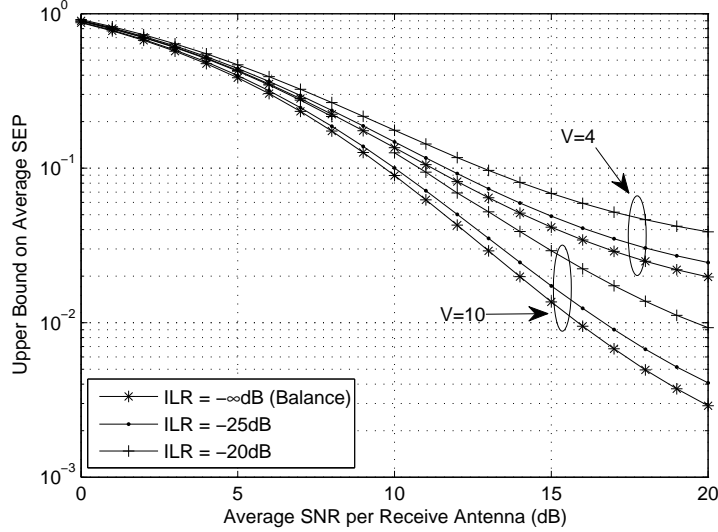


Figure 5.3: Upper bound on average SEP versus average SNR per receive antenna of MIMO MRC for different values of ILR and V in the cases with or without I/Q imbalance ($n_T = n_R = 2$, 16QAM).

receive antenna in the case without compensation, taking the modulation order as parameter and $n_T = n_R = 2$, in comparison with simulation results. As for the image-leakage ratio of the I/Q imbalance, we choose $ILR = -20$ dB. We set $V = 4$, thus 16 pilot symbols are used to perform the channel estimation in the case with I/Q imbalance. The average SEP in the case without I/Q imbalance is taken as the performance baseline, where curves with perfect and imperfect channel estimation are plotted. As for the case with ideal I/Q branches and imperfect channel estimation, the estimation error is the same as in the case with I/Q imbalance. From Fig. 5.2, we observe how the degradation caused by the I/Q imbalance on the average SEP increases as the average SNR per receive antenna $\bar{\gamma}$ gets larger, i.e., the I/Q imbalance becomes more serious in the high SNR region. In addition, given the same requirement on the average SEP, the $\bar{\gamma}$ penalty is the largest for 64-QAM and the least for QPSK. As 64-QAM works in the high SNR region, the I/Q imbalance yields higher interference.

To further illustrate the effect of I/Q imbalance on the average SEP, we plot in Fig. 5.3 the average SEP for different values of ILR and V , taking 16QAM as the

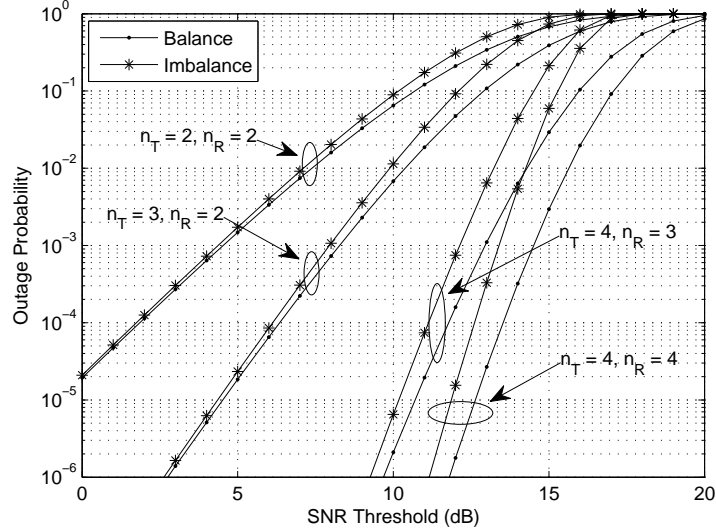


Figure 5.4: Outage probability versus SNR threshold γ_{th} of MIMO MRC for different values of n_T and n_R in the cases with or without I/Q imbalance ($\bar{\gamma} = 10$ dB, $V = 8$).

modulation scheme in the $n_T = n_R = 2$ MIMO configuration. As observed, the higher the image-leakage ratio of the I/Q imbalance is, the larger the average SEP will be. Moreover, the average SEP of the MIMO MRC system using the proposed channel estimation can be reduced at the cost of high number of pilot symbols, since the channel estimation MSE is lower in the case with more pilot symbols.

Fig. 5.4 illustrates the outage probability versus SNR threshold γ_{th} , without using I/Q imbalance compensation, and shows the effects of varying n_T and n_R in the case with $\bar{\gamma} = 10$ dB, $ILLR = -20$ dB and $V = 8$. The outage probability is reduced by increasing the numbers of transmit and/or receive antennas. For arbitrary antenna deployment scenarios, the effect of I/Q imbalance is more visible at high SNR thresholds. Furthermore, the higher the number of antennas is, the larger the increment in outage probability due to I/Q imbalance will be. Therefore, the I/Q imbalance should be given a particular attention in the scenario with high numbers of transmit and receive antennas.

In Fig. 5.5, we show the relationship between the lower bound on ergodic capacity and the average SNR per receive antenna for the case with $n_T = n_R = 2$. Three cases of I/Q imbalances are considered: 1) $ILLR = -30$ dB; 2) $ILLR = -25$ dB;

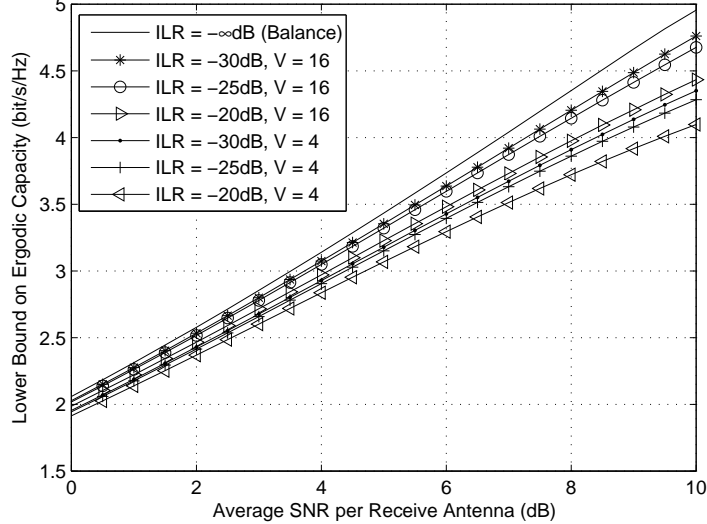


Figure 5.5: Lower bound on ergodic capacity versus average SNR per receive antenna of MIMO MRC for different values of ILR and V in the cases with or without I/Q imbalance ($n_T = n_R = 2$).

and 3) $ILR = -20$ dB. As noticed, the interference due to I/Q imbalance results in a decrease in the capacity of MIMO MRC systems, and the deterioration in the case with $ILR = -20$ dB is more important than that of the other two scenarios. Moreover, reducing the number of pilot symbols results in a reduction in the ergodic capacity.

Next, we analyze the proposed I/Q imbalance compensation scheme, and compare its performance with that of the case without I/Q imbalance and the one with I/Q imbalance but without compensation. The channel estimation is assumed to be perfect and the comparisons are carried out in terms of average SEP, outage probability and ergodic capacity.

Fig. 5.6 demonstrates the average SEP performance as a function of the average SNR per receive antenna for different modulation formats in the cases with and without compensation. The parameters are set to be $n_T = n_R = 2$, $ILR = -20$ dB, and $U = 32$, which means that 32 pilot symbols are used to estimate the coefficients $K_1 \mathbf{z}^H \mathbf{H} \mathbf{w}$ and $K_2 (\mathbf{z}^H \mathbf{H} \mathbf{w})^*$ in the I/Q imbalance compensation. It can be observed that the average SEP obtained using compensation can approach the baseline, i.e.,

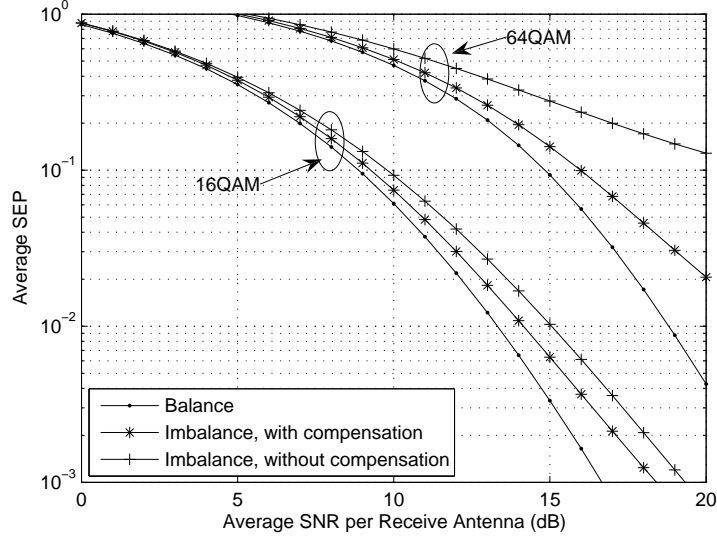


Figure 5.6: Average SEP versus average SNR per receive antenna of MIMO MRC for different modulation formats in the cases with or without compensation (perfect channel estimation, $n_T = n_R = 2$).

the one in the scenario without I/Q imbalance, for arbitrary modulation formats, which implies that the I/Q imbalance can be efficiently compensated for using the proposed method.

In Fig. 5.7, the effect of the number of pilot symbols used to estimate the coefficients $K_1 \mathbf{z}^H \mathbf{H} \mathbf{w}$ and $K_2 (\mathbf{z}^H \mathbf{H} \mathbf{w})^*$, i.e., U , on the average SEP in the case with I/Q imbalance compensation is presented for the $n_T = n_R = 2$ MIMO configuration and 16QAM. Here, we set $ILR = -20$ dB. As observed, by making use of the proposed I/Q imbalance compensation scheme and employing enough pilot symbols, the average SEP can be reduced to approach the performance with ideal I/Q branches.

Fig. 5.8 shows the outage probability versus SNR threshold, using I/Q imbalance compensation, and demonstrates the benefits of increasing n_T , n_R and U on performance in the case with $\bar{\gamma} = 10$ dB and $ILR = -20$ dB. We can see that for arbitrary $n_T \times n_R$ MIMO configurations, the outage probability drops as the value of U becomes larger.

Finally, Fig. 5.9 plots the ergodic capacity as a function of the average SNR per receive antenna for the cases with and without compensation. The parameters are

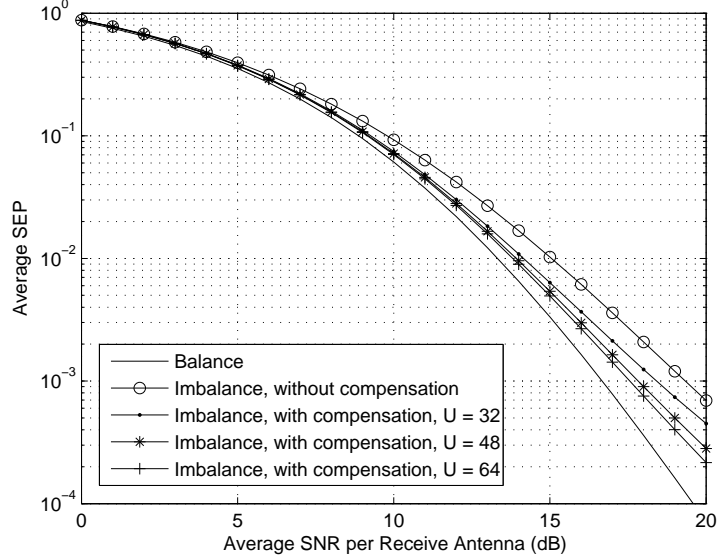


Figure 5.7: Average SEP versus average SNR per receive antenna of MIMO MRC for different values of U in the case with I/Q imbalance compensation (perfect channel estimation, $n_T = n_R = 2$, 16QAM).

set to be $ILR = -20$ dB and $U = 16$. It is observed that by making use of the proposed compensation scheme, the ergodic capacity in the case with I/Q imbalance can approach the performance of the case without I/Q imbalance, for arbitrary $n_T \times n_R$ MIMO configurations.

5.7 Summary

In this chapter, a MIMO MRC system model that takes I/Q imbalance into account was developed. A channel estimation scheme considering the I/Q imbalance was proposed to perform the MIMO MRC, where the length of pilot symbols used to achieve the same estimation performance as in the case with ideal I/Q branches is twice as that in the latter. Furthermore, we proposed a compensation algorithm for the I/Q imbalance, which can efficiently mitigate the deterioration that results from said imbalance. The effect of I/Q imbalance and the proposed compensation algorithm on the performance for MIMO MRC systems was evaluated in terms of average SEP, outage probability and system capacity, which were derived considering

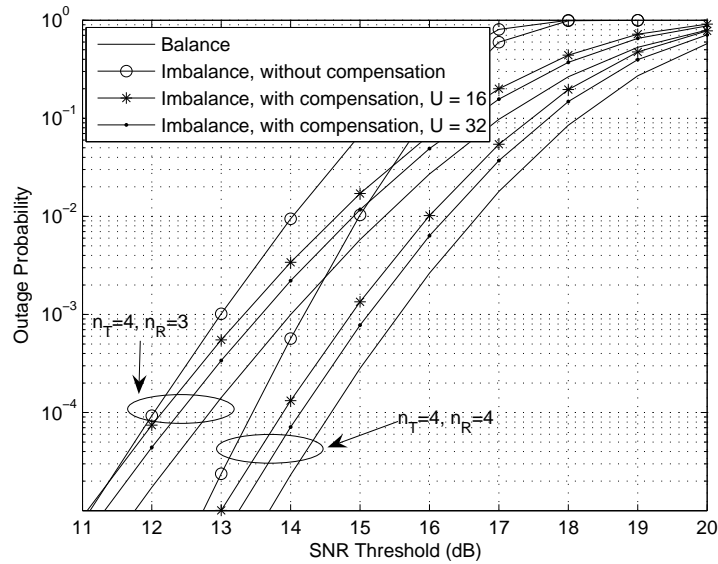


Figure 5.8: Outage probability versus SNR threshold of MIMO MRC for different values of n_T , n_R and U in the case with I/Q imbalance compensation (perfect channel estimation, $\bar{\gamma} = 10$ dB).

transmission over uncorrelated Rayleigh fading channels. Numerical and simulation results showing the effects of several system parameters, such as the image-leakage ratio, numbers of transmit and receive antennas, modulation order of QAM, and length of pilot symbols, on the system performance, were studied and discussed.

In the next chapter, the performance of MIMO wireless communication systems in the presence of another RF impairment, namely, crosstalk, will be evaluated.

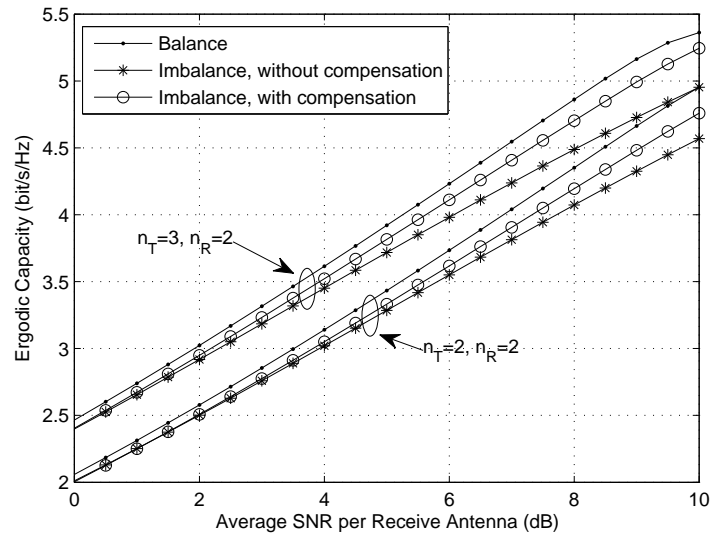


Figure 5.9: Ergodic capacity versus average SNR per receive antenna of MIMO MRC for different values of n_T and n_R in the cases with and without I/Q imbalance compensation (perfect channel estimation).

Chapter 6

Analysis of the Effects of Crosstalk

6.1 Introduction

Crosstalk indicates unintended electromagnetic coupling between PCB lands, traces, wires, or other electrical components that are in close distance to each other and subject to electromagnetic field disturbance [57]. It concerns the intrasystem interference performance. In other words, the source of the electromagnetic emission and the receptor of this emission are within the same system. The current research effort that dealt with the issue of crosstalk was discussed in Section 1.1.6.

In this chapter, we focus on the so-called MIMO MRC technique implementing MRT with the linear crosstalk. Specifically, we investigate the performance of beamforming for MIMO transmit-receive diversity systems in the presence of crosstalk. Here, the beamforming weight-vector and combining vector of the MIMO MRC system are chosen according to the value of the crosstalk. For the outlined communication system, we derive the average SEP and system capacity, considering that the system operates under uncorrelated quasi-static frequency-flat Rayleigh fading. Furthermore, numerical results are provided, and the effects of the crosstalk, numbers of transmit and receive antennas, and modulation order of phase-shift keying (PSK), on the overall system performance, are discussed.

The remainder of this chapter is organized as follows: Section 6.2 introduces the MIMO MRC system model, considering crosstalk at the transmitter and receiver.

In Section 6.3, the effects of crosstalk on the average SEP and system capacity of the MIMO MRC system are analyzed. Numerical results and comparisons are then presented in Section 6.4, followed by the summary in Section 6.5.

6.2 System Model

We consider a MIMO MRC system equipped with n_T transmit and n_R receive antennas, and assume a discrete-time baseband channel model subject to quasi-static frequency-flat Rayleigh fading.

In the absence of impairments, the MIMO signal model can be expressed as $\mathbf{y}_{\text{id}} = \mathbf{H}\mathbf{w}x + \mathbf{n}$, where x denotes the transmitted symbol with average power P_0 , \mathbf{w} represents the $n_T \times 1$ unit beamforming weight vector, \mathbf{n} refers to the $n_R \times 1$ noise vector with elements belonging to independent and identically distributed (i.i.d.) complex circular Gaussian distribution $\mathcal{CN}(0, N_0)$ uncorrelated with the transmitted symbols, and $\mathbf{H} = [h_{i,j}]_{i,j=1}^{n_R, n_T}$ expresses the $n_R \times n_T$ channel random matrix with $h_{i,j}$ representing the channel coefficient between the j th transmit and i th receive antennas. The entries of the channel gain matrix are i.i.d. complex Gaussian random variables, each with a $\mathcal{CN}(0, 1)$ distribution.

In practice, crosstalk occurs between the wires and PCB lands of the MIMO transceivers, due to the fact that the PCB paths use the same operating frequency [57]. In the presence of crosstalk, the block diagram for the considered MIMO MRC system can be illustrated as shown in Fig. 6.1. As such, the MIMO MRC signal model in the presence of crosstalk can be expressed as

$$\mathbf{y} = \mathbf{A}_R \mathbf{H} \mathbf{A}_T \mathbf{w} x + \mathbf{n}, \quad (6.1)$$

where \mathbf{A}_T and \mathbf{A}_R denote the $n_T \times n_T$ and $n_R \times n_R$ crosstalk matrices at the transmitter and receiver, respectively. Herein, we consider symmetric crosstalk, and assume that the crosstalk takes effect between adjacent signal paths only [64, 133]. Then, the

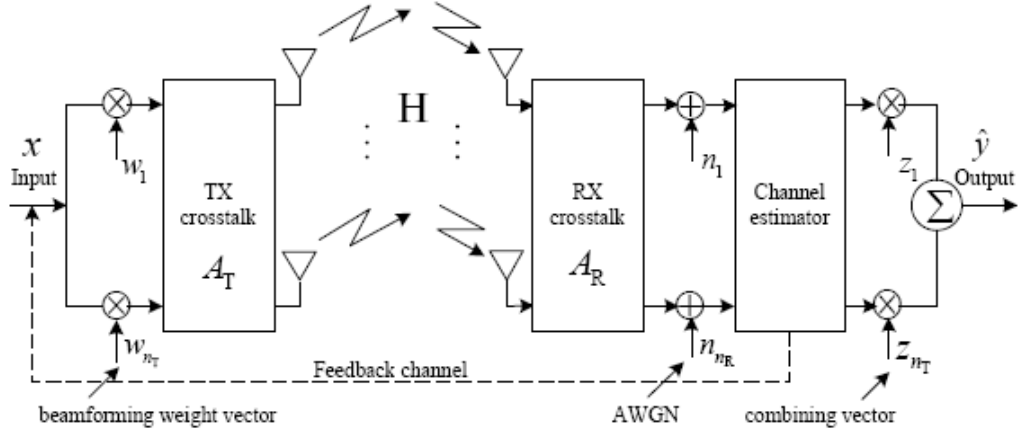


Figure 6.1: Block diagram of the MIMO MRC system with crosstalk.

elements of \mathbf{A}_T and \mathbf{A}_R are of the form

$$\mathbf{A}_T(i, j) = \begin{cases} 1, & i - j = 0 \\ \alpha_T, & |i - j| = 1 \\ 0, & \text{else,} \end{cases} \quad (6.2)$$

$$\mathbf{A}_R(i, j) = \begin{cases} 1, & i - j = 0 \\ \alpha_R, & |i - j| = 1 \\ 0, & \text{else,} \end{cases} \quad (6.3)$$

where α_T and α_R represent the crosstalk between adjacent signal paths at the transmitter and receiver, respectively.

At the receiver side, signals from all the antenna branches are weighted by the $n_R \times 1$ combining vector \mathbf{z} . Thus, the combined signal at the receiver is given by

$$\hat{y} = \mathbf{z}^H \mathbf{A}_R \mathbf{H} \mathbf{A}_T \mathbf{w} x + \mathbf{z}^H \mathbf{n}, \quad (6.4)$$

where $(\cdot)^H$ denotes the Hermitian operator. It is assumed that knowledge of the crosstalk matrices and of the channel gain matrix is available at the transmitter and

the receiver. Thereby, the output SNR, γ , can be expressed as

$$\gamma = \bar{\gamma} \frac{|\mathbf{z}^H \mathbf{A}_R \mathbf{H} \mathbf{A}_T \mathbf{w}|^2}{\|\mathbf{z}\|_F^2}, \quad (6.5)$$

where $\|\cdot\|_F$ denotes the Frobenius norm, and $\bar{\gamma} = P_0/N_0$ represents the pre-processing average SNR. In a beamforming and combining system, the key problem is to choose \mathbf{w} and \mathbf{z} that maximize the output SNR [121]. Without loss of generality, we fix $\|\mathbf{z}\|_F = 1$. A receiver where \mathbf{z} maximizes $|\mathbf{z}^H \mathbf{A}_R \mathbf{H} \mathbf{A}_T \mathbf{w}|$ given \mathbf{w} is called an MRC receiver. Under MRC, it can be seen that $\mathbf{z} = \mathbf{A}_R \mathbf{H} \mathbf{A}_T \mathbf{w} / \|\mathbf{A}_R \mathbf{H} \mathbf{A}_T \mathbf{w}\|_F$. Then, the output SNR can be expressed as

$$\gamma = \bar{\gamma} \mathbf{w}^H \mathbf{A}_T^H \mathbf{H}^H \mathbf{A}_R^H \mathbf{A}_R \mathbf{H} \mathbf{A}_T \mathbf{w}. \quad (6.6)$$

The matrix $\mathbf{A}_R \mathbf{H} \mathbf{A}_T$ in (6.6) can be rewritten using the common Kronecker structure, according to

$$\mathbf{A}_R \mathbf{H} \mathbf{A}_T = \sqrt{(1 + |\alpha_T|^2)(1 + |\alpha_R|^2)} \Phi_R^{1/2} \mathbf{H} \Phi_T^{1/2}, \quad (6.7)$$

where Φ_T and Φ_R denote the equivalent transmit and receive correlation matrices with unit diagonal entries, respectively, and are given by

$$\Phi_T = \frac{1}{1 + |\alpha_T|^2} \mathbf{A}_T^H \mathbf{A}_T, \quad (6.8)$$

$$\Phi_R = \frac{1}{1 + |\alpha_R|^2} \mathbf{A}_R^H \mathbf{A}_R. \quad (6.9)$$

Then, the output SNR (6.6) can be rewritten as

$$\gamma = \bar{\gamma}_{ct} \mathbf{w}^H \left(\Phi_R^{1/2} \mathbf{H} \Phi_T^{1/2} \right)^H \Phi_R^{1/2} \mathbf{H} \Phi_T^{1/2} \mathbf{w}, \quad (6.10)$$

where $\bar{\gamma}_{ct} = (1 + |\alpha_T|^2)(1 + |\alpha_R|^2) \bar{\gamma}$.

Furthermore, MRT is employed to maximize γ with respect to \mathbf{w} . Set $\|\mathbf{w}\|_F = 1$ to keep a constant average transmit power, irrespective of n_T . By denoting λ_{\max} as the largest eigenvalue of the Wishart matrix $\left(\Phi_R^{1/2} \mathbf{H} \Phi_T^{1/2} \right)^H \Phi_R^{1/2} \mathbf{H} \Phi_T^{1/2}$, the output

SNR of the optimal MIMO MRC system is given by

$$\gamma = \bar{\gamma}_{ct} \lambda_{\max}. \quad (6.11)$$

In this scenario, \mathbf{w} is the unit-norm eigenvector associated with λ_{\max} .

Note that the crosstalk can have constructive or destructive effects, depending on whether the gain in the average SNR, i.e., $\bar{\gamma}_{ct}/\bar{\gamma}$, or the correlation caused by the crosstalk plays the major role in the performance variation.

For arbitrary $n_T \times n_R$ MIMO configurations, the expression for the CDF of λ_{\max} is too complex to achieve tractable performance analysis. Herein, we concentrate on MIMO MRC implementing $2 \times m$ or $m \times 2$ multi-element antennas with crosstalk. The CDF of λ_{\max} has been previously presented in (3.6).

6.3 Performance Analysis

In this section, we analyze the performance of the MIMO MRC system with crosstalk under uncorrelated quasi-static frequency-flat Rayleigh fading, in terms of average symbol error probability and system capacity.

6.3.1 Average Symbol Error Probability

The average SEP for general modulation formats in the scenario with additive white Gaussian noise can be expressed as [105]

$$P_s = E \left\{ aQ \left(\sqrt{2b\gamma} \right) \right\}, \quad (6.12)$$

where $E \{ \cdot \}$ denotes the expectation operator, $Q(\cdot)$ represents the Gaussian Q-function, and a and b are modulation-specific constants. For instance, as samples of the values of a and b for specific modulation schemes, $a = 1$, $b = 1$ for BPSK, and $a \approx 2$, $b \approx \sin^2(\pi/M)$ for M -PSK [105].

Based on integration by parts, a useful alternative expression for (6.12) is given

by

$$P_s = \frac{a\sqrt{b}}{2\sqrt{\pi}} \int_0^\infty \frac{e^{-bu}}{\sqrt{u}} F_{\lambda_{\max}} \left(\frac{u}{\bar{\gamma}_{ct}} \right) du. \quad (6.13)$$

By making use of the similar methodology as that in Section 3.4.1, we obtain the following expression for the average SEP of the MIMO MRC system in the presence of crosstalk:

$$\begin{aligned} P_s &= \frac{a\sqrt{b} \det(\mathbf{\Omega})}{2\sqrt{\pi} \Delta_2(\mathbf{\Omega}) \Delta_m(\mathbf{\Sigma})} \sum_{s=1}^m \sum_{t=1, t \neq s}^m (-1)^{s+\vartheta(t)} (\sigma_s \sigma_t)^{m-1} \Delta_{m-2}(\sigma^{[s,t]}) \\ &\times \left\{ 2\bar{\gamma}_{ct} \left[\sqrt{\pi \left(b + \frac{1}{\omega_2 \sigma_s \bar{\gamma}_{ct}} \right)} + \sqrt{\pi \left(b + \frac{1}{\omega_1 \sigma_t \bar{\gamma}_{ct}} \right)} - \sqrt{\pi \left(b + \frac{1}{\omega_2 \sigma_s \bar{\gamma}_{ct}} + \frac{1}{\omega_1 \sigma_t \bar{\gamma}_{ct}} \right)} \right] \right. \\ &+ \sum_{k=1}^{m-1} \frac{(-1)^k (2k-3)!! \sqrt{\pi}}{k! (2\bar{\gamma}_{ct})^{k-1}} \\ &\times \left. \left[\frac{b^{\frac{1}{2}-k}}{(\omega_1 \sigma_t)^k} + \frac{b^{\frac{1}{2}-k}}{(\omega_2 \sigma_s)^k} - \frac{1}{(\omega_1 \sigma_t)^k} \left(\frac{1}{\omega_2 \sigma_s \bar{\gamma}_{ct}} + b \right)^{\frac{1}{2}-k} - \frac{1}{(\omega_2 \sigma_s)^k} \left(\frac{1}{\omega_1 \sigma_t \bar{\gamma}_{ct}} + b \right)^{\frac{1}{2}-k} \right] \right\}. \end{aligned} \quad (6.14)$$

6.3.2 System capacity

By using the similar methodology as that in Section 3.4.2, the system capacity of the MIMO MRC system in the presence of crosstalk can be obtained in [bits/s/Hz] as

$$\begin{aligned} C &= \frac{\det(\mathbf{\Omega})}{\bar{\gamma}_{ct} \ln 2 \Delta_2(\mathbf{\Omega}) \Delta_m(\mathbf{\Sigma})} \sum_{s=1}^m \sum_{t=1, t \neq s}^m (-1)^{s+\vartheta(t)} (\sigma_s \sigma_t)^{m-1} \Delta_{m-2}(\sigma^{[s,t]}) \\ &\times \left\{ \bar{\gamma}_{ct}^2 \left[\ln \left(\frac{1}{\omega_2 \sigma_s \bar{\gamma}_{ct}} + \frac{1}{\omega_1 \sigma_t \bar{\gamma}_{ct}} \right) - \ln \left(\frac{1}{\omega_2 \sigma_s \bar{\gamma}_{ct}} \right) - \ln \left(\frac{1}{\omega_1 \sigma_t \bar{\gamma}_{ct}} \right) - e^{\frac{1}{\omega_1 \sigma_t \bar{\gamma}}} E_1 \left(\frac{1}{\omega_1 \sigma_t \bar{\gamma}_{ct}} \right) \right. \right. \\ &+ e^{\frac{1}{\omega_2 \sigma_s \bar{\gamma}_{ct}} + \frac{1}{\omega_1 \sigma_t \bar{\gamma}_{ct}}} E_1 \left(\frac{1}{\omega_2 \sigma_s \bar{\gamma}_{ct}} + \frac{1}{\omega_1 \sigma_t \bar{\gamma}_{ct}} \right) - e^{\frac{1}{\omega_2 \sigma_s \bar{\gamma}_{ct}}} E_1 \left(\frac{1}{\omega_2 \sigma_s \bar{\gamma}_{ct}} \right) \left. \right] \\ &+ \sum_{k=1}^{m-1} \frac{(-1)^k}{k} \left[\left(\frac{1}{\omega_1 \sigma_t} \right)^k e^{\frac{1}{\omega_2 \sigma_s \bar{\gamma}_{ct}}} \sum_{l=1}^k \bar{\gamma}_{ct}^{l-k+1} \left(\frac{1}{\omega_2 \sigma_s} \right)^{1-l} \Gamma \left(-k+l, \frac{1}{\omega_2 \sigma_s \bar{\gamma}_{ct}} \right) \right. \\ &+ \left. \left(\frac{1}{\omega_2 \sigma_s} \right)^k e^{\frac{1}{\omega_1 \sigma_t \bar{\gamma}_{ct}}} \sum_{l=1}^k \bar{\gamma}_{ct}^{l-k+1} \left(\frac{1}{\omega_1 \sigma_t} \right)^{1-l} \Gamma \left(-k+l, \frac{1}{\omega_1 \sigma_t \bar{\gamma}_{ct}} \right) \right] \left. \right\}. \end{aligned} \quad (6.15)$$

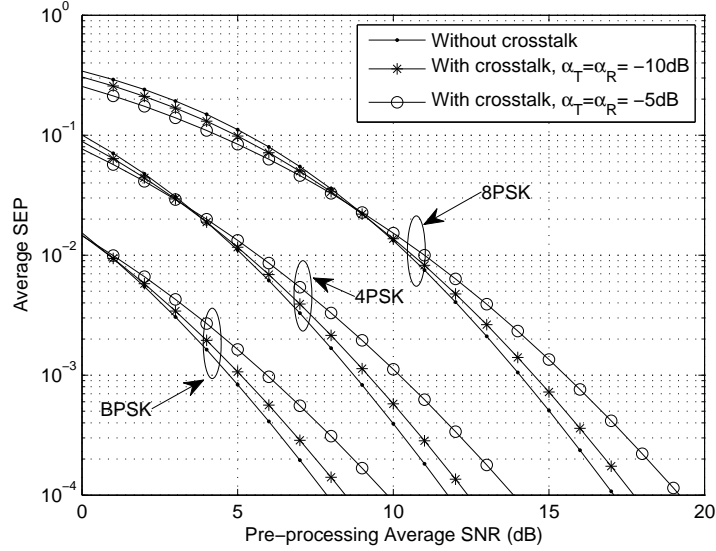


Figure 6.2: Average SEP versus $\bar{\gamma}$ of MIMO MRC with crosstalk for different modulation formats ($n_T = n_R = 2$).

6.4 Numerical Results

Hereafter, we present numerical results illustrating the performance of the MIMO MRC system in the presence of crosstalk over uncorrelated Rayleigh fading channels, specifically on the average SEP and system capacity.

First, we evaluate the average SEP versus the pre-processing average SNR $\bar{\gamma}$ for the 2×2 MIMO configuration, taking the modulation order and crosstalk as parameters. From Fig. 6.2, we observe the degradation caused by the crosstalk on the average SEP in the high $\bar{\gamma}$ range, which increases as $\bar{\gamma}$ gets larger. On the other hand, in the low $\bar{\gamma}$ range, the average SEP is reduced, profiting from the crosstalk. This phenomenon is due to the fact that in the high $\bar{\gamma}$ range, the effect of the equivalent correlation caused by the crosstalk is larger than that of the gain in the average SNR, i.e., $\bar{\gamma}_{ct}/\bar{\gamma}$, while in the low $\bar{\gamma}$ range, the gain in the average SNR is more visible, compared to the pre-processing average SNR, $\bar{\gamma}$. Furthermore, the cross point in $\bar{\gamma}$ between the constructive and destructive effects of the crosstalk becomes larger when using high-order modulations, which implies that the correlation impact caused by the crosstalk is smaller in the low and medium $\bar{\gamma}$ ranges for high-order modulation schemes, e.g.,

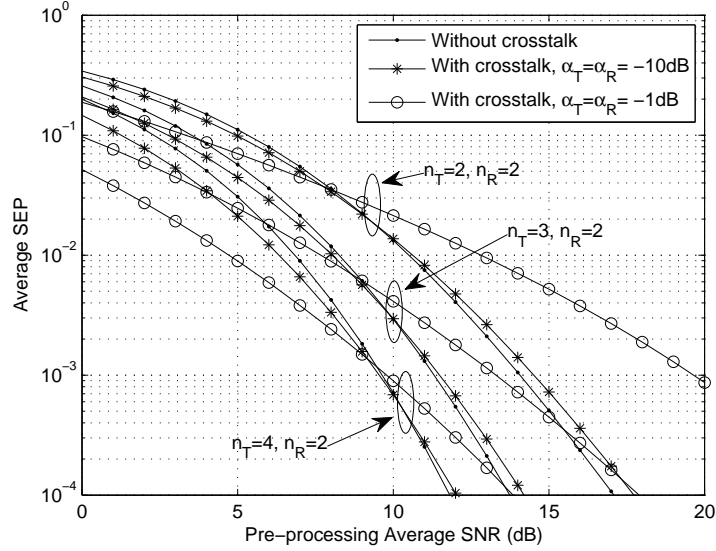


Figure 6.3: Average SEP versus $\bar{\gamma}$ of MIMO MRC with crosstalk for different values of n_T and n_R (8PSK).

8PSK.

In Fig. 6.3, the effect of crosstalk on the average SEP is further analyzed for different values of n_T and n_R , taking 8PSK as the modulation scheme. As observed, increasing the numbers of transmit and receive antennas enlarges the effect of the gain in the average SNR, and weakens the impact of the correlation due to the crosstalk. As a result, the cross point in $\bar{\gamma}$ between the constructive and destructive effects of crosstalk is larger in the case with high antenna numbers. Moreover, the cross point moves to higher $\bar{\gamma}$ values as the crosstalk increases.

Finally, Fig. 6.4 shows the system capacity versus the pre-processing average SNR for the 2×2 MIMO configuration, in the presence of crosstalk. It can be observed that the system capacity improves, profiting from the crosstalk, which implies that the effect of the correlation due to crosstalk is much lower than that of the gain in the average SNR. However, as noticed from Fig. 6.5, the resulting system capacity improvement approaches a limited value when the crosstalk becomes too significant, since in this case the correlations at the transmitter and receiver are so severe that the desired signal cannot be efficiently detected.

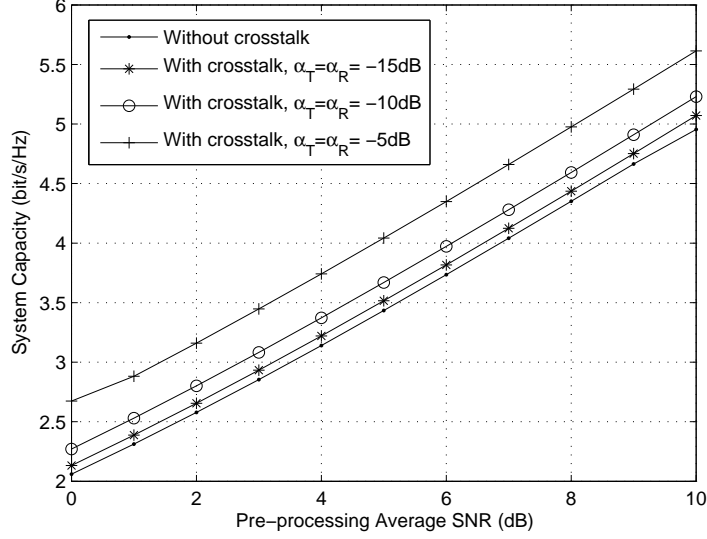


Figure 6.4: System capacity versus $\bar{\gamma}$ of MIMO MRC with crosstalk for different values of α_T and α_R ($n_T = n_R = 2$).

6.5 Summary

A beamforming technique for MIMO transmit-receive diversity systems with crosstalk was studied in this chapter. In particular, the impact of crosstalk on the performance of MIMO MRC was evaluated in terms of average symbol error probability and system capacity, which were derived considering transmission over uncorrelated Rayleigh fading channels. Numerical results showing the effects of several system parameters on performance were presented and discussed. Importantly, it was observed that the impact of crosstalk on performance can be constructive or destructive.

Investigation on RF impairments, including HPA nonlinearity, I/Q imbalance and crosstalk as well as their compensation methods have been carried out separately in Chapters 4, 5 and 6. In the next chapter, a comprehensive compensation mechanism for multiple RF impairments together in MIMO wireless communication systems will be proposed.

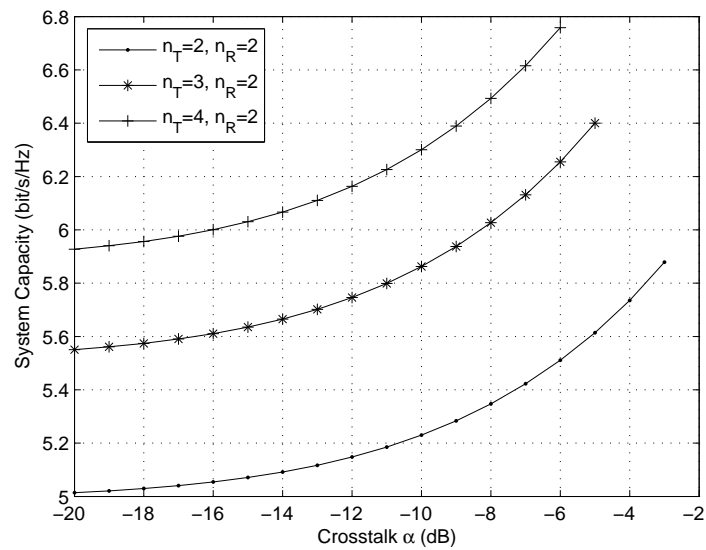


Figure 6.5: System capacity versus crosstalk of MIMO MRC for different values of n_T and n_R ($\alpha_T = \alpha_R = \alpha$, $\bar{\gamma} = 10$ dB).

Chapter 7

Compensation for Multiple RF Impairments

7.1 Introduction

RF impairments, including HPA nonlinearity, I/Q imbalance and crosstalk, are inherent phenomena in wireless communication systems. HPA nonlinearity results from operation of the amplifier in a nonlinear region, especially at high-power signal levels [34]. Models to describe nonlinear HPAs can be classified into two categories: memoryless models with frequency-flat responses, which are characterized by their AM/AM and AM/PM conversions, and memory models with frequency-selective responses. As for I/Q imbalance, it represents the mismatch between the components in the I and Q branches, which happens due to the limited accuracy of the analog hardware, such as finite tolerances of capacitors and resistors [49]. Crosstalk, on the other hand, indicates unintended electromagnetic coupling between PCB lands, traces, wires, or other electrical components that are in close distance to each other and subject to electromagnetic field disturbance [57].

Recently, the issue of HPA nonlinearity, I/Q imbalance and crosstalk in MIMO systems has been investigated. For instance, several compensation schemes for HPA nonlinearity have been proposed, which can be classified into two categories: com-

compensation at the transmitter or at the receiver. Methods implemented at the transmitter include power back-off, PAPR reduction techniques, and linearization techniques [34, 42]. On the other hand, in order to eliminate or at least mitigate the effect of I/Q imbalance on the performance of wireless communication systems, several compensation methods for this kind of impairment have been proposed, which can be classified into two categories: compensation methods with estimation of the I/Q imbalance parameters and those without such estimation [49, 55]. In addition, a crossover digital predistorter was proposed for the compensation of HPA nonlinearity and crosstalk in MIMO systems, and was evaluated through simulations [64]. However, compensation methods and comprehensive theoretical analysis of several RF impairments together, in MIMO communications systems, are extremely challenging.

In this chapter, we investigate the combined effects of HPA nonlinearity, I/Q imbalance and crosstalk in MIMO TB systems, where the MRC at the receiver is performed at the RF level. We propose a compensation method for HPA nonlinearity, I/Q imbalance and crosstalk together. First, the estimation of the equivalent channel in the presence of the three kinds of impairments is performed using the LS rule. Then, we determine the optimal beamforming weight vector and combining vector for the MIMO TB system with these three impairments. Furthermore, we employ the LS rule to estimate the coefficients of the equivalent channel gain matrix, equivalent beamforming and combining weight vectors, and parameters of I/Q imbalance jointly, and then use the received signal together with its conjugation to detect the transmitted signal. Subsequently, an upper bound on the average SEP and a lower bound on the system capacity of the MIMO TB under study over uncorrelated Rayleigh fading channels are derived.

The remainder of this chapter is organized as follows: Section 7.2 introduces the MIMO TB system model with HPA nonlinearity, I/Q imbalance and crosstalk. In Section 7.3, we investigate the estimation of the equivalent channel. In Section 7.4, we propose a compensation scheme for the three impairments. In Section 7.5, the performance of the MIMO TB system is analyzed in terms of average SEP and system capacity. Numerical results and comparisons are then presented in Section

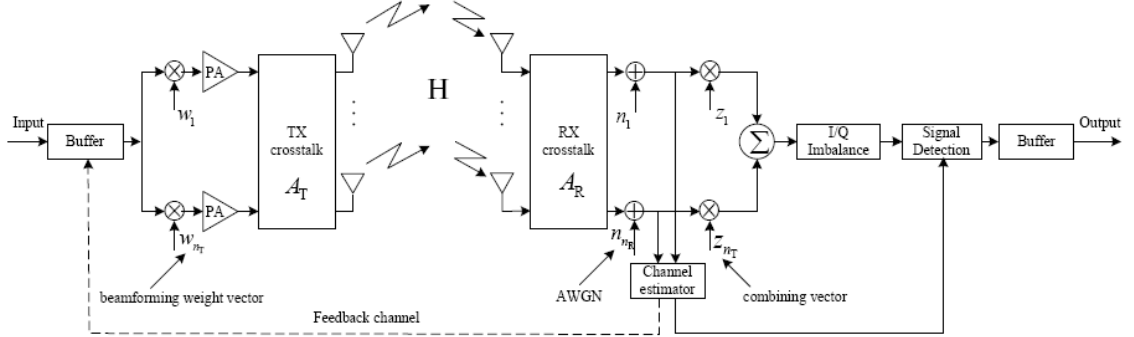


Figure 7.1: Block diagram of the MIMO TB system in the presence of HPA nonlinearity, I/Q imbalance and crosstalk.

7.6, followed by the summary in Section 7.7.

7.2 System Model

We consider a MIMO TB system equipped with n_T transmit and n_R receive antennas, and assume a discrete-time baseband channel model subject to quasi-static frequency-flat Rayleigh fading. In the MIMO TB transmission chain, we consider three RF impairments, namely, HPA nonlinearity at the transmitter, I/Q imbalance at the receiver, and crosstalk at both ends of the transmission link. The system block diagram is shown in Fig. 7.1. Above all, due to the crosstalk which occurs in the PCB design, the equivalent channel gain matrix is given by

$$\mathbf{H}_e = \mathbf{A}_R \mathbf{H} \mathbf{A}_T, \quad (7.1)$$

where $\mathbf{H} = [h_{i,j}]_{i,j=1}^{n_R, n_T}$ denotes the $n_R \times n_T$ channel gain matrix with $h_{i,j}$ indicating the channel coefficient between the j th transmit and i th receive antennas, and where \mathbf{A}_T and \mathbf{A}_R represent the $n_T \times n_T$ and $n_R \times n_R$ crosstalk matrices at the transmitter and receiver, respectively. The entries of \mathbf{H} are independent and identically distributed (i.i.d.) complex Gaussian random variables, each with a $\mathcal{CN}(0, 1)$ distribution. It is assumed that the crosstalk is symmetric and takes effect between adjacent signal

paths only [64]. Specifically, the elements of \mathbf{A}_T are given by

$$\mathbf{A}_T(i, j) = \begin{cases} 1, & i - j = 0 \\ \alpha_T, & |i - j| = 1 \\ 0, & \text{else,} \end{cases} \quad (7.2)$$

where α_T represents the crosstalk between adjacent signal paths at the transmitter. The expression for \mathbf{A}_R is similar to that of \mathbf{A}_T , after replacing α_T with α_R in the right-hand-side of (7.2), with α_R denoting the crosstalk between adjacent signal paths at the receiver. The equivalent channel gain matrix $\mathbf{H}_e = \mathbf{A}_R \mathbf{H} \mathbf{A}_T$ can be rewritten using the common Kronecker structure, according to:

$$\mathbf{A}_R \mathbf{H} \mathbf{A}_T = \beta_{ct} \mathbf{\Phi}_R^{1/2} \mathbf{H} \mathbf{\Phi}_T^{1/2}, \quad (7.3)$$

where $\beta_{ct} = \sqrt{(1 + |\alpha_T|^2)(1 + |\alpha_R|^2)}$ and where $\mathbf{\Phi}_T$ and $\mathbf{\Phi}_R$ denote the equivalent transmit and receive correlation matrices, respectively, and are given by

$$\mathbf{\Phi}_T = \frac{1}{1 + |\alpha_T|^2} \mathbf{A}_T^H \mathbf{A}_T, \quad (7.4)$$

$$\mathbf{\Phi}_R = \frac{1}{1 + |\alpha_R|^2} \mathbf{A}_R^H \mathbf{A}_R. \quad (7.5)$$

In addition, the HPA at the RF module may operate in its nonlinear region. In a generic way, denote the signal at the input of the HPA as

$$x_{\text{in}} = r e^{j\theta}, \quad (7.6)$$

where r and θ denote the amplitude and phase of x_{in} , respectively, and $j^2 = -1$. Then, the symbol at the output of the memoryless nonlinear HPA can be expressed as

$$x_{\text{out}} = f_A(r) e^{j f_P(r)} e^{j\theta}, \quad (7.7)$$

where $f_A(\cdot)$ and $f_P(\cdot)$ denote the AM/AM and AM/PM conversions, respectively.

The HPA parameters are assumed to be perfectly known at the transmitter and the receiver. Moreover, for simplicity of the analysis, HPAs at all transmitting branches of the MIMO TB system under study are assumed to have the same nonlinear behavior. Then, the received signal in the presence of crosstalk and HPA nonlinearity is given by

$$\mathbf{y} = \mathbf{H}_e \mathbf{u} + \mathbf{n}, \quad (7.8)$$

where \mathbf{n} denotes the $n_R \times 1$ noise vector with elements belonging to i.i.d. complex circular Gaussian distribution $\mathcal{CN}(0, N_0)$ uncorrelated with the transmitted symbols, and $\mathbf{u} = [u_1, u_2, \dots, u_{n_T}]^T$ represents the transmit symbol vector processed by the $n_T \times 1$ unit-norm beamforming weight vector $\mathbf{w} = [w_1, w_2, \dots, w_{n_T}]^T$ and the HPAs, with $()^T$ representing the transpose operator. Specifically, the weighted and distorted signal u_i , $i = 1, 2, \dots, n_T$, can be expressed as

$$u_i = f_A(|w_i x|) \exp[j(\theta_x + \varphi_i + f_P(|w_i x|))], \quad (7.9)$$

where x represents the transmitted symbol with average power P_0 and where θ_x and φ_i denote the phases of the input signal x and the beamforming weight w_i , respectively.

Furthermore, at the receiver side, I/Q imbalance occurs in the RF processing, due to the limited accuracy of the analog hardware. Herein, we consider the case that the MRC is performed at the RF level, which requires only one RF chain [129]. At the receiver, the signals from all antenna branches are combined using the $n_R \times 1$ weight vector \mathbf{z} . Thus, the combined signal is given by

$$\hat{y} = K_1 (\mathbf{z}^H \mathbf{H}_e \mathbf{u} + \mathbf{z}^H \mathbf{n}) + K_2 (\mathbf{z}^H \mathbf{H}_e \mathbf{u} + \mathbf{z}^H \mathbf{n})^*, \quad (7.10)$$

where $(\cdot)^*$ denotes the conjugate operator. The coefficients K_1 and K_2 are given by $K_1 = (1 + ge^{-j\theta})/2$ and $K_2 = (1 - ge^{j\theta})/2$, where g and θ denote the gain imbalance and phase imbalance, respectively [49]. These coefficients are related through $K_2 = 1 - K_1^*$. Besides, the image-rejection ratio is defined as $IRR = \left| \frac{K_1}{K_2} \right|^2$ and the image-leakage ratio is given by $ILLR = \left| \frac{K_2}{K_1} \right|^2$.

7.3 Estimation of the Equivalent Channel Under HPA Nonlinearity, I/Q Imbalance and Crosstalk

In this section, we present the estimation algorithm of the equivalent channel gain matrix taking into account crosstalk, in the presence of HPA nonlinearity and I/Q imbalance. As the channels are assumed to be quasi-static, the channel gain matrix remains invariant in each frame and may vary from frame to frame. Under this assumption, the receive antenna elements can be multiplexed to the RF chain during the training period [129]. $n_T \times V n_R$ pilot symbols $[\mathbf{S}_p \ \mathbf{S}_p \ \dots \ \mathbf{S}_p]$, with an average power of ξ_p per pilot, are used to perform the channel estimation, where \mathbf{S}_p denotes the $n_T \times V$ transmitted pilot symbol matrix. The RF chain is connected to the first receive antenna during the first part of the pilot sequence, then to the second receive antenna during the second part, and so on. The equivalent received signal in the presence of HPA nonlinearity, I/Q imbalance and crosstalk can be expressed as

$$\mathbf{Y}_p = K_1 \left(\mathbf{H}_e \tilde{\mathbf{S}}_p + \mathbf{N}_p \right) + K_2 \left(\mathbf{H}_e \tilde{\mathbf{S}}_p + \mathbf{N}_p \right)^*, \quad (7.11)$$

where \mathbf{N}_p denotes the $n_R \times V$ noise matrix with elements belonging to i.i.d. complex circular Gaussian distribution $\mathcal{CN}(0, N_0)$ uncorrelated with the transmitted pilot symbols, and $\tilde{\mathbf{S}}_p$ denotes the pilot symbol matrix after nonlinear amplification.

Making use of a similar methodology as that in Section 5.3.1, the LS estimate $\hat{\mathbf{\Omega}} = \begin{bmatrix} \hat{\mathbf{H}}_e & \hat{\mathbf{H}}_e^* \end{bmatrix}$ can be expressed as

$$\hat{\mathbf{\Omega}} = (\mathbf{Y}_p + \mathbf{Y}_p^*) \mathbf{Z}_p^H (\mathbf{Z}_p \mathbf{Z}_p^H)^{-1}, \quad (7.12)$$

where $\mathbf{Z}_p = \begin{bmatrix} \tilde{\mathbf{S}}_p & \tilde{\mathbf{S}}_p^* \end{bmatrix}^T$. A lower bound on the MSE between the equivalent channel gain matrix \mathbf{H}_e and its estimation $\hat{\mathbf{H}}_e$ is given by

$$\sigma_{\mathbf{H}_e, \text{low}}^2 = \frac{2n_R n_T N_0}{V f_A^2 (\sqrt{\xi_p})}. \quad (7.13)$$

Subsequently, the estimation error for each element of \mathbf{H}_e is given by $\sigma_{h_e}^2 = \frac{\sigma_{\mathbf{H}_e}^2}{n_T n_R}$.

The relationship between \mathbf{H}_e and $\hat{\mathbf{H}}_e$ can be expressed as

$$\mathbf{H}_e = \rho_{h_e} \hat{\mathbf{H}}_e + \Theta, \quad (7.14)$$

where $\rho_{h_e} = \frac{1}{1 + \sigma_{h_e}^2 / \beta_{ct}^2}$ and each component of Θ is complex Gaussian distributed variable, with zero mean and variance $\sigma_{\Theta}^2 = \frac{\sigma_{h_e}^2}{1 + \sigma_{h_e}^2 / \beta_{ct}^2}$, and is uncorrelated with the elements of \mathbf{H}_e .

7.4 Compensation for HPA Nonlinearity, I/Q Imbalance and Crosstalk

In this section, we describe the proposed compensation technique for HPA nonlinearity, I/Q imbalance and crosstalk together. Firstly, we start by determining the optimal beamforming weight vector and combining vector to adapt the MIMO TB system for operation under HPA nonlinearity, I/Q imbalance and crosstalk. Then, we describe the process of signal detection with the compensation for the three impairments.

7.4.1 Optimal TB Scheme

We now determine the optimal beamforming scheme with the optimal beamforming weight vector and combining vector in the presence of HPA nonlinearity, I/Q imbalance and crosstalk. The detected signal at the receiver after the MRC in the presence of the considered impairments can be re-expressed as

$$\hat{y} = K_1 (\mathbf{z}^H \mathbf{H}_e \mathbf{v} x + \mathbf{z}^H \mathbf{n}) + K_2 (\mathbf{z}^H \mathbf{H}_e \mathbf{v} x + \mathbf{z}^H \mathbf{n})^*, \quad (7.15)$$

where $\mathbf{v} = [v_1, v_2, \dots, v_{n_T}]^T$, with $v_i = \frac{f_A(|w_i x|)}{|x|} \exp[j(\varphi_i + f_P(|w_i x|))]$. Our objectives are to choose \mathbf{w} and \mathbf{z} for the MIMO MRC scheme, i.e., using MRT at the transmitter and MRC at the receiver [98]. In this case, \mathbf{z} maximizes $|\mathbf{z}^H \mathbf{H}_e \mathbf{v}|$ given \mathbf{v} , according to $\mathbf{z} = \hat{\mathbf{H}}_e \mathbf{v} / \left\| \hat{\mathbf{H}}_e \mathbf{v} \right\|_F$, due to the imperfect estimation of the equivalent channel, and

MRT is employed to maximize the output SNR. Thus, \mathbf{v} is the eigenvector associated with the largest eigenvalue of matrix $\hat{\mathbf{H}}_e^H \hat{\mathbf{H}}_e / (1 + \sigma_{h_e}^2 / \beta_{ct}^2)$, λ_{\max} . Consequently, \mathbf{v} can be rewritten as

$$\mathbf{v} = d\tilde{\mathbf{w}}, \quad (7.16)$$

where $\tilde{\mathbf{w}}$ denotes the unit-norm eigenvector of $\hat{\mathbf{H}}_e^H \hat{\mathbf{H}}_e / (1 + \sigma_{h_e}^2 / \beta_{ct}^2)$ associated with its largest eigenvalue. Accordingly, the optimal combining vector, \mathbf{z} , can be expressed as $\mathbf{z} = \hat{\mathbf{H}}_e \tilde{\mathbf{w}} / \left\| \hat{\mathbf{H}}_e \tilde{\mathbf{w}} \right\|_F$.

Then, a methodology similar to that in Section 4.2.3 is used to determine the values of the optimal beamforming weight vector \mathbf{w} and the coefficient d . The solution is given by

$$\begin{cases} |w_i| = \frac{f_A^{-1}(d|\tilde{w}_i x|)}{|x|}, & i = 1, 2, \dots, n_T, \\ \varphi_i = \tilde{\varphi}_i - f_P[f_A^{-1}(d|\tilde{w}_i x|)], & i = 1, 2, \dots, n_T, \end{cases} \quad (7.17)$$

where the coefficient d is the solution of the following equation

$$\sum_{i=1}^{n_T} [f_A^{-1}(d|\tilde{w}_i x|)]^2 = |x|^2. \quad (7.18)$$

7.4.2 Estimation of Coefficients $K_1 \mathbf{z}^H \mathbf{H}_e \mathbf{v}$ and $K_2 (\mathbf{z}^H \mathbf{H}_e \mathbf{v})^*$

The coefficients $K_1 \mathbf{z}^H \mathbf{H}_e \mathbf{v}$ and $K_2 (\mathbf{z}^H \mathbf{H}_e \mathbf{v})^*$ are estimated before the signal detection. At the transmitter side, U pilot symbols are inserted before the data symbols in each frame. Each pilot symbol is transmitted using the beamforming scheme. Taking the HPA nonlinearity, I/Q imbalance and crosstalk into account, the received signal can be expressed as

$$\hat{\mathbf{y}}_{p,C} = K_1 \mathbf{z}^H \mathbf{H}_e \mathbf{v} \tilde{\mathbf{s}}_{p,C} + K_2 (\mathbf{z}^H \mathbf{H}_e \mathbf{v})^* \tilde{\mathbf{s}}_{p,C}^* + K_1 \mathbf{z}^H \mathbf{N}_{p,C} + K_2 (\mathbf{z}^H \mathbf{N}_{p,C})^*, \quad (7.19)$$

where $\mathbf{s}_{p,C}$ represents the $1 \times U$ transmitted pilot symbol vector, with an average power of ξ_p per pilot, $\tilde{\mathbf{s}}_{p,C}$ denotes the distorted version of $\mathbf{s}_{p,C}$ due to HPA nonlinearity, and $\mathbf{N}_{p,C}$ is the $n_R \times U$ noise matrix with elements belonging to i.i.d. complex circular Gaussian distribution $\mathcal{CN}(0, N_0)$ uncorrelated with the transmitted pilot symbols.

Then, making use of a similar methodology as the one adopted in our previous work, the estimate of $\Phi_C = [\phi_{C,1} \ \phi_{C,2}] = [K_1 \mathbf{z}^H \mathbf{H}_e \mathbf{v} \ K_2 (\mathbf{z}^H \mathbf{H}_e \mathbf{v})^*]$ using the LS method can be expressed as

$$\hat{\Phi}_C = \hat{\mathbf{y}}_{p,C} \mathbf{Q}_{p,C}^H (\mathbf{Q}_{p,C} \mathbf{Q}_{p,C}^H)^{-1}, \quad (7.20)$$

where $\mathbf{Q}_{p,C} = [\tilde{\mathbf{s}}_{p,C} \ \tilde{\mathbf{s}}_{p,C}^*]^T$. Consequently, the lower bound on the MSE between the coefficient vector Φ_C and its estimation $\hat{\Phi}_C$ is given by

$$\sigma_{C,\text{low}}^2 = \frac{2(|K_1|^2 + |K_2|^2) N_0}{U f_A^2 (\sqrt{\xi_p})}. \quad (7.21)$$

Then denoting Ψ as the estimation error vector, the relationship between $\hat{\Phi}_C$ and Φ_C can be expressed as

$$\hat{\Phi}_C = \Phi_C + \Psi, \quad (7.22)$$

where each element of vector $\Psi = [\psi_1 \ \psi_2]$ is a complex Gaussian distributed random variable, with zero mean and variance $\frac{\sigma_C^2}{2}$, uncorrelated with the elements of Φ_C .

7.4.3 Signal Detection Using Compensation for RF Impairments

Based on the estimation of the equivalent channel gain matrix \mathbf{H}_e and the coefficients vector Φ_C , the received signal of the considered system (7.10) can be rewritten as

$$\hat{y} = \phi_{C,1} x + \phi_{C,2} x^* + K_1 \mathbf{z}^H \mathbf{n} + K_2 (\mathbf{z}^H \mathbf{n})^*. \quad (7.23)$$

Then, the detection of $\mathbf{X} = [x \ x^*]^T$ can be obtained using a similar methodology as that in our previous work. Accordingly, we obtain

$$\hat{\mathbf{X}} = \hat{\Phi}_d^{-1} \mathbf{Y}, \quad (7.24)$$

where $\hat{\Phi}_d = \begin{bmatrix} \hat{\phi}_{C,1} & \hat{\phi}_{C,2} \\ \hat{\phi}_{C,2}^* & \hat{\phi}_{C,1}^* \end{bmatrix}$ and $\mathbf{Y} = [\hat{y} \ \hat{y}^*]^T$.

7.5 Performance Analysis

In this section, we analyze the performance of the MIMO TB scheme when implementing the proposed compensation method for HPA nonlinearity, I/Q imbalance and crosstalk, in uncorrelated Rayleigh fading channels. The performance metrics are the average SEP and the system capacity.

Based on (4.60) and (5.51), the approximate output SNR for the considered MIMO TB system is given by

$$\hat{\gamma} = d^2 \omega \bar{\gamma} \lambda_{\max}, \quad (7.25)$$

where $\omega = \frac{(|K_1|^2 - |K_2|^2)^2}{(|K_1|^2 + |K_2|^2)(|K_1|^2 + |K_2|^2 + \bar{\gamma} \sigma_c^2)}$ and where $\bar{\gamma} = P_0/N_0$ denotes the average SNR per receive antenna. A lower bound on d can be obtained as

$$d_{\text{low}} = \sqrt{\frac{1}{P_0}} f_A(\sqrt{P_0}), \quad (7.26)$$

which is achieved when $|\tilde{w}_i| = 1, |\tilde{w}_j| = 0$ ($j = 1, 2, \dots, n_T, j \neq i$).

Making use of a similar methodology as that in Section 5.5.1, it is observed that the Wishart matrix $\hat{\mathbf{H}}_e^H \hat{\mathbf{H}}_e / (1 + \sigma_{h_e}^2 / \beta_{ct}^2)$ has the same PDF as that of the matrix $\mathbf{H}_e^H \mathbf{H}_e$. Thus, the output SNR can be finally rewritten as

$$\hat{\gamma} = d^2 \omega \beta_{ct}^2 \bar{\gamma} \lambda_{\max}^e, \quad (7.27)$$

where λ_{\max}^e is the largest eigenvalue of the Wishart matrix $(\Phi_R^{1/2} \mathbf{H} \Phi_T^{1/2})^H \Phi_R^{1/2} \mathbf{H} \Phi_T^{1/2}$.

However, the provided expressions are too complex to achieve tractable performance analysis, such as average SEP and system capacity, for arbitrary $n_T \times n_R$ MIMO configurations. Herein, we focus on MIMO TB implementing $2 \times m$ or $m \times 2$ multi-element antennas. Above all, let $n = \min(n_T, n_R)$, $m = \max(n_T, n_R)$, and denote $\mathbf{\Omega} \in \mathcal{C}^{n \times n}$ and $\mathbf{\Sigma} \in \mathcal{C}^{m \times m}$ as

$$\mathbf{\Omega} \triangleq \begin{cases} \Phi_R, & n_R \leq n_T, \\ \Phi_T, & n_R > n_T, \end{cases} \quad (7.28)$$

$$\Sigma \triangleq \begin{cases} \Phi_{\text{T}}, & n_{\text{R}} \leq n_{\text{T}}, \\ \Phi_{\text{R}}, & n_{\text{R}} > n_{\text{T}}, \end{cases} \quad (7.29)$$

with eigenvalues $\omega_1 < \dots < \omega_n$ and $\sigma_1 < \dots < \sigma_m$, respectively. Then, the CDF of λ_{\max}^e is given by [100]:

$$F_{\lambda_{\max}^e}(\lambda) = \frac{\det(\mathbf{\Omega})}{\Delta_2(\mathbf{\Omega}) \Delta_m(\mathbf{\Sigma})} \times \sum_{s=1}^m \sum_{t=1, t \neq s}^m (-1)^{s+\vartheta(t)} (\sigma_s \sigma_t)^{m-1} \Delta_{m-2}(\sigma^{[s,t]}) Q_{s,t}(\lambda), \quad (7.30)$$

where

$$\vartheta(t) = \begin{cases} t, & t < s, \\ t-1, & t > s, \end{cases} \quad (7.31)$$

$$\sigma^{[s,t]} = \{\sigma_k; k = 1, \dots, m \setminus \{s, t\}\}, \quad (7.32)$$

$$Q_{s,t}(\lambda) = \frac{1}{\lambda} e^{-\frac{\lambda}{\omega_2 \sigma_s}} \text{P}\left(m, -\frac{\lambda}{\omega_2 \sigma_s}\right) e^{-\frac{\lambda}{\omega_1 \sigma_t}} \text{P}\left(m, -\frac{\lambda}{\omega_1 \sigma_t}\right), \quad (7.33)$$

with $\text{P}(\ell, y) = 1 - e^{-y} \sum_{k=0}^{\ell-1} \frac{y^k}{k!}$, and $\Delta_m(\cdot)$ denoting a Vandermonde determinant in the eigenvalues of the m -dimensional matrix argument, expressed as $\Delta_m(\mathbf{\Sigma}) = \prod_{k < l}^m (\sigma_l - \sigma_k)$.

7.5.1 Average Symbol Error Probability

The average SEP for general modulation formats in the scenario with additive white Gaussian noise can be expressed as [105]

$$P_s = E \left\{ aQ \left(\sqrt{2b\gamma} \right) \right\}, \quad (7.34)$$

where $E\{\cdot\}$ denotes the expectation operator, $Q(\cdot)$ represents the Gaussian Q-function, and (a, b) are modulation-specific constants, e.g., $(a, b) = (1, 1)$ for BPSK, and $(a \approx 2, b \approx \sin^2(\pi/M))$ for M -PSK [105].

Now, we recall that the entries of the effective post-processing noise caused by the three impairments are not necessarily Gaussian distributed. However, an upper bound on the average SEP can be obtained under the assumption that the interference

and noise are Gaussian random variables.

Using a similar methodology as that in Section 3.4.1, the upper bound on the average SEP can be expressed as

$$\begin{aligned}
P_s^{\text{up}} &= \frac{a\sqrt{b} \det(\mathbf{\Omega})}{2\sqrt{\pi} \Delta_2(\mathbf{\Omega}) \Delta_m(\mathbf{\Sigma})} \sum_{s=1}^m \sum_{t=1, t \neq s}^m (-1)^{s+\vartheta(t)} \times (\sigma_s \sigma_t)^{m-1} \Delta_{m-2}(\sigma^{[s,t]}) \\
&\left\{ 2c_{\text{RF}} \left[\sqrt{\pi \left(b + \frac{1}{\omega_2 \sigma_s c_{\text{RF}}} \right)} + \sqrt{\pi \left(b + \frac{1}{\omega_1 \sigma_t c_{\text{RF}}} \right)} - \sqrt{\pi \left(b + \frac{1}{\omega_2 \sigma_s c_{\text{RF}}} + \frac{1}{\omega_1 \sigma_t c_{\text{RF}}} \right)} \right] \right. \\
&+ \sum_{k=1}^{m-1} \frac{(-1)^k (2k-3)!! \sqrt{\pi}}{k! (2c_{\text{RF}})^{k-1}} \left[-\frac{1}{(\omega_2 \sigma_s)^k} \left(\frac{1}{\omega_1 \sigma_t c_{\text{RF}}} + b \right)^{\frac{1}{2}-k} \right. \\
&\left. \left. - \frac{1}{(\omega_1 \sigma_t)^k} \left(\frac{1}{\omega_2 \sigma_s c_{\text{RF}}} + b \right)^{\frac{1}{2}-k} + \frac{b^{\frac{1}{2}-k}}{(\omega_1 \sigma_t)^k} + \frac{b^{\frac{1}{2}-k}}{(\omega_2 \sigma_s)^k} \right] \right\}. \tag{7.35}
\end{aligned}$$

where $c_{\text{RF}} = d_{\text{low}}^2 \omega \beta_{ct}^2 \bar{\gamma}$.

7.5.2 System Capacity

A lower bound on the system capacity of the considered MIMO TB system with compensation for HPA nonlinearity, I/Q imbalance and crosstalk can be expressed in [bps/Hz] as

$$C^{\text{low}} = E_{\lambda_{\text{max}}^e} \{ \log_2(1 + c_{\text{RF}} \lambda_{\text{max}}^e) \}. \tag{7.36}$$

Making use of a similar methodology as that in Section 3.4.2, a lower bound on the system capacity is given by

$$\begin{aligned}
C^{\text{low}} &= \frac{\det(\mathbf{\Omega})}{c_{\text{RF}} \ln 2 \Delta_2(\mathbf{\Omega}) \Delta_m(\mathbf{\Sigma})} \sum_{s=1}^m \sum_{t=1, t \neq s}^m (-1)^{s+\vartheta(t)} (\sigma_s \sigma_t)^{m-1} \times \Delta_{m-2}(\sigma^{[s,t]}) \\
&\times \left\{ c_{\text{RF}}^2 \left[-\ln \left(\frac{1}{\omega_1 \sigma_t c_{\text{RF}}} \right) - \ln \left(\frac{1}{\omega_2 \sigma_s c_{\text{RF}}} \right) + \ln \left(\frac{1}{\omega_2 \sigma_s c_{\text{RF}}} + \frac{1}{\omega_1 \sigma_t c_{\text{RF}}} \right) \right] \right.
\end{aligned}$$

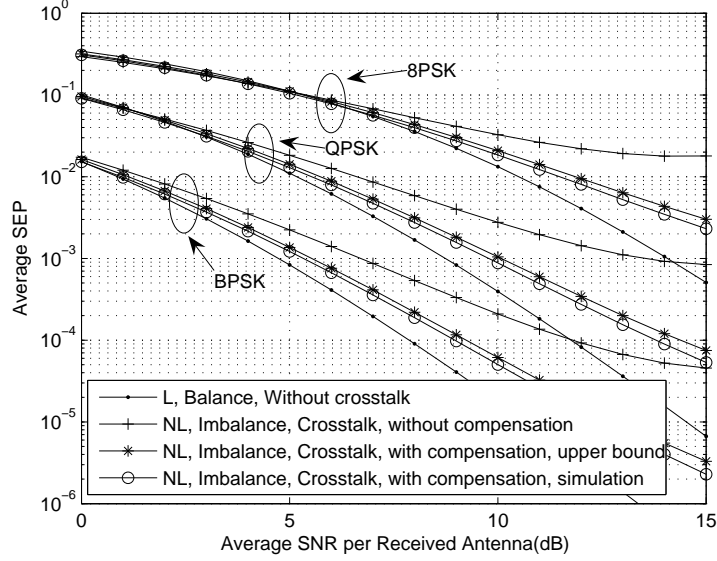


Figure 7.2: Average SEP versus $\bar{\gamma}$ of MIMO TB with RF impairments for different modulations formats ($n_T = n_R = 2$, $\beta = 1$, $ILR = -20$ dB, $U=32$, $\alpha_T = \alpha_R = -10$ dB).

$$\begin{aligned}
& - e^{\frac{1}{\omega_2 \sigma_s c_{RF}}} E_1 \left(\frac{1}{\omega_2 \sigma_s c_{RF}} \right) + e^{\frac{1}{\omega_2 \sigma_s c_{RF}} + \frac{1}{\omega_1 \sigma_t c_{RF}}} E_1 \left(\frac{1}{\omega_2 \sigma_s c_{RF}} + \frac{1}{\omega_1 \sigma_t c_{RF}} \right) \\
& - e^{\frac{1}{\omega_1 \sigma_t c_{RF}}} \times E_1 \left(\frac{1}{\omega_1 \sigma_t c_{RF}} \right) \Big] + \sum_{k=1}^{m-1} \frac{(-1)^k}{k} \left[\left(\frac{1}{\omega_1 \sigma_t} \right)^k e^{\frac{1}{\omega_2 \sigma_s c_{RF}}} \right. \\
& \times \sum_{l=1}^k c_{RF}^{l-k+1} \left(\frac{1}{\omega_2 \sigma_s} \right)^{1-l} \times \Gamma \left(-k + l, \frac{1}{\omega_2 \sigma_s c_{RF}} \right) \\
& \left. + \left(\frac{1}{\omega_2 \sigma_s} \right)^k \times e^{\frac{1}{\omega_1 \sigma_t c_{RF}}} \sum_{l=1}^k c_{RF}^{l-k+1} \left(\frac{1}{\omega_1 \sigma_t} \right)^{1-l} \Gamma \left(-k + l, \frac{1}{\omega_1 \sigma_t c_{RF}} \right) \right] \Big\}. \quad (7.37)
\end{aligned}$$

where $\Gamma(\alpha, x) = \int_x^{+\infty} t^{\alpha-1} e^{-t} dt$ denotes the complementary incomplete Gamma function and $E_1(\mu) = \int_1^{\infty} \frac{e^{-\mu t}}{t} dt$ represents the exponential integral function of the first order.

7.6 Numerical Results

In this section, we present numerical results illustrating the performance of the MIMO TB system with compensation for HPA nonlinearity, I/Q imbalance and

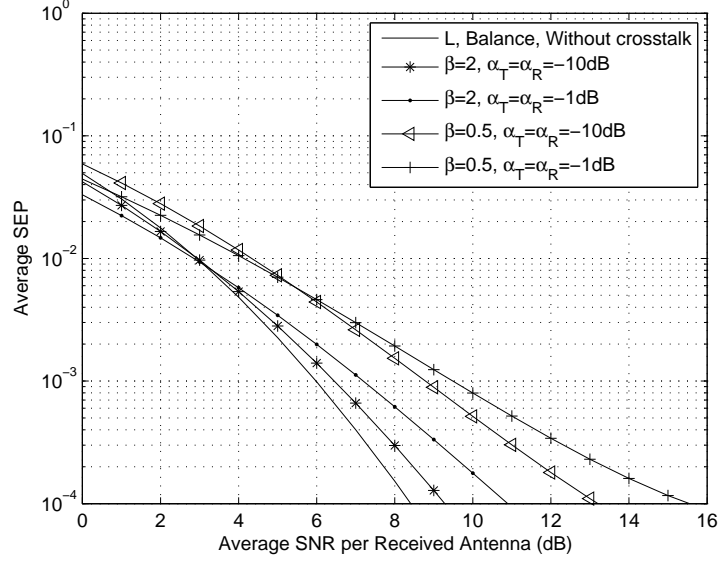


Figure 7.3: Average SEP versus $\bar{\gamma}$ of MIMO TB with RF impairments for different values of α_T , α_R and β ($n_T = 3$, $n_R = 2$, QPSK, $ILR = -20$ dB, $U=32$).

crosstalk over uncorrelated Rayleigh fading channels, specifically on the average SEP and system capacity. Herein, we consider the SSPA model for the nonlinear HPA, with the output saturation voltage set to $A_{os} = 1$. We fix the ratio of the pilot power to the noise power spectral density ξ_p/N_0 at 10 dB.

First, we show the average SEP versus the average SNR per receive antenna $\bar{\gamma}$ for the 2×2 MIMO configuration, taking the modulation order as parameter, in comparison with simulation results. We consider $\beta = 1$ in the SSPA model. As for the image-leakage ratio of the I/Q imbalance, we choose $ILR = -20$ dB. Furthermore, we set $U = 32$ and $\alpha_T = \alpha_R = -10$ dB. The average SEP of the MIMO MRT/MRC system in the case without HPA nonlinearity, I/Q imbalance and crosstalk is taken as the performance baseline. Fig. 7.2 indicates that the HPA nonlinearity, I/Q imbalance and crosstalk can be efficiently compensated using the proposed method in the presence of crosstalk. The residual degradation on the average SEP, due to these three impairments, increases as $\bar{\gamma}$ gets larger.

To further illustrate the effects of HPA nonlinearity, I/Q imbalance and crosstalk on the average SEP, results for different values of α_T , α_R and β , taking QPSK as the

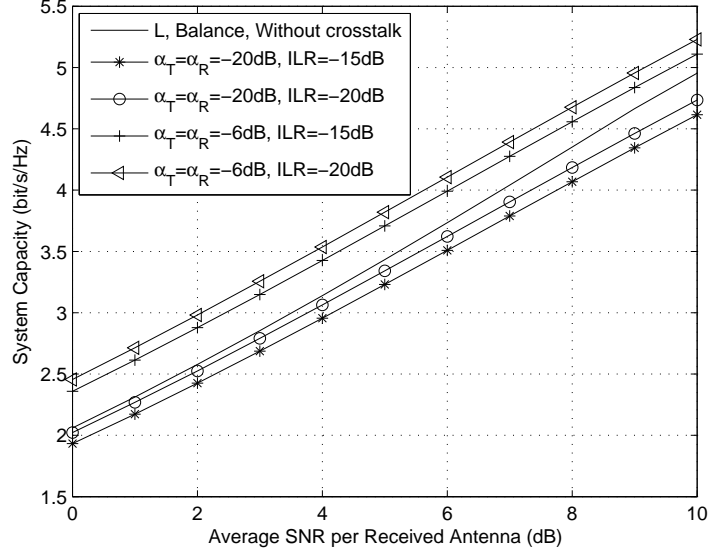


Figure 7.4: System capacity versus $\bar{\gamma}$ of MIMO TB with RF impairments for different values of α_T , α_R and ILR ($n_T = n_R = 2$, $\beta = 1$, $U=32$).

modulation scheme in the 3×2 MIMO configuration are provided in Fig. 7.3. In this case, we set $ILR = -20$ dB and $U = 32$. As observed, the average SEP decreases as the HPA parameter β becomes larger. In addition, the degradation caused by the crosstalk on the average SEP increases in the high $\bar{\gamma}$ range. On the other hand, for low values of $\bar{\gamma}$, the average SEP is reduced, profiting from the crosstalk. Furthermore, the cross point in $\bar{\gamma}$ between the constructive and destructive effects of the crosstalk becomes larger when the parameter β decreases.

In Fig. 7.4, we show the the lower bound on the system capacity versus the average SNR per receive antenna $\bar{\gamma}$ in the case with $n_T = n_R = 2$, $\beta = 1$ and $U = 32$. As noticed, the distortion due to HPA nonlinearity and I/Q imbalance results in a decrease in the capacity of MIMO TB systems. On the other hand, the capacity improves, profiting from the crosstalk.

Finally, in Fig. 7.5, we represent the lower bound on the system capacity as a function of the crosstalk, taking into account the three impairments, for the case with $\bar{\gamma} = 10$ dB and $ILR = -20$ dB. The effects of n_T and β on performance are shown in this figure. It is observed that for arbitrary MIMO configurations and parameter β ,

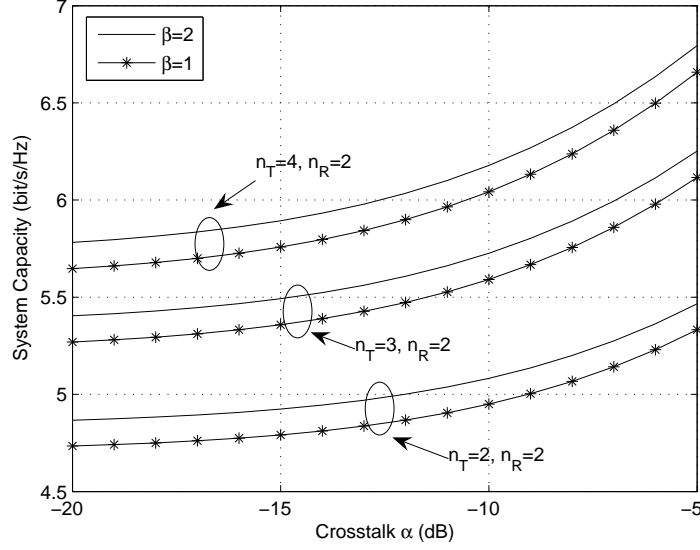


Figure 7.5: System capacity versus crosstalk of MIMO TB with RF impairments for different values of n_T , n_R and β ($\alpha_T = \alpha_R = \alpha$, $\bar{\gamma} = 10$ dB, $ILR = -20$ dB).

the system capacity increases as the crosstalk parameters α_T and α_R become larger.

7.7 Summary

In this chapter, MIMO TB systems with multiple RF impairments, including HPA nonlinearity, I/Q imbalance and crosstalk, were studied. We proposed a compensation method for the joint effect of HPA nonlinearity, I/Q imbalance and crosstalk. Then, we obtained an upper bound on the average SEP and a lower bound on capacity of the considered MIMO TB system using the proposed compensation method in Rayleigh fading environment. Numerical results showing the effects of several system parameters on performance were presented and discussed.

Chapter 8

Conclusions and Further Research

8.1 Conclusions of the Dissertation

In this dissertation, we investigated the analysis and compensation of channel impairments (spatially-correlated and keyhole fading channels, impairments in M-to-M communications) and RF impairments (HPA nonlinearity, I/Q imbalance and crosstalk) both separately and together for MIMO wireless communications systems. Analytical expressions for different performance metrics were derived in closed-form or approximate-form. This gave a comprehensive understanding on how channel and RF impairments can affect the performance of MIMO systems. The investigation on the channel and RF impairments made the advantages of MIMO systems, such as diversity gain and multiplexing gain, easy to be achieved in practical system implementations. Moreover, it provided a comprehensive method to investigate channel and RF impairments in other communication systems such as cognitive radio networks and cooperative communications. Specifically, the contribution of the dissertation is concluded as follows:

In Chapter 2, we proposed a cross-layer design for MIMO OSTBC over spatially-correlated and keyhole Nakagami- m fading channels. Numerical results were also presented to illustrate the effects of various parameters on the system performance. In particular, the ASE was shown to become more discrete and the oscillatory behavior of the average PLR curves increases as the spatial correlation becomes smaller. In

addition, the discrete property of the ASE and the oscillatory behavior of the average PLR curves become less visible in keyhole Nakagami- m fading channels, compared to the i.i.d. Nakagami- m case.

In Chapter 3, impairments in M-to-M communications were investigated. The performance of M-to-M MIMO MRC systems in double-correlated channels was evaluated in terms of average SEP, ergodic capacity and outage probability. The receive and transmit correlation functions were investigated taking into account fast fading and shadowing in a 3D M-to-M MIMO channel model. Numerical results and comparisons were presented. In particular, the average SEP was shown to increase as the shadowing standard derivation increases. It was also shown that the larger the degree of scattering around the transmitter in the x-y plane is, the higher the outage probability will be due to the higher non-isotropic scattering, and that the effect of path loss on performance is more visible than that of spatial correlation.

In addition to the investigation on channel impairments addressed in Chapters 2 and 3, the analysis and compensation of RF impairments were studied. In Chapter 4, a MIMO-OSTBC system that accounts for HPA nonlinearity was considered. We proposed a constellation-based compensation method and a SMC-based compensation algorithm for HPA nonlinearity in the case with and without knowledge of the HPA parameters, respectively. Using the proposed compensation schemes, the system performance was analyzed in terms of average SEP, TD and system capacity, when the system operates under uncorrelated Nakagami- m fading. It was shown that the constellation-based compensation method can efficiently mitigate the effect of HPA nonlinearity with low implementation complexity, and that the SMC-based compensation scheme is effective in the case without knowledge of the HPA parameters.

MIMO TB schemes with nonlinear HPAs were also studied in Chapter 4. It was illustrated that the conventional MRT/MRC scheme becomes suboptimal in the presence of HPA nonlinearity, where the spatial diversity cannot be efficiently obtained by the MRC. Then, we sought the optimal TB scheme with the optimal beamforming weight vector and combining vector for operation under HPA nonlinearity, by maximizing the output SNR. In addition, an alternative suboptimal but much simpler TB

scheme, namely, QEGT/MRC, was investigated, which is feasible in the case with nonlinear HPA, profiting from the property that the elements of the beamforming weight vector have the same constant modulus. We derived lower and upper bounds on the average SEP and mutual information with Gaussian input for the proposed optimal TB scheme in the presence of HPA nonlinearity, when operating under uncorrelated quasi-static frequency-flat Rayleigh fading. Moreover, a lower bound on the average SEP and an upper bound on the mutual information were provided for the QEGT/MRC scheme.

In Chapter 5, a MIMO MRC system model that takes another RF impairment, namely, I/Q imbalance, into account was developed. A channel estimation scheme considering the I/Q imbalance was proposed to perform the MIMO MRC, where the length of pilot symbols used to achieve the same estimation performance as in the case with ideal I/Q branches is twice that in the latter. Furthermore, we proposed a compensation algorithm for the I/Q imbalance, which can efficiently mitigate the deterioration that results from said imbalance. The effect of I/Q imbalance and proposed compensation algorithm on the performance for MIMO MRC systems was evaluated in terms of average SEP, outage probability and system capacity, which were derived considering transmission over uncorrelated Rayleigh fading channels.

Moreover, another RF impairment, namely, crosstalk, was evaluated in Chapter 6. In particular, the impact of crosstalk on the performance of MIMO TB systems was evaluated in terms of average symbol error probability and system capacity, which were derived considering transmission over uncorrelated Rayleigh fading channels. Importantly, it was observed that the impact of crosstalk on performance can be constructive or destructive.

Finally, in Chapter 7, a compensation method for the joint effect of HPA nonlinearity, I/Q imbalance and crosstalk was proposed for MIMO TB systems. Then, we obtained an upper bound on the average SEP and a lower bound on capacity of the considered MIMO TB system using the proposed compensation method in a Rayleigh fading environment.

8.2 Topics for Future Research

In the following, we provide some topics for further research, which are articulated for the research fields examined in this dissertation.

RF-Baseband Co-Design for Further Wireless Communication Systems with RF Impairments

This research theme aims at investigating RF-baseband co-design for further wireless communication systems with various RF impairments. Hybrid compensation techniques at both RF and baseband levels for RF impairments, including HPA non-linearity, LNA nonlinearity, I/Q imbalance, crosstalk, antenna coupling, phase noise, imperfect timing synchronization and echo, are to be proposed to eliminate or mitigate the impacts of RF impairments. The proposed RF-baseband co-design will make cooperation between device level design and system level compensation. Based on this, it will give new criteria for the design of further wireless systems.

The areas of this research include the baseband design, advanced RF front-end design, power amplifier design and linearization, MIMO-OFDM transceiver design, design of circuits and systems, digital signal processing/field-programmable gate array (DSP/FPGA) development, and noise measurement techniques. The required facilities include computer aided design (CAD) based software tools, test benches, and rapid prototyping setups. Therefore, it is an interdisciplinary investigation for the general communications field, which will undoubtedly make significant contributions to the scientific community and bring a new trend for the design and analysis of future wireless communication systems. It will provide a comprehensive method to investigate RF impairments in various communication systems such as cognitive radio networks, cooperative communications, “green” networks, 3GPP LTE-Advanced, WLAN and WiMAX.

Appendix A

Appendix

A.1 Proof of Proposition 1

Denote the term

$$\frac{1}{W} \sum_{i_1=1}^N \sum_{i_2=1}^N \cdots \sum_{i_{n_T}=1}^N w_{i_1, i_2, \dots, i_{n_T}} \left\| \hat{\mathbf{H}} \hat{\mathbf{X}}_p (\boldsymbol{\Psi}_{i_1, i_2, \dots, i_{n_T}}) - \mathbf{Y}_p \right\|_F^2 \quad (\text{A.1})$$

in (4.36) as $g(\hat{\mathbf{H}})$. This term can be rewritten as

$$\begin{aligned} g(\hat{\mathbf{H}}) &= \frac{1}{W} \sum_{i_1=1}^N \sum_{i_2=1}^N \cdots \sum_{i_{n_T}=1}^N w_{i_1, i_2, \dots, i_{n_T}} \\ &\quad \times \text{Tr} \left[\left(\hat{\mathbf{H}} \hat{\mathbf{X}}_p (\boldsymbol{\Psi}_{i_1, i_2, \dots, i_{n_T}}) - \mathbf{Y}_p \right) \left(\hat{\mathbf{H}} \hat{\mathbf{X}}_p (\boldsymbol{\Psi}_{i_1, i_2, \dots, i_{n_T}}) - \mathbf{Y}_p \right)^H \right] \\ &= \frac{1}{W} \sum_{i_1=1}^N \sum_{i_2=1}^N \cdots \sum_{i_{n_T}=1}^N w_{i_1, i_2, \dots, i_{n_T}} \\ &\quad \times \text{Tr} \left[\left(\hat{\mathbf{H}} \hat{\mathbf{X}}_p (\boldsymbol{\Psi}_{i_1, i_2, \dots, i_{n_T}}) - \mathbf{Y}_p \right) \left(\hat{\mathbf{X}}_p^H (\boldsymbol{\Psi}_{i_1, i_2, \dots, i_{n_T}}) \hat{\mathbf{H}}^H - \mathbf{Y}_p^H \right) \right] \end{aligned}$$

$$\begin{aligned}
&= \frac{1}{W} \sum_{i_1=1}^N \sum_{i_2=1}^N \cdots \sum_{i_{n_T}=1}^N w_{i_1, i_2, \dots, i_{n_T}} \left\{ \text{Tr} \left[\hat{\mathbf{H}} \hat{\mathbf{X}}_p \left(\Psi_{i_1, i_2, \dots, i_{n_T}} \right) \hat{\mathbf{X}}_p^H \left(\Psi_{i_1, i_2, \dots, i_{n_T}} \right) \hat{\mathbf{H}}^H \right] \right. \\
&\quad \left. - \text{Tr} \left[\mathbf{Y}_p \hat{\mathbf{X}}_p^H \left(\Psi_{i_1, i_2, \dots, i_{n_T}} \right) \hat{\mathbf{H}}^H \right] - \text{Tr} \left[\hat{\mathbf{H}} \hat{\mathbf{X}}_p \left(\Psi_{i_1, i_2, \dots, i_{n_T}} \right) \mathbf{Y}_p^H \right] + \text{Tr} \left(\mathbf{Y}_p \mathbf{Y}_p^H \right) \right\}, \tag{A.2}
\end{aligned}$$

where $\text{Tr}(\cdot)$ denotes the trace of a matrix. Then, the differential of $g(\hat{\mathbf{H}})$ can be found as

$$\begin{aligned}
\frac{\partial \left[g(\hat{\mathbf{H}}) \right]}{\partial \hat{\mathbf{H}}^*} &= \frac{1}{W} \sum_{i_1=1}^N \sum_{i_2=1}^N \cdots \sum_{i_{n_T}=1}^N w_{i_1, i_2, \dots, i_{n_T}} \left\{ - \frac{\partial \left[\text{Tr} \left(\hat{\mathbf{H}} \hat{\mathbf{X}}_p \left(\Psi_{i_1, i_2, \dots, i_{n_T}} \right) \mathbf{Y}_p^H \right) \right]}{\partial \hat{\mathbf{H}}^*} \right. \\
&\quad - \frac{\partial \left[\text{Tr} \left(\mathbf{Y}_p \hat{\mathbf{X}}_p^H \left(\Psi_{i_1, i_2, \dots, i_{n_T}} \right) \hat{\mathbf{H}}^H \right) \right]}{\partial \hat{\mathbf{H}}^*} \\
&\quad \left. + \frac{\partial \left[\text{Tr} \left(\hat{\mathbf{H}} \hat{\mathbf{X}}_p \left(\Psi_{i_1, i_2, \dots, i_{n_T}} \right) \hat{\mathbf{X}}_p^H \left(\Psi_{i_1, i_2, \dots, i_{n_T}} \right) \hat{\mathbf{H}}^H \right) \right]}{\partial \hat{\mathbf{H}}^*} \right\} \\
&= \frac{1}{W} \sum_{i_1=1}^N \sum_{i_2=1}^N \cdots \sum_{i_{n_T}=1}^N w_{i_1, i_2, \dots, i_{n_T}} \\
&\quad \times \left[\hat{\mathbf{H}} \hat{\mathbf{X}}_p \left(\Psi_{i_1, i_2, \dots, i_{n_T}} \right) \hat{\mathbf{X}}_p^H \left(\Psi_{i_1, i_2, \dots, i_{n_T}} \right) - \mathbf{Y}_p \hat{\mathbf{X}}_p^H \left(\Psi_{i_1, i_2, \dots, i_{n_T}} \right) \right]. \tag{A.3}
\end{aligned}$$

Finally, by setting the differential to zero, the estimate $\hat{\mathbf{H}}_{LS}$ is obtained as

$$\begin{aligned}
\hat{\mathbf{H}}_{LS} &\approx \sum_{i_1=1}^N \sum_{i_2=1}^N \cdots \sum_{i_{n_T}=1}^N w_{i_1, i_2, \dots, i_{n_T}} \mathbf{Y}_p \hat{\mathbf{X}}_p^H \left(\Psi_{i_1, i_2, \dots, i_{n_T}} \right) \\
&\quad \times \left[\sum_{i_1=1}^N \sum_{i_2=1}^N \cdots \sum_{i_{n_T}=1}^N w_{i_1, i_2, \dots, i_{n_T}} \hat{\mathbf{X}}_p \left(\Psi_{i_1, i_2, \dots, i_{n_T}} \right) \hat{\mathbf{X}}_p^H \left(\Psi_{i_1, i_2, \dots, i_{n_T}} \right) \right]^{-1}. \tag{A.4}
\end{aligned}$$

A.2 Proof of Theorem 1

Assuming that $\sigma_C^2 \ll 1$, the term $\hat{\Phi}_d^{-1}$ in (5.30) can be approximated by the linear part of a Taylor expansion as

$$\begin{aligned}\hat{\Phi}_d^{-1} &= (\Phi_d + \Psi_d)^{-1} \\ &= \Phi_d^{-1} \sum_{n=0}^{\infty} (-1)^n (\Psi_d \Phi_d^{-1})^n \\ &\cong \Phi_d^{-1} (\mathbf{I}_2 - \Psi_d \Phi_d^{-1}).\end{aligned}\tag{A.5}$$

Hence, substituting (5.28) and (A.5) into (5.30), the estimate of the transmitted symbols can be further expressed as

$$\hat{\mathbf{X}}_{\text{WI\&WC}} \approx \mathbf{X} + \Phi_d^{-1} \mathbf{N}_d - \Phi_d^{-1} \Psi_d \mathbf{X} - \Phi_d^{-1} \Psi_d \Phi_d^{-1} \mathbf{N}_d.\tag{A.6}$$

We denote the effective post-processing noise as

$$\begin{aligned}\tilde{\mathbf{N}}_d &= \hat{\mathbf{X}}_{\text{WI\&WC}} - \mathbf{X} \\ &\approx \Phi_d^{-1} \mathbf{N}_d - \Phi_d^{-1} \Psi_d \mathbf{X} - \Phi_d^{-1} \Psi_d \Phi_d^{-1} \mathbf{N}_d,\end{aligned}\tag{A.7}$$

whose covariance matrix can be obtained using an approach similar to that taken to derive [134, eq. (11)], as follows,

$$\begin{aligned}E \left[\tilde{\mathbf{N}}_d \tilde{\mathbf{N}}_d^H \right] &\approx E \left[\Phi_d^{-1} (\Phi_d^{-1})^H \right] \left\{ (|K_1|^2 + |K_2|^2) N_0 \right. \\ &\quad \left. + P_0 \sigma_C^2 + \frac{\sigma_C^2}{2} (|K_1|^2 + |K_2|^2) N_0 E \left[\text{tr} \left(\Phi_d^{-1} (\Phi_d^{-1})^H \right) \right] \right\}.\end{aligned}\tag{A.8}$$

Moreover, by taking into account the estimation error for the channel gain matrix \mathbf{H} specified in Section 5.3.1, matrix Φ_d is given by

$$\Phi_d = \Phi_{d,\hat{\mathbf{H}}} + \Theta_{d,\hat{\mathbf{H}}}, \quad (\text{A.9})$$

where

$$\Phi_{d,\hat{\mathbf{H}}} = \begin{bmatrix} K_1 \rho_h \frac{\mathbf{w}^H \hat{\mathbf{H}}^H \hat{\mathbf{H}} \mathbf{w}}{\|\hat{\mathbf{H}} \mathbf{w}\|_F} & K_2 \left(\rho_h \frac{\mathbf{w}^H \hat{\mathbf{H}}^H \hat{\mathbf{H}} \mathbf{w}}{\|\hat{\mathbf{H}} \mathbf{w}\|_F} \right)^* \\ K_2^* \rho_h \frac{\mathbf{w}^H \hat{\mathbf{H}}^H \hat{\mathbf{H}} \mathbf{w}}{\|\hat{\mathbf{H}} \mathbf{w}\|_F} & K_1^* \left(\rho_h \frac{\mathbf{w}^H \hat{\mathbf{H}}^H \hat{\mathbf{H}} \mathbf{w}}{\|\hat{\mathbf{H}} \mathbf{w}\|_F} \right)^* \end{bmatrix}, \quad (\text{A.10})$$

$$\Theta_{d,\hat{\mathbf{H}}} = \begin{bmatrix} K_1 \frac{\mathbf{w}^H \hat{\mathbf{H}}^H \Theta \mathbf{w}}{\|\hat{\mathbf{H}} \mathbf{w}\|_F} & K_2 \left(\frac{\mathbf{w}^H \hat{\mathbf{H}}^H \Theta \mathbf{w}}{\|\hat{\mathbf{H}} \mathbf{w}\|_F} \right)^* \\ K_2^* \frac{\mathbf{w}^H \hat{\mathbf{H}}^H \Theta \mathbf{w}}{\|\hat{\mathbf{H}} \mathbf{w}\|_F} & K_1^* \left(\frac{\mathbf{w}^H \hat{\mathbf{H}}^H \Theta \mathbf{w}}{\|\hat{\mathbf{H}} \mathbf{w}\|_F} \right)^* \end{bmatrix}. \quad (\text{A.11})$$

Under the assumption that $\sigma_{h,\text{WI}}^2 \ll 1$, and making use of a Taylor expansion, the matrix Φ_d^{-1} can be approximated as

$$\Phi_d^{-1} \cong \Phi_{d,\hat{\mathbf{H}}}^{-1} \left(\mathbf{I}_2 - \Theta_{d,\hat{\mathbf{H}}} \Phi_{d,\hat{\mathbf{H}}}^{-1} \right). \quad (\text{A.12})$$

Thus, the term $E \left[\Phi_d^{-1} (\Phi_d^{-1})^H \right]$ in (A.8) can be expressed as

$$E \left[\Phi_d^{-1} (\Phi_d^{-1})^H \right] \approx \left(\Phi_{d,\hat{\mathbf{H}}}^H \Phi_{d,\hat{\mathbf{H}}} \right)^{-1} \times \left(1 + (|K_1|^2 + |K_2|^2) \sigma_{\Theta}^2 \text{tr} \left(\left(\Phi_{d,\hat{\mathbf{H}}}^H \Phi_{d,\hat{\mathbf{H}}} \right)^{-1} \right) \right). \quad (\text{A.13})$$

It can be obviously shown that the first term in the right-hand-side of (A.13) is given by

$$\left(\Phi_{d,\hat{\mathbf{H}}}^H \Phi_{d,\hat{\mathbf{H}}} \right)^{-1} = \left(\frac{1 + \sigma_{h,\text{WI}}^2}{(|K_1|^2 - |K_2|^2) \lambda_{\max}} \right)^2 \begin{bmatrix} M_{1,1} & M_{2,1}^* \\ M_{2,1} & M_{1,1} \end{bmatrix}, \quad (\text{A.14})$$

where

$$M_{1,1} = \frac{(|K_1|^2 + |K_2|^2) \lambda_{\max}}{1 + \sigma_{h,\text{WI}}^2}, \quad (\text{A.15})$$

$$M_{2,1} = -2K_1K_2^* \left(\rho_h \frac{\mathbf{w}^H \hat{\mathbf{H}}^H \hat{\mathbf{H}} \mathbf{w}}{\|\hat{\mathbf{H}} \mathbf{w}\|_F} \right)^2, \quad (\text{A.16})$$

and λ_{\max} and $\sigma_{h,\text{WI}}^2$ are as defined in Section 5.3. Then, substituting (A.14) into (A.13), the term $E \left[\Phi_d^{-1} (\Phi_d^{-1})^H \right]$ can be further expressed as

$$\begin{aligned} E \left[\Phi_d^{-1} (\Phi_d^{-1})^H \right] &\approx \left(\frac{1 + \sigma_{h,\text{WI}}^2}{(|K_1|^2 - |K_2|^2) \lambda_{\max}} \right)^2 \\ &\times \left(1 + \left(\frac{|K_1|^2 + |K_2|^2}{|K_1|^2 - |K_2|^2} \right)^2 \frac{2\sigma_{h,\text{WI}}^2}{\lambda_{\max}} \right) \begin{bmatrix} M_{1,1} & M_{2,1}^* \\ M_{2,1} & M_{1,1} \end{bmatrix}. \end{aligned} \quad (\text{A.17})$$

Based on the above, the term $E \left[\text{Tr} \left(\Phi_d^{-1} (\Phi_d^{-1})^H \right) \right]$ in (A.8) is given by

$$\begin{aligned} E \left[\text{Tr} \left(\Phi_d^{-1} (\Phi_d^{-1})^H \right) \right] &\approx \frac{2(|K_1|^2 + |K_2|^2)(1 + \sigma_{h,\text{WI}}^2)}{(|K_1|^2 - |K_2|^2)^2 \lambda_{\max}} \\ &\times \left[1 + \left(\frac{|K_1|^2 + |K_2|^2}{|K_1|^2 - |K_2|^2} \right)^2 \frac{2\sigma_{h,\text{WI}}^2}{\lambda_{\max}} \right]. \end{aligned} \quad (\text{A.18})$$

Finally, by substituting (A.17) and (A.18) into (A.8), and applying the latter to the SNR definition $\gamma_{\text{WI\&WC}}^{\text{MRT/MRC}} = \frac{P_0}{(E[\tilde{\mathbf{N}}_d \tilde{\mathbf{N}}_d^H])_{1,1}}$, where $(E[\tilde{\mathbf{N}}_d \tilde{\mathbf{N}}_d^H])_{1,1}$ denotes the (1,1) element of the matrix $E[\tilde{\mathbf{N}}_d \tilde{\mathbf{N}}_d^H]$, the effective output SNR of the MIMO MRC system under study can be approximated as (5.31).

Bibliography

- [1] D. N. C. Tse and P. Viswanath, *Fundamentals of Wireless Communication*, Cambridge University Press, New York, 2005.
- [2] *Requirements for further advancements for Evolved Universal Terrestrial Radio Access (E-UTRA) (LTE-Advanced) (Release 9)*, 3rd Generation Partnership Project, 3GPP TR 36.913 V. 9.0.0, Dec. 2009.
- [3] *Wireless LAN Medium Access Control (MAC) and Physical Layer (PHY) Specifications: High Speed Physical Layer in the 5 Ghz Band*, IEEE Std 802.11a, 1999.
- [4] *Wireless LAN Medium Access Control (MAC) and Physical Layer (PHY) Specifications: Further Higher-Speed Physical Layer Extension in the 2.4GHz Band*, IEEE Std 802.11g, 2003.
- [5] *IEEE Standard for Local and Metropolitan Area Networks Part 16: Air Interface for Fixed and Mobile Broadband Wireless Access Systems*, IEEE Std 802.16e, 2006.
- [6] *IEEE Standard for Local and Metropolitan Area Networks Part 20: Air Interface for Mobile Broadband Wireless Access Systems Supporting Vehicular Mobility—Physical and Media Access Control Layer Specification*, IEEE Std 802.20, 2008.
- [7] *Draft Standard for Wireless Regional Area Networks Part 22: Cognitive Wireless RAN Medium Access Control (MAC) and Physical Layer (PHY) Specifications: Policies and Procedures for Operation in the TV Bands*, IEEE Std 802.22/DRAFT v2.0, May 2009.

- [8] D. Chizhik, G. J. Foschini, and R. A. Valenzuela, "Capacities of multi-element transmit and receive antennas: Correlations and keyholes," *IEE Electron. Lett.*, vol. 36, no. 13, pp. 1099–1100, June 2000.
- [9] X. Cai and G. B. Giannakis, "Differential space-time modulation with eigenbeamforming for correlated MIMO fading channels," *IEEE Trans. Signal Process.*, vol. 54, no. 4, pp. 1279–1288, Apr. 2006.
- [10] X. Cai, G. B. Giannakis, and M. D. Zoltowski, "Space-time spreading and block coding for correlated fading channels in the presence of interference," *IEEE Trans. Commun.*, vol. 53, no. 3, pp. 515–525, Mar. 2005.
- [11] H. Boche and E. A. Jorswieck, "On the ergodic capacity as a function of the correlation properties in systems with multiple transmit antennas without CSI at the transmitter," *IEEE Trans. Commun.*, vol. 52, no. 10, pp. 1654–1657, Oct. 2004.
- [12] E. A. Jorswieck and H. Boche, "Channel capacity and capacity-range of beamforming in MIMO wireless systems under correlated fading with covariance feedback," *IEEE Trans. Wireless Commun.*, vol. 3, no. 5, pp. 1543–1553, Sept. 2004.
- [13] M. Kang and M. S. Alouini, "Impact of correlation on the capacity of MIMO channels," in *Proc. IEEE Int. Conf. Commun. (ICC'03)*, Ottawa, Canada, May 2003, vol. 4, pp. 2623–2627.
- [14] J. S. Kwak, H. Kang, Y. Li, and G. L. Stüber, "Effects of spatial correlation on MIMO adaptive antenna system with optimum combining," *IEEE Trans. Wireless Commun.*, vol. 6, no. 5, pp. 1722–1731, May 2007.
- [15] R. H. Y. Louie, M. R. McKay, I. B. Collings, and B. Vucetic, "Capacity approximations for multiuser MIMO-MRC with antenna correlation," in *Proc. IEEE International Conf. on Commun. (ICC'07)*, Glasgow, Scotland, June 2007, pp. 5195–5200.

- [16] C. Martin and B. Ottersten, "Asymptotic eigenvalue distributions and capacity for MIMO channels under correlated fading," *IEEE Trans. Wireless Commun.*, vol. 3, no. 4, pp. 1350–1359, July 2004.
- [17] H. Shin, M. Z. Win, J. H. Lee, and M. Chiani, "On the capacity of doubly correlated MIMO channels," *IEEE Trans. Wireless Commun.*, vol. 5, no. 8, pp. 2253–2265, Aug. 2006.
- [18] V. V. Veeravalli, Y. Liang, and A. M. Sayeed, "Correlated MIMO wireless channels: Capacity, optimal signaling, and asymptotics," *IEEE Trans. Inf. Theory*, vol. 51, no. 6, pp. 2058–2072, June 2005.
- [19] M. Chiani, M. Z. Win, and A. Zanella, "On the capacity of spatially correlated MIMO Rayleigh-fading channels," *IEEE Trans. Inf. Theory*, vol. 49, no. 10, pp. 2363–2371, Oct. 2003.
- [20] M. Kang and M. S. Alouini, "Capacity of correlated MIMO Rayleigh channels," *IEEE Trans. Wireless Commun.*, vol. 5, no. 1, pp. 143–155, Jan. 2006.
- [21] L. Musavian and M. R. Nakhai, "On the capacity of orthogonalised correlated MIMO channels under different adaptive transmission techniques," *IET Commun.*, vol. 1, no. 3, pp. 464–471, June 2007.
- [22] L. Yang and J. Qin, "Performance of STBCs with antenna selection: Spatial correlation and keyhole effects," *IEE Proc.-Commun.*, vol. 153, no. 1, pp. 15–20, Feb. 2006.
- [23] D. Chizhik, G. J. Foschini, M. J. Gans, and R. A. Valenzuela, "Keyholes, correlations, and capacities of multielement transmit and receive antennas," *IEEE Trans. Wireless Commun.*, vol. 1, no. 2, pp. 361–368, Apr. 2002.
- [24] A. Muller and J. Speidel, "Bit error rate analysis of orthogonal space-time block codes in Nakagami- m keyhole channels," in *Proc. Int. Conf. Commun. and Networking in China (ChinaCom '06)*, Beijing, China, Oct. 2006, pp. 1–5.

- [25] A. Maaref and S. Aïssa, “Impact of spatial fading correlation and keyhole on the capacity of MIMO systems with transmitter and receiver CSI,” *IEEE Trans. Wireless Commun.*, vol. 7, no. 8, pp. 3218–3229, Aug. 2008.
- [26] M. Pätzold, B. O. Hogstad, N. Youssef, and D. Kim, “A MIMO mobile-to-mobile channel model: Part I—the reference model,” in *Proc. IEEE Symp. Personal, Indoor and Mobile Radio Commun. (PIMRC’05)*, Berlin, Germany, Sept. 2005, vol. 1, pp. 573–578.
- [27] D. Shiu, G. J. Foschini, M. J. Gans, and J. M. Khan, “Fading correlation and its effect on the capacity of multielement antenna systems,” *IEEE Trans. Commun.*, vol. 48, no. 3, pp. 502–513, Mar. 2000.
- [28] H. S. Rad and S. Gazor, “Space-time-frequency characterization of 3D non-isotropic MIMO multicarrier propagation channels employing directional antennas,” in *Proc. IEEE Wireless Commun. and Networking Conf. (WCNC’07)*, Hong Kong, China, Mar. 2007, pp. 1888–1893.
- [29] A. G. Zajić and G. L. Stüber, “A three-dimensional MIMO mobile-to-mobile channel model,” in *Proc. IEEE Wireless Commun. and Networking Conf. (WCNC’07)*, Hong Kong, China, Mar. 2007, pp. 1883–1887.
- [30] T. Aulin, “A modified model for the fading at a mobile radio channel,” *IEEE Trans. Veh. Tech.*, vol. VT-28, pp. 182–203, 1979.
- [31] J. D. Parsons and A. M. D. Turkmani, “Characterisation of mobile radio signals: Model description,” in *Proc. IEE Commun., Speech, and Vision*, Dec. 1991, vol. 138, pp. 549–556.
- [32] S. Y. Leong, Y. R. Zheng, and C. Xiao, “Space-time fading correlation functions of a 3-D MIMO channel model,” in *Proc. IEEE Wireless Commun. and Networking Conf. (WCNC’04)*, Atlanta, Georgia, USA, Mar. 2004, pp. 1127–1132.

- [33] A. G. Zajić and G. L. Stüber, “Influence of 3-D spatial correlation on the capacity of MIMO mobile-to-mobile channels,” in *Proc. IEEE Veh. Technol. Conf. (VTC’07)*, Dublin, Ireland, Apr. 2007, pp. 461–465.
- [34] F. H. Gregorio, *Analysis and Compensation of Nonlinear Power Amplifier Effects in Multi-antenna OFDM Systems*, Ph.D thesis, Helsinki University of Technology, Espoo, Finland, Nov. 2007.
- [35] A. Saleh, “Frequency-independent and frequency-dependent nonlinear models of TWT amplifiers,” *IEEE Trans. Commun.*, vol. 29, no. 11, pp. 1715–1720, Nov. 1981.
- [36] C. Rapp, “Effects of HPA nonlinearity on a 4-DPSK/OFDM signal for a digital sound broadcasting system,” in *Proc. Eur. Conf. Satellite Commun.*, Liege, Belgium, Oct. 1991, vol. 1, pp. 179–184.
- [37] H. E. Rowe, “Memoryless nonlinearities with Gaussian inputs: Elementary results,” *Bell Syst. Tech. J.*, vol. 61, no. 7, pp. 1519–1525, Sept. 1982.
- [38] J. Boccuzzi, “Performance evaluation of non-linear transmit power amplifiers for North American digital cellular portables,” *IEEE Trans. Veh. Technol.*, vol. 44, no. 2, pp. 220–228, Aug. 1995.
- [39] A. I. Sulyman and M. Ibnkahla, “Performance of space time codes over nonlinear MIMO channels,” in *Proc. IEEE Int. Symp. Signal Process. and Its Applications (ISSPA ’05)*, Sydney, Australia, Aug. 2005, vol. 1, pp. 407–410.
- [40] E. K. S. Au and W. H. Mow, “Effect of non-linearity on the performance of a MIMO zero-forcing receiver with channel estimation errors,” in *Proc. IEEE Int. Conf. Commun. (ICC’07)*, Glasgow, Scotland, June 2007, pp. 4150–4155.
- [41] D. Dardari, V. Tralli, and A. Vaccari, “A theoretical characterization of non-linear distortion effects in OFDM systems,” *IEEE Trans. Commun.*, vol. 48, no. 10, pp. 1755–1764, Oct. 2000.

- [42] A. Katz, "Linearization: Reducing distortion in power amplifiers," *IEEE Microw. Mag.*, vol. 2, no. 4, pp. 37–49, Dec. 2001.
- [43] A. I. Sulyman and M. Ibnkahla, "Performance of MIMO systems with antenna selection over nonlinear fading channels," *IEEE J. Sel. Topics Signal Process.*, vol. 2, no. 2, pp. 159–170, Apr. 2008.
- [44] J. K. Cavers and M. W. Liao, "Adaptive compensation for imbalance and offset losses in direct conversion transceivers," *IEEE Trans. Veh. Technol.*, vol. 42, no. 4, pp. 581–588, Nov. 1993.
- [45] P. Rykaczewski, M. Valkama, and M. Renfors, "On the connection of I/Q imbalance and channel equalization in direct-conversion transceivers," *IEEE Trans. Veh. Technol.*, vol. 57, no. 3, pp. 1630–1636, May 2008.
- [46] D. Tandur and M. Moonen, "Joint adaptive compensation of transmitter and receiver IQ imbalance under carrier frequency offset in OFDM-based systems," *IEEE Trans. Signal Process.*, vol. 55, no. 11, pp. 5246–5252, Nov. 2007.
- [47] G. Xing, M. Shen, and H. Liu, "Frequency offset and I/Q imbalance compensation for direct-conversion receivers," *IEEE Trans. Wireless Commun.*, vol. 4, no. 2, pp. 673–680, Mar. 2005.
- [48] Y. Zou, M. Valkama, and M. Renfors, "Compensation of frequency-selective I/Q imbalances in space-time coded multi-antenna OFDM systems," in *Proc. IEEE Int. Symp. Commun., Control and Signal Process. (ISCCSP'08)*, St. Julians, Malta, Mar. 2008, pp. 123–128.
- [49] Y. Zou, M. Valkama, and M. Renfors, "Digital compensation of I/Q imbalance effects in space-time coded transmit diversity systems," *IEEE Trans. Signal Process.*, vol. 56, no. 6, pp. 2496–2508, June 2008.
- [50] S. Krone and G. Fettweis, "On the capacity of OFDM systems with receiver I/Q imbalance," in *Proc. IEEE Int. Conf. Commun. (ICC'08)*, Beijing, China, May 2008, pp. 1317–1321.

- [51] H. Zareian and V. T. Vakili, "Analytical BER performance of M-QAM-OFDM systems in the presence of IQ imbalance," in *Proc. IFIP Int. Conf. Wireless and Optical Commun. Networks (WOCN'07)*, Singapore, July 2007, pp. 1–5.
- [52] M. Valkama, M. Renfors, and V. Koivunen, "Advanced methods for I/Q imbalance compensation in communication receivers," *IEEE Trans. Signal Process.*, vol. 49, no. 10, pp. 2335–2344, Oct. 2001.
- [53] L. Anttila, M. Valkama, and M. Renfors, "Circularity-based I/Q imbalance compensation in wideband direct-conversion receivers," *IEEE Trans. Veh. Technol.*, vol. 57, no. 4, pp. 2099–2113, July 2008.
- [54] A. Tarighat, R. Bagheri, and A. H. Sayed, "Compensation schemes and performance analysis of IQ imbalances in OFDM receivers," *IEEE Trans. Signal Process.*, vol. 53, no. 8, pp. 3257–3268, Aug. 2005.
- [55] A. Tarighat and A. H. Sayed, "MIMO OFDM receivers for systems with IQ imbalances," *IEEE Trans. Signal Process.*, vol. 53, no. 9, pp. 3583–3596, Sept. 2005.
- [56] M. Windisch and G. Fettweis, "Adaptive I/Q imbalance compensation in low-IF transmitter architectures," in *Proc. IEEE Veh. Technol. Conf. (VTC'04-Fall)*, Los Angeles, USA, Sept. 2004, vol. 3, pp. 2096–2100.
- [57] C. R. Paul, *Introduction to Electromagnetic Compatibility*, Wiley, Hoboken, New Jersey, 4th edition, Jan. 2006.
- [58] B. J. LaMeres and S. P. Khatri, "Encoding-based minimization of inductive cross-talk for off-chip data transmission," in *Proc. Design, Automation and Test in Europe (DATE'05)*, Munich, Germany, Mar. 2005, pp. 1318–1323.
- [59] A. Mahanfar, "On the parameterization of the cross-talk in printed circuit board traces," in *Proc. IEEE Int. Symp. Electromagn. Compat. (EMC'04)*, Santa Clara, CA, USA, Aug. 2004, vol. 2, pp. 383–385.

- [60] Y. Palaskas, A. Ravi, and S. Pellerano, et al, "A 5-GHz 108-Mb/s 2×2 MIMO transceiver RFIC with fully integrated 20.5-dBm P_{1dB} power amplifiers in 90-nm CMOS," *IEEE J. Solid-State Circuit*, vol. 41, no. 12, pp. 2746–2756, Dec. 2006.
- [61] K.-J. Sham, *Crosstalk Mitigation Techniques in High-Speed Serial Links*, Ph.D thesis, University of Minnesota, Minnesota, USA, Apr. 2009.
- [62] R. Sharma, T. Chakravarty, and A. B. Bhattacharyya, "Analytical model for optimum signal integrity in PCB interconnects using ground tracks," *IEEE Trans. Electromagn. Compat.*, vol. 51, no. 1, pp. 67–77, Feb. 2009.
- [63] T. Stefanński and B. J. Janiczak, "Experimental and numerical investigation of crosstalk effect in coupled coplanar waveguidespart I: Bi-mode coupled-line representation," *IEEE Trans. Electromagn. Compat.*, vol. 48, no. 4, pp. 669–676, Nov. 2006.
- [64] S. A. Bassam, M. Helaoui, and F. M. Ghannouchi, "Crossover digital predistorter for the compensation of crosstalk and nonlinearity in MIMO transmitters," *IEEE Trans. Microw. Theory Tech.*, vol. 57, no. 5, pp. 1119–1128, May 2009.
- [65] M. I. Montrose, *Crosstalk Mitigation Techniques in High-speed Serial links*, IEEE, New York, 1999.
- [66] J. Qi, S. Aïssa, and Amine Maaref, "Cross-layer design for MIMO systems over spatially correlated and keyhole Nakagami- m fading channels," *Wiley Journal Wireless Commun. and Mobile Computing*, vol. 10, no. 8, pp. 1055–1067, Aug. 2010, online publication, July 2009.
- [67] J. Qi and S. Aïssa, "Cross-layer design for multiuser MIMO MRC systems with feedback constraints," *IEEE Trans. Veh. Technol.*, vol. 58, no. 7, pp. 3347–3360, Sept. 2009.

- [68] J. Qi and S. Aïssa, “Cross-layer design of enhanced AMC with truncated ARQ protocols,” in *Proc. IEEE Global Telecommun. Conf. (Globecom’07)*, Washington D.C., USA, Nov. 2007, pp. 3353–3357.
- [69] J. Qi, S. Aïssa, and Xinsheng Zhao, “Optimal frame length for keeping normalized goodput with lowest requirement on BER,” in *IEEE Int. Conf. Innovations in Inf. Technol. (Innovations’07)*, Dubai, Nov. 2007, pp. 715–719.
- [70] J. Qi and S. Aïssa, “Mobile-to-mobile MIMO transmit-receive diversity systems: analysis and performance in 3D double-correlated channels,” *Wiley Journal Wireless Commun. and Mobile Computing*, revised.
- [71] J. Qi and S. Aïssa, “Performance analysis of MIMO MRC systems in 3D mobile-to-mobile double-correlated channel,” in *Proc. IEEE Global Telecommun. Conf. (Globecom’08)*, New Orleans, LA, USA, Nov.–Dec. 2008.
- [72] J. Qi and S. Aïssa, “Analysis and compensation of power amplifier nonlinearity in MIMO transmit diversity systems,” *IEEE Trans. Veh. Technol.*, vol. 59, no. 6, pp. 2921–2931, July 2010.
- [73] J. Qi and S. Aïssa, “On the effect of power amplifier nonlinearity on MIMO transmit diversity systems,” in *Proc. IEEE Int. Conf. Commun. (ICC’09)*, Dresden, Germany, June 2009.
- [74] J. Qi and S. Aïssa, “On the power amplifier nonlinearity in MIMO transmit beamforming systems,” *IEEE Trans. Commun.*, revised.
- [75] J. Qi and S. Aïssa, “Optimal beamforming in MIMO systems with HPA nonlinearity,” in *Proc. IEEE Symp. Personal, Indoor and Mobile Radio Commun. (PIMRC’10)*, Istanbul, Turkey, Sept. 2010, pp. 910–914.
- [76] J. Qi and S. Aïssa, “Impact of HPA nonlinearity on MIMO systems with quantized equal gain transmission,” in *Proc. IEEE Symp. Personal, Indoor and Mobile Radio Commun. (PIMRC’09)*, Tokyo, Japan, Sept. 2009, pp. 2891–2895.

- [77] J. Qi and S. Aïssa, “Analysis and compensation of I/Q imbalance in MIMO transmit-receive diversity systems,” *IEEE Trans. Commun.*, vol. 58, no. 5, pp. 1546–1556, May 2010.
- [78] J. Qi and S. Aïssa, “On the effect of I/Q imbalance on MIMO transmit-receive diversity systems,” in *Proc. IEEE Wireless Commun. and Networking Conf. (WCNC’09)*, Budapest, Hungary, Apr. 2009.
- [79] J. Qi and S. Aïssa, “Beamforming for MIMO transmit-receive diversity systems with crosstalk,” in *Proc. IEEE Int. Conf. Commun. (ICC’10)*, Cape Town, South Africa, May 2010.
- [80] J. Qi and S. Aïssa, “Adaptive switching for spatial transmission modes in MIMO systems with RF impairments,” *IEEE Trans. Wireless Commun.*, to be submitted.
- [81] J. Qi and S. Aïssa, “Analysis and compensation for the joint effects of HPA nonlinearity, I/Q imbalance and crosstalk in MIMO beamforming systems,” in *Proc. IEEE Wireless Commun. and Networking Conf. (WCNC’11)*, Cancun, Quintana-Roo, Mexico, Mar. 2011, pp. 328–333.
- [82] J. Qi and S. Aïssa, “Compensation for HPA nonlinearity and I/Q imbalance in MIMO beamforming system,” in *Proc. IEEE Int. Conf. on Wireless and Mobile Computing, Networking and Commun. (WiMob’10)*, Niagara Falls, Canada, Oct. 2010, pp. 78–82.
- [83] *Physical layer aspects of UTRA High Speed Downlink Packet Access (Release 4)*, 3rd Generation Partnership Project, 3GPP TR 25.848 V. 4.0.0, Mar. 2001.
- [84] *Feasibility Study for Enhanced Uplink for UTRA FDD (Release 6)*, 3rd Generation Partnership Project, 3GPP TR 25.896 V. 6.0.0, Mar. 2004.
- [85] S. Vishwanath and A. J. Goldsmith, “Variable-rate variable power MQAM for fading channels,” *IEEE Trans. Commun.*, vol. 45, no. 10, pp. 1218–1230, Oct. 1997.

- [86] Q. Liu, S. Zhou, and G. B. Giannakis, "Cross-layer combining of adaptive modulation and coding with truncated ARQ over wireless links," *IEEE Trans. Wireless Commun.*, vol. 3, no. 5, pp. 1746–1755, Sep. 2004.
- [87] X. Zhao, J. Qi, H. Liang, and X. Yu, "An analytical method for capacity dimensioning of WCDMA with high speed wireless link," in *Proc. IEEE Wireless Commun. and Networking Conf. (WCNC'07)*, Hong Kong, China, Mar. 2007, pp. 4175–4179.
- [88] S. M. Alamouti, "A simple transmit diversity technique for wireless communications," *IEEE J. Select. Areas Commun.*, vol. 16, no. 8, pp. 1451–1458, Oct. 1998.
- [89] V. Tarokh, H. Jafarkhani, and A. R. Calderbank, "Space-time block coding for wireless communications: Performance results," *IEEE J. Select. Areas Commun.*, vol. 17, no. 3, pp. 451–460, Mar. 1999.
- [90] V. Tarokh, H. Jafarkhani, and A. R. Calderbank, "Space-time block codes from orthogonal designs," *IEEE Trans. Inform. Theory*, vol. 45, no. 5, pp. 1456–1467, July 1999.
- [91] A. Maaref and S. Aïssa, "Performance analysis of orthogonal space-time block codes in spatially correlated MIMO Nakagami fading channels," *IEEE Trans. Wireless Commun.*, vol. 5, no. 4, pp. 807–817, Apr. 2006.
- [92] H. Shin and J. H. Lee, "Performance analysis of space-time block codes over keyhole Nakagami- m fading channels," *IEEE Trans. Veh. Technol.*, vol. 53, no. 2, pp. 351–362, Mar. 2004.
- [93] I. S. Gradshteyn and I. M. Ryzhik, *Tables of Integrals, Series, and Products*, Academic, San Diego, CA, 5th edition, 1994.
- [94] E. Malkamaki and H. Leib, "Performance of truncated type-II hybrid ARQ schemes with noisy feedback over block fading channels," *IEEE Trans. Commun.*, vol. 48, no. 9, pp. 1477–1487, Sept. 2000.

- [95] K. Cho and D. Yoon, "On the general BER expression of one-and two-dimensional amplitude modulations," *IEEE Trans. Commun.*, vol. 50, no. 6, pp. 11074–1080, July 2002.
- [96] M.-S. Alouini and A. J. Goldsmith, "Adaptive modulation over Nakagami fading channels," *Kluwer Journal on Wireless Commun.*, vol. 13, no. 1-2, pp. 119–143, July 2002.
- [97] V. A. Aalo, "Performance of maximal-ratio diversity systems in a correlated Nakagami-fading environment," *IEEE Trans. Commun.*, vol. 43, no. 8, pp. 2360–2369, Aug. 1995.
- [98] P. A. Dighe, R. K. Mallik, and S. S. Jamuar, "Analysis of transmit-receive diversity in Rayleigh fading," *IEEE Trans. Commun.*, vol. 51, no. 4, pp. 694–703, Apr. 2003.
- [99] A. Maaref and S. Aïssa, "Eigenvalue distributions of Wishart-type random matrices with application to the performance analysis of MIMO MRC systems," *IEEE Trans. Wireless Commun.*, vol. 6, no. 7, pp. 2678–2689, July 2007.
- [100] M. R. McKay, A. J. Grant, and I. B. Collings, "Performance analysis of MIMO-MRC in double-correlated Rayleigh environments," *IEEE Trans. Commun.*, vol. 55, no. 3, pp. 497–507, Mar. 2007.
- [101] S. Jin, M. R. McKay, X. Gao, and I. B. Collings, "Asymptotic SER and outage probability of MIMO MRC in correlated fading," *IEEE Signal Process. Lett.*, vol. 14, no. 1, pp. 9–12, Jan. 2007.
- [102] F. Graziosi and F. Santucci, "A general correlation model for shadow fading in mobile radio systems," *IEEE Commun. Lett.*, vol. 6, no. 3, pp. 102–104, Mar. 2002.
- [103] H. Claussen, "Efficient modelling of channel maps with correlated shadow fading in mobile radio systems," in *Proc. IEEE Symp. Personal, Indoor and*

- Mobile Radio Commun. (PIMRC'05)*, Berlin, Germany, Sept. 2005, vol. 1, pp. 512–516.
- [104] A. Abdi, J. A. Barger, and M. Kaveh, “A parametric model for the distribution of the angle of arrival and the associated correlation function and power spectrum at the mobile station,” *IEEE Trans. Veh. Technol.*, vol. 51, no. 3, pp. 425–434, May 2002.
- [105] J. G. Proakis, *Digital Communications*, McGraw-Hill, New York, 4th edition, 2001.
- [106] M.-S. Alouini and A. J. Goldsmith, “Capacity of Rayleigh fading channels under different adaptive transmission and diversity-combining techniques,” *IEEE Trans. Veh. Technol.*, vol. 48, no. 4, pp. 1165–1181, July 1999.
- [107] M. Shabany and P. G. Gulak, “Efficient compensation of the nonlinearity of solid-state power amplifiers using adaptive sequential Monte Carlo methods,” *IEEE Trans. Circuits and Systems*, vol. 55, no. 10, pp. 2007–2019, Sept. 2008.
- [108] P. M. Djurić, J. H. Kotecha, J. Zhang, Y. Huang, T. Ghirmai, M. F. Bugallo, and J. Míguez, “Particle filtering,” *IEEE Signal Process. Mag.*, vol. 20, no. 5, pp. 19–38, Sep. 2003.
- [109] J. H. Kotecha and P. M. Djurić, “Gaussian particle filtering,” *IEEE Trans. Signal Process.*, vol. 51, no. 10, pp. 2592–2601, Oct. 2003.
- [110] F. Septier, Y. Delignon, A. Menhaj-Rivenq, and C. Garnier, “Monte Carlo methods for channel, phase noise, and frequency offset estimation with unknown noise variances in OFDM systems,” *IEEE Trans. Signal Process.*, vol. 56, no. 8, pp. 3613–3626, Aug. 2008.
- [111] Z. Yang and X. Wang, “A sequential Monte Carlo blind receiver for OFDM systems in frequency-selective fading channels,” *IEEE Trans. Signal Process.*, vol. 50, no. 2, pp. 271–280, Feb. 2002.

- [112] R. A. Iltis, "A sequential Monte Carlo filter for joint linear/nonlinear state estimation with application to DS-CDMA," *IEEE Trans. Signal Process.*, vol. 51, no. 2, pp. 417–426, Feb. 2003.
- [113] J. W. Craig, "A new, simple and exact result for calculating the probability of error for two-dimensional signal constellations," in *Proc. IEEE Conf. Military Commun. (MILCOM'91)*, McLean, VA, USA, Nov. 1991, vol. 2, pp. 571–575.
- [114] M.-S. Alouini and M. K. Simon, "An MGF-based performance analysis of generalized selection combining over Rayleigh fading channels," *IEEE Trans. Commun.*, vol. 48, no. 3, pp. 401–415, Mar. 2000.
- [115] A. Conti, D. Dardari, and V. Tralli, "An analytical framework for CDMA systems with a nonlinear amplifier and AWGN," *IEEE Trans. Commun.*, vol. 50, no. 7, pp. 1110–1120, July 2002.
- [116] G. Caire and S. Shamai, "On the capacity of some channels with channel state information," *IEEE Trans. Inf. Theory*, vol. 45, no. 6, pp. 2007–2019, Sept. 1999.
- [117] J. J. Bussgang, "Cross correlation function of amplitude-distorted Gaussian input signals," *Res. Lab Electron., M.I.T., Cambridge, MA, Tech. Rep. 216*, vol. 3, Mar. 1952.
- [118] S. M. Kay, *Fundamentals of Statistical Signal Processing: Estimation Theory*, vol. 1, Prentice Hall, New Jersey, NJ, 1th edition, 1993.
- [119] D. Gu and C. Leung, "Performance analysis of transmit diversity scheme with imperfect channel estimation," *IEE Elect. Lett.*, vol. 39, pp. 402–403, Feb. 2003.
- [120] A. Maaref and S. Aïssa, "Spectral efficiency limitations of maximum ratio transmission in the presence of channel estimation errors," in *Proc. IEEE Veh. Technol. Conf. (VTC'05-Fall)*, Dallas, Texas, USA, Sept. 2005, vol. 1, pp. 502–506.

- [121] A. Maaref and S. Aïssa, “Closed-form expressions for the outage and ergodic Shannon capacity of MIMO MRC systems,” *IEEE Trans. Commun.*, vol. 53, no. 7, pp. 1092–1095, July 2005.
- [122] M. Medard, “The effect upon channel capacity in wireless communications of perfect and imperfect knowledge of the channel,” *IEEE Trans. Inf. Theory*, vol. 46, no. 3, pp. 933–946, May 2000.
- [123] L. Musavian and S. Aïssa, “On the achievable sum-rate of correlated mimo multiple access channel with imperfect channel estimation,” *IEEE Trans. Wireless Commun.*, vol. 7, no. 7, pp. 2549–2559, July 2008.
- [124] T. Yoo and A. Goldsmith, “Capacity and power allocation for fading MIMO channels with channel estimation errors,” *IEEE Trans. Inf. Theory*, vol. 52, no. 5, pp. 2203–2214, May 2006.
- [125] D. J. Love, R. W. Heath, Jr., and T. Strohmer, “Grassmannian beamforming for multiple-input multiple-output wireless systems,” *IEEE Trans. Inf. Theory*, vol. 49, no. 10, pp. 2735–2747, Oct. 2003.
- [126] D. J. Love and R. W. Heath, Jr., “Equal gain transmission in multiple-input multiple-output wireless systems,” *IEEE Trans. Commun.*, vol. 51, no. 7, pp. 1102–1110, July 2003.
- [127] K. K. Mukkavilli, A. Sabharwal, E. Erkip, and B. Aazhang, “On beamforming with finite rate feedback in multiple-antenna systems,” *IEEE Trans. Inf. Theory*, vol. 49, no. 10, pp. 2562–2579, Oct. 2003.
- [128] S. Zhou, Z. Wang, and G. B. Giannakis, “Quantifying the power-loss when transmit-beamforming relies on finite rate feedback,” *IEEE Trans. Wireless Commun.*, vol. 4, no. 10, pp. 1948–1957, July 2005.
- [129] S. W. Kim and Z. Wang, “Maximum ratio diversity combining receiver using single radio frequency chain and single matched filter,” in *Proc. IEEE*

- Global Telecommun. Conf. (Globecom'07)*, Washington D.C., USA, Nov. 2007, pp. 4081–4085.
- [130] T. C. W. Schenk, P. F. M. Smulders, and E. R. Fledderus, “Estimation and compensation of frequency selective TX/RX IQ imbalance in MIMO OFDM systems,” in *Proc. IEEE Int. Conf. Commun. (ICC'06)*, Istanbul, Turkey, June 2006, vol. 1, pp. 251–256.
- [131] Y. Chen and C. Tellambura, “Distribution function of selection combiner output in equally correlated Rayleigh, Rician, and Nakagami- m fading channels,” *IEEE Trans. Commun.*, vol. 52, no. 11, pp. 1948–1956, Nov. 2004.
- [132] B. Hassibi and B. M. Hochwald, “How much training is needed in multiple-antenna wireless links?,” *IEEE Trans. Inf. Theory*, vol. 49, no. 4, pp. 951–963, Apr. 2003.
- [133] G. Kim, D. G. Kam, S. J. Lee, J. Kim, M. Ha, K. Koo, J. S. Pak, and J. Kim, “Modeling of eye-diagram distortion and data-dependent jitter in meander delay lines on high-speed printed circuit boards (PCBs) based on a time-domain even-mode and odd-mode analysis,” *IEEE Trans. Microw. Theory Tech.*, vol. 56, no. 8, pp. 1962–1972, Aug. 2008.
- [134] C. Wang, E. K. S. Au, R. D. Murch, W. H. Mow, R. S. Cheng, and V. Lau, “On the performance of the MIMO zero-forcing receiver in the presence of channel estimation error,” *IEEE Trans. Wireless Commun.*, vol. 6, no. 3, pp. 805–810, Mar. 2007.

Appendix B

Résumé

B.1 Introduction

B.1.1 Contexte et Motivation

Systemes de Communication Sans Fil MIMO

La croissance sans précédent, au cours des dernières décennies, de la demande de communications haut débit fiables afin de soutenir des applications multiples, par exemple, la voix, la vidéo, le *Voice over Internet Protocol* (VoIP), et la navigation sur le Web, met en évidence la nécessité de nouvelles techniques de transmission prometteuses. Dans les années 1990, les techniques *multiple-input multiple-output* (MIMO) ont été inventées et représentent un moyen efficace pour améliorer la capacité du canal et la fiabilité de la transmission, à savoir, un gain de multiplexage et un gain de diversité. Les techniques MIMO peuvent être classées en plusieurs types, à savoir, le *space-time block code* (STBC), le *space-time trellis code* (STTC), les codes espace-temps en couche et le MIMO *maximal ratio combining* (MRC) avec *transmit beamforming* (TB). Les systèmes STBC peuvent atteindre une diversité de trans-

mission et de réception en utilisant un processus de transmission-réception simple, mais efficace. Le STTC peut atteindre un gain de codage par rapport à STBC mais avec un coût de complexité de décodage accru, où la structure en treillis détermine les symboles codés à transmettre à partir des différents éléments d'antenne. Comme pour le code espace-temps en couches, ils se concentrent sur le gain de multiplexage spatial. D'autre part, si la *channel state information* (CSI) est parfaitement connue à l'émetteur, le TB et la technique de *water filling* associés à la MRC peuvent être utilisés pour obtenir un gain de diversité et une capacité plus grande. En raison de ces grands avantages, les techniques MIMO ont été incluses dans plusieurs normes pour les systèmes de communication sans fil futurs, tels que le *3rd Group Partnership Project* (3GPP) *Long Term Evolution* (LTE) et LTE-Avancée [2].

Cependant, tous les schémas MIMO mentionnés ci-dessus sont des techniques de communication en bande de base et sont liés à la condition de canal et à la *radio frequency* (RF) pour les opérations. En pratique, la performance du système est affectée par des déficiences des canaux et du RF, tels que canaux à évanouissements spatialement corrélés et à *keyhole*, les canaux *mobile-to-mobile* (M-to-M), la nonlinéarité *high-power amplifier* (HPA), le déséquilibre *in-phase and quadrature-phase* (I/Q), la diaphonie, la nonlinéarité *low-noise amplifier* (LNA), le couplage d'antenne, le bruit de phase, le décalage en fréquence, la synchronisation temporelle imparfaite et l'écho. Dans cette thèse, nous nous concentrons sur les canaux à évanouissements spatialement corrélés et à *keyhole*, les canaux M-to-M, la nonlinéarité HPA, le déséquilibre I/Q et la diaphonie.

Canaux à Évanouissements Spatialement Corrélés et à *Keyhole*

Dans la pratique, les canaux à évanouissement sur lesquels les régimes du MIMO fonctionnent ne peuvent pas être *indépendent and identiquement distribués* (i.i.d.) en

raison de la corrélation spatiale ou des phénomènes du trou de serrure (*keyhole*) [8]. La corrélation spatiale peut surgir lorsque les éléments de la transmission/réception des réseaux d'antennes ne sont pas suffisamment espacés et/ou en raison des mauvaises conditions de dispersion [9]. D'autre part, en présence du phénomène du trou de serrure dans l'environnement de la propagation MIMO, l'onde radio émise par l'émetteur au récepteur doit se propager travers le trou de la serrure dans l'espace [22]. Les propriétés des corrélations spatiales et les trous ont été étudiées dans [23], où des modèles canoniques physiques de trous de serrure ont été présentés.

Communications Mobile-à-Mobile

Dans les systèmes de communication sans fil, les émetteurs et les récepteurs peuvent à la fois être en mouvement: le canal est alors dénommé par le canal de communication M-to-M. En outre, dans des environnements riches en diffusion, par exemple, les zones urbaines à forte densité de bâtiments, les ondes peuvent ne pas se diffuser seulement dans le plan horizontal uniquement. Dans ce cas, la modélisation géométrique 3D représente un outil adéquat pour décrire l'environnement de propagation sans fil. Pour les systèmes de communication M-to-M équipés d'antennes de faible altitude et émetteurs-récepteurs multi-antennes mobiles, les canaux de diffusion 3D peuvent être caractérisés par le modèle à deux cylindres, avec un cylindre autour de l'émetteur et l'autre autour du récepteur [29].

Nonlinéarité HPA

HPA est un bloc primaire des systèmes de communication sans fil, qui opère au niveau du RF. En pratique, les distorsions non linéaires, y compris les distorsions d'amplitude et de phase, sont introduites dans les symboles transmis, qui à leur tour peuvent provoquer des distorsions des canaux adjacents et des pertes de puissance.

À cet égard, plusieurs régimes de compensation pour la non-linéarité HPA ont été proposés, et peuvent être classés en deux catégories: la compensation au niveau de l'émetteur ou du récepteur. Les méthodes mises en œuvre à l'émetteur incluent la puissance marche-arrière, les techniques de réduction *peak-to-average power ratio* (PAPR) et les techniques de linéarisation [34, 42]. Par exemple, la méthode prédictive, la méthode de rétroaction et la prédistorsion, représentent des techniques de linéarisation. D'autre part, le scénario de transmission de liaison montante exige une compensation de la nonlinéarité HPA au récepteur, par exemple, la postdistorsion, la péréquation non linéaire et la détection itérative [34].

Déséquilibre I/Q

Le déséquilibre I/Q fait référence à la discordance entre les composants *in-phase* (I) et *quadrature-phase* (Q), c'est-à-dire, le décalage entre les parties réelle et imaginaire du signal complexe [44]. Cela se produit en raison de la précision limitée du matériel analogique, telles que les tolérances limitées des condensateurs et des résistances. Récemment, plusieurs régimes d'indemnisation pour les déséquilibre I/Q ont été proposés et peuvent être divisés en deux types: les méthodes de compensation et les méthodes sans estimation des paramètres du déséquilibre I/Q, respectivement. Par exemple, la compensation de l'interférence fondée sur l'annulation et la compensation basée sur la séparation aveugle de source, qui ne nécessite pas de signaux de formation, représente des méthodes dédommagement sans estimation des paramètres du déséquilibre I/Q [49, 52, 53]. D'autre part, le signal émis peut être détecté après que le gain de canal et les paramètres de déséquilibre I/Q sont estimés en utilisant des signaux de formation. Par exemple, une méthode de compensation basée sur des propriétés algébriques des modèles de signaux dérivés combinée avec des données de pilotage appropriée a été proposée pour les systèmes MIMO STBC dans [49].

Diaphonie

Dans *printed circuit board* (PCB), un des aspects les importants est la diaphonie, qui se réfère aux couplages électromagnétiques imprévus entre les traces, les fils, les terres de PCB, ainsi que tout autres objets des composants électriques sujets aux perturbations des champs électroniques et qui sont à proximité les uns aux autres [57]. Pour éviter la diaphonie dans le PCB, des techniques de design et de *layout* ont été proposées, telles que la maximisation des distance de séparation entre les composants, ce qui porte les traces à un plan de référence [65]. Cependant, les effets de la diaphonie ne peuvent pas être complètement éliminés dans la cadre de PCB et des méthodes de compensation de bande de base sont nécessaires pour éliminer ou atténuer les effets de diaphonie résiduelle.

Dans le cas de dégradations de canal et RF, des avantages des systèmes MIMO, tels que le gain de diversité et le gain de multiplexage , ne sont pas visible ou ne peuvent plus être atteints. Par conséquent, il est essentiel d'étudier l'impact du canal et des déficiences RF sur les systèmes de communication MIMO et les méthodes de recherche d'indemnisation efficace pour éliminer ou atténuer ces déficiences.

B.1.2 Objectifs de la Recherche

Le thème de recherche de cette thèse vise à étudier les déficiences du canal et du RF dans les systèmes de communication sans fil MIMO. Tout d'abord, nous comprenons les concepts mentionnés ci-dessus à savoir déficiences du canal et du RF et évaluons leurs effets sur la performance des systèmes MIMO par l'analyse théorique et assistée par simulation ordinateur. Plus précisément, les modèles de système MIMO modifiés prenant en compte le canal et les déficiences du RF seront fournis, ainsi que les expressions correspondantes pour les mesures de performance dans une expression

analytiques ou une forme approximative. Sur cette base, nous allons donner un critère pour la conception des systèmes MIMO, tels que les méthodes de compensation pour les déficiences et les paramètres de réglage pour la conception émetteur-récepteur. La recherche fera que le gain de diversité et le gain de multiplexage faciles sont à atteindre dans les implémentations d'un système pratique.

B.1.3 Contribution de la Dissertation

La contribution de cette thèse peut se résumer en quelques égards comme suit:

i) Un design de régime inter-couches qui combine l'*adaptive modulation and coding* (AMC) de la couche physique avec la *truncated automatic repeat request* (T-ARQ) de la couche de liaison est proposé pour les systèmes MIMO employant l'OSTBC. La performance de la proposition de la conception d'inter-couches est évaluée en termes de *average spectral efficiency* (ASE), de *average packet loss rate* (PLR) et de probabilité de panne, pour lesquels des expressions analytiques sont dérivées, considérant la transmission sur deux types de canaux à évanouissement du MIMO, à savoir, les canaux à évanouissement spatialement corrélés Nakagami- m et les canaux à *keyhole* Nakagami- m .

ii) Nous considérons le système M-to-M MIMO MRC et évaluons ses performances dans les canaux spatialement corrélés. L'analyse suppose les canaux à évanouissement doublement-corrélés Rayleigh-et-Lognormal et est effectuée en termes du SEP moyen, de la probabilité de coupure et de la capacité ergodique. Pour obtenir les fonctions de corrélation spatiale pour la réception et la transmission nécessaires à l'analyse des performances, un modèle MIMO 3D M-to-M de canal, qui prend en compte des effets de l'évanouissement rapide et l'ombre, est utilisé. Les expressions pour les paramètres considérés sont dérivés en fonction du *average signal-to-noise*

ratio (SNR) par antenne de réception en forme analytique, et une harmonisation plus poussée à l'aide de la méthode adaptative récursive quadrature Simpson.

iii) Les systèmes MIMO-OSTBC en présence de nonlinéarité HPA sont étudiés dans cette thèse. Plus précisément, nous proposons une méthode de compensation basée sur la constellation de la nonlinéarité pour les HPA dans le cas avec connaissance des paramètres de la HPA à l'émetteur et au récepteur, où les régions constellation et la décision du signal déformé transmis sont connues à l'avance. En outre, dans le scénario sans connaissance des paramètres de la HPA, une méthode de *sequential Monte Carlo* (SMC) de compensation basée sur la nonlinéarité HPA est proposée, qui estime, premièrement, la matrice du gain du canal au moyen de la méthode SMC, et qui utilise, ensuite, l'algorithme basé SMC pour détecter le signal désiré.

iv) Les systèmes MIMO TB en présence de nonlinéarité HPA sont étudiés dans cette thèse. Plus précisément, nous proposons le régime optimal TB avec le vecteur poids beamforming et le vecteur combinant optimaux, pour les systèmes MIMO avec la nonlinéarité HPA. En outre, une d'autre alternative sous-optimale mais beaucoup plus simple, à savoir, le *quantized equal gain transmission* (QEGT), est proposée. Ces bénéfices proviennent de la propriété que les éléments de la formation de faisceaux vecteur de poids ont un même module constant. La performance du régime TB-optimal proposé et la technique QEGT/MRC en présence de la nonlinéarité HPA est évaluée en termes de SEP moyenne et d'information mutuelle avec entrée gaussienne, en tenant compte d'une transmission sur un canal de Rayleigh, décooeeélé, quasi-statique et à fréquences plates.

v) On étudie les effets du déséquilibre I/Q sur les performances des systèmes MIMO MRC qui exécutent la combinaison au niveau RF. Nous proposons un algorithme d'estimation de canal qui compte pour le déséquilibre I/Q. En outre, un algorithme de compensation pour les déséquilibres I/Q dans les systèmes MIMO MRC est

proposé: il emploie la technique LS pour estimer les coefficients de la matrice de gain du canal, du beamforming et la combinaison des vecteurs de poids, et les paramètres de déséquilibre I/Q conjointement, puis utilise le signal reçu avec son conjugué pour détecter le signal transmis. Les performances du système MIMO MRC à l'étude sont évalués en termes de SEP moyenne, probabilité de coupure et de la capacité ergodique, qui sont dérivées en considant la transmission sur les canaux Rayleigh.

vi) Les performances des systèmes MIMO MRC, en présence de diaphonie sont réévaluées dans cette thèse. L'effet de la diaphonie sur les performances du MIMO MRC est étudiée en termes de la SEP et de la capacité du système, considérant la transmission sur des canaux Rayleigh corrélés d'une moyenne.

vii) Nous étudions les effets conjoints de non-linéarité HPA, déséquilibre I/Q et de la diaphonie, sur les performances des systèmes MIMO TB, et proposons une méthode de compensation pour les trois modes ensemble. Les performances des systèmes MIMO TB équipés du régime d'indemnisation proposé sont évalués en termes de SEP moyenne et la capacité lorsque les transmissions sont effectuées sur un canal de Rayleigh corrélé.

B.2 Canaux à Évanouissements Spatialement Corrélés et à *Keyhole*

Dans cette section, nous proposons un design d'inter-couches combinant la couche physique d'AMC et la couche de liaison de systèmes T-ARQ pour les systèmes MIMO dans des canaux spatialement corrélés et *keyhole* Nakagami- m . Le schéma correspondant est représenté sur la Fig. B.1. AMC au niveau de la couche physique est utilisée pour améliorer l'efficacité spectrale des systèmes sans fil, en sélectionnant la *mod-*

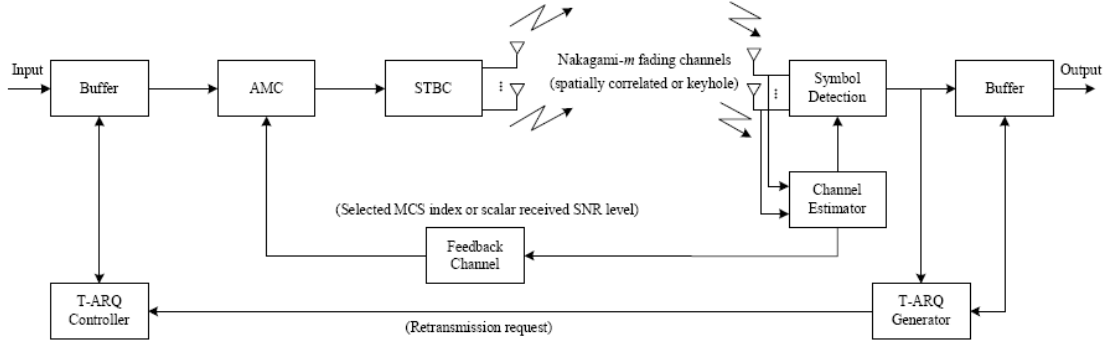


Figure B.1: Schéma pour la conception inter-couches basée sur les MIMO-OSTBC systèmes.

ulation and coding scheme (MCS), conformes aux variations du SNR reçu, tout en satisfaisant le système en exigence sur la PLR [83]. Les canaux MIMO sont convertis en un scalaire équivalent *signal-input single-output* (SISO) pour que les MCSs puissent être choisies en fonction du SNR effectif sur le canal équivalent. Le *automatic repeat request* (ARQ) dans le lien de couche peut aussi être utilisé pour augmenter la fiabilité de la transmission en renvoyant un paquet de données à chaque échec d'une précédente tentative de transmission. Les effets du canal déficient, la corrélation spatiale décoloration et à *Keyhole*, sont évalués sur la base de notre mécanisme inter-couches.

La corrélation spatiale survient lorsque les éléments de la transmission/réception sur les réseaux d'antennes ne sont pas suffisamment espacé et/ou en raison de mauvaises conditions de dispersion. D'autre part, dans certains environnements de propagation MIMO, les ondes radio envoyées par l'émetteur au récepteur doivent se propager à travers le trou de la serrure dans l'espace. La matrice du gain de canal à *Keyhole* MIMO Nakagami- m peut être exprimé comme [92]

$$\mathbf{H}_{\text{Kh}} = \mathbf{h}_R \mathbf{h}_T^H, \quad (\text{B.1})$$

où \mathbf{h}_T et \mathbf{h}_R désignent des vecteurs $n_T \times 1$ et $n_R \times 1$ modélisant les coefficients d'évanouissement au niveau émetteur et récepteur, respectivement. Notez que toutes les entrées du canal matriciel du gain \mathbf{H}_{Kh} ne sont pas corrélées, mais $\text{rank}(\mathbf{H}_{Kh}) = 1$.

La performance est évaluée en termes de l'ASE, la moyenne du PLR et la probabilité de panne. Les résultats numériques sont présentés pour illustrer les effets de divers paramètres sur les performances du système. En particulier, l'ASE devient de plus en plus discrète et le comportement oscillatoire des courbes de la moyenne PLR augmente à mesure que la corrélation spatiale devient plus petite. En outre, la propriété discrète de l'ASE et le comportement oscillatoire des courbes de la moyenne PLR devient visible moins en canaux à évanouissement à *keyhole* Nakagami- m par rapport au cas i.i.d Nakagami- m .

B.3 Communications Mobile-à-Mobile

Les canaux 3D M-to-M peuvent être considérés comme un type général de la double-corrélation des canaux à évanouissement, où l'émission et la réception de la corrélations sont dues à la diffusion et l'ombrage. Les travaux actuels sur modélisation M-to-M de canal examinent les facteurs des effets des évanouissements rapides causés par les trajets multiples, tels que le décalage de phase aléatoire, le retard de propagation et l'effet Doppler, dans la modélisation de la variables dans le temps de réponse impulsionnelle du canal. Dans cette section, l'effet de la corrélation spatiale sur la performance des systèmes MRC M-to-M MIMO est évaluée pour les transmissions sur des canaux à évanouissement Rayleigh-et-Lognormal doublement-corrélés considérant l'évanouissement et l'ombrage rapide. Nous considérons un environnement de diffusion 3D à propagation NLoS, qui peut être caractérisé par le modèle à deux cylindres

adaptative de quadrature de Simpson.

En outre, les résultats numériques sont fournis et l'effet de paramètres du système, tels que la distance entre les éléments d'antenne, l'angle d'élévation maximum de diffuseurs, l'angle d'orientation de réseau d'antennes dans le plan x-y, l'angle entre le plan x-y et l'orientation réseau d'antennes, et le degré de dispersion dans les x-y plans, les performances du système, sont étudiés et discutés. Notamment, la performance de SEP moyenne en fonction des angles relatifs entre le réseau d'antennes et les diffuseurs locaux autour de l'émetteur et le récepteur, c'est à dire, $|\theta_T - \mu_T|$ et $|\theta_R - \mu_R|$, montre une réduction de façon spectaculaire avec des valeurs croissantes de $|\theta_T - \mu_T|$ lorsque l'angle entre le plan x-y et le transmette orientation antenne réseau diminue. En outre, le SEP moyen augmente avec la déviation standard de l'ombrage. Il est également montré que plus le degré de dispersion autour de l'émetteur dans le plan x-y est élevé, plus la probabilité de coupure augmente, ceci est due à la diffusion non-isotrope, et que l'effet de la perte de trajet sur la performance est plus visible que celui de corrélation spatiale.

B.4 Analyse et Rémunération de la Nonlinéarité

HPA

B.4.1 Analyse et Rémunération de la Nonlinéarité HPA dans le Systèmes MIMO OSTBC

Dans cette section, nous nous concentrons sur la non-linéarité dans les systèmes HPA OSTBC. Le schéma pour le système considéré MIMO-OSTBC est représenté sur la Fig. B.3. Pour le cas où les paramètres de la HPA sont parfaitement connus à l'émetteur et au récepteur, nous proposons un régime d'indemnisation qui détermine

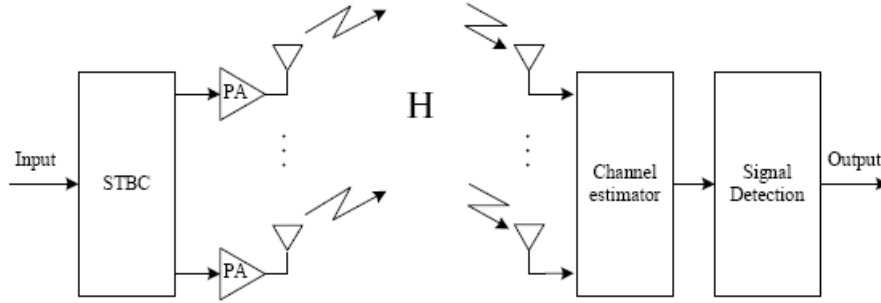


Figure B.3: Schéma pour le système considéré MIMO-OSTBC dans le présence de non linéaires HPA.

la constellation et les régions de décision du signal affecté transmis à l'avance. De cette façon, la complexité de l'émetteur peut être efficacement réduite en utilisant le système de compensation proposé, par rapport à d'autres méthodes de compensation mises en œuvre à l'émetteur seulement, ce qui est crucial pour la mise en œuvre du système, en particulier dans les scénarios à liaison montante pour la transmission. Pour la chaîne de transmission décrite, nous dérivons les expressions pour le SEP moyen et TD, et obtenons les bornes supérieures et inférieures sur la capacité du système, qui sont évalués pour les modèles non linéaires HPA sans mémoire, en considérant un canal Nakagami- m décorrélé.

D'autre part, les paramètres de l'HPA non linéaire peuvent être parfois inconnus ou variables dans le temps. Ces variations sont dues à des processus de transfert comme c'est le cas dans les réseaux cellulaires, de la limitations de fabrication ou des effets environnementaux comme la température et le vieillissement [107]. Dans ce scénario, la méthode est employée le SMC, pour compenser la non-linéarité de l'HPAs dans un seul systèmes d'antenne dans un canal AWGN [107]. Le SMC (ou filtrage particulière) est une technique de calcul commune récursive de distributions de la probabilité utilisant le concept de l'importance l'échantillonnage et l'approximation des distributions de la probabilité avec mesures discrètes aléatoires (voir [108] et

même module constant, nous avons également cherché une alternative sous-optimale mais plus simple pour le régime TB, à savoir, QEGT, qui est un mécanisme efficace dans le cas nonlinéaire avec l'HPA. Pour le régime de la TB optimale proposée, nous dérivons les bornes inférieure et supérieure pour le SEP moyen et l'information mutuelle avec entrée Gaussienne, considérant que le système fonctionne dans un canal Rayleigh corrélés, quasi-statique et à fréquence plates. En outre, une limite inférieure du SEP moyen et une borne supérieure à l'information mutuelle avec l'entrée gaussienne sont prévus pour le régime QEGT/MRC.

Les résultats numériques sont fournis et montrent les effets des paramètres système, tels que les paramètres de l'HPA, le nombre d'antennes, l'ordre QAM, le nombre de symboles pilotes, et la cardinalité des mots de codes pour le vecteur poids de beamforming pour QEGT, sur la performance du système. En particulier, le SEP moyen du beamforming optimal en utilisant le projet de l'estimation du canal est réduite mais au prix de nombre de pilotes symboles, en raison du fait que l'MSE de l'estimation du canal est plus faible dans le cas de plus de symboles pilotes. Pour les configurations arbitraires MIMO, une plus importante information mutuelle est atteint en utilisant, plus de symboles pilotes pour effectuer l'estimation de canal.

B.5 Analyse et Rémunération des Déséquilibre I/Q

Dans cette section, nous nous concentrons sur la technique MRC MIMO meltaut en œuvre le MRT, qui requiert une connaissance complète du gain de canal de chaque antenne d'émission-réception lié à l'émetteur [98]. Ici, nous considérons un tel système où la MRC est effectuée au niveau RF, et présentns les modèles du système en considérant le déséquilibre I/Q. Le schéma pour le système considéré MIMO MRC est représenté sur la Fig. B.5.

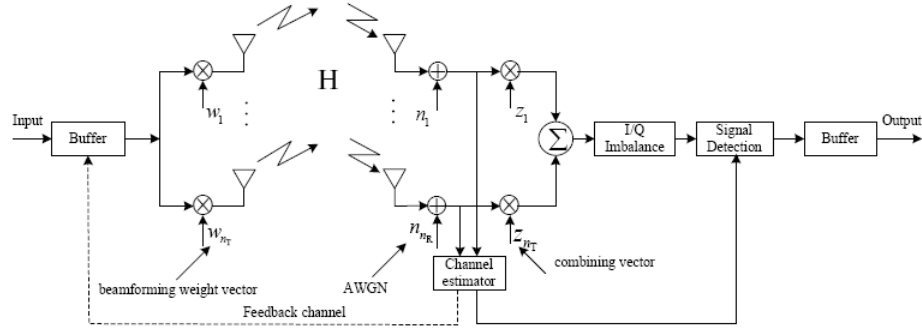


Figure B.5: Schéma pour le système considéré MIMO MRC dans le présence d'I/Q déséquilibré.

La MRC était supposée effectuée au niveau RF, le signal combiné en tenant compte de déséquilibre I/Q peut s'exprimer comme

$$\hat{y} = K_1 (\mathbf{z}^H \mathbf{H} \mathbf{w} x + \mathbf{z}^H \mathbf{n}) + K_2 (\mathbf{z}^H \mathbf{H} \mathbf{w} x + \mathbf{z}^H \mathbf{n})^*, \quad (\text{B.2})$$

où $K_2 \tilde{y}^*$ est l'image du signal $K_1 \tilde{y}$, x est le symbole transmis, \mathbf{w} est le vecteur $n_T \times 1$ unité de poids de formation de faisceaux, \mathbf{n} se rapporte au vecteur de bruit $n_R \times 1$, et $\mathbf{H} = [h_{i,j}]_{i,j=1}^{n_R, n_T}$ exprime la matrice $n_R \times n_T$ de gain de canal, avec n_T and n_R représentant le nombre d'antennes de transmission et de réception, respectivement. Les coefficients K_1 et K_2 sont de la forme $K_1 = (1 + g e^{-j\theta})/2$ et $K_2 = (1 - g e^{j\theta})/2$, où g et θ représentent le déséquilibre de gain et de déséquilibre de phase, respectivement.

Nous proposons un algorithme d'estimation de canal en tenant compte des déséquilibres I/Q, où la longueur des symboles pilotes utilisés pour atteindre les mêmes performances d'estimation de canal comme dans le cas de branches I/Q idéales est de deux fois supérieur à ce dernier. En présence d'estimation de canal imparfaite, les expressions des PDF et CDF du SNR de sortie sont obtenus sous la forme analytique à l'examen de la transmission sur des canaux de Rayleigh non corrélé. Par la suite,

nous obtenons une borne supérieure du SEP moyen, l'expression de la probabilité de coupure en forme analytique, et fournissons une borne inférieure sur la capacité ergodique. En outre, un schéma d'indemnisation pour les déséquilibres I/Q est proposé, qui emploie, tout d'abord, la règle LS pour estimer les coefficients de la matrice de gain de canal, la formation de faisceau et la combinaison des vecteurs de poids, et les paramètres de déséquilibre I/Q conjoints, ensuite, utilise les signaux reçus avec leurs conjugués pour détecter le signal transmis. Les expressions approximatives pour le SEP moyen, la probabilité de panne et la capacité ergodique du système MIMO MRC sur les canaux de Rayleigh corrélés en utilisant le système de compensation proposé sont dérivées.

En outre, les résultats numériques et les comparaisons sont fournis et montrent les effets des paramètres du système, tels que l'image de rapport fuite, le nombre d'antennes de transmission et réception, la modulation d'ordre de QAM, et la longueur des symboles pilotes, sur les performances du système MIMO MRC en présence de déséquilibre I/Q. En particulier, le SEP moyen obtenu par l'utilisation de la compensation peut approcher la ligne de base, c'est-à-dire, l'une dans le scénario sans déséquilibre I/Q, pour les formats arbitraires de la modulation, ce qui implique que déséquilibre I/Q peut être efficacement compensé en utilisant la méthode proposée. En utilisant de la proposition de compensation du déséquilibre I/Q et en engageant assez de symboles pilotes, le SEP moyen peut être réduit à l'approche de la performance avec des branches I/Q idéales.

B.6 Analyse des Effets de la Diaphonie

Dans cette section, nous nous concentrons sur la technique MIMO MRC mettant en œuvre le MRT. Plus précisément, nous étudions les performances de beamforming

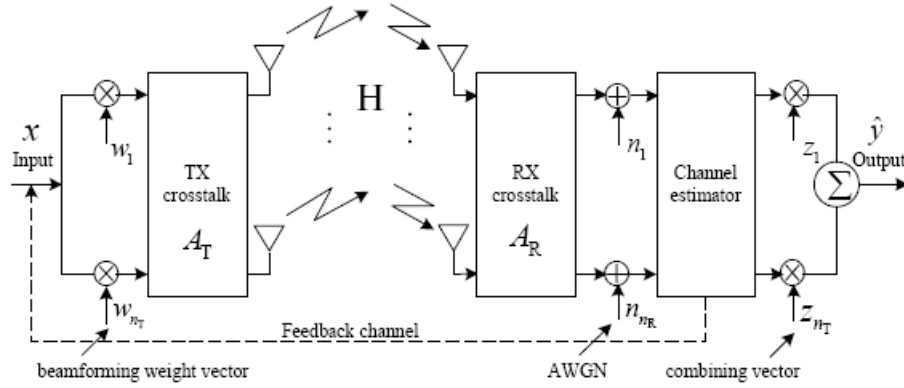


Figure B.6: Schéma du système MIMO MRC avec diaphonie.

pour MIMO des systèmes à diversité d'émission-réception en présence de diaphonie. Le schéma pour le système MIMO MRC peut être illustré comme le montre la Fig B.6. Ici, nous considérons la diaphonie symétrique, et supposons que les diaphonies prennent les effets entre les chemins de signaux adjacents seulement [64]. Plus précisément, les éléments de matrices de diaphonie à l'émetteur \mathbf{A}_T sont donnés par

$$\mathbf{A}_T(i, j) = \begin{cases} 1, & i - j = 0 \\ \alpha_T, & |i - j| = 1 \\ 0, & \text{sinon,} \end{cases} \quad (\text{B.3})$$

où α_T représente la diaphonie entre chemins sinon adjacents du signal à l'émetteur. L'expression de matrices de diaphonie au niveau du récepteur \mathbf{A}_R est similaire à celle de \mathbf{A}_T , après avoir remplacé α_T avec α_R dans le membre de droite de (B.3), avec α_R désignant la diaphonie entre les voies de signaux adjacents au niveau du récepteur. Ici, le poids du vecteur beamforming et le vecteur combinaison du système MIMO MRC sont choisis en fonction de la valeur de la diaphonie. Pour le système de communication décrits, nous dérivons le SEP moyen et la capacité du système, considérant que le système opérationnel sous un canal de Rayleigh décorrélaté quasi-

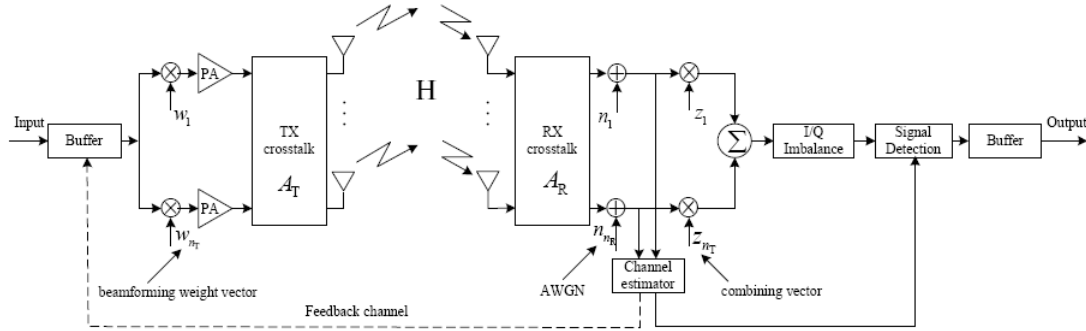


Figure B.7: Schéma du système MIMO TB en présence de nonlinéarité HPA, I/Q déséquilibre et de la diaphonie.

statique, à fréquence plates. En outre, les résultats numériques sont fournis, et les effets de la diaphonie, le nombre d'antennes de transmission et de réception, et pour la modulation de l'ordre du *phase-shift keying* (PSK), sur la performances globales du système, sont discutées. La diaphonie est représenté pour produire un effet constructif sur le SEP moyen dans la faible gamme SNR, et un effet destructif pour le SNR élevé.

B.7 Indemnisation des Multiples Déficiences RF

Dans cette section, nous étudions les effets combinés de nonlinéarité HPA, du déséquilibre I/Q et de la diaphonie dans les systèmes MIMO TB, où la MRC au niveau du récepteur est effectué au niveau RF. Le schéma du système est présenté sur la Fig. B.7. Nous proposons une méthode de compensation pour la non-linéarité HPA, le déséquilibre I/Q et la diaphonie ensemble. Tout d'abord, l'estimation du canal l'équivalent en présence des trois types de déficiences est réalisé en utilisant la règle de LS. Puis, nous déterminons la vecteur beamforming de poids optimal et le vecteur pour système MIMO TB avec ces trois déficiences. En outre, nous utilisons la règle LS pour estimer les coefficients de la matrice de gain de canal équivalent, soit l'équivalent de formation de faisceaux, la combinaison des vecteurs de poids, et

paramètres de déséquilibre I/Q conjointement, puis utilisons le signal reçu avec son conjugué pour détecter la signal transmis. Par la suite, une limite supérieure du SEP moyen et une borne inférieure sur la capacité du système MIMO TB à sous un canal de Rayleigh décorrélé sont dérivés. Les résultats numériques montrent que les effets des paramètres du système sur plusieurs performances sont présentés et discutés. En particulier, le SEP moyen diminue quand le paramètre HPA β devient plus grand. En outre, la dégradation causée par la diaphonie sur les SEP moyen augmente pour la gamma de $\bar{\gamma}$ élevée. D'autre part, pour les faibles valeurs de $\bar{\gamma}$, le SEP moyen est réduit, en profitant de la diaphonie. En outre, le point d'intersection de $\bar{\gamma}$ entre les effets constructives et les effets destructives de la diaphonie devient plus important lorsque le paramètre β diminue.

B.8 Conclusions et Recherches Supplémentaires

B.8.1 Conclusions de la Dissertation

Dans cette thèse, nous avons étudié l'analyse et la compensation des dégradations du canal et du RF, y compris les canaux à évanouissements spatialement-corrélés et à *keyhole*, les troubles de communications M-to-M, la nonlinéarité HPA, le déséquilibre I/Q et la diaphonie à la fois, séparé et ensemble pour les systèmes MIMO. Plus précisément, un système de design inter-couches a été proposé pour les systèmes MIMO utilisant OSTBC sur des canaux Nakagami- m spatialement corrélés et à *keyhole*. En outre, la performance de l'analyse de systèmes M-to-M MIMO MRC a été réalisée, sur le canal à évanouissement doublement-corrélé de Rayleigh-et-Lognormal. À ce égard, un modèle de canal 3D, qui prend en compte les effets d'un évanouissement rapide et l'ombrage, a été utilisé pour obtenir les fonctions de corrélation spatiale d'émission

et de réception. D'autre part, nous proposons des méthodes de compensation basées sur la constellation et la SMC pour nonlinéarité HPA dans le cas, avec et sans connaissance des paramètres HPA, respectivement, pour les systèmes MIMO OSTBC. Quant à la nonlinéarité HPA dans les systèmes MIMO TB, la régimes optimal TB avec le vecteur poids optimal et vecteur beamforming combinant a été proposé. En outre, un schéma sous-optimal mais plus simple, à savoir, QEGT, a également été évaluée en présence nonlinéarité HPA. Nous avons également proposé un algorithme de compensation pour le déséquilibre I/Q dans les systèmes MIMO MRC, qui exploite la règle LS est pour estimer les coefficients de la matrice de gain de canal, la formation de faisceau et la combinaison des vecteurs de poids, et les paramètres de déséquilibre I/Q conjointe, puis fait usage du signal reçu avec son conjugué pour détecter le signal transmis. En outre, la performance de MIMO MRC en présence de la diaphonie a été évaluée. Enfin, nous avons proposé une méthode de compensation globale pour de multiples déficiences du RF dans les systèmes MIMO TB.

B.8.2 Thèmes pour de Futures Recherches

Le thème de recherche futur vise à étudier le RF en bande de base de co-design pour les systèmes de communication avec des différents déficiences du RF. Les techniques de compensation hybride à la fois au niveau RF et bande de base pour les déficiences du RF, y compris la nonlinéarité HPA, la nonlinéarité LNA, le déséquilibre I/Q, la diaphonie, le couplage d'antenne, le bruit de phase, de synchronisation temporelle imparfaite et de l'écho, doivent être proposés. Le co-design RF-bande de base préposé permettra la coopération entre la conception et l'indemnisation au niveau de l'appareil et au niveau du système. Le domaine de la recherche comprend la conception de bande de base, conception *front-ends* RF avancés, la conception d'amplificateurs

de puissance et de linéarisation, le design émetteur-récepteur MIMO-OFDM, la conception de circuits et systèmes, le développement de *digital signal processing/field-programmable gate array* (DSP/FPGA) , et les techniques de la mesure du bruit. Les outils nécessaires comprennent le *computer aided design* (CAD) à base de outils, de bancs d'essais, de prototypages rapide et de configurations.